SCHIZOPHRENIA-RELEVANT *DISC1* INTERRUPTION ALTERS WNT SIGNALING AND CELL FATE IN HUMAN iPSC-DERIVED NEURONS

A dissertation presented

by

Priya Srikanth

to

The Division of Medical Sciences

In partial fulfillment of the requirements

for the degree of

Doctor of Philosophy

In the subject of

Neurobiology

Harvard University

Cambridge, Massachusetts

May 2015

Dissertation Advisors: Dennis Selkoe & Tracy Young-Pearse Priya Srikanth

Schizophrenia-Relevant *DISC1* Interruption Alters Wnt Signaling and Cell Fate in Human iPSC-Derived Neurons

Abstract

The advent of human induced pluripotent stem cell (iPSC) technology has allowed for unprecedented investigation into the pathophysiology of human neurological and psychiatric diseases. Use of human iPSC-derived neural cells to study disease is complicated by the genetic heterogeneity of cell lines and diversity of differentiation protocols. Here, I address issues surrounding neuropsychiatric disease modeling with human iPSCs.

Dozens of published protocols exist to differentiate iPSCs into forebrain neuronal cultures. Among the factors that distinguish these methods are: use of small molecules, monolayer vs. aggregate culture, choice of plating substrates, method of NPC isolation, and glial co-culture. Each of these factors is evaluated here, creating a resource that directly compares a variety of differentiation procedures. The most efficient and reproducible method was an embryoid aggregate differentiation protocol, including aggregate plating onto a Matrigel substrate, enzymatic neural rosette selection, and neuronal dissociation and plating onto Matrigel.

This optimized protocol is used to model a schizophrenia-relevant mutation in human neural cells. Genetic and clinical association studies have identified disrupted-in-schizophrenia 1 (*DISC1*) as a strong candidate risk gene for major mental illness. *DISC1* was initially associated with mental illness upon the discovery that its coding sequence is interrupted by a balanced chr(1;11) translocation in a Scottish family, in which the translocation cosegregates with psychiatric disorders. I investigate the functional and biochemical consequences of *DISC1* interruption in human neurons using TALENs or CRISPR-Cas9 to introduce *DISC1* frameshift mutations into iPSCs. I show that disease-relevant *DISC1* targeting results in decreased DISC1

protein expression by nonsense-mediated decay, increases baseline Wnt signaling in neural progenitor cells, and causes a shift in neural cell fate. DISC1-dependent Wnt signaling and cell fate changes can be reversed by antagonizing the Wnt pathway during a critical window in neural progenitor development. These experiments suggest that *DISC1*-disruption increases Wnt signaling, which alters the balance and identity of neural progenitors, thereby subtly modifying cell fate.

These studies evaluate the use of multiple differentiation procedures in neural disease modeling, shed light on the roles of DISC1 during human brain development, and further our understanding of the pathogenesis of major mental illness.

Table of Contents

Acknowledgments

First and foremost, I would like to thank my thesis advisors, Tracy Young-Pearse and Dennis Selkoe, for their superb guidance throughout my PhD. Tracy and Dennis have been fantastic mentors, providing me with encouragement and keeping me motivated when I didn't think I would ever finish my PhD. Having two mentors provided me with twice the opportunities for mentorship and two incredible models of success. They embody all the things I would like to be as a scientist, and I can only hope to one day be as creative, rigorous, enthusiastic, and respected as they each are. I would also like to thank my dissertation advisory committee members (past and present), Bernardo Sabatini, Stephen Haggarty, Gabriel Corfas, and Kevin Eggan for their scientific advice throughout my thesis.

I thank all the past and present members of the Young-Pearse, Selkoe, and LaVoie labs for their technical and emotional support over the years. They have made the long hours in lab worthwhile, rewarding, and fun. I especially thank Christina Muratore for teaching me everything I know about stem cells and commiserating with me in all things in and out of the lab; Dana Callahan for keeping the TYP lab running and being the most upbeat and efficient person I've ever met; Meichen Liao for always distracting me with cat pictures; and Heather Rice for her talent of keeping me entertained in lab. I would also like to thank all the students I have mentored for their hard work and for reminding me how much fun it can be to teach, particularly Jenny Makovkina and Karam Han, who each contributed amazing efforts to help me finish my PhD.

I also owe thanks to those people outside of the lab who helped get me here. I am grateful to Philip Stahl, who was such an incredible mentor to me when I was an undergraduate student at Washington University in St. Louis, and without whom I certainly would not be where I

am today. I thank all my MD-PhD classmates, who are my greatest support network at Harvard, especially Cristy Garza-Mayers, Morgan Hennessy, Veena Venkatachalam, and Christine Eckhardt. Finally, I thank my family for providing the inspiration that keeps me going every day: to Galen, for keeping me sane and happy, and being the most supportive partner anyone could ask for; my Dad, who is the most brilliant person I know; my sister Maya, who constantly shows me the kind of scientist, doctor, and person I want to be; and to my Mom, who is the reason I have dreamed of being a scientist since I was five years old.

Chapter I.
Introduction

Modeling neurodevelopmental and neurodegenerative diseases using human iPSCs

The majority of this chapter was previously published as:

Srikanth P, Young-Pearse TL. Stem cells on the brain: modeling neurodevelopmental and neurodegenerative diseases using human induced pluripotent stem cells. *J Neurogenet*. 2014 Mar-Jun; 28(0): 5–29. PMID: 24628482

INTRODUCTION

The alleviation of human suffering through the prevention and treatment of disease is the ultimate goal of biomedical research. In order to target the causes of a particular disease, it is beneficial to first understand the molecular mechanisms that underlie the pathology. Studying diseases of the nervous system comes with certain unique challenges due to the complexity of the systems involved and the lack of accessibility of the human brain to direct observation. Recent advances in stem cell technology have allowed researchers to establish human induced pluripotent stem cell (hiPSC) lines from patients[1-3] and direct the differentiation of these cells to various neuronal and glial fates of the nervous system. The hope is that these advancements will allow researchers to model neurological diseases at a cellular level in a dish, providing an opportunity to both study disease mechanisms and test therapeutic strategies in the cell types most affected in these diseases.

As these cells can be maintained and expanded in culture, human iPSCs provide a theoretically unlimited source of disease-relevant human cells for experimentation. Since the initial description of the technology, researchers in the field of neuroscience have established dozens of lines from patients with neurodegenerative and neurodevelopmental diseases, and have modified and expanded neuronal differentiation protocols used with embryonic stem cells (ESCs) to be used with iPSCs. Here, we review the progress in the field in modeling neurologic and psychiatric diseases, providing an overview of the lines created for different diseases and disorders, the cell fates examined for each, and the cell and molecular phenotypes observed. We highlight the challenges involved in studying phenotypes associated with different categories of genetic alterations, and the potential pitfalls in the interpretations of results obtained with hiPSC models. Finally, we discuss the possibilities for expanding the utility of hiPSCs through manipulations of the *in vitro* environment to generate more physiological

models of brain development and aging. As this review focuses on the analysis of stem cells, we will use the term “phenotype” to refer to specific assay outcomes such as gene expression, protein cleavage or phosphorylation, or electrophysiological measures, rather than organismal-level observations. As such, each cell line may display an array of phenotypes that are either a direct result of the genetic lesion (i.e. a truncated protein resulting directly from a nonsense mutation) or are progressively more distantly related to the genetic lesion. We will refer to the former as “proximal” phenotypes, and the latter as “distal” phenotypes. Finally, we include three tables describing published patient-derived iPSC lines and protocols for differentiation to neural fates. While these were meant to be an all-inclusive resource for the community, the rapidly growing literature of the iPSC field makes this challenging. We apologize for any unintentional omissions in these tables. For additional information regarding iPSC usage, we direct the reader to reviews pertaining to the careful modeling of disease-associated genetic variants with stem cells[4,5], direct induction as an alternative to iPSC generation[6], drug screening using stem cells[7], genomic variation between stem cell lines[8], methods of iPSC derivation[6,8], and the study of aging-related disorders using iPSCs[9].

EXAMINING EFFECTS OF GENETIC MUTATIONS AND MODIFIERS USING HUMAN IPSCS

The identification of genetic variants that predispose to disease is of tremendous importance when attempting to identify the molecular and cellular underpinnings of a pathological process. Genetic modifiers of various strengths and prevalence have been found for a variety of diseases (Fig 1.1a). Different strategies can be (and perhaps should be) used to model disease based upon each of these kinds of variants. The influence of genomic variants on cellular phenotypes in question depends on a number of factors, including: (1) the penetrance of the mutation/variant, (2) the proximity of the phenotype to be studied to the mutation of interest, and (3) the technical and biological reproducibility of the phenotype. For

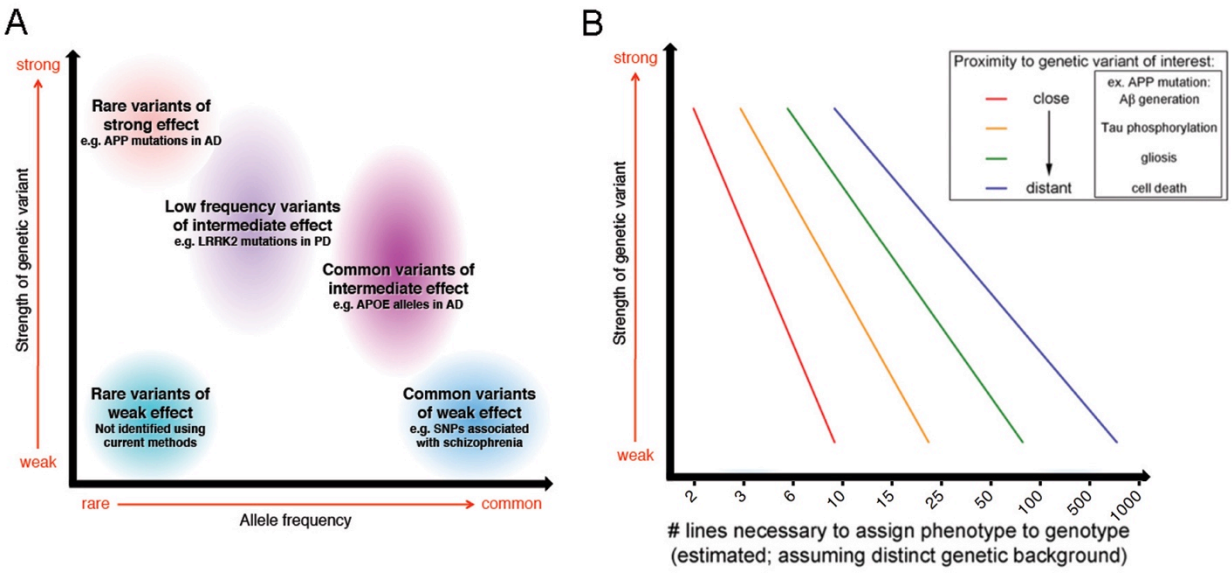

Figure 1.1. Relationship of allele frequency, variant strength, and number of iPSC lines needed to study disease processes. (A) Distributions of disease-predisposing genetic variants and allele frequency. Nearly all identified rare variants that confer an increased disease risk are high in penetrance, such as autosomal dominant mutations causing early-onset familial Parkinson's disease (e.g. in *SCNA*), early-onset familial Alzheimer's disease (e.g. in *APP* or *PSEN1/2*), or familial ALS (e.g. in *SOD1*). There also are low frequency variants, with lower penetrance than the aforementioned rare alleles, which greatly increase disease risk, such as *LRRK2* mutation in Parkinson's disease. Relatively common alleles have been identified that carry a substantially increased risk, such as the *APOE* ε4 allele, with an allelic odds ratio of ~4 for Alzheimer's disease[10]. Many genome-wide association study (GWAS)-identified loci mark common variants of weak effect, as is the case for most SNPs associated with neuropsychiatric disease. Finally, there almost certainly exist rarer variants than those currently known, which confer a small increase in disease risk. However, current methods are unable to discern such genetic variants due to lack of statistical power. **(B)** Estimate of the number of disease and control-derived iPSC lines needed to attribute a phenotype to the genotype under examination. For strong genetic variants with high increased disease risk and penetrance, fewer lines will generally be needed. Similarly, when analyzing phenotypes that are closer functionally to the genetic alteration of interest, fewer lines will be required. The graph above relays an estimate of how the variables of variant strength and phenotypic 'distance' might combine to achieve statistically significant results, based upon published studies. Example phenotypes listed pertain to the study of a familial Alzheimer's disease mutation, i.e. *APP* mutation.

these reasons, the widespread genetic variation that exists between iPSC lines derived from unrelated individuals is likely to affect analyses of weaker disease-predisposing mutations and phenotypes more distant from the mutation. Thus, when studying genetic variants that only mildly increase disease risk or phenotypes far removed from the genetic alteration, it is especially important to control for other genetic variation. Using genetically related, unaffected family-derived control lines would lessen genomic variability, but this is ideally done using gene correction methods (outlined below). On the other hand, rare but highly penetrant variants may be capable of recapitulating disease phenotypes even in the presence of other genomic variation, especially when examining phenotypes proximal to the disease-causing mutation.

For example, fully penetrant mutations have been identified that cause early-onset familial Alzheimer's disease (fAD). Hundreds of such mutations have been identified in Amyloid Precursor Protein (*APP*) and Presenilin 1 or 2 (*PSEN1/2*) (reviewed here[10]). *APP* encodes the precursor protein for β-amyloid (Aβ), and presenilins encode the active site of the enzyme that cleaves APP to generate Aβ of differing lengths. An example of a so-called "proximal" phenotype to these mutations would be the generation of different lengths of Aβ. Based upon pathological findings in fAD patients and animal models, progressively more "distal" phenotypes may include tau phosphorylation, gliosis, neuritic dystrophy, synaptic failure, and ultimately, cell death. Alzheimer's disease genetics also provide an example of a relatively common allelic variant of strong effect. The *APOE* ε4 allele increases risk for AD 3-12 fold, depending on allele dosage, and is present in ~15% of subjects of European ancestry[11,12]. A proximal phenotype of *APOE* allelic variation may be expression, secretion, or cholesterol-binding abilities of APOE variants, while more distal phenotypes may overlap with those of *APP* and *PSEN* mutations. In order to achieve sufficient statistical power using iPSC modeling, the number of lines required for analysis would vary based upon these variables of penetrance/strength of genetic variant and the proximity of the phenotype to the genetic alteration (schematized in Fig 1.1b).

Investigating the proximal effects of strong genetic variants in neurological disease are the "low hanging fruit" that most iPSC studies published to date have presented. Many of these have confirmed the findings from animal models, heterologous cell lines (such as CHO, HEK, HELA, and others) and postmortem studies (see Tables 1.1 and 1.2). While it is valuable to re-examine these phenotypes in living human neuronal and glial cells, it will be important to examine additional phenotypes that may or may not be specific to cell type, and identify sites of convergence of multiple predisposing genetic variants (Fig 1.2). However, other genetic loci are more likely to impact these phenotypes the further removed they are from the mutation of interest, which underlies the predicted requirement for increased numbers of iPSC lines to study such phenotypes (Fig 1.1b). Known genetic variants can be modeled with "isogenic" cell lines, where a patient-derived iPSC line has been gene-corrected (e.g. using zinc-finger nucleases [ZFNs], transcription-activator-like effector nucleases [TALENs], clustered regularly interspaced short palindromic repeat [CRISPR]-Cas9, or other methods), reverting a mutant line to the wild-type genotype or vice-versa. It may be more desirable to correct a mutant line than to induce mutation in a wild-type line, as beginning with an iPSC line from a patient manifesting disease ensures that the genetic background is permissive to disease progression in the presence of the mutation in question.

The recent expansion of gene-editing nuclease technologies has greatly enhanced the possibilities for genomic editing in iPSCs. TALENs and ZFNs are similar in action, in that they both involve a custom DNA binding domain conjugated to FokI nuclease, which induces a DNA break upon dimerization with another FokI nuclease within a certain spacer distance. The identification of a simple DNA recognition "code" for TALENs has made TALEN design far simpler and more predictable than ZFN design, which was largely based on testing many nucleases for activity at the target site[86]. For all cleavage-based methods, DNA-binding and cleavage specificity is a concern, as off-target mutations may induce aberrant phenotypes or

Table 1.1. Human iPS cell lines created to study neurodegenerative diseases
This table outlines published studies that generated novel hiPSC lines to study a subset of neurodegenerative diseases. The number of lines listed indicates the number of distinct *subjects* from whom iPSC lines were derived (i.e. "1x" may represent a single line or multiple clonal lines derived from a single subject). All mutations are heterozygous unless otherwise indicated (het: heterozygous, homo: homozygous). The differentiated cell types are listed as identified in the original paper. A-T: ataxia telangiectasia, AD: Alzheimer's disease, ALS: amyotrophic lateral sclerosis, ER: endoplasmic reticulum, FA: Friedreich's ataxia, FD: familial dysautonomia, FTD: frontotemporal dementia, HD: Huntington's disease, MMR: mismatch repair, NCL: neuronal ceroid lipofuscinosis, ND: no data, NMJ: neuromuscular junction, NPC: neural progenitor cell, PD: Parkinson's disease, ROS: reactive oxygen species, RP: retinitis pigmentosa, RPE: retinal pigment epithelium, SMA: spinal muscular atrophy, TH: tyrosine hydroxylase, wt: wild-type.

Year	Novel iPSC lines generated (# of subjects per genotype/phenotype)	Differentiated cell type(s) identified and analyzed	Phenotypes described	Reference
Alzheimer's disease				
2011	1x PSEN1 A246E, 1x PSEN2 N141I	Neurons	Aβ generation	13
2012	2x sporadic AD, 2x APP duplication, 1x wt	Neurons, co-culture with astrocytes	Aβ generation, Tau phosphorylation, GSK3b phosphorylation, endosome size	14
2013	1x APP homo E693Δ, 1x APP V717L, 2x sporadic AD, 3x wt	Cortical neurons	Aβ generation, localization, and oligomerization state, levels of cellular stress	15
2014	2x APP V717I	Cortical neurons	Aβ and sAPPα/β generation, APP & Tau levels, Tau phosphorylation, APP early endosomal localization	16
Amyotrophic lateral sclerosis				
2008	2x SOD1 L144F	Motor neurons and astrocytes	ND	17
2010	16x idiopathic ALS, 10x wt	Cortical neurons, motor neurons, co-cultured with astrocytes	TDP-43 aggregation	18
2011	4x VAPB P56S, 3x wt	Motor neurons	VAPB protein levels, VAPB aggregates	19
2012	1x TARDBP M337V, 2x wt	Motor neurons	TDP-43 protein levels, cell death	20
2013	4x C9ORF72 GGGGCC expansion (3x ALS, 1x ALS/FTLD, 1x >70, 3x >800 repeats), 4x wt	Motor neurons	C9ORF72 GGGGCC repeat stability, C9ORF72 expression, RNA foci, RNA binding protein sequestration, gene expression, motor neuron survival	21

Table 1.1 (Continued)

2013	4x C9ORF72 GGGGCC expansion (1x >620, 2x >850, 1x >1150 repeats), 2x SOD1 A4V, 2x SOD1 D90A, 5x wt	Motor neurons	C9ORF72 expression, C9ORF72 GGGGCC repeat stability, RNA foci, gene expression, RNA binding protein sequestration, C9ORF72 RAN translation, excitotoxicity	22
Ataxia telangiectasia				
2012	1x ATM het, 1x ATM homo (ATM c.7004delCA and/or ATM c.7886delTATTA)	Neurons	Radiation-induced signaling, radiosensitivity, DNA damage signaling pathways, mitochondrial and pentose phosphate pathways	23
2013	1x ATM homo c.103C>T, 1x ATM compound het c.967A>G;c.3802delG, 1x wt	NPCs and neurons	Activation of ATM activity, DNA repair, mitochondrial function	24
Best vitelliform macular dystrophy				
2013	1x BEST1 A146K, 1x BEST1 N296H, 2x wt	RPE, co-cultured with photoreceptor outer segments	Fluid flux, rhodopsin degradation, stimulated calcium responses, oxidative stress measures	25
Familial dysautonomia				
2009	3x IKBKAP homo c.2507+6T>C, 1x wt	Neural crest, NPCs	IKBKAP splicing, cell motility	26
Friedreich's ataxia				
2010	2x FXN homo GAA (330;380 and 541;420)	No neurons created	Global gene expression, FXN expression, FXN GAA repeat instability, MMR enzyme expression and localization to FXN gene	27
2011	2x FXN homo GAA expansion (527;1058 and 751;1027)	Neurons, neural crest, peripheral sensory neurons, cardiomyocytes	FXN expression, FXN GAA repeat instability	28
2013	2x FXN homo GAA expansion (800;600 and 900;400), 2x wt (<20 FXN GAA)	Neurons, cardiomyocytes	FXN expression, FXN GAA repeat stability, morphology, viability, electrophysiological properties, mitochondrial structure and membrane potential, MMR enzyme levels	29
2013	2x FXN homo GAA expansion (500;750 and 580;620)	Neural crest, peripheral sensory neurons	FXN expression	30
Frontotemporal dementia				
2012	1x FTD sporadic, 1x GRN S116X, 1x wt	Neurons (majority glutamatergic, some GABAergic)	GRN/PGRN expression, sensitivity to cellular stress, S6K2 expression	31

Table 1.1 (Continued)

2013	2x C9ORF72 >1,000 GGGGCC	Neurons (majority glutamatergic, some GABAergic), some astrocytes	C9ORF72 expression, C9ORF72 GGGGCC repeat stability, RNA foci, RNA binding protein sequestration, C9ORF72 RAN translation, viability in response to inhibitors of autophagy	32
Gaucher's disease				
2013	1x GBA1 compound het L444P;G202R (acute neuronopathic [type 2] Gaucher's disease)	Dopaminergic neurons, macrophages	Acid-β-glucosidase activity	33
Gyrate atrophy				
2011	1x OAT homo A226V	RPE	OAT activity	34
Hereditary spastic paraplegia				
2013	1x SPAST c.683-1G>T, ≥1x wt	Telencephalic glutamatergic neurons	Axonal swellings, mitochondrial transport, spastin protein levels, tubulin acetylation	35
Huntington's disease				
2012	3x HTT CAG expansion (180;18, 109;19, 60;18), 3x wt (HTT 33;18, 28;21, 21;17 CAG).	NPCs, forebrain neurons, striatal neurons	Adhesion, cytoskeletal properties, electrophysiological activity, gene expression profiles, ATP levels, susceptibility to glutamate toxicity and other stressors	36
2012	1x HTT 73;19 CAG expansion, corrected to HTT 21;20 CAG	NPCs, striatal neurons	Gene expression, cell death following growth factor withdrawal, mitochondrial bioenergetics, xenografting into striatum	37
2012	2x HTT CAG expansion (50;ND, 109;ND CAG), 1x wt (HTT 28;ND CAG)	Neurons, astrocytes	Clear cytoplasmic vacuole formation	38
2012	3x HTT CAG expansion (42;44, 39;42, 17;45), 2x wt (HTT 15;17, 15;18 CAG)	Neurons	Lysosomal activity	39
Neuronal ceroid lipofuscinosis				
2013	2x CLN2 compound het c.509-1G>C;R208X (late-infantile NCL), 3x CLN3 homo 1.02 kb del (juvenile NCL), 1x CLN3 compound het c.1056+3 A>C;D416G (juvenile NCL), 1x CLN3 het 1.02 kb del, 1x wt	NPCs, neurons	Organelle morphology, lysosomal storage material	40

Table 1.1 (Continued)

Niemann-Pick type C1 disease				
2013	1x NPC1 compound het c.1628delC;E612D, 1x wt	NPCs, neurons	Electrophysiological properties, cholesterol accumulation	41
Parkinson's disease				
2009	5x idiopathic PD, 3x non-PD	Dopaminergic neurons	ND	42
2011	1x LRRK2 homo G2019S, 1x wt	Dopaminergic neurons and other midbrain neuronal types	α-synuclein accumulation, measures of oxidative stress, cell death in response to stressors	43
2011	2x PINK1 homo Q456X, 1x PINK1 homo V170G, 1x wt	Dopaminergic neurons	Stress-induced Parkin mitochondrial translocation, mitochondrial copy number, and PGC-1a expression	44
2011	1x SCNA A53T with gene correction	Dopaminergic neurons	ND	45
2011	1x SCNA triplication, 1x wt	Dopaminergic neurons	Expression of a-synuclein and other triplicated genes	46
2011	1x SCNA triplication, 1x wt	Dopaminergic neurons	a-synuclein expression, oxidative stress, peroxide-induced cell death	47
2012	7x idiopathic PD, 4x LRRK2 G2019S, 4x wt	Ventral midbrain dopaminergic neurons	a-synuclein accumulation, cell death, autophagy	48
2012	2x PINK1 homo Q456X, 1x LRRK2 homo G2019S, 2x LRRK2 R1441C, 2x wt	Neurons, dopaminergic neurons	Response to stressors as measured by, mitochondrial respiration, proton leakage, mitochondrial mobility	49
2012	1x PARK2 homo ex2-4 del, 1x PARK2 homo ex6-7 del	Dopaminergic neurons	Oxidative stress, mitochondrial morphology and homeostasis, changes in Nrf2 pathway, a-synuclein accumulation	50
2012	1x LRRK2 G2019S with gene correction	NPCs, neurons	LRRK2 activity, nuclear morphology, susceptibility to proteosomal stress, neuronal differentiation	51
2013	2x LRRK2 G2019S with gene correction, 4x wt	Dopaminergic neurons	Neurite outgrowth, cell death in response to certain toxins, tau and a-synuclein expression	52
2013	1x LRRK2 homo G2019S, 1x wt	Dopaminergic neurons	Mitochondrial morphology, ATP levels, mitochondrial ROS generation, lysosomal activity	53
2013	3x LRRK2 G2019S with gene correction, 1x wt	NPCs, dopaminergic neurons	Mitochondrial DNA damage	54
2013	1x PINK1 homo Q456X, 1x PARK2 homo c.1072delT,	Dopaminergic neurons,	Age-associated markers, dendritic length, gene	55

Table 1.1 (Continued)

	1x PARK2 R275W, 2x wt	fibroblasts	expression, xenografting into striatum, cell death, neuromelanin accumulation, mitochondrial size & ROS, Lewy body-precursor inclusions	
Retinitis pigmentosa				
2011	1x RP1 c.2161insC, 2x RP9 H137L, 1x PRPH2 W316G, 1x RHO G188R	Rod photoreceptor cells	Cell degeneration, oxidative stress, ER stress, response to antioxidants	56
2011	1x MAK homo ex 9 353bp Alu repeat ins, 1x non-MAK RP	Postmitotic retinal cells	MAK expression	57
2012	1x RHO G188R	Rod photoreceptor cells	RHO protein distribution, ER stress, cell degeneration	58
Spinal muscular atrophy				
2012	2x type I SMA (1x homo SMN1 del, 1x unknown genotype) with targeted conversion of SMN2 to SMN1, 1x SMN1 het del, 1x wt	Spinal motor neurons, co-cultured with myotubes	Motor neuron number and size, axon length, endplate size and number (NMJ) when co-cultured with myotubes, number of nuclear gems, xenografting into spinal cord	59
Tauopathy				
2013	1x MAPT A152T with gene correction to wt or MAPT homo A152T	Neurons	Tau fragmentation, phosphorylation, axonal degeneration, cell death	60

Table 1.2. Human iPS cell lines created to study neurodevelopmental and neuropsychiatric diseases

This table outlines published studies that generated novel hiPSC lines to study a subset of neurodevelopmental and neuropsychiatric disorders. The number of lines listed indicates the number of distinct *subjects* from whom iPSC lines were derived (i.e. "1x" may represent a single line or multiple clonal lines derived from a single subject). All mutations are heterozygous unless otherwise indicated (het: heterozygous, homo: homozygous). The differentiated cell types are listed as identified in the original paper. AS: Angelman's syndrome, F: female, FXS: fragile X syndrome, ND: no data, NPC: neural progenitor cell, pre-FXS: FMR1 premutation carrier, M: male, PWS: Prader-Willi syndrome, RG: radial glia, ROS: reactive oxygen species, SCZ: schizophrenia, SCZoid: schizoid, sE/IPSCs: spontaneous excitatory/inhibitory post-synaptic currents, wt: wild-type.

Year	Novel iPSC lines generated (# of subjects per genotype/phenotype)	Differentiated cell type(s) identified and analyzed	Phenotypes described	Reference
Angelman/Prader-Willi syndromes				
2010	2x AS maternal 15q11-13 del, 1x PWS paternal 15q11-13 del, 1x wt	Neurons, astrocytes	Methylation imprint, UBE3A and UBE3A-ATS expression	61
Dravet syndrome				
2013	1x SCN1A c.IVS14+3A>T, 1x SCN1A Y325X, 3x wt	Forebrain neurons (primarily GABAergic)	SCN1A expression, sodium current density, various electrophysiological measures of excitability	62
2013	1x SCN1A F1415I, 1x SCN1A Q1923R, 1x wt	Primarily glutamatergic neurons, some GABAergic; co-cultured with astrocytes	Various electrophysiological measures of excitability	63
2013	1x SCN1A R1645X	GABAergic neurons	SCN1A expression, various electrophysiological measures of excitability	64
Fragile X syndrome				
2010	3x FXS (FMR1 >200 CGG), 2x wt	No neurons created	CpG methlyation in the FMR1 promoter region, FMR1 expression	65
2011	3x FXS (FMR1 > 200 CGG, 1x FMR1 142 CGG derived from mosaic FXS patient), 1x wt	NPCs, neurons	CpG methlyation in the FMR1 promoter region, FMR1 expression, neuronal differentiation	66

Table 1.2 (Continued)

2012	1x pre-FXS (F) with derivation of isoautosomal lines containing either FMR1 94 CGG- or FMR1 30 CGG-active chrX	Neurons, astrocytes	FMR1 mRNA expression, PSD95 expression, synaptic density, neurite length, spontaneous Ca++ transient frequency and amplitude, altered response to glutamate uptake	67
Lesch-Nyhan syndrome				
2013	1x HPRT1 -/Y (M), 1x HPRT1 +/- (F) with derivation of isoautosomal lines containing either wt- or mutation-active chrX (both M & F lines: complex HPRT1 rearrangement involving ex6-9 inv & del), 1x wt (M), 1x wt (F)	Neurons	HGPRT activity, X-inactivation status, neuronal differentiation, neurite length	68
Phelan-McDermid syndrome				
2013	2x 22q13 del (1x 825 kb del, 1x 871 kb del)	Mature forebrain neurons	SHANK3 expression, action potential characteristics, sE/IPSCs, presence of structural and functional synapses	69
Microcephaly				
2013	1x CDK5RAP2 compound het E1516X;R1558X	Cerebral organoids	Neuroepithelial and progenitor region sizes, neuronal outgrowth, RG and neuronal number, neurogenic divisions, RG spindle orientation	70
Rett syndrome				
2009	1x MeCP2 R306C (F)	No neurons created	ND	71
2010	1x MeCP2 T158M (F), 1x MeCP2 Q244X (F), 1x MeCP2 R306C (F), 1x MeCP2 c.1155del32 (F), 3x wt (M), 2x wt (F)	Neurons	MeCP2 expression, X-inactivation, glutamatergic synapse number, spine density, soma size, Ca2+ oscillations, sE/IPSP frequency	72
2011	1x MeCP2 ex3-4 del (F), isoautosomal lines with either wt- or mutation-active chrX	Neurons	MeCP2 RNA and protein expression, soma size, X-inactivation	73
2011	1x CDKL5 T288I (M), 1x CDKL5 Q347X (F) with isoautosomal lines with either wt- or mutation-active chrX	Neurons	X-inactivation	74
2011	1x MeCP2 T158M (F), 1x MeCP2 Q244X (F), 1x MeCP2 R306C (F), 1x MeCP2 X487W (F), 1x	Neurons	X-inactivation, neuronal maturation	75

Table 1.2 (Continued)

	MeCP2 c.705delG, isoautosomal lines with either wt- or mutation-active chrX			
2011	1x MeCP2 T158M (F), 1x MeCP2 V247X (F), 1x MeCP2 R306C (F), 1x MeCP2 R294X (F), isoautosomal lines with either wt- or mutation-active chrX	Neurons	Nuclear size, X-inactivation	76
Schizophrenia				
2011, 2014	2x SCZ, 1x major depression (DISC1 c.2420_2423del) with gene correction of 2 lines, 2x wt, 2x wt edited to DISC1 c.2420_2423del mutation	Glutamatergic forebrain neurons	DISC1 expression, synaptic puncta density, spontaneous synaptic current amplitude & frequency, vesicle release, presynaptic protein expression levels	77,78
2011	1x childhood onset-SCZ, 2x SCZ/SCZoid, 1x SCZ-affective, 5x wt	NPCs, neurons	Connectivity, neurite number, PSD95 and glutamate receptor levels	79
2011	1x SCZ 22q11.2 del, 1x childhood-onset SCZ, 1x SCZ, 2x wt	Glutamatergic neurons	ND	80
2012	4x SCZ, 4x wt	No neurons created	ND	81
2012	1x SCZ, 1x wt	NPCs	Extramitochondrial oxygen consumption, ROS generation	82
2013	3x SCZ, 2x wt	NPCs, glutamatergic neurons, dopaminergic neurons	Differentiation capacity, cell area, neurite length & number, monoamine levels, mitochondrial distribution	83
2014	3x 15q11.2 del, 3x wt	NPCs	Neural rosette polarity, reversed with CYFIP expression	84
Timothy syndrome				
2011	2x CACNA1C c.1216G>A, 3x wt	Cortical neurons	Ca2+ signaling, activity-dependent gene expression, cell fate and differentiation to lower cortical layer and callosal projection neurons	85

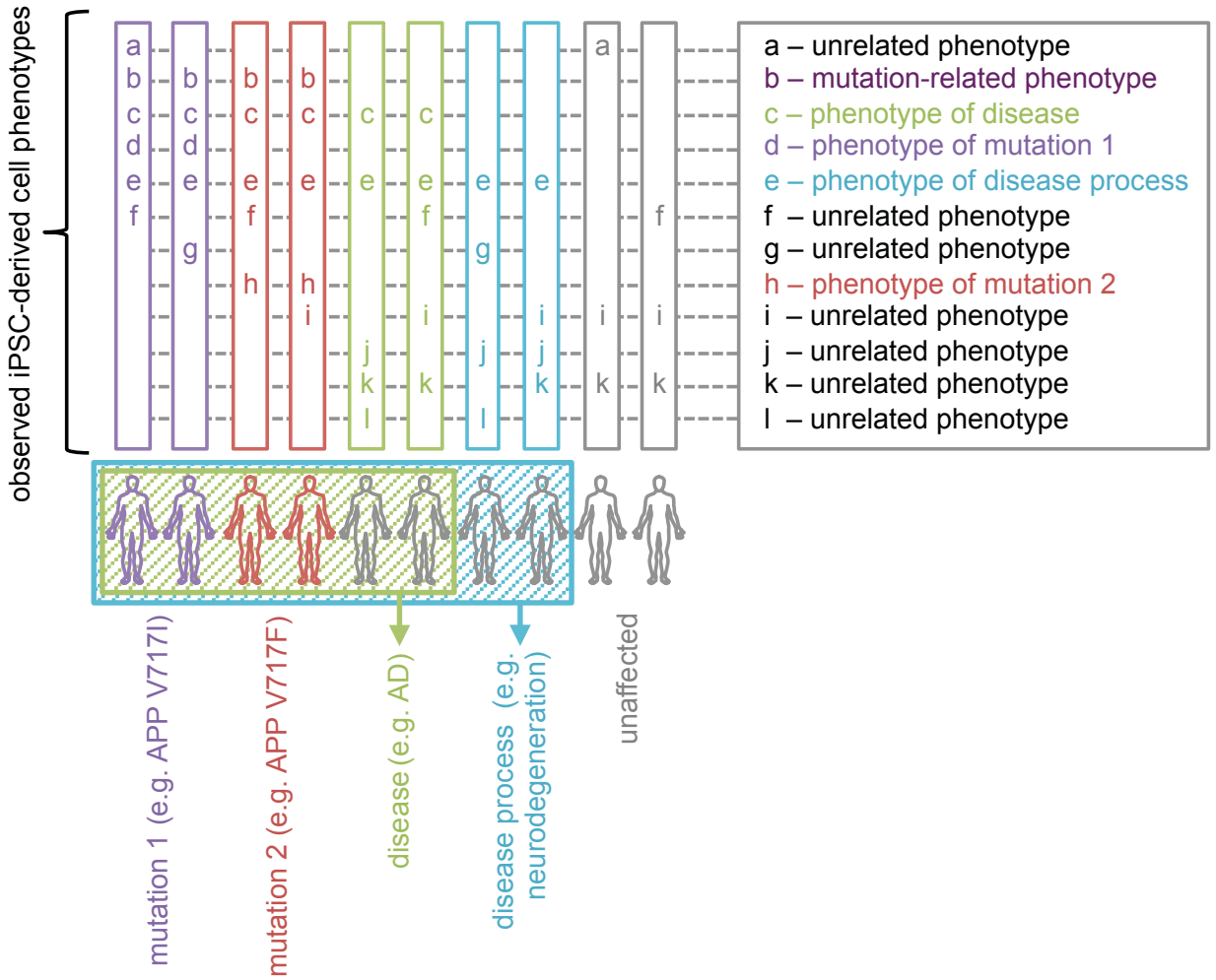

Figure 1.2. Schematic of biological causes of observed phenotypes. Given the study of any particular mutation, several genuine phenotypes attributable to biological (rather than technical) causes may exist. This diagram depicts a subset of meaningful biological causes of phenotypes, which each should be considered when interpreting an observed phenotype. On the bottom from left to right: patients with a particular disease-causing mutation (mutation 1, purple), those with a distinct disease-causing mutation (mutation 2, orange), others with sporadic disease (green), patients experiencing a disease process that encompasses the disease in question (blue), and finally unaffected individuals. Above, hypothetical phenotypes altered in iPSC-derived cells from the individual directly below are shown in boxes. In the given set of individuals, some phenotypes will be common among certain sets of iPSCs, whereas others will be unique. Combinations of lines with similar and distinct origins help to parse out how the phenotype relates to the mutation of interest (e.g. phenotypes b, d, h), the disease of interest (e.g. phenotype c), an overarching disease process (e.g. phenotype e), or that particular individual's genetic background (e.g. all other phenotypes listed above).

even obscure true phenotypes resulting from mutation at the desired site. One proposed method to improve ZFN and TALEN specificity is to use a mutated FokI nuclease, making it an obligate heterodimer[87-92]. The obligate heterodimer approach ensures that FokI dimerization and nuclease activity can only occur if both the forward *and* reverse TALENs/ZFNs bind to neighboring sites. Other FokI mutations have been engineered to reduce toxicity, enhance nuclease activity, or restrict activity to single-stranded cutting ("nickases")[93-97]. Fortunately, TALENs and ZFNs have not been found to induce off-target genomic mutations with appreciable frequency thus far[45,89,98]. The recently-discovered CRISPR-Cas9 system (an RNA-guided nuclease) demonstrates higher genome editing efficiency than TALENs[99], but also has increased potential for initiating off-target cleavage events[100-103]. Similar strategies to those used with ZFNs and TALENs have recently been employed to improve CRISPR-Cas9 specificity, by employing a mutant Cas9 "nickase," which requires two guide RNA sites in close proximity to create a double-stranded DNA break[101,102,104-106]. Although there has been concern for off-target mutation events using CRISPR-Cas9 in screening-based systems, those studies that have examined CRISPR-Cas9 editing in human stem cells have found minimal evidence of off-target effects, reducing concern for widespread mutagenesis using this system[4,5,107,108]. The various nuclease activities, specificities, and target site requirements of each system should be examined before attempting genomic editing in hiPSCs. Additional information thoroughly outlining the advantages and disadvantages of ZFNs, TALENs, and CRISPR-Cas9 methods is provided in other reviews[86,109,110].

In addition to the widespread genetic variability between lines from different individuals, it is also important to consider the impact of epigenetic variation on iPSC studies. The parental cell from which iPSCs are derived impacts the resulting epigenome, altering gene expression and potentially cellular functions[111-113]. This epigenetic "memory" can impact the study of certain disease loci, which may remain silenced after reprogramming[61,65,67,68,73-76,114,115]. The

reprogramming and differentiation processes can themselves affect genomic and epigenetic stability in ways that affect phenotypes of interest. A 2010 report showed that reprogramming iPSCs derived from patients with CGG repeat expansion in the *FMR1* gene (causing fragile X syndrome, or FXS) fails to reactivate *FMR1* expression[65]. This contrasted with results from FXS mutation ESCs, which did express the mutant *FMR1* in the ESC state but silenced it during differentiation. Notably, iPSCs reprogrammed from FXS-ESC-derived differentiated cells also failed to rescue *FMR1* expression, indicating that this disease-associated locus is resistant to reprogramming.

Furthermore, different groups have come to variable conclusions regarding repeat instability during reprogramming and differentiation of iPSCs from patients with repeat expansion disorders. In one study of Huntington's disease, a repeat-expanded *HTT* line showed stable repeat numbers in fibroblasts, iPSCs, and iPSC-derived neurons, with occasional repeat contraction seen with increasing iPSC passage number (loss of 2 out of 44 repeats)[39]. A model of frontotemporal dementia (FTD) using *C9ORF72* repeat expansion lines found differential repeat stability in iPSC reprogramming from fibroblasts of a single patient (≥200 repeat loss or no loss), as well as repeat contraction with neuronal differentiation[32]. Generation of iPSCs from Friedreich's ataxia *FXN* GAA-repeat fibroblasts showed repeat expansion as well as contraction[28]. Finally, iPSCs derived from FXS patients showed *FMR1* repeat instability during reprogramming in one study[66] but relative repeat stability in two others[65,67]. The divergence between studies may arise due to various reasons that are both biological (e.g. differences between patient cells) or technical (e.g. differences in reprogramming or culture methods). Repeat instability may introduce artifactual genomic variation during iPSC culture, or could alternatively recapitulate mosaicism seen in certain disease states[32,66,72].

The X inactivation status of reprogrammed female iPSCs and iPSC-derived differentiated cells introduces another layer of epigenetic variability. Lines derived from the same individual

may not be functionally “isogenic” if they each maintain a different inactivated X chromosome. X-inactivation is of particular importance when the disease-causing mutation occurs on a single X chromosome (e.g. *MeCP2* mutation in Rett syndrome, *FMR1* mutation in fragile X syndrome, *HPRT* mutation in Lesch-Nyhan syndrome). When modeling X-linked disorders with female iPSCs, the specific X chromosome that is inactivated is crucial for the presentation of a mutation-dependent phenotype, as only the mutant gene is expressed when one X chromosome is inactivated, and only the wild-type gene is expressed when the other is inactivated, drastically impacting resulting neuronal characteristics[67,68,72-76,114,115]. It is important to note that in *any* female iPSC lines, X-inactivation status can impact neuronal phenotypes, as several neuronal genes are present on the X chromosome, where significant allele-biased expression occurs during neuronal differentiation[116]. X-inactivation may thus have broad, though subtle, confounding effects on a variety of neuronal phenotypes in any model. This could potentially minimize a genuine disease-associated phenotype or lead to variable results from studies of the same mutation in different lines or labs, such as studies of the same autosomal mutation in a male- vs. a female-derived iPSC line.

CHOOSING A CELL FATE: EXPLORING CELL TYPE-SPECIFIC PHENOTYPES

In addition to deriving cells from patients with mutations or diseases of interest, pluripotent stem cells are an exciting tool because of their ability to generate a multitude of cell types from an identical genetic background. This property of iPSCs provides an opportunity for investigating the nature and causes of selective cellular vulnerability seen in neurological diseases using human cells. Differentiating to distinct neuronal or glial subtypes may reveal phenotypes only in a subset of cell fates, and/or cell autonomous vs. non-autonomous phenotypes. A number of reports have investigated cell type-specificity of phenotypes in fibroblasts vs. iPSCs vs. differentiated cells[20,26,43], but fewer have examined phenotypes across

distinct neuronal subtypes[18,43,117]. This underutilized power of iPSCs represents a missed opportunity (but potential future strength) to investigate the molecular mechanisms underlying selective vulnerability in neurological diseases.

The ability to make a specific cell fate is of particular interest in the study of diseases with well-characterized and limited affected cell populations. A 2011 paper utilized dopaminergic neuron-directed differentiation to study effects of the Parkinson's disease-predisposing *LRRK2* G2019S mutation[43]. *LRRK2* G2019S-homozygous dopaminergic (DA) neurons were more susceptible to H_2O_2-induced cell death than wild-type DA neurons. However, both wild-type and *LRRK2* G2019S tyrosine hydroxylase (TH)-negative neurons were less susceptible to peroxide-induced cell death than TH-positive neurons. *LRRK2* G2019S DA neuron-enriched cultures also showed increased α-synuclein protein levels and increased expression of oxidative stress pathway genes (the latter phenotype seen in day 35, but not day 50 or 55, neurons). A 2010 study examined cellular phenotypes of amyotrophic lateral sclerosis (ALS), a motor neuron disorder, in motor neurons from sporadic and familial ALS patient-derived iPSCs. Burkhardt, et al. reported TDP-43 aggregates in select sporadic ALS iPSC-derived motor neurons. These aggregates were less commonly found in other types of neurons in the same cultures (neurons lacking ISLET1/HB9 expression) and were absent in wild-type and *SOD1*-mutant iPSC-derived motor neurons[18]. Neural crest-directed differentiation was used by the Studer lab to investigate the molecular basis of familial dysautonomia, a fatal peripheral neuropathy, in *IKBKAP*-mutant iPSCs[26]. *IKBKAP* mutant iPSC-derived neural crest precursors (the progenitor cells of the peripheral nervous system) displayed abnormal *IKBKAP* splicing, decreased *ASCL1* expression, and reduced neuronal differentiation and migratory capacity. These studies and others (Tables 1.1 and 1.2) demonstrate the capacity of iPSC disease models to recapitulate cell-type specific phenotypes.

Cell-type-specific directed differentiation is of limited utility when studying diseases

without a clear fate-restricted cellular origin, as is the case with many developmental and neuropsychiatric diseases. In these instances, it may be possible to identify alterations present in broad groups of neurons (e.g. altered spine density), which may only noticeably affect specific circuits *in vivo.* In some cases, it is valuable to study specific neuronal subtypes in the context of a milieu of cell types. The differentiation protocols currently available produce cultures that are heterogeneous to variable extents, whether they contain a wide variety of neural cell types or cells of more fate-restricted neural lineages (Table 1.3).

As alluded to above, the cellular context of the cells to be studied may significantly affect the phenotype of interest. For example, the presence of a pool of neural progenitor cells in a neuronal culture could mask disease-associated phenotypes by continuing to produce newborn neurons (discussed here[5]). This will particularly confound analyses of phenotypes that dramatically change over the course of neuronal maturation, such as neurite architecture, soma size, synaptic density, electrophysiological activity, and gene expression[118-120], and could in theory conceal a cell death phenotype by replenishing viable neurons. Alternatively, some phenotypes may *only* be discernible in a heterogeneous culture. Non-cell autonomous effects have been carefully studied in models of ALS, which have revealed cytotoxicity of *SOD1*-mutant astrocytes on motor neurons[117,121,122]. The Eggan lab found that wild-type hESC-derived motor neurons displayed increased cell death when cultured with *SOD1* G93A-overexpressing human astrocytes relative to wild-type astrocytes. Interestingly, *SOD1* wt-overexpressing astrocytes did not cause motor neuron death, interneurons were not susceptible to *SOD1* G93A astrocyte-induced cytotoxicity, and *SOD1* G93A-overexpressing fibroblasts did not induce motor neuron death[117]. In parallel, the Gage lab showed similar cytotoxic effects of *SOD1* G37R- (but not wild-type *SOD1*-) overexpressing human astrocytes on hESC-derived motor neurons, whereas GABAergic neurons were unaffected[122]. These studies highlight the importance of choice of cell type when studying a human disease process. The predicted pathogenic and/or affected cell

Table 1.3. Protocols for human ES or iPS cell differentiation

Dozens of protocols have been published for the production of various types of neurons from human ESCs and iPSCs. As many hESC differentiation protocols have been successfully used in hiPSCs, protocols using both cell types are included here. Readers should refer to the papers listed for further information on the efficiency of directed differentiation to each cell fate listed.
*For GABAergic neuron generation, only protocols that specifically direct differentiation to an inhibitory fate (rather than observation of inhibitory neuron generation) are listed. In contrast, studies that reported generation of astrocytes or oligodendrocytes are included whether they intentionally biased cells toward these cell fates, or if these cells were observed as a by-product of another differentiation method.
**Protocols listed include studies that performed direct conversion of human somatic cells (non-stem cells) to neurons.

Cell type	References
Forebrain neuronal precursors or neurons	38,70,72,118,120,125,128-145
Motor neuron precursors or neurons	125,132,133,135,137,139,146-152
Dopaminergic neurons	130,132-135,138,139,143,153-165
GABAergic neuronal precursors or neurons (enriched*)	136,166-170
Medium spiny neurons	171-174
Forebrain cholinergic neurons	175-177
Serotonergic neurons	133
Hippocampal neurons	178
Hypothalamic neurons	179,180
Caudal neurons	129,143
Cerebellar neurons	181,182
Astrocytes (observed or enriched*)	38,118,128,133,134,139,140,142,163,183-185
Oligodendrocytes (observed or enriched*)	128,133,134,163,184-189
Neural crest precursors or derivatives (including peripheral neurons, nociceptors, melanocytes, Schwann cells)	28,30,190-200
Cranial placode derivatives	201
Retinal cells	34,56,57,124,202-210
Lineage reprogramming*	
Neural progenitors	211,212
Mixed neurons or uncharacterized	213-219
Glutamatergic neurons (predominantly)	220-223
GABAergic neurons	222,224
Dopaminergic neurons	225-228
Motor neurons	152,229
Medium spiny neurons	230
Peripheral sensory neurons	231
Cholinergic neurons	232
Serotonergic neurons	233
Astrocytes	234
Oligodendrocytes or oligodendrocyte precursors	235

subtypes should be carefully evaluated when deciding what cell types will be used to interrogate disease-relevant processes.

The development of lineage reprogramming as a differentiation method has yielded a plethora of protocols with accelerated timescales and, depending on the protocol, relatively homogenous cell fates (Table 1.3). These methods employ forced expression of critical regulators of cell fate, driving differentiation toward specific cell types. Specific transcription factors and miRNA “cocktails” have been identified by multiple groups that enable direct reprogramming of human cells into multiple types of brain cells (Table 1.3). Interestingly, these methods can facilitate transdifferentiation, allowing use of multiple initial cell types to make neurons, including fibroblasts, pericytes, astrocytes, and adipocytes (Table 1.3, reviewed here[25]). In comparison to the embryoid-aggregate-based method, transdifferentiation protocols often result in cells that mature more quickly, and which may circumvent the protracted differentiation of aggregate-based methods. Lineage reprogramming can provide an opportunity to examine more mature neuronal fates, which may be more relevant to some disease processes. Increased culture homogeneity also reduces differentiation variability, which may reveal otherwise obscured subtle cell-type-specific effects of disease mutations.

While these “induced neurons” open many possibilities for screening and disease modeling, this approach has yet to be used to successfully identify disease-associated phenotypes in human neural cells. In addition, there are potential pitfalls of transdifferentiation methods related to the introduction of strong genetic drivers that bypass normal differentiation. As lineage-reprogrammed cells are directly converted to a final cell type, it may be difficult to study neurodevelopmental processes using these cells. A few protocols exist to directly convert cells to human neural progenitor cells (Table 1.3), which may allow study of particular neural progenitor cell subtypes. Overexpression of strong transcription factors or miRNAs could also mask effects of disease mutations by overpowering a subtle mutation-associated effect on cell

fate or gene expression. Furthermore, while the potential uniformity of resulting cultures presents an opportunity to study effects of disease-associated mutations in one cell type, this assumes prior knowledge that the particular cell type is implicated in disease pathophysiology. As previously discussed, the exact cell types affected by certain disease processes are unknown, making less biased and more "endogenous" differentiation methods an attractive way to examine neurodevelopment and to study multiple cell types simultaneously.

Studying selective neuronal vulnerability or cell fate-specific phenotypes is limited to those cell fates that can be generated using available protocols (Table 1.3). The breadth of neuronal and glial cell fate protocols is constantly expanding, and these are continually being improved to yield higher efficiencies at lower cost. However, this perpetual refinement of protocols also presents a challenge to researchers - how do we compare similar cell fates generated by distinct protocols? Differences in differentiation methods (e.g. use of small molecules or genes, monolayer vs. aggregate, small molecule/growth factor concentrations and sources, differentiation time, cell purification by MACS/FACS, lab environment) could considerably alter the population of resulting neurons. In addition, different iPSC lines have incredibly variable neuronal differentiation capacities[74,113,117,123-127], which can complicate analyses of presumed neuronal differentiation-impairment resulting from mutation[75,80,83]. As a result, it is essential that as a research community we thoroughly characterize the cell populations we study (by gene expression studies, immunostaining, electrophysiological characterization, etc.) and maintain a high level of transparency in data reporting (recording number of lines used, number of differentiations, and number of cells/wells studied for each experiment).

SPECIFICITY OF PHENOTYPE

There are many factors that may contribute to the presence or absence of any particular

phenotype in iPSC-derived cells. Technical variables can be a prominent source of phenotypic variation between iPSC lines or within one iPSC line used in multiple laboratories. Each step from somatic cell harvesting to phenotypic assay introduces multiple variables that may differ between lines, differentiation rounds, and labs. Included among the many technical variables are: somatic cell source and age at harvest, reprogramming method, iPSC culture conditions, differentiation method (including use of small molecules and exogenous transcripts and/or proteins), and phenotypic assay protocol. These factors can influence the epigenome and genome, potentially altering specific cellular phenotypes, including the capacity to differentiate to a particular cell lineage. Indeed, recent studies have shown that different iPSC lines each have their own propensities to differentiate to particular cell lineages (addressed above), although this can be partially overcome by modified protocols, such as extended iPSC passaging[236], DMSO treatment prior to differentiation[237], and FGF2 and/or dual SMAD inhibition during differentiation[125,126]. This is a vital concern when studying a potential phenotype of altered differentiation potential, and requires that multiple distinct lines and/or isogenic lines be used.

Of equal importance to technical variables are the biological causes of phenotypic variation between iPSC lines (Fig 1.2). These biologically-significant variable phenotypes can be grouped as follows: (1) a phenotype that is unique to cell lines from that particular person, (2) a phenotype specific for a mutation of interest, and (3) a phenotype of a pathological process. A person-specific phenotype would likely result from genomic or epigenomic variation other than the mutation of interest. In contrast, a phenotype could be a biological result of a certain mutation, but may not result from other mutations linked to the same disease. For example, the *SOD1* G93A mutation causing ALS could result in a specific biochemical phenotype that does not occur with other ALS-causing mutations in *SOD1* or ALS-causing mutations in other genes, such as *TDP-43* or *C9ORF72*. Findings such as these reveal interesting aspects of the basic molecular and cell biology of the proteins implicated in disease, but may reduce the possibility

that the unique phenotype is absolutely required for disease pathogenesis. Finally, a phenotype may be characteristic of a specific disease, such as ALS, or a disease spectrum, such as neurodegeneration.

Although it would be time- and resource-intensive to tease out each of these possibilities in any one study, compilation of data from multiple studies can reveal patterns that indicate into which group a specific phenotype falls. Targeted strategies can be revealing, including using multiple iPSC lines with the same mutation, iPSC lines with different disease-causing mutations, and iPSCs derived from patients with sporadic disease. When possible, rescue experiments in which the suspected disease cause is corrected can demonstrate the dependence of an observed phenotype on a mutation or other characteristic. Complementary methods are also critical for determining the relevance of any iPSC-derived finding. This can include non-iPSC cell culture, postmortem human tissue studies, and animal models, each of which provide a distinct set of advantages and disadvantages when compared to iPSCs. For example, disease processes characterized by loss of a developmentally- and regionally-restricted cell type can be studied using xenografting of hiPSC-derived cells into rodent disease models, followed by examination for symptomatic alleviation. Examples of this sort have been carried out in the literature in the study of spinal muscular atrophy (SMA)[59], Huntington's disease[37,238], Parkinson's disease[164], and congenital hypomyelination[185].

One such report generated iPSCs from *SMN1* mutation-homozygous SMA patients (SMA-iPSCs) and gene-corrected one copy of the *SMN2* gene to an *SMN1*-like sequence by single-stranded oligonucleotide treatment (TR-iPSCs), enabling expression of a functional homolog of SMN1 from one *SMN2* allele[59]. SMA-iPSC-derived, but not isogenic TR-iPSC-derived, spinal motor neurons displayed degenerative phenotypes *in vitro*. Corti, et al. subsequently transplanted SMA-iPSC- or TR-iPSC-derived motor neurons into SMA transgenic mice, and found that TR-neurons engrafted with higher efficiency than SMA-neurons, while both rescued

deficits in SMA transgenic mice in proportion to motor neuron engraftment[59]. These types of iPSC-based studies that incorporate non-iPSC methods will expand our knowledge of the characteristics and potential applications of iPSC-derived cells.

LIMITATIONS OF THE DISH: BRINGING *IN VITRO* CLOSER TO *IN VIVO*

Although iPSCs are an exciting and appealing tool for studying the molecular and cellular phenotypes underlying human disease states, we must recognize the many caveats and limitations that accompany this method. As iPSCs are an *in vitro* system, they lack many of the characteristics of a developing and mature brain. The microenvironment of the developing brain cannot yet be fully recapitulated, but certainly affects the extracellular cues presented to differentiating cells. The lack of physically disparate regional identities also obfuscates area-specific phenotypes. For example, it is difficult to study neuronal circuitry using iPSCs, particularly when investigating phenotypes unique to specific neuronal circuits of the adult brain. However, it may be possible to reproduce inter-regional cellular connections using co-culture of cells resulting from distinct directed differentiation methods. Adding to the challenge of recapitulating the endogenous nervous system, the cell types that can be made using iPSCs have intrinsic limitations. No matter the extent of characterization of gene expression, protein expression, morphology, and electrophysiology, it is nearly impossible to map an iPSC-derived cell to a corresponding *in vivo* cell fate. Although a cell may express a set of proteins and display firing characteristics of a layer V excitatory pyramidal neuron, it is impossible to know if this neuron is a faithful representation of a neuron that exists *in vivo* at any time over the life of a human. This theoretically insurmountable obstacle is minimized with detailed phenotypic examination of the cell types to be studied, but must always be acknowledged when interpreting data.

One strategy to bring more *in vivo* relevance to iPSC use is xenografting of iPSC-derived

neurons into the developing or mature rodent CNS environment. Transplantation has been utilized by several groups to characterize the differentiation and functional capacity of neural cell types resulting from differentiation[38,119,120,143,163,164,166,167,169,170,173,182,185,188,239-242]. In addition, a handful of studies have used xenografting of wild-type or gene-corrected iPSC-derived cells into disease-model rodent brains to observe resulting engraftment and behavioral rescue[37,59,164,185,238]. If would be of interest to extend these studies to examine cellular defects relating to processes such as neuronal migration and maturation, axon guidance, and synapse formation in mutant vs. wild-type iPSC-derived cells.

The developmental timeline of human stem cells *in vitro* is restrictive, as iPSC/ESC neuronal differentiation recapitulates early *in vivo* neurodevelopment, producing embryonic-like neurons that proceed through the neurodevelopmental stages of neural progenitor cell proliferation, neuronal migration, and neurite outgrowth and arborization[70,131,144,169,170,243-247]. However, using currently available methods, these cells lack many characteristics of adult neurons[248], complicating the study of adult-onset diseases using stem cell-derived neurons. Human neurodevelopment continues for decades postnatally, with continuing changes in synapse number, myelination of axons, and neuronal maturation[249-251]. In contrast, hiPSC-derived neurons used to study mechanisms of disease are often differentiated for anywhere from 14 to greater than 100 days[118,135,139]. These differentiation times fall far short of the delayed onset of symptoms that accompanies many neurological diseases studied with iPSCs (fragile X syndrome: neonatal [252], Rett syndrome: 6-18 months[253,254], schizophrenia: 15-30 years[255], Huntington's disease: average ~40 years[256,257], ALS: average ~60 years[258,259], Parkinson's disease: ≥ 60 years[260], Alzheimer's disease: ≥ 65 years[261]), calling into question whether cellular phenotypes of these disorders could be observed *in vitro* in a matter of weeks or months. The *in vitro* differentiation process is more relevant for neurodevelopmental and neuropsychiatric disorders, which are often hypothesized to stem (at least in part) from defects in early brain

development (Table 1.2)[251,262-264]. However, even late-onset neurological diseases can have early cellular endophenotypes that manifest before clinically-observed symptoms. For example, neurons derived from patients with late-onset disorders can reveal early mechanisms underlying disease pathophysiology prior to the development of overt pathology, such as altered gene expression and protein processing (Table 1.1).

While certain molecular phenotypes may be observable in neurons at early developmental stages, other downstream phenotypes may only be observed in fully-mature, "aged" neurons. To this end, a number of methods are currently being developed to accelerate the aging and maturation process of hiPSC-derived neurons. Xenografting stem cell-derived neurons into rodent brain stimulates neuronal maturation[120,265], and could be used to 'age' neurons prior to assaying for a phenotype of interest. In addition, neurons may be artificially aged in culture by presenting cells with exogenous stressors (see Table 1.1). Aging could also be accelerated by introducing mutations in genes implicated in cellular aging regulation, such as *LMNA*, which is mutated in the premature aging disorder Hutchinson-Gilford progeria syndrome (HGPS). HGPS iPSC-derived cells display premature senescence, dysmorphic nuclei, DNA damage, increased mitochondrial reactive oxygen species, and reduced telomere length, thus recapitulating aspects of accelerated cellular aging *in vitro*[55,266,267]. Such 'aging' mutations could theoretically be manipulated to hasten neuronal aging in culture. Indeed, a recent study was able to recapitulate aspects of neuronal aging *in vitro* by overexpressing progerin (the truncated transcript resulting from HGPS-associated *LMNA* mutations) in control and Parkinson's disease (PD) iPS-derived cells. In this report, progerin-induced aging was able to reveal PD-specific phenotypes that were previously unobservable in wild-type and PD-derived neurons[55]. These strategies facilitate the study of late-onset disorders *in vitro* on a more practical timescale.

The ability to produce cerebral "organoids" presents the possibility of studying a disease phenotype in a specific cell type or group of cell fates in the context of a three-dimensional (3D)

model of human neurodevelopment [26]. These organoids also facilitate the study of phenotypes which may only manifest in a 3D system, or which are easier to study in a 3D context, such as alterations in neural progenitor proliferation, neuronal migration, cortical layering, and axon guidance. While these processes can occur to varying extents in two-dimensional culture systems, they are likely more ordered and closer to their *in vivo* counterparts when occurring in 3D. This is of interest especially when studying common neurodevelopmental and neuropsychiatric disorders, which often do not display striking neuroanatomical phenotypes, but are characterized by subtle perturbations in cortical organization[27]. Cerebral organoids do recapitulate some area-restricted neuronal identities (e.g. prefrontal lobe, hippocampal, and ventral cortical neuron marker expression), indicating the possibility of using organoids to study inter-regional phenotypes. No current method can exactly replicate the *in vivo* ratios of relevant cell fates, extra-cerebral influences on disease processes (e.g. immune cells, blood-brain barrier), or the 3D structure of neurodevelopment, preventing the study of human disease-associated states in a precise human *in vivo* environment. However, further characterization of this recent technique compared to more traditional differentiation protocols and *in vivo* neurodevelopment will help identify those phenotypes that are better studied in this 3D environment.

Another approach to make *in vitro* systems more physiological involves tissue engineering to mimic *in vivo* structures “on a chip”. Microfluidic devices can be used to improve nutrient delivery and waste removal in tissues or cultures *in vitro* [28], simulate the blood-brain barrier[268], model a neurovascular unit[269], and manipulate neuronal connectivity[270] or organization[271]. These devices could be used to characterize the behavior of iPSC-derived vs. rodent brain-derived neurons, as well as provide opportunities to investigate disease-associated phenotypic alterations that may not be accessible in traditional culture systems. Although these have yet to be widely used in the field, tissue engineering presents many exciting possible avenues for

future applications with iPSC-derived neurons[272].

CONCLUDING REMARKS

Since the first descriptions of human iPSC methodologies, hundreds of laboratories in academia and industry have adopted the technology for the study of neurological and psychiatric disorders. Lines from over one hundred patients with brain diseases have been published (Tables 1.1 and 1.2), but thousands more are in the process of being characterized. As the number of iPSC lines developed goes through exponential expansion, it is crucial that the iPSC community develop a standard format for sharing information about these lines. The format used should allow the information to be described using a consistent vocabulary and to be easily discovered online. There are already several repositories that share information on their individual websites (coriell.org, atcc.org, wicell.org, hsci.harvard.edu, and nyscf.org), and informational sites that share data about existing lines (umassmed.edu/iscr, nimhstemcells.org, and eagle-i.net). While the number of lines is still manageable, these groups should work together to drive the standardization of cell line description and of the format for sharing iPS cell information.

While many have embraced the potential of this technology, others remain skeptical that hiPSCs will reveal significant insights into the mechanisms of and treatments for neurological diseases. As with any new technology, the early years of adoption have resulted in a wave of studies of varying caliber. Several important initial studies with hiPSCs confirmed known effects of certain genetic variants, but for the first time in *human* neurons, while others where able to reveal novel insights into the effects of such variants on neuronal function. In some studies reporting novel phenotypes in patient-derived lines, concerns have been raised about the specificity of the phenotype for the disease state or even for the genetic alteration being studied. For example, it has been described that first-generation neuronal differentiation protocols show

variable efficiencies, even between multiple lines derived from the same subject[125] (also see Tables 1.1 and 1.2). Therefore, phenotypes relating to neuronal differentiation (such as neurite outgrowth, neuronal marker expression, electrophysiology) must be carefully interpreted in the context of appropriate controls.

Despite the concerns mentioned above, human iPSCs allow unprecedented investigation into the causative events in disease progression. In addition, for the first time, this technology allows neuroscientists to test therapeutics in the cell types of interest derived from the patients to be treated. As differentiation protocols become more efficient and reliable, and novel strategies are optimized to make the *in vitro* environment more physiological, the insights garnered from studies using hiPSCs will be broadened.

REFERENCES

1. Takahashi, K. *et al.* Induction of pluripotent stem cells from adult human fibroblasts by defined factors. *Cell* **131,** 861–872 (2007).

2. Yu, J. *et al.* Induced pluripotent stem cell lines derived from human somatic cells. *Science* **318,** 1917–1920 (2007).

3. Park, I.-H. *et al.* Reprogramming of human somatic cells to pluripotency with defined factors. *Nature* **451,** 141–146 (2008).

4. Merkle, F. T. & Eggan, K. Modeling human disease with pluripotent stem cells: from genome association to function. *Cell Stem Cell* **12,** 656–668 (2013).

5. Sandoe, J. & Eggan, K. Opportunities and challenges of pluripotent stem cell neurodegenerative disease models. *Nat Neurosci* **16,** 780–789 (2013).

6. Tran, N. N., Ladran, I. G. & Brennand, K. J. Modeling schizophrenia using induced pluripotent stem cell-derived and fibroblast-induced neurons. *Schizophrenia Bulletin* **39,** 4–10 (2013).

7. Marchetto, M. C. N., Winner, B. & Gage, F. H. Pluripotent stem cells in neurodegenerative and neurodevelopmental diseases. *Human Molecular Genetics* **19,** R71–6 (2010).

8. Vaccarino, F. M. *et al.* Induced pluripotent stem cells: a new tool to confront the challenge of neuropsychiatric disorders. *Neuropharmacology* **60,** 1355–1363 (2011).

9. Liu, G.-H., Ding, Z. & Izpisua Belmonte, J. C. iPSC technology to study human aging and aging-related disorders. *Curr. Opin. Cell Biol.* **24,** 765–774 (2012).

10. Bertram, L., Lill, C. M. & Tanzi, R. E. The genetics of Alzheimer disease: back to the future. *Neuron* **68,** 270–281 (2010).

11. Verghese, P. B., Castellano, J. M. & Holtzman, D. M. Apolipoprotein E in Alzheimer's disease and other neurological disorders. *Lancet Neurol* **10,** 241–252 (2011).

12. Mahley, R. W. & Rall, S. C. Apolipoprotein E: far more than a lipid transport protein. *Annu Rev Genomics Hum Genet* **1,** 507–537 (2000).

13. Yagi, T. *et al.* Modeling familial Alzheimer's disease with induced pluripotent stem cells. *Human Molecular Genetics* **20,** 4530–4539 (2011).

14. Israel, M. A. *et al.* Probing sporadic and familial Alzheimer's disease using induced pluripotent stem cells. *Nature* **482,** 216–220 (2012).

15. Kondo, T. *et al.* Modeling Alzheimer's disease with iPSCs reveals stress phenotypes associated with intracellular Aβ and differential drug responsiveness. *Cell Stem Cell* **12,** 487–496 (2013).

16. Muratore, C. R. *et al.* The familial Alzheimer's disease APPV717I mutation alters APP processing and Tau expression in iPSC-derived neurons. *Human Molecular Genetics* **23,** 3523–3536 (2014).

17. Dimos, J. T. *et al.* Induced pluripotent stem cells generated from patients with ALS can be differentiated into motor neurons. *Science* **321,** 1218–1221 (2008).

18. Burkhardt, M. F. *et al.* A cellular model for sporadic ALS using patient-derived induced pluripotent stem cells. *Mol Cell Neurosci* **56,** 355–364 (2013).

19. Mitne-Neto, M. *et al.* Downregulation of VAPB expression in motor neurons derived from induced pluripotent stem cells of ALS8 patients. *Human Molecular Genetics* **20,** 3642–3652 (2011).

20. Bilican, B. *et al.* Mutant induced pluripotent stem cell lines recapitulate aspects of TDP-43 proteinopathies and reveal cell-specific vulnerability. *Proceedings of the National Academy of Sciences* **109,** 5803–5808 (2012).

21. Sareen, D. *et al.* Targeting RNA foci in iPSC-derived motor neurons from ALS patients with a C9ORF72 repeat expansion. *Science Translational Medicine* **5,** 208ra149 (2013).

22. Donnelly, C. J. *et al.* RNA toxicity from the ALS/FTD C9ORF72 expansion is mitigated by antisense intervention. *Neuron* **80,** 415–428 (2013).

23. Nayler, S. *et al.* Induced pluripotent stem cells from ataxia-telangiectasia recapitulate the cellular phenotype. *Stem Cells Translational Medicine* **1,** 523–535 (2012).

24. Lee, P. *et al.* SMRT compounds abrogate cellular phenotypes of ataxia telangiectasia in neural derivatives of patient-specific hiPSCs. *Nature Communications* **4,** 1824 (2013).

25. Singh, R. *et al.* iPS cell modeling of Best disease: insights into the pathophysiology of an inherited macular degeneration. *Human Molecular Genetics* **22,** 593–607 (2013).

26. Lee, G. *et al.* Modelling pathogenesis and treatment of familial dysautonomia using patient-specific iPSCs. *Nature* **461,** 402–406 (2009).

27. Ku, S. *et al.* Friedreich's ataxia induced pluripotent stem cells model intergenerational GAA · TTC triplet repeat instability. *Cell Stem Cell* **7,** 631–637 (2010).

28. Liu, J. *et al.* Generation of induced pluripotent stem cell lines from Friedreich ataxia patients. *Stem Cell Rev and Rep* **7,** 703–713 (2011).

29. Hick, A. *et al.* Neurons and cardiomyocytes derived from induced pluripotent stem cells as a model for mitochondrial defects in Friedreich's ataxia. *Dis Model Mech* **6,** 608–621 (2013).

30. Eigentler, A., Boesch, S., Schneider, R., Dechant, G. & Nat, R. Induced pluripotent stem cells from friedreich ataxia patients fail to upregulate frataxin during in vitro differentiation to peripheral sensory neurons. *Stem Cells and Development* **22,** 3271–

3282 (2013).

31. Almeida, S. *et al.* Induced pluripotent stem cell models of progranulin-deficient frontotemporal dementia uncover specific reversible neuronal defects. *CellReports* **2,** 789–798 (2012).

32. Almeida, S. *et al.* Modeling key pathological features of frontotemporal dementia with C9ORF72 repeat expansion in iPSC-derived human neurons. *Acta Neuropathol.* **126,** 385–399 (2013).

33. Tiscornia, G. *et al.* Neuronopathic Gaucher's disease: induced pluripotent stem cells for disease modelling and testing chaperone activity of small compounds. *Human Molecular Genetics* **22,** 633–645 (2013).

34. Meyer, J. S. *et al.* Optic vesicle-like structures derived from human pluripotent stem cells facilitate a customized approach to retinal disease treatment. *Stem Cells* **29,** 1206–1218 (2011).

35. Denton, K. R. *et al.* Loss of spastin function results in disease-specific axonal defects in human pluripotent stem cell-based models of hereditary spastic paraplegia. *Stem Cells* **32,** 414–423 (2014).

36. HD iPSC Consortium. Induced pluripotent stem cells from patients with Huntington's disease show CAG-repeat-expansion-associated phenotypes. *Cell Stem Cell* **11,** 264–278 (2012).

37. An, M. C. *et al.* Genetic correction of Huntington's disease phenotypes in induced pluripotent stem cells. *Cell Stem Cell* **11,** 253–263 (2012).

38. Juopperi, T. A. *et al.* Astrocytes generated from patient induced pluripotent stem cells recapitulate features of Huntington's disease patient cells. *Molecular Brain* **5,** 17 (2012).

39. Camnasio, S. *et al.* The first reported generation of several induced pluripotent stem cell lines from homozygous and heterozygous Huntington's disease patients demonstrates mutation related enhanced lysosomal activity. *Neurobiology of Disease* **46,** 41–51 (2012).

40. Lojewski, X. *et al.* Human iPSC models of neuronal ceroid lipofuscinosis capture distinct effects of TPP1 and CLN3 mutations on the endocytic pathway. *Human Molecular Genetics* (2013). doi:10.1093/hmg/ddt596

41. Trilck, M. *et al.* Niemann-Pick type C1 patient-specific induced pluripotent stem cells display disease specific hallmarks. *Orphanet J Rare Dis* **8,** 144 (2013).

42. Soldner, F. *et al.* Parkinson's disease patient-derived induced pluripotent stem cells free of viral reprogramming factors. *Cell* **136,** 964–977 (2009).

43. Nguyen, H. N. *et al.* LRRK2 mutant iPSC-derived DA neurons demonstrate increased susceptibility to oxidative stress. *Cell Stem Cell* **8,** 267–280 (2011).

44. Seibler, P. *et al.* Mitochondrial Parkin recruitment is impaired in neurons derived from mutant PINK1 induced pluripotent stem cells. *Journal of Neuroscience* **31,** 5970–5976 (2011).

45. Soldner, F. *et al.* Generation of isogenic pluripotent stem cells differing exclusively at two early onset Parkinson point mutations. *Cell* **146,** 318–331 (2011).

46. Devine, M. J. *et al.* Parkinson's disease induced pluripotent stem cells with triplication of the α-synuclein locus. *Nature Communications* **2,** 440 (2011).

47. Byers, B. *et al.* SNCA triplication Parkinson‘s patient’s iPSC-derived DA neurons accumulate α-synuclein and are susceptible to oxidative stress. *PLoS ONE* **6,** e26159 (2011).

48. Sánchez-Danés, A. *et al.* Disease-specific phenotypes in dopamine neurons from human iPS-based models of genetic and sporadic Parkinson's disease. *EMBO Mol Med* **4,** 380–395 (2012).

49. Cooper, O. *et al.* Pharmacological rescue of mitochondrial deficits in iPSC-derived neural cells from patients with familial Parkinson's disease. *Science Translational Medicine* **4,** 141ra90 (2012).

50. Imaizumi, Y. *et al.* Mitochondrial dysfunction associated with increased oxidative stress and α-synuclein accumulation in PARK2 iPSC-derived neurons and postmortem brain tissue. *Molecular Brain* **5,** 35 (2012).

51. Liu, G.-H. *et al.* Progressive degeneration of human neural stem cells caused by pathogenic LRRK2. *Nature* **491,** 603–607 (2012).

52. Reinhardt, P. *et al.* Genetic correction of a LRRK2 mutation in human iPSCs links parkinsonian neurodegeneration to ERK-dependent changes in gene expression. *Cell Stem Cell* **12,** 354–367 (2013).

53. Su, Y.-C. & Qi, X. Inhibition of excessive mitochondrial fission reduced aberrant autophagy and neuronal damage caused by LRRK2 G2019S mutation. *Human Molecular Genetics* **22,** 4545–4561 (2013).

54. Sanders, L. H. *et al.* LRRK2 mutations cause mitochondrial DNA damage in iPSC-derived neural cells from Parkinson's disease patients: Reversal by gene correction. *Neurobiology of Disease* **62C,** 381–386 (2013).

55. Miller, J. D. *et al.* Human iPSC-based modeling of late-onset disease via progerin-induced aging. *Cell Stem Cell* **13,** 691–705 (2013).

56. Jin, Z.-B. *et al.* Modeling retinal degeneration using patient-specific induced pluripotent stem cells. *PLoS ONE* **6,** e17084 (2011).

57. Tucker, B. A. *et al.* Exome sequencing and analysis of induced pluripotent stem cells identify the cilia-related gene male germ cell-associated kinase (MAK) as a cause of

retinitis pigmentosa. *Proceedings of the National Academy of Sciences* **108,** E569–76 (2011).

58. Jin, Z.-B., Okamoto, S., Xiang, P. & Takahashi, M. Integration-free induced pluripotent stem cells derived from retinitis pigmentosa patient for disease modeling. *Stem Cells Translational Medicine* **1,** 503–509 (2012).

59. Corti, S. *et al.* Genetic correction of human induced pluripotent stem cells from patients with spinal muscular atrophy. *Science Translational Medicine* **4,** 165ra162 (2012).

60. Fong, H. *et al.* Genetic correction of tauopathy phenotypes in neurons derived from human induced pluripotent stem cells. *Stem Cell Reports* **1,** 226–234 (2013).

61. Chamberlain, S. J. *et al.* Induced pluripotent stem cell models of the genomic imprinting disorders Angelman and Prader-Willi syndromes. *Proceedings of the National Academy of Sciences* **107,** 17668–17673 (2010).

62. Liu, Y. *et al.* Dravet syndrome patient-derived neurons suggest a novel epilepsy mechanism. *Ann Neurol.* **74,** 128–139 (2013).

63. Jiao, J. *et al.* Modeling Dravet syndrome using induced pluripotent stem cells (iPSCs) and directly converted neurons. *Human Molecular Genetics* **22,** 4241–4252 (2013).

64. Higurashi, N. *et al.* A human Dravet syndrome model from patient induced pluripotent stem cells. *Molecular Brain* **6,** 19 (2013).

65. Urbach, A., Bar-Nur, O., Daley, G. Q. & Benvenisty, N. Differential modeling of fragile X syndrome by human embryonic stem cells and induced pluripotent stem cells. *Cell Stem Cell* **6,** 407–411 (2010).

66. Sheridan, S. D. *et al.* Epigenetic characterization of the FMR1 gene and aberrant neurodevelopment in human induced pluripotent stem cell models of fragile X syndrome. *PLoS ONE* **6,** e26203 (2011).

67. Liu, J. *et al.* Signaling defects in iPSC-derived fragile X premutation neurons. *Human Molecular Genetics* **21,** 3795–3805 (2012).

68. Mekhoubad, S. *et al.* Erosion of dosage compensation impacts human iPSC disease modeling. *Cell Stem Cell* **10,** 595–609 (2012).

69. Shcheglovitov, A. *et al.* SHANK3 and IGF1 restore synaptic deficits in neurons from 22q13 deletion syndrome patients. *Nature* **503,** 267–271 (2013).

70. Lancaster, M. A. *et al.* Cerebral organoids model human brain development and microcephaly. *Nature* **501,** 373–379 (2013).

71. Hotta, A. *et al.* Isolation of human iPS cells using EOS lentiviral vectors to select for pluripotency. *Nat Meth* **6,** 370–376 (2009).

72. Marchetto, M. C. N. *et al.* A model for neural development and treatment of Rett syndrome using human induced pluripotent stem cells. *Cell* **143,** 527–539 (2010).

73. Cheung, A. Y. L. *et al.* Isolation of MECP2-null Rett Syndrome patient hiPS cells and isogenic controls through X-chromosome inactivation. *Human Molecular Genetics* **20,** 2103–2115 (2011).

74. Amenduni, M. *et al.* iPS cells to model CDKL5-related disorders. *Eur J Hum Genet* **19,** 1246–1255 (2011).

75. Kim, K.-Y., Hysolli, E. & Park, I.-H. Neuronal maturation defect in induced pluripotent stem cells from patients with Rett syndrome. *Proceedings of the National Academy of Sciences* **108,** 14169–14174 (2011).

76. Ananiev, G., Williams, E. C., Li, H. & Chang, Q. Isogenic pairs of wild type and mutant induced pluripotent stem cell (iPSC) lines from Rett syndrome patients as in vitro disease model. *PLoS ONE* **6,** e25255 (2011).

77. Chiang, C.-H. *et al.* Integration-free induced pluripotent stem cells derived from schizophrenia patients with a DISC1 mutation. *Mol Psychiatry* **16,** 358–360 (2011).

78. Wen, Z. *et al.* Synaptic dysregulation in a human iPS cell model of mental disorders. *Nature* 1–15 (2014). doi:10.1038/nature13716

79. Brennand, K. J. *et al.* Modelling schizophrenia using human induced pluripotent stem cells. *Nature* **473,** 221–225 (2011).

80. Pedrosa, E. *et al.* Development of patient-specific neurons in schizophrenia using induced pluripotent stem cells. *J. Neurogenet.* **25,** 88–103 (2011).

81. Vitale, A. M. *et al.* Variability in the generation of induced pluripotent stem cells: importance for disease modeling. *Stem Cells Translational Medicine* **1,** 641–650 (2012).

82. Paulsen, B. D. S. *et al.* Altered oxygen metabolism associated to neurogenesis of induced pluripotent stem cells derived from a schizophrenic patient. *ct* **21,** 1547–1559 (2012).

83. Robicsek, O. *et al.* Abnormal neuronal differentiation and mitochondrial dysfunction in hair follicle-derived induced pluripotent stem cells of schizophrenia patients. *Mol Psychiatry* **18,** 1067–1076 (2013).

84. Yoon, K.-J. *et al.* Modeling a Genetic Risk for Schizophreniain iPSCs and Mice Reveals Neural Stem Cell Deficits Associated with Adherens Junctions and Polarity. *Stem Cell* **15,** 79–91 (2014).

85. Paşca, S. P. *et al.* Using iPSC-derived neurons to uncover cellular phenotypes associated with Timothy syndrome. *Nature Medicine* **17,** 1657–1662 (2011).

86. Carlson, D. F., Fahrenkrug, S. C. & Hackett, P. B. Targeting DNA With Fingers and

TALENs. *Mol Ther Nucleic Acids* **1,** e3 (2012).

87. Miller, J. C. *et al.* An improved zinc-finger nuclease architecture for highly specific genome editing. *Nat Biotechnol* **25,** 778–785 (2007).

88. Doyon, Y. *et al.* Enhancing zinc-finger-nuclease activity with improved obligate heterodimeric architectures. *Nat Meth* **8,** 74–79 (2011).

89. Hockemeyer, D. *et al.* Genetic engineering of human pluripotent cells using TALE nucleases. *Nat Biotechnol* **29,** 731–734 (2011).

90. Huang, P. *et al.* Heritable gene targeting in zebrafish using customized TALENs. *Nat Biotechnol* **29,** 699–700 (2011).

91. Tesson, L. *et al.* Knockout rats generated by embryo microinjection of TALENs. *Nat Biotechnol* **29,** 695–696 (2011).

92. Wood, A. J. *et al.* Targeted genome editing across species using ZFNs and TALENs. *Science* **333,** 307 (2011).

93. Szczepek, M. *et al.* Structure-based redesign of the dimerization interface reduces the toxicity of zinc-finger nucleases. *Nat Biotechnol* **25,** 786–793 (2007).

94. Guo, J., Gaj, T. & Barbas, C. F. Directed evolution of an enhanced and highly efficient FokI cleavage domain for zinc finger nucleases. *J. Mol. Biol.* **400,** 96–107 (2010).

95. Ramirez, C. L. *et al.* Engineered zinc finger nickases induce homology-directed repair with reduced mutagenic effects. *Nucleic Acids Res* **40,** 5560–5568 (2012).

96. Kim, E. *et al.* Precision genome engineering with programmable DNA-nicking enzymes. *Genome Research* **22,** 1327–1333 (2012).

97. Wang, J. *et al.* Targeted gene addition to a predetermined site in the human genome using a ZFN-based nicking enzyme. *Genome Research* **22,** 1316–1326 (2012).

98. Ding, Q. *et al.* A TALEN genome-editing system for generating human stem cell-based disease models. *Cell Stem Cell* **12,** 238–251 (2013).

99. Ding, Q. *et al.* Enhanced efficiency of human pluripotent stem cell genome editing through replacing TALENs with CRISPRs. *Cell Stem Cell* **12,** 393–394 (2013).

100. Fu, Y. *et al.* High-frequency off-target mutagenesis induced by CrIsPr-Cas nucleases in human cells. *Nat Biotechnol* **31,** 822–826 (2013).

101. Hsu, P. D. *et al.* DNA targeting specificity of RNA-guided Cas9 nucleases. *Nat Biotechnol* **31,** 827–832 (2013).

102. Mali, P. *et al.* CAS9 transcriptional activators for target specificity screening and paired nickases for cooperative genome engineering. *Nat Biotechnol* **31,** 833–838 (2013).

103. Pattanayak, V. *et al.* High-throughput profiling of off-target DNA cleavage reveals RNA-programmed Cas9 nuclease specificity. *Nat Biotechnol* **31,** 839–843 (2013).

104. Cong, L. *et al.* Multiplex genome engineering using CRISPR/Cas systems. *Science* **339,** 819–823 (2013).

105. Mali, P. *et al.* RNA-guided human genome engineering via Cas9. *Science* **339,** 823–826 (2013).

106. Ran, F. A. *et al.* Double nicking by RNA-guided CRISPR Cas9 for enhanced genome editing specificity. *Cell* **154,** 1380–1389 (2013).

107. Smith, C. *et al.* Whole-genome sequencing analysis reveals high specificity of CRISPR/Cas9 and TALEN-based genome editing in human iPSCs. *Cell Stem Cell* **15,** 12–13 (2014).

108. Veres, A. *et al.* Low incidence of off-target mutations in individual CRISPR-Cas9 and TALEN targeted human stem cell clones detected by whole-genome sequencing. *Cell Stem Cell* **15,** 27–30 (2014).

109. Urnov, F. D., Rebar, E. J., Holmes, M. C., Zhang, H. S. & Gregory, P. D. Genome editing with engineered zinc finger nucleases. *Nat Rev Genet* **11,** 636–646 (2010).

110. Gaj, T., Gersbach, C. A. & Barbas, C. F. ZFN, TALEN, and CRISPR/Cas-based methods for genome engineering. *Trends in Biotechnology* **31,** 397–405 (2013).

111. Marchetto, M. C. N. *et al.* Transcriptional signature and memory retention of human-induced pluripotent stem cells. *PLoS ONE* **4,** e7076 (2009).

112. Kim, K. *et al.* Epigenetic memory in induced pluripotent stem cells. *Nature* **467,** 285–290 (2010).

113. Bock, C. *et al.* Reference Maps of human ES and iPS cell variation enable high-throughput characterization of pluripotent cell lines. *Cell* **144,** 439–452 (2011).

114. Farra, N. *et al.* Rett syndrome induced pluripotent stem cell-derived neurons reveal novel neurophysiological alterations. *Mol Psychiatry* **17,** 1261–1271 (2012).

115. Larimore, J. *et al.* MeCP2 regulates the synaptic expression of a Dysbindin-BLOC-1 network component in mouse brain and human induced pluripotent stem cell-derived neurons. *PLoS ONE* **8,** e65069 (2013).

116. Lin, M. *et al.* Allele-biased expression in differentiating human neurons: implications for neuropsychiatric disorders. *PLoS ONE* **7,** e44017 (2012).

117. Di Giorgio, F. P., Boulting, G. L., Bobrowicz, S. & Eggan, K. C. Human embryonic stem cell-derived motor neurons are sensitive to the toxic effect of glial cells carrying an ALS-causing mutation. *Cell Stem Cell* **3,** 637–648 (2008).

118. Shi, Y., Kirwan, P., Smith, J., Robinson, H. P. C. & Livesey, F. J. Human cerebral cortex development from pluripotent stem cells to functional excitatory synapses. *Nat Neurosci*

15, 477–486 (2012).

119. Takazawa, T. *et al.* Maturation of spinal motor neurons derived from human embryonic stem cells. *PLoS ONE* **7,** e40154 (2012).

120. Espuny-Camacho, I. *et al.* Pyramidal neurons derived from human pluripotent stem cells integrate efficiently into mouse brain circuits in vivo. *Neuron* **77,** 440–456 (2013).

121. Di Giorgio, F. P., Carrasco, M. A., Siao, M. C., Maniatis, T. & Eggan, K. Non-cell autonomous effect of glia on motor neurons in an embryonic stem cell-based ALS model. *Nat Neurosci* **10,** 608–614 (2007).

122. Marchetto, M. C. N. *et al.* Non-cell-autonomous effect of human SOD1 G37R astrocytes on motor neurons derived from human embryonic stem cells. *Cell Stem Cell* **3,** 649–657 (2008).

123. Osafune, K. *et al.* Marked differences in differentiation propensity among human embryonic stem cell lines. *Nat Biotechnol* **26,** 313–315 (2008).

124. Meyer, J. S. *et al.* Modeling early retinal development with human embryonic and induced pluripotent stem cells. *Proceedings of the National Academy of Sciences* **106,** 16698–16703 (2009).

125. Hu, B.-Y. *et al.* Neural differentiation of human induced pluripotent stem cells follows developmental principles but with variable potency. *Proceedings of the National Academy of Sciences* **107,** 4335–4340 (2010).

126. Boulting, G. L. *et al.* A functionally characterized test set of human induced pluripotent stem cells. *Nat Biotechnol* **29,** 279–286 (2011).

127. Koyanagi-Aoi, M. *et al.* Differentiation-defective phenotypes revealed by large-scale analyses of human pluripotent stem cells. *Proceedings of the National Academy of Sciences* **110,** 20569–20574 (2013).

128. Zhang, S. C., Wernig, M., Duncan, I. D., Brüstle, O. & Thomson, J. A. In vitro differentiation of transplantable neural precursors from human embryonic stem cells. *Nat Biotechnol* **19,** 1129–1133 (2001).

129. Pankratz, M. T. *et al.* Directed neural differentiation of human embryonic stem cells via an obligated primitive anterior stage. *Stem Cells* **25,** 1511–1520 (2007).

130. Sonntag, K.-C. *et al.* Enhanced yield of neuroepithelial precursors and midbrain-like dopaminergic neurons from human embryonic stem cells using the bone morphogenic protein antagonist noggin. *Stem Cells* **25,** 411–418 (2007).

131. Eiraku, M. *et al.* Self-organized formation of polarized cortical tissues from ESCs and its active manipulation by extrinsic signals. *Cell Stem Cell* **3,** 519–532 (2008).

132. Elkabetz, Y. *et al.* Human ES cell-derived neural rosettes reveal a functionally distinct

early neural stem cell stage. *Genes & Development* **22,** 152–165 (2008).

133. Erceg, S. *et al.* Differentiation of human embryonic stem cells to regional specific neural precursors in chemically defined medium conditions. *PLoS ONE* **3,** e2122 (2008).

134. Wernig, M. *et al.* Neurons derived from reprogrammed fibroblasts functionally integrate into the fetal brain and improve symptoms of rats with Parkinson's disease. *Proceedings of the National Academy of Sciences* **105,** 5856–5861 (2008).

135. Chambers, S. M. *et al.* Highly efficient neural conversion of human ES and iPS cells by dual inhibition of SMAD signaling. *Nat Biotechnol* **27,** 275–280 (2009).

136. Li, X.-J. *et al.* Coordination of sonic hedgehog and Wnt signaling determines ventral and dorsal telencephalic neuron types from human embryonic stem cells. *Development* **136,** 4055–4063 (2009).

137. Wada, T. *et al.* Highly efficient differentiation and enrichment of spinal motor neurons derived from human and monkey embryonic stem cells. *PLoS ONE* **4,** e6722 (2009).

138. Zhang, X.-Q. & Zhang, S.-C. in *Methods in Molecular Biology* **584,** 355–366 (Humana Press, 2009).

139. Zeng, H. *et al.* Specification of region-specific neurons including forebrain glutamatergic neurons from human induced pluripotent stem cells. *PLoS ONE* **5,** e11853 (2010).

140. Gupta, K. *et al.* Human embryonic stem cell derived astrocytes mediate non-cell-autonomous neuroprotection through endogenous and drug-induced mechanisms. *Cell Death Differ.* **19,** 779–787 (2012).

141. Yuan, S. H. *et al.* Cell-surface marker signatures for the isolation of neural stem cells, glia and neurons derived from human pluripotent stem cells. *PLoS ONE* **6,** e17540 (2011).

142. Emdad, L., D'Souza, S. L., Kothari, H. P., Qadeer, Z. A. & Germano, I. M. Efficient differentiation of human embryonic and induced pluripotent stem cells into functional astrocytes. *Stem Cells and Development* **21,** 404–410 (2012).

143. Kirkeby, A. *et al.* Generation of regionally specified neural progenitors and functional neurons from human embryonic stem cells under defined conditions. *CellReports* **1,** 703–714 (2012).

144. Mariani, J. *et al.* Modeling human cortical development in vitro using induced pluripotent stem cells. *Proceedings of the National Academy of Sciences* **109,** 12770–12775 (2012).

145. Lancaster, M. A. & Knoblich, J. A. Generation of cerebral organoids from human pluripotent stem cells. *Nat Protoc* **9,** 2329–2340 (2014).

146. Li, X.-J. *et al.* Specification of motoneurons from human embryonic stem cells. *Nat*

Biotechnol **23,** 215–221 (2005).

147. Singh Roy, N. *et al.* Enhancer-specified GFP-based FACS purification of human spinal motor neurons from embryonic stem cells. *Experimental Neurology* **196,** 224–234 (2005).

148. Lee, H. *et al.* Directed differentiation and transplantation of human embryonic stem cell-derived motoneurons. *Stem Cells* **25,** 1931–1939 (2007).

149. Li, X.-J. *et al.* Directed differentiation of ventral spinal progenitors and motor neurons from human embryonic stem cells by small molecules. *Stem Cells* **26,** 886–893 (2008).

150. Hu, B.-Y. & Zhang, S.-C. Differentiation of spinal motor neurons from pluripotent human stem cells. *Nat Protoc* **4,** 1295–1304 (2009).

151. Nizzardo, M. *et al.* Human motor neuron generation from embryonic stem cells and induced pluripotent stem cells. *Cell. Mol. Life Sci.* **67,** 3837–3847 (2010).

152. Hester, M. E. *et al.* Rapid and efficient generation of functional motor neurons from human pluripotent stem cells using gene delivered transcription factor codes. *Molecular Therapy* **19,** 1905–1912 (2011).

153. Perrier, A. L. *et al.* Derivation of midbrain dopamine neurons from human embryonic stem cells. *Proc Natl Acad Sci USA* **101,** 12543–12548 (2004).

154. Park, C.-H. *et al.* In vitro and in vivo analyses of human embryonic stem cell-derived dopamine neurons. *J Neurochem* **92,** 1265–1276 (2005).

155. Yan, Y. *et al.* Directed differentiation of dopaminergic neuronal subtypes from human embryonic stem cells. *Stem Cells* **23,** 781–790 (2005).

156. Roy, N. S. *et al.* Functional engraftment of human ES cell-derived dopaminergic neurons enriched by coculture with telomerase-immortalized midbrain astrocytes. *Nature Medicine* **12,** 1259–1268 (2006).

157. Iacovitti, L., Donaldson, A. E., Marshall, C. E., Suon, S. & Yang, M. A protocol for the differentiation of human embryonic stem cells into dopaminergic neurons using only chemically defined human additives: Studies in vitro and in vivo. *Brain Res* **1127,** 19–25 (2007).

158. Ko, J.-Y. *et al.* Human embryonic stem cell-derived neural precursors as a continuous, stable, and on-demand source for human dopamine neurons. *J Neurochem* **103,** 1417–1429 (2007).

159. Cho, M.-S., Hwang, D.-Y. & Kim, D. W. Efficient derivation of functional dopaminergic neurons from human embryonic stem cells on a large scale. *Nat Protoc* **3,** 1888–1894 (2008).

160. Cho, M.-S. *et al.* Highly efficient and large-scale generation of functional dopamine

neurons from human embryonic stem cells. *Proceedings of the National Academy of Sciences* **105,** 3392–3397 (2008).

161. Karumbayaram, S. *et al.* Directed differentiation of human-induced pluripotent stem cells generates active motor neurons. *Stem Cells* **27,** 806–811 (2009).

162. Cooper, O. *et al.* Differentiation of human ES and Parkinson's disease iPS cells into ventral midbrain dopaminergic neurons requires a high activity form of SHH, FGF8a and specific regionalization by retinoic acid. *Mol Cell Neurosci* **45,** 258–266 (2010).

163. Swistowski, A. *et al.* Efficient generation of functional dopaminergic neurons from human induced pluripotent stem cells under defined conditions. *Stem Cells* **28,** 1893–1904 (2010).

164. Kriks, S. *et al.* Dopamine neurons derived from human ES cells efficiently engraft in animal models of Parkinson's disease. *Nature* **480,** 547–551 (2011).

165. Morizane, A., Doi, D. & Takahashi, J. Neural induction with a dopaminergic phenotype from human pluripotent stem cells through a feeder-free floating aggregation culture. *Methods Mol. Biol.* **1018,** 11–19 (2013).

166. Goulburn, A. L. *et al.* A targeted NKX2.1 human embryonic stem cell reporter line enables identification of human basal forebrain derivatives. *Stem Cells* **29,** 462–473 (2011).

167. Goulburn, A. L., Stanley, E. G., Elefanty, A. G. & Anderson, S. A. Generating GABAergic cerebral cortical interneurons from mouse and human embryonic stem cells. *Stem Cell Research* **8,** 416–426 (2012).

168. Liu, Y. *et al.* Directed differentiation of forebrain GABA interneurons from human pluripotent stem cells. *Nat Protoc* **8,** 1670–1679 (2013).

169. Maroof, A. M. *et al.* Directed differentiation and functional maturation of cortical interneurons from human embryonic stem cells. *Cell Stem Cell* **12,** 559–572 (2013).

170. Nicholas, C. R. *et al.* Functional maturation of hPSC-derived forebrain interneurons requires an extended timeline and mimics human neural development. *Cell Stem Cell* **12,** 573–586 (2013).

171. Aubry, L. *et al.* Striatal progenitors derived from human ES cells mature into DARPP32 neurons in vitro and in quinolinic acid-lesioned rats. *Proceedings of the National Academy of Sciences* **105,** 16707–16712 (2008).

172. Ma, L. *et al.* Human embryonic stem cell-derived GABA neurons correct locomotion deficits in quinolinic acid-lesioned mice. *Cell Stem Cell* **10,** 455–464 (2012).

173. Carri, A. D. *et al.* Developmentally coordinated extrinsic signals drive human pluripotent stem cell differentiation toward authentic DARPP-32+ medium-sized spiny neurons. *Development* **140,** 301–312 (2013).

174. Delli Carri, A. *et al.* Human pluripotent stem cell differentiation into authentic striatal projection neurons. *Stem Cell Rev and Rep* **9,** 461–474 (2013).

175. Nilbratt, M., Porras, O., Marutle, A., Hovatta, O. & Nordberg, A. Neurotrophic factors promote cholinergic differentiation in human embryonic stem cell-derived neurons. *J. Cell. Mol. Med.* **14,** 1476–1484 (2010).

176. Wicklund, L. *et al.* B-amyloid 1-42 oligomers impair function of human embryonic stem cell-derived forebrain cholinergic neurons. *PLoS ONE* **5,** e15600 (2010).

177. Bissonnette, C. J. *et al.* The controlled generation of functional basal forebrain cholinergic neurons from human embryonic stem cells. *Stem Cells* **29,** 802–811 (2011).

178. Yu, D. X. *et al.* Modeling hippocampal neurogenesis using human pluripotent stem cells. *Stem Cell Reports* **2,** 295–310 (2014).

179. Wang, L. *et al.* Differentiation of hypothalamic-like neurons from human pluripotent stem cells. *J. Clin. Invest.* **125,** 796–808 (2015).

180. Merkle, F. T. *et al.* Generation of neuropeptidergic hypothalamic neurons from human pluripotent stem cells. *Development* **142,** 633–643 (2015).

181. Erceg, S., Lukovic, D., Moreno-Manzano, V., Stojkovic, M. & Bhattacharya, S. S. *Derivation of Cerebellar Neurons from Human Pluripotent Stem Cells*. (John Wiley & Sons, Inc., 2007). doi:10.1002/9780470151808.sc01h05s20

182. Erceg, S. *et al.* Efficient differentiation of human embryonic stem cells into functional cerebellar-like cells. *Stem Cells and Development* **19,** 1745–1756 (2010).

183. Lee, D. S. *et al.* Cyclopamine treatment of human embryonic stem cells followed by culture in human astrocyte medium promotes differentiation into nestin- and GFAP-expressing astrocytic lineage. *Life Sci.* **80,** 154–159 (2006).

184. Czepiel, M. *et al.* Differentiation of induced pluripotent stem cells into functional oligodendrocytes. *Glia* **59,** 882–892 (2011).

185. Wang, S. *et al.* Human iPSC-derived oligodendrocyte progenitor cells can myelinate and rescue a mouse model of congenital hypomyelination. *Cell Stem Cell* **12,** 252–264 (2013).

186. Nistor, G. I., Totoiu, M. O., Haque, N., Carpenter, M. K. & Keirstead, H. S. Human embryonic stem cells differentiate into oligodendrocytes in high purity and myelinate after spinal cord transplantation. *Glia* **49,** 385–396 (2005).

187. Kang, S.-M. *et al.* Efficient induction of oligodendrocytes from human embryonic stem cells. *Stem Cells* **25,** 419–424 (2007).

188. Krencik, R., Weick, J. P., Liu, Y., Zhang, Z.-J. & Zhang, S.-C. Specification of transplantable astroglial subtypes from human pluripotent stem cells. *Nat Biotechnol* **29,**

528–534 (2011).

189. Ogawa, S.-I., Tokumoto, Y., Miyake, J. & Nagamune, T. Induction of oligodendrocyte differentiation from adult human fibroblast-derived induced pluripotent stem cells. *In Vitro Cell. Dev. Biol. Anim.* **47,** 464–469 (2011).

190. Pomp, O., Brokhman, I., Ben-Dor, I., Reubinoff, B. & Goldstein, R. S. Generation of peripheral sensory and sympathetic neurons and neural crest cells from human embryonic stem cells. *Stem Cells* **23,** 923–930 (2005).

191. Lee, G. *et al.* Isolation and directed differentiation of neural crest stem cells derived from human embryonic stem cells. *Nat Biotechnol* **25,** 1468–1475 (2007).

192. Lee, G., Chambers, S. M., Tomishima, M. J. & Studer, L. Derivation of neural crest cells from human pluripotent stem cells. *Nat Protoc* **5,** 688–701 (2010).

193. Ziegler, L., Grigoryan, S., Yang, I. H., Thakor, N. V. & Goldstein, R. S. Efficient generation of schwann cells from human embryonic stem cell-derived neurospheres. *Stem Cell Rev and Rep* **7,** 394–403 (2011).

194. Menendez, L., Yatskievych, T. A., Antin, P. B. & Dalton, S. Wnt signaling and a Smad pathway blockade direct the differentiation of human pluripotent stem cells to multipotent neural crest cells. *Proceedings of the National Academy of Sciences* **108,** 19240–19245 (2011).

195. Chambers, S. M. *et al.* Combined small-molecule inhibition accelerates developmental timing and converts human pluripotent stem cells into nociceptors. *Nat Biotechnol* **30,** 715–720 (2012).

196. Lee, K. S. *et al.* Human sensory neurons derived from induced pluripotent stem cells support varicella-zoster virus infection. *PLoS ONE* **7,** e53010 (2012).

197. Liu, Q. *et al.* Human neural crest stem cells derived from human ESCs and induced pluripotent stem cells: induction, maintenance, and differentiation into functional schwann cells. *Stem Cells Translational Medicine* **1,** 266–278 (2012).

198. Chambers, S. M., Mica, Y., Lee, G., Studer, L. & Tomishima, M. J. Dual-SMAD Inhibition/WNT Activation-Based Methods to Induce Neural Crest and Derivatives from Human Pluripotent Stem Cells. *Methods Mol. Biol.* (2013). doi:10.1007/7651_2013_59

199. Menendez, L. *et al.* Directed differentiation of human pluripotent cells to neural crest stem cells. *Nat Protoc* **8,** 203–212 (2013).

200. Mica, Y., Lee, G., Chambers, S. M., Tomishima, M. J. & Studer, L. Modeling neural crest induction, melanocyte specification, and disease-related pigmentation defects in hESCs and patient-specific iPSCs. *CellReports* **3,** 1140–1152 (2013).

201. Dincer, Z. *et al.* Specification of functional cranial placode derivatives from human pluripotent stem cells. *CellReports* **5,** 1387–1402 (2013).

202. Lamba, D. A., Karl, M. O., Ware, C. B. & Reh, T. A. Efficient generation of retinal progenitor cells from human embryonic stem cells. *Proc Natl Acad Sci USA* **103,** 12769–12774 (2006).

203. Osakada, F. *et al.* Toward the generation of rod and cone photoreceptors from mouse, monkey and human embryonic stem cells. *Nat Biotechnol* **26,** 215–224 (2008).

204. Buchholz, D. E. *et al.* Derivation of functional retinal pigmented epithelium from induced pluripotent stem cells. *Stem Cells* **27,** 2427–2434 (2009).

205. Hirami, Y. *et al.* Generation of retinal cells from mouse and human induced pluripotent stem cells. *Neurosci Lett* **458,** 126–131 (2009).

206. Osakada, F. *et al.* In vitro differentiation of retinal cells from human pluripotent stem cells by small-molecule induction. *J Cell Sci* **122,** 3169–3179 (2009).

207. Osakada, F., Ikeda, H., Sasai, Y. & Takahashi, M. Stepwise differentiation of pluripotent stem cells into retinal cells. *Nat Protoc* **4,** 811–824 (2009).

208. Kokkinaki, M., Sahibzada, N. & Golestaneh, N. Human induced pluripotent stem-derived retinal pigment epithelium (RPE) cells exhibit ion transport, membrane potential, polarized vascular endothelial growth factor secretion, and gene expression pattern similar to native RPE. *Stem Cells* **29,** 825–835 (2011).

209. Nakano, T. *et al.* Self-formation of optic cups and storable stratified neural retina from human ESCs. *Cell Stem Cell* **10,** 771–785 (2012).

210. Phillips, M. J. *et al.* Blood-derived human iPS cells generate optic vesicle-like structures with the capacity to form retinal laminae and develop synapses. *Investigative Ophthalmology & Visual Science* **53,** 2007–2019 (2012).

211. Ring, K. L. *et al.* Direct reprogramming of mouse and human fibroblasts into multipotent neural stem cells with a single factor. *Cell Stem Cell* **11,** 100–109 (2012).

212. Zou, Q. *et al.* Direct conversion of human fibroblasts into neuronal restricted progenitors. *Journal of Biological Chemistry* **289,** 5250–5260 (2014).

213. Pang, Z. P. *et al.* Induction of human neuronal cells by defined transcription factors. *Nature* **476,** 220–223 (2011).

214. Ladewig, J. *et al.* Small molecules enable highly efficient neuronal conversion of human fibroblasts. *Nat Meth* **9,** 575–578 (2012).

215. Xue, Y. *et al.* Direct conversion of fibroblasts to neurons by reprogramming PTB-regulated microRNA circuits. *Cell* **152,** 82–96 (2013).

216. Torper, O. *et al.* Generation of induced neurons via direct conversion in vivo. *Proceedings of the National Academy of Sciences* **110,** 7038–7043 (2013).

217. Pfisterer, U. *et al.* Efficient induction of functional neurons from adult human fibroblasts. *Cell Cycle* **10,** 3311–3316 (2011).

218. Yoo, A. S. *et al.* MicroRNA-mediated conversion of human fibroblasts to neurons. *Nature* **476,** 228–231 (2011).

219. Lau, S., Rylander Ottosson, D., Jakobsson, J. & Parmar, M. Direct neural conversion from human fibroblasts using self-regulating and nonintegrating viral vectors. *CellReports* **9,** 1673–1680 (2014).

220. Chanda, S. *et al.* Generation of induced neuronal cells by the single reprogramming factor ASCL1. *Stem Cell Reports* **3,** 282–296 (2014).

221. Ambasudhan, R. *et al.* Direct reprogramming of adult human fibroblasts to functional neurons under defined conditions. *Cell Stem Cell* **9,** 113–118 (2011).

222. Heinrich, C. *et al.* Directing astroglia from the cerebral cortex into subtype specific functional neurons. *PLoS Biol.* **8,** e1000373 (2010).

223. Yang, Y. *et al.* Direct conversion of adipocyte progenitors into functional neurons. *Cell Reprogram* **15,** 484–489 (2013).

224. Karow, M. *et al.* Reprogramming of pericyte-derived cells of the adult human brain into induced neuronal cells. *Cell Stem Cell* **11,** 471–476 (2012).

225. Sánchez-Danés, A. *et al.* Efficient generation of A9 midbrain dopaminergic neurons by lentiviral delivery of LMX1A in human embryonic stem cells and induced pluripotent stem cells. *Hum. Gene Ther.* **23,** 56–69 (2012).

226. Theka, I. *et al.* Rapid generation of functional dopaminergic neurons from human induced pluripotent stem cells through a single-step procedure using cell lineage transcription factors. *Stem Cells Translational Medicine* **2,** 473–479 (2013).

227. Pfisterer, U. *et al.* Direct conversion of human fibroblasts to dopaminergic neurons. *Proceedings of the National Academy of Sciences* **108,** 10343–10348 (2011).

228. Caiazzo, M. *et al.* Direct generation of functional dopaminergic neurons from mouse and human fibroblasts. *Nature* **476,** 224–227 (2011).

229. Son, E. Y. *et al.* Conversion of mouse and human fibroblasts into functional spinal motor neurons. *Cell Stem Cell* **9,** 205–218 (2011).

230. Victor, M. B. *et al.* Generation of human striatal neurons by microRNA-dependent direct conversion of fibroblasts. *Neuron* **84,** 311–323 (2014).

231. Blanchard, J. W. *et al.* Selective conversion of fibroblasts into peripheral sensory neurons. *Nat Neurosci* **18,** 25–35 (2015).

232. Liu, M.-L. *et al.* Small molecules enable neurogenin 2 to efficiently convert human

fibroblasts into cholinergic neurons. *Nature Communications* **4,** 2183 (2013).

233. Kumar, M., Kaushalya, S. K., Gressens, P., Maiti, S. & Mani, S. Optimized derivation and functional characterization of 5-HT neurons from human embryonic stem cells. *Stem Cells and Development* **18,** 615–627 (2009).

234. Caiazzo, M. *et al.* Direct conversion of fibroblasts into functional astrocytes by defined transcription factors. *Stem Cell Reports* **4,** 25–36 (2015).

235. Maire, C. L. *et al.* Directing human neural stem/precursor cells into oligodendrocytes by overexpression of Olig2 transcription factor. *J. Neurosci. Res.* **87,** 3438–3446 (2009).

236. Kondo, T., Johnson, S. A., Yoder, M. C., Romand, R. & Hashino, E. Sonic hedgehog and retinoic acid synergistically promote sensory fate specification from bone marrow-derived pluripotent stem cells. *Proc Natl Acad Sci USA* **102,** 4789–4794 (2005).

237. Chetty, S. *et al.* A simple tool to improve pluripotent stem cell differentiation. *Nat Meth* **10,** 553–556 (2013).

238. Jeon, I. *et al.* Neuronal properties, in vivo effects, and pathology of a Huntington's disease patient-derived induced pluripotent stem cells. *Stem Cells* **30,** 2054–2062 (2012).

239. Li, W. *et al.* Rapid induction and long-term self-renewal of primitive neural precursors from human embryonic stem cells by small molecule inhibitors. *Proc Natl Acad Sci USA* **108,** 8299–8304 (2011).

240. Morgan, P. J. *et al.* Human neural progenitor cells show functional neuronal differentiation and regional preference after engraftment onto hippocampal slice cultures. *Stem Cells and Development* **21,** 1501–1512 (2012).

241. Tønnesen, J. *et al.* Functional integration of grafted neural stem cell-derived dopaminergic neurons monitored by optogenetics in an in vitro Parkinson model. *PLoS ONE* **6,** e17560 (2011).

242. Kumamaru, H. *et al.* Direct isolation and RNA-seq reveal environment-dependent properties of engrafted neural stem/progenitor cells. *Nature Communications* **3,** 1140 (2012).

243. Watanabe, K. *et al.* Directed differentiation of telencephalic precursors from embryonic stem cells. *Nat Neurosci* **8,** 288–296 (2005).

244. Krencik, R. & Zhang, S.-C. Stem cell neural differentiation: A model for chemical biology. *Curr Opin Chem Biol* **10,** 592–597 (2006).

245. Dhara, S. K. & Stice, S. L. Neural differentiation of human embryonic stem cells. *J. Cell. Biochem.* **105,** 633–640 (2008).

246. Gaspard, N. *et al.* An intrinsic mechanism of corticogenesis from embryonic stem cells.

Nature **455,** 351–357 (2008).

247. Liu, H. & Zhang, S.-C. Specification of neuronal and glial subtypes from human pluripotent stem cells. *Cell. Mol. Life Sci.* **68,** 3995–4008 (2011).

248. Erraji-Benchekroun, L. *et al.* Molecular aging in human prefrontal cortex is selective and continuous throughout adult life. *Biol Psychiatry* **57,** 549–558 (2005).

249. Jaaro-Peled, H. Gene models of schizophrenia: DISC1 mouse models. *Prog Brain Res* **179,** 75–86 (2009).

250. Tau, G. Z. & Peterson, B. S. Normal development of brain circuits. *Neuropsychopharmacology* **35,** 147–168 (2010).

251. Pescosolido, M. F., Yang, U., Sabbagh, M. & Morrow, E. M. Lighting a path: genetic studies pinpoint neurodevelopmental mechanisms in autism and related disorders. *Dialogues Clin Neurosci* **14,** 239–252 (2012).

252. Jacquemont, S., Hagerman, R. J., Hagerman, P. J. & Leehey, M. A. Fragile-X syndrome and fragile X-associated tremor/ataxia syndrome: two faces of FMR1. *Lancet Neurol* **6,** 45–55 (2007).

253. Chahrour, M. & Zoghbi, H. Y. The story of Rett syndrome: from clinic to neurobiology. *Neuron* **56,** 422–437 (2007).

254. Amir, R. E. *et al.* Rett syndrome is caused by mutations in X-linked MECP2, encoding methyl-CpG-binding protein 2. *Nat Genet* **23,** 185–188 (1999).

255. Stilo, S. A. & Murray, R. M. The epidemiology of schizophrenia: replacing dogma with knowledge. *Dialogues Clin Neurosci* **12,** 305–315 (2010).

256. Walker, F. O. Huntington's disease. *Lancet* **369,** 218–228 (2007).

257. Myers, R. H. Huntington's disease genetics. *NeuroRx* **1,** 255–262 (2004).

258. Chiò, A. *et al.* Global epidemiology of amyotrophic lateral sclerosis: a systematic review of the published literature. *Neuroepidemiology* **41,** 118–130 (2013).

259. Huisman, M. H. B. *et al.* Population based epidemiology of amyotrophic lateral sclerosis using capture-recapture methodology. *J. Neurol. Neurosurg. Psychiatr.* **82,** 1165–1170 (2011).

260. de Lau, L. M. L. & Breteler, M. M. B. Epidemiology of Parkinson's disease. *Lancet Neurol* **5,** 525–535 (2006).

261. Thies, W., Bleiler, L.Alzheimer's Association. 2013 Alzheimer's disease facts and figures. *Alzheimers Dement* **9,** 208–245 (2013).

262. Lewis, D. A. & Levitt, P. Schizophrenia as a disorder of neurodevelopment. *Annu Rev Neurosci* **25,** 409–432 (2002).

263. Brandon, N. J. & Sawa, A. Linking neurodevelopmental and synaptic theories of mental illness through DISC1. *Nat Rev Neurosci* **12,** 707–722 (2011).

264. Mitchell, K. J. The genetics of neurodevelopmental disease. *Curr Opin Neurobiol* **21,** 197–203 (2011).

265. Tabar, V. *et al.* Migration and differentiation of neural precursors derived from human embryonic stem cells in the rat brain. *Nat Biotechnol* **23,** 601–606 (2005).

266. Liu, G.-H. *et al.* Recapitulation of premature ageing with iPSCs from Hutchinson-Gilford progeria syndrome. *Nature* **472,** 221–225 (2011).

267. Zhang, J. *et al.* A human iPSC model of Hutchinson Gilford Progeria reveals vascular smooth muscle and mesenchymal stem cell defects. *Cell Stem Cell* **8,** 31–45 (2011).

268. Griep, L. M. *et al.* BBB on chip: microfluidic platform to mechanically and biochemically modulate blood-brain barrier function. *Biomed Microdevices* **15,** 145–150 (2013).

269. Achyuta, A. K. H. *et al.* A modular approach to create a neurovascular unit-on-a-chip. *Lab Chip* **13,** 542–553 (2013).

270. Berdichevsky, Y., Staley, K. J. & Yarmush, M. L. Building and manipulating neural pathways with microfluidics. *Lab Chip* **10,** 999–1004 (2010).

271. Kunze, A., Giugliano, M., Valero, A. & Renaud, P. Micropatterning neural cell cultures in 3D with a multi-layered scaffold. *Biomaterials* **32,** 2088–2098 (2011).

272. Khademhosseini, A., Langer, R., Borenstein, J. & Vacanti, J. P. Microscale technologies for tissue engineering and biology. *Proc Natl Acad Sci USA* **103,** 2480–2487 (2006).

Chapter II.

Comparison and optimization of hiPSC forebrain cortical differentiation protocols

The majority of this chapter was previously published as:

Muratore CR*, **Srikanth P***, Callahan DG, and Young-Pearse TL. Comparison and Optimization of hiPSC Forebrain Cortical Differentiation Protocols. *PLOS ONE*. 2014; 9(8): e105807. PMID: 25165848

Experimental contributions to this chapter: CRM performed the majority of experimental work contributing to Figures 2.1-2.4. PS performed the majority of experimental work contributing to Figures 2.5-2.7. DGC assisted with qPCR.

ABSTRACT

Several protocols have been developed for human induced pluripotent stem cell neuronal differentiation. We compare several methods for forebrain cortical neuronal differentiation by assessing cell morphology, immunostaining and gene expression. We evaluate embryoid aggregate vs. monolayer with dual SMAD inhibition differentiation protocols, manual vs. AggreWell aggregate formation, plating substrates, neural progenitor cell (NPC) isolation methods, NPC maintenance and expansion, and astrocyte co-culture. The embryoid aggregate protocol, using a Matrigel substrate, consistently generates a high yield and purity of neurons. NPC isolation by manual selection, enzymatic rosette selection, or FACS all are efficient, but exhibit some differences in resulting cell populations. Expansion of NPCs as neural aggregates yields higher cell purity than expansion in a monolayer. Finally, co-culture of iPSC-derived neurons with astrocytes increases neuronal maturity by day 40. This study directly compares commonly employed methods for neuronal differentiation of iPSCs, and can be used as a resource for choosing between various differentiation protocols.

INTRODUCTION

Since the advent of human induced pluripotent stem cell (hiPSC) technology, numerous studies have utilized these cells for neuronal differentiation. Several groups have independently developed hiPSC neuronal differentiation protocols, often adapted from existing protocols for human embryonic stem cells (ESCs) or mouse iPSCs/ESCs[1-10]. These protocols are constantly being improved and revised, creating a plethora of techniques to differentiate hiPSCs to neuronal fates. The ability to differentiate, culture, and manipulate human neurons is of tremendous interest to labs seeking to study human neurodevelopment and neurological diseases. For a group that is new to stem cell culture and differentiation, the multitude of available neuronal differentiation protocols can be overwhelming. Here, we aim to directly

compare some of the most commonly used techniques in human neuronal differentiation, using gene expression, cell morphology, and immunostaining to benchmark efficiency. We hope this study may provide useful information to aid in other groups' future decisions regarding iPSC differentiation methods and reagents.

Many groups have taken advantage of somatic cell reprogramming technology to generate patient-specific iPSC lines in order to model neurodegenerative and neurodevelopmental disorders (reviewed here[11]). Furthermore, there have been many advancements in protocols to create neurons of a particular identity (e.g. motor neurons, dopaminergic neurons or interneurons)[12-18]. There are often multiple protocols to differentiate stem cells to a particular neuronal fate of interest. While a comparison of neuronal patterning protocols would certainly be informative, it is outside the scope of this study. Here, we focus on methods for differentiating iPSCs to a "default" forebrain cortical neuronal fate.

For the differentiation of iPSCs to forebrain neurons, two base protocols are often utilized: an embryoid aggregate-based technique and a monolayer dual SMAD inhibition method[8,19]. In the embryoid aggregate procedure, iPSC colonies in iPSC media are allowed to form aggregates in suspension in the absence of exogenous growth factors or small molecules. The media is then changed at day 5 to a neural induction media with a DMEM/F12 base, containing non-essential amino acids, heparin, and N2 supplement, which supplies transferrin and insulin, among other components ("*N2 neural induction media*"). The primitive neuroectodermal aggregates are plated at day 7 onto an adherence-promoting substrate, and cultured for 10 days, promoting formation of definitive neuroectoderm. At day 17, neural progenitor cells, organized into neural "rosette" structures, are selectively removed from the plate and cultured in suspension. These neural aggregates are cultured in a similar neural induction medium, but with the addition of B27 supplement (containing biotin, DL alpha tocopherol, vitamin A, BSA, catalase, insulin, transferrin, and superoxide dismutase, among

other components), cyclic AMP (cAMP), and insulin growth factor-1 (IGF-1) ("*N2/B27 neural induction media*"). After being cultured in suspension for 7 days, the neural aggregates are plated on an adherent substrate in a differentiation-promoting media. This "*neural differentiation media*" is made with a neurobasal base media supplemented with non-essential amino acids, N2, B27, cAMP, IGF-1, brain-derived neurotrophic factor (BDNF), and glial cell-derived neurotrophic factor (GDNF). Differentiated neurons are visible from day 25 onwards, and can be cultured as long as is desired for experimental purposes[19]. There exist multiple variations on this protocol, including aggregate formation techniques, the use of different plating substrates, neural progenitor cell isolation methods, and co-culture of neuronal cells with astrocytes.

The monolayer dual SMAD inhibition protocol[8] involves dissociating iPSCs and plating them as a feeder-free adherent monolayer before rapidly inducing neuroectoderm formation by antagonizing the bone-morphogenetic protein (BMP) and transforming growth factor beta (TGF-beta) signaling pathways (e.g. by using Noggin and SB431542, respectively). The morphogen Noggin and small molecule SB431542 induce conversion of hiPSCs or hESCs to a neural progenitor cell fate by day 7, in a neural induction media made with a DMEM/F12 base and insulin, N2, and B27 ("*3N neural induction media*")[10]. At day 11, cells are dissociated and re-plated in neural differentiation-promoting media ("neural differentiation media," defined above). Thus the media used by the dual SMAD inhibition protocol is largely similar to those utilized in the embryoid aggregate method. Two main differences exist between these two protocols: 1) morphogens/small molecules block the BMP and TGF-beta pathways in the dual SMAD inhibition protocol, and 2) the monolayer (dual SMAD inhibition protocol) versus the three-dimensional aggregate (embryoid aggregate technique) culture. The resulting timelines of these methods are also distinct, with neuroectoderm at day 17 vs. day 7, and neurons at day 25 vs. day 12 in the embryoid aggregate vs. dual SMAD inhibition protocols, respectively.

Multiple studies have utilized each of these methods, often with modifications, to

generate human iPSC-derived neurons. These variations involve the use of different reagents at multiple stages of differentiation to achieve a common goal: culture of human neurons. It is not always clear from a published study why a particular method was chosen and how the method employed compares to other available protocols. Here we examine both the embryoid aggregate and dual SMAD inhibition protocols and compare commonly used experimental paradigms for aggregate formation, plating substrates, NPC isolation and expansion, and neuronal maturation. We evaluate these various techniques through the use of common metrics such as morphology, immunostaining and gene expression.

RESULTS

Differentiation of human iPSCs into neurons using an aggregate method

To examine various differentiation strategies, we first utilized an embryoid aggregate protocol[19] originally based on methods developed for hESCs[20]. Fig 2.1A shows the timeline schematic for the protocol, in which human iPSCs are differentiated to neuronal fates over the course of ~40 days. Aggregates were formed by dissociating iPSCs as large clusters at day 1, followed by suspension in culture for five days in serum-free iPS media (without FGF2). At day 5, aggregate media was changed to N2 neural induction media. Aggregates then were plated on Matrigel for the formation of primitive neuroepithelial cells (Fig 2.1B, day 10) in N2 neural induction media. At day 17, neural rosette structures were manually selected from plates and suspended in flasks for another week in N2/B27 neural induction media. This step aims to select for definitive neuroepithelial cells since many non-neuroepithelial cell types adhere to the flask. At day 24, aggregates were plated on Matrigel and allowed to mature for an additional 15-30 days in neural differentiation media.

In order to qualitatively assess the progression of differentiation, we performed immunostaining for various markers indicative of the differentiation process (Fig 2.1C).

Figure 2.1. Embryoid body differentiation of hiPSCs. (A) Time course of differentiation for embryoid aggregates. iPSC colonies were dissociated from mouse embryonic fibroblasts at day 1 (D1) and cultured as aggregates in suspension. Aggregates were plated onto culture dishes at day 7 (D7), forming primitive neuroepithelial (NE) structures. By day 17 (D17), definitive NE structures were present; NE structures were manually isolated and further cultured in suspension. Cells were plated for final differentiation at day 24 (D24). Arrows indicate media changes across differentiation. Boxes indicate differentiation state. This protocol was performed in 11 independent lines, with all lines performing similarly; representative images are shown. **(B)** Bright-field microscopy images showing morphological changes spanning differentiation from the earliest time-point (iPSCs) to day 40 (D40) neurons. Scale bars from left to right: 100, 200, 200, 500, 500 μm. **(C)** Cells were immunostained at various time-points during neuronal differentiation. Confocal microscopy images at days 0 (iPS colony), 18, 26, and 40. Scale bars=100 μm. TOPRO3, nuclear marker. **D)** qPCR analysis of markers over differentiation. Ct data normalized to *GAPDH*. For Oct4: iPS n=14, D17 n=23, D40-50 n=19 with data points all normalized to iPS; MAP2: iPS n=15, D17 n=25, D40-50 n=26 with data points all normalized to D40-50; Tbr1: iPS n=14, D17 n=25, D40-50 n=26 with data points all normalized to D40-50, from 6 independent differentiations. Data are represented as mean ± SEM.

Figure 2.1 (Continued)

A.

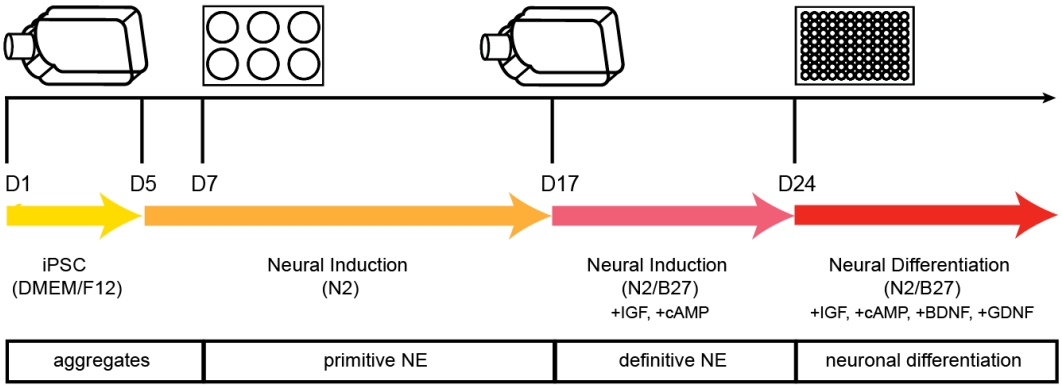

B.

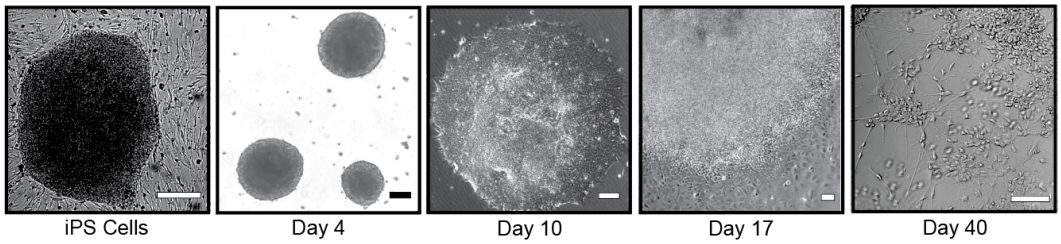

C.

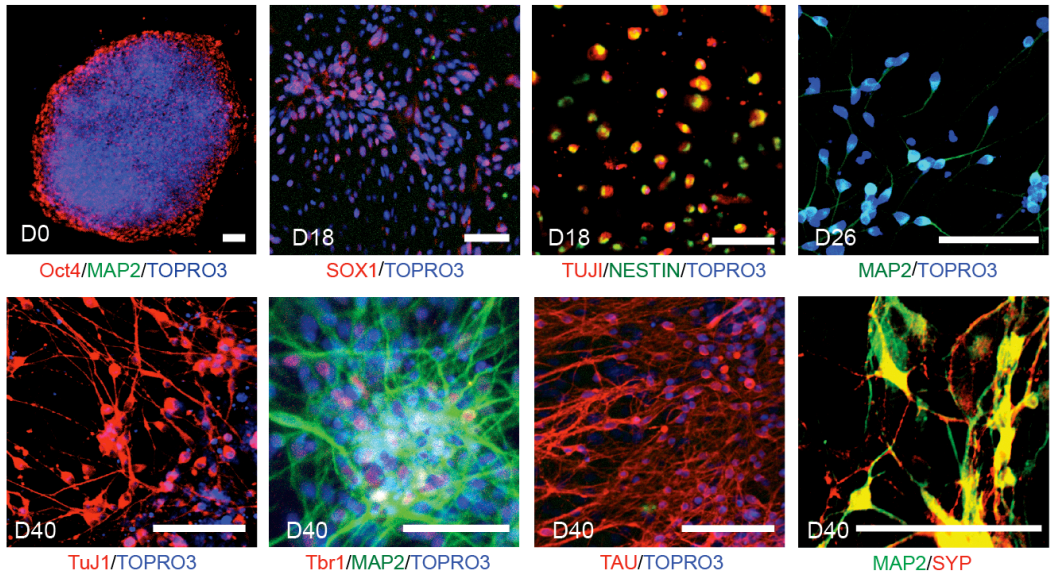

D.

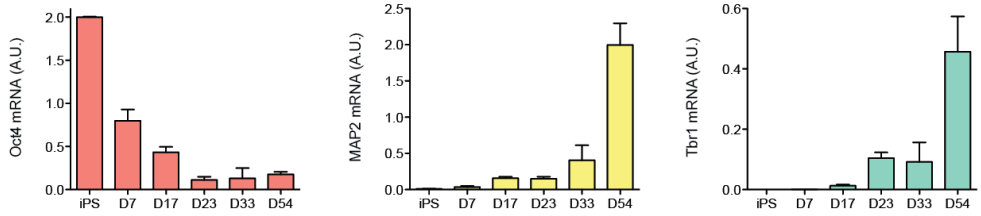

Undifferentiated iPSC colonies expressed the pluripotent marker Oct4 (POU5F1), but lacked expression of neuronal cytoskeletal markers such as MAP2. The intermediate time-point day 18 shows the expression of neural progenitor markers Sox1 and Nestin. Neurons differentiated for 40 days express neuronal proteins such as MAP2, TuJ1, and Tau, the cortical marker Tbr1, and synaptic markers such as synaptophysin (SYP) (Fig 2.1C, bottom row). Functional analyses were performed using a microelectrode array platform. Spontaneous potentials were observed at around 50 days of differentiation, as previously reported using this protocol [21]. In order to quantitatively assess and compare differentiation progression across multiple wells, qPCR was performed for multiple cell-fate markers (Fig 2.1D). Data show that with an increase in differentiation time, mRNA expression of *Oct4* (*POU5F1*) decreases, while neuronal markers such as *MAP2* and *Tbr1* increase, and this expression pattern is consistent between wells of the same experiment and between differentiation rounds. To complement the qPCR data and determine the absolute percentage of neuronal cells derived using this method, the percentage of cells expressing MAP2 was quantified from immunostained wells, with 93% (±1.5 SEM) of cells expressing MAP2 by day 40.

Generation of neurons utilizing dual SMAD inhibition in monolayer culture

We next sought to compare a monolayer-based protocol to this aggregate method. Fig 2.2A illustrates the timeline schematic that was utilized, based on the technique of dual SMAD inhibition[8]. At the start of differentiation (day 0), iPSCs were dissociated to single cells and re-plated as a monolayer with a concentration of 20,000 cells/cm^2 in MEF conditioned media, supplemented with FGF2. After cells reached 90% confluency, media was changed to 3N neural induction media supplemented with Noggin (200 ng/mL) and SB431542 (10 μM)[10]. Cells were split at day 11 using dispase and re-plated in neural differentiation media onto 96-well plates coated with Matrigel. The bright-field images in Fig 2.2B illustrate the morphological changes over the course of differentiation. At day 7, the cells begin to form early rosette structures. After

Figure 2.2. Monolayer differentiation of hiPSCs. (A) Time course of differentiation using dual-SMAD inhibition. iPSC colonies were dissociated from mouse embryonic fibroblasts at day 1 (D1) and plated as a monolayer. Small molecules and growth factors were added as indicated. This protocol was performed in at least 6 independent lines; representative images from the most efficient differentiations are shown. **(B)** Bright-field images spanning differentiation from the earliest time-point day 0 (D0) to day 40 (D40). Scale bars=50 μm. **(C)** Cells were immunostained at various time-points during neuronal differentiation. Confocal images at days 0, 7, 11, 27 and 40. Scale bars=100 μm. TOPRO, nuclear marker. **(D)** qPCR analysis of markers over differentiation. Ct data normalized to *GAPDH*. For Oct 4: iPS n=3, D1 n=3, D7 n=3, D11 n=6, D40 n=5; MAP2: iPS n=3, D1 n=4, D7 n=4, D11 n=6, D40 n=5; Tbr1: n=2, D1 n=3, D7 n=3, D11 n=5, D40 n=5. Data are represented as mean ± SEM.

Figure 2.2 (Continued)

A.

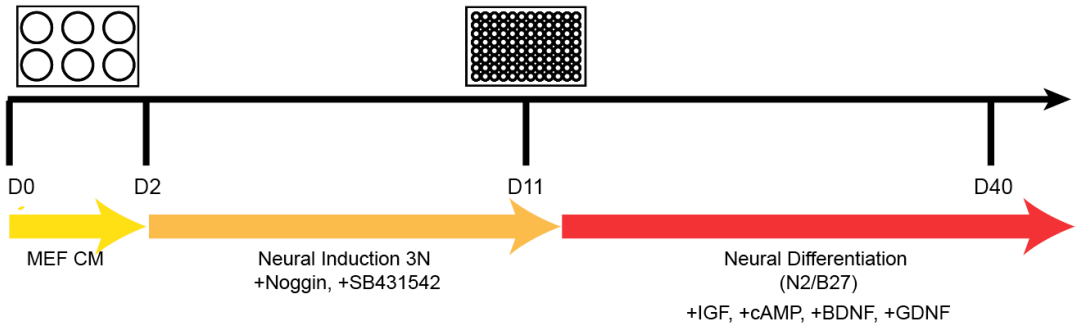

B.

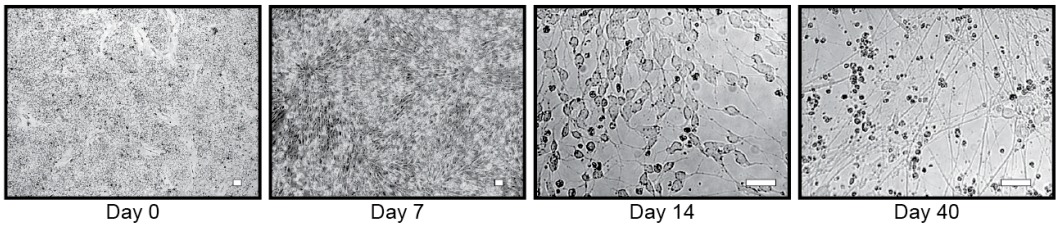

C.

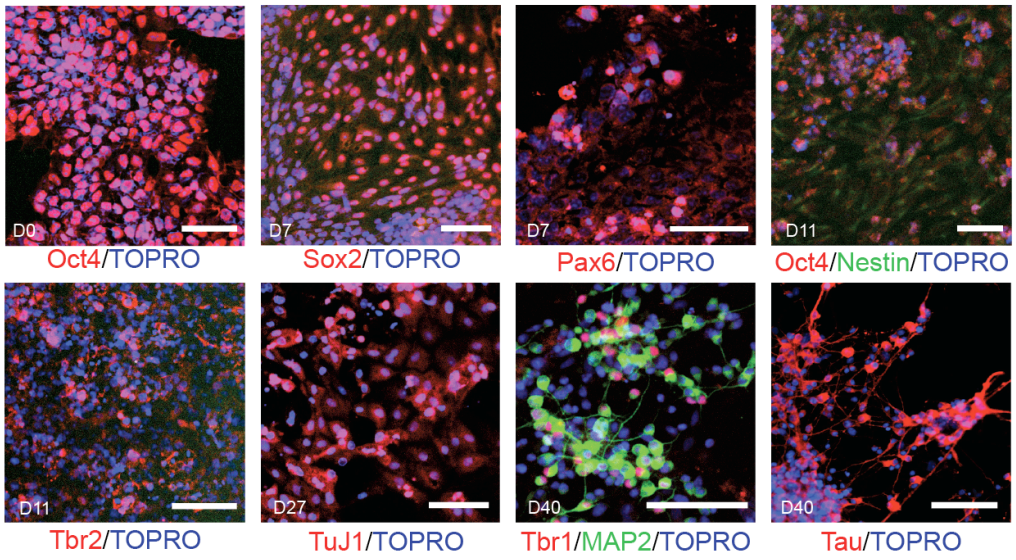

D.

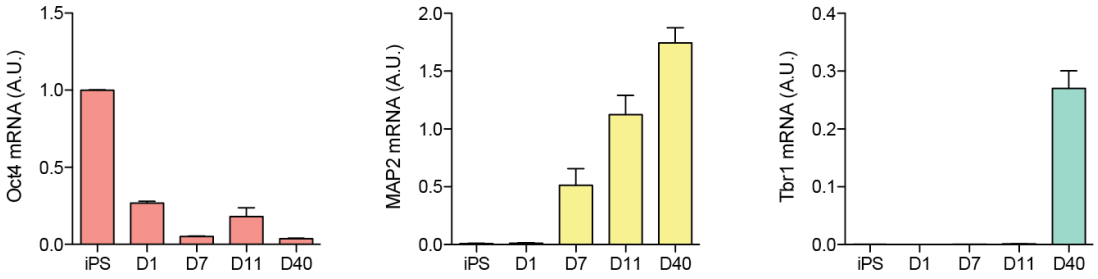

re-plating the cells at day 11, small processes begin to emerge (day 14), followed by more mature neuronal morphology at day 40 (Fig 2.2B, last panel).

Both immunostaining and qPCR were employed to examine differentiation efficiency over time. Cells begin to express progenitor markers Sox2 and Pax6 at day 7 and Nestin and Tbr2 at day 11. From its maximal expression at day 0, Oct4 expression is markedly decreased at day 11 (Fig 2.2C). From day 27 through day 40, neuronal markers Tau, MAP2, Tbr1 and TuJ1 are expressed. Based on quantification of immunostaining, approximately 45% (±4.6 SEM) of cells expressed MAP2. Similarly to the aggregate method, when we probed mRNA from harvested cells, *Oct4* (*POU5F1*) decreased over differentiation time while *MAP2* and *Tbr1* increased up to day 40 (Fig 2.2D). However, this method often resulted in "failed" differentiations due to high levels of cell death between days 10-17 of differentiation. Neuronal differentiation using the dual-SMAD inhibition protocol without splitting led to cultures that either died or did not produce MAP2+ neurons (10/10 differentiation rounds), due to over-confluent cultures between days 10-17. However with a revision in the protocol that included splitting the cultures at day 11 (Chambers and Studer, personal communication), we observed MAP2+ cells in 3/5 differentiation rounds. Based on these initial results, we chose to focus upon optimizing the embryoid aggregate differentiation protocol.

Comparison of embryoid aggregate formation: manual versus AggreWell

We hypothesized that differentiation efficiency could be improved by creating embryoid aggregates of a more uniform size, using AggreWell plates. At day 0, iPSCs were dissociated manually using dispase and either resuspended in flasks or triturated and plated in AggreWell plates. With AggreWell plates, cells were force-pelleted into microwells by centrifugation. After 24 hours, dissociated cells formed aggregate structures and were further cultured following the protocol outlined in Fig 2.1A. We made aggregates of two different types: 3,000 and 8,000 cells/aggregate. Manually formed aggregates consisted of varying shapes and sizes (Fig 2.3A),

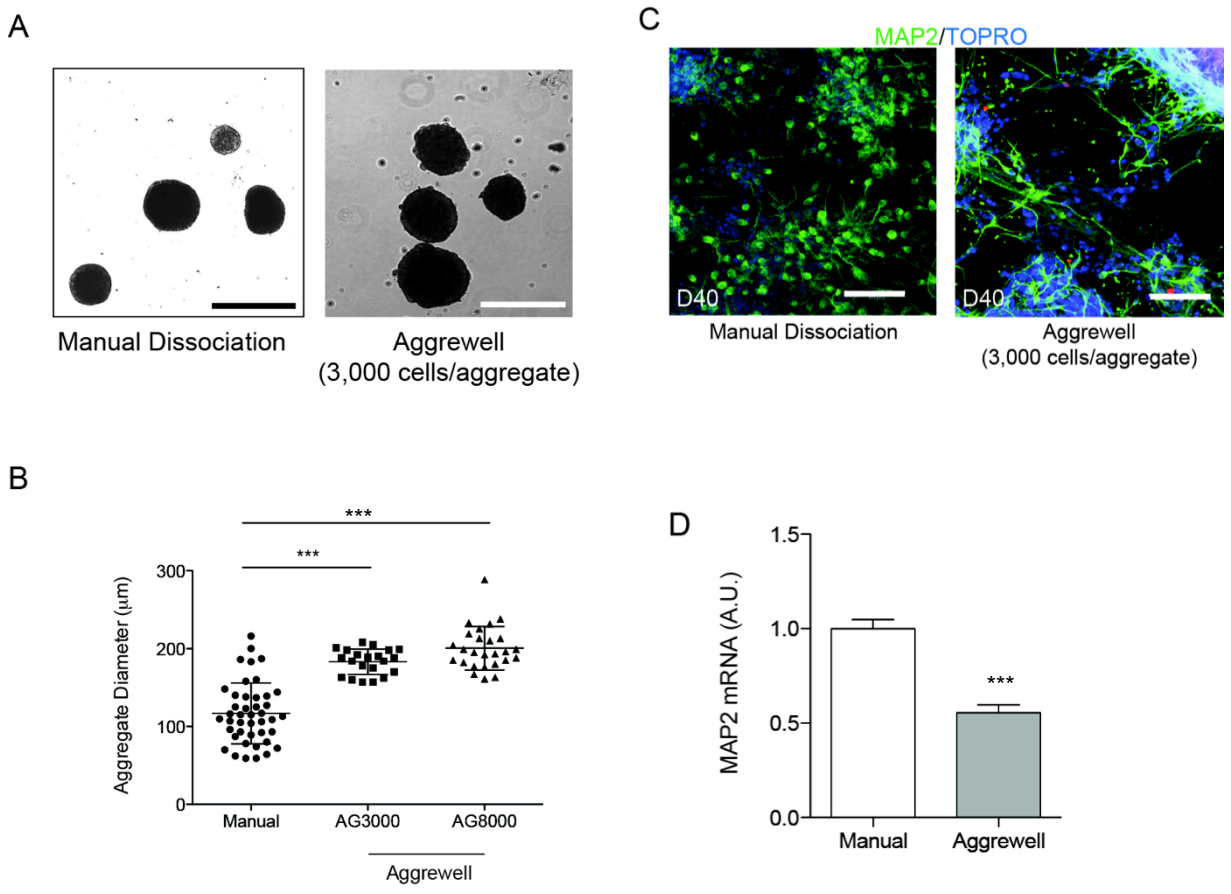

Figure 2.3. Comparison of embryoid body formation. (A,B) Embryoid bodies were either formed by dissociating iPSCs (using dispase and trituration) or by AggreWell plate technology, followed by culture in non-adherent flasks. **(B**) Quantification of aggregate size from manually-formed or 3,000- or 8,000-cell aggregates. Mean diameter for manually formed aggregates=118.3 µm; mean diameter for 3,000 cells/aggregate=183.1 µm; mean diameter for 8,000 cells/aggregate=195.2 µm. Scale bars=200 µm. Data are represented as mean ± SEM, from 3 independent differentiations, n=21-43. Significance determined by one-way ANOVA with a Tukey's post-test: ***, $p<0.0001$. F-tests between groups showed significantly different variances, with $p<0.05$ between manual vs. 3,000 cells/aggregate and manual vs. 8,000 cells/aggregate. Data are represented as mean ± SEM. **(C**) Immunostaining of day 40 (D40) neurons, following differentiation using either manual formation or AggreWell plates. TOPRO, nuclear marker. Scale bars=100 µm. Representative images are shown. **(D**) qPCR was performed using RNA harvested from day 40 cultures. Data normalized to *GAPDH* expression. Manual n=10, AggreWell n=10. Error bars represent SEM. Significance was determined by student's t-test: ***, $p<0.0001$.

whereas aggregates formed using AggreWell were visually more uniform in size and shape. These size differences were quantified by measuring the diameter of aggregates (Fig 2.3B). The mean diameter for manually formed aggregates was 118.3 μm (±6.0 SEM), whereas the mean diameter was 183.1 μm (±3.6 SEM) for 3,000 cells/aggregate and 195.2 μm (±5.5 SEM) for 8,000 cells/aggregate. Both sizes of AggreWell aggregates were significantly larger than manually formed aggregates, and although there was a trend for an increased aggregate diameter between 3,000 and 8,000 cells/aggregate, it did not reach statistical significance. As the AggreWell system is designed to incorporate 3,000 versus 8,000 cells into each aggregate, the insignificant difference in aggregate size may reflect a difference in aggregate density, with 8,000 cells/aggregate being more densely packed than 3,000 cells/aggregate. Not surprisingly, the variance of aggregate size distribution was significantly greater with manual aggregate formation than with either AggreWell size. Immunostaining for MAP2 in cells following aggregate formation with the use of AggreWell is shown in Fig 2.3C (right). Immunostaining at day 40 showed that approximately 46% (±1.6 SEM) of AggreWell-differentiated cells were MAP2+, compared to 93% MAP2+ cells with manually formed aggregate differentiation. Quantification of *MAP2* mRNA from day 40 neurons that were cultured in the AggreWell format also showed a corresponding significant decrease in *MAP2* mRNA levels (Fig 2.3D).

Comparison of plating substrates: Matrigel vs. poly-o-laminin

The choice of plating substrates for differentiation varies among labs and protocols. By far, the two most commonly used substrates are Matrigel and a poly-ornithine/laminin combination (POL). We sought to compare the results of using Matrigel versus POL substrate at the two plating steps of the embryoid aggregate technique (Fig 2.1A). We found that using Matrigel for the first aggregate plating (day 7) was sufficient to direct differentiation to a neuroepithelial fate (Fig 2.4A). However, when we attempted to plate aggregates on POL at the

Figure 2.4. Comparison of plating substrates. Aggregates were plated on either Matrigel or poly-o/laminin (POL) coated plates at days 7 or 24. **(A,D)** Aggregates plated at day 7 (D7) and imaged at day 10 (D10) on Matrigel (**A**) formed typical neuroepithelial structures, while aggregates plates on POL (**D**) failed to adhere after two days. **(B,E)** Aggregates were plated on either Matrigel or POL coated plates for final differentiation on day 24 (D24) and imaged at day 40 (D40). Aggregates plated on Matrigel (**B**) exhibited an increased density of processes, while aggregates plates on POL (**E**) displayed increased cell body migration from the plated aggregate. **(C,F)** Neural aggregates were dissociated at day 24 and plated on either Matrigel (**C**) or POL (**F**). **(G)** Aggregates were plated on either Matrigel (top row) or POL (bottom row) at day 24 and allowed to mature until day 40, followed by immunostaining and confocal microscopy for neuronal markers. Scale bars=100 μm. Representative images are shown. **(H)** qPCR was performed using RNA harvested from day 40 cultures. Data normalized to *GAPDH* expression. Matrigel n=10, POL n=10. Error bars represent SEM. **(I)** Aggregates were single-cell dissociated and plated on either Matrigel (top row) or POL (bottom row) at day 24 and allowed to mature until day 40, followed by immunostaining and confocal microscopy for neuronal markers. Scale bars=100 μm. Representative images are shown. **(J)** qPCR was performed using RNA harvested from day 40 cultures. Data normalized to *GAPDH* expression. Matrigel n=22, POL n=22. Significance determined by student's t-test: **, $p<0.01$; ***, $p<0.001$. Data are represented as mean ± SEM.

Figure 2.4 (Continued)

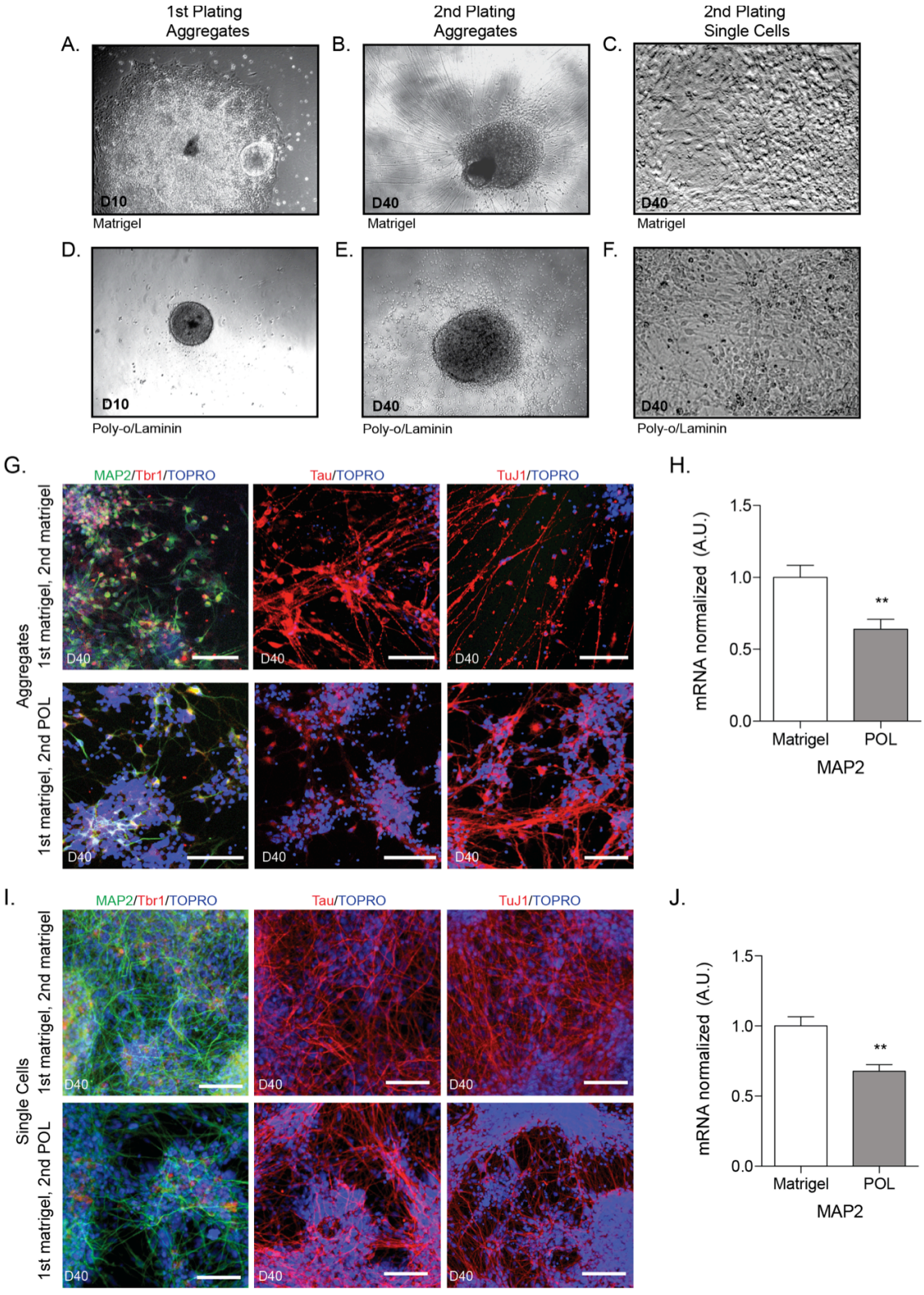

same time-point, aggregates did not reliably adhere to the plate (Fig 2.4D). For the second plating of neural aggregates at day 24, cells were plated on either Matrigel (Fig 2.4B) or POL (Fig 2.4E). For both plating substrates, aggregates were able to adhere to the plate, and cells with neuronal morphology were visible. However, aggregates plated on POL displayed sparser distribution of cell processes and more migration of cell bodies away from aggregates (Fig 2.4E) compared to aggregates plated on Matrigel (Fig 2.4B). Immunostaining of day 40 differentiated neurons showed decreased MAP2 staining (Fig 2.4G, bottom row) as well as low levels of Tau staining, in POL versus Matrigel-plated neurons (Fig 2.4G, top row). TuJ1 staining appeared to be consistent between the two plating conditions. *MAP2* mRNA levels from day 40 differentiated neurons, plated on either Matrigel or POL, were quantified using qPCR (Fig 2.4H). Cells from POL-plated aggregates expressed significantly less *MAP2* mRNA than cells plated on Matrigel. Based on immunostaining, approximately 56% (±3.5 SEM) of differentiated neurons expressed MAP2 on POL, compared to 93% MAP2+ cells with Matrigel plating.

While plating aggregates for final differentiation induces efficient neuron generation, for some purposes it may be desirable to have a culture that is more monolayer in nature. For example, aggregates can interfere with imaging as it is difficult to visualize cells in or near large aggregates. In an effort to create a monolayer cell culture, aggregates were dissociated with Accutase at day 24 and plated on either Matrigel or POL (Fig 2.4C,F). Immunostaining revealed similar results to those seen in Fig 2.4G. Dissociated single cells plated on POL exhibited less dense cultures than neurons plated on Matrigel, with less overall staining of neuronal processes (MAP2, Tau, TuJ1) (Fig 2.4I, bottom row). *MAP2* mRNA from day 40 dissociated/single-cell neurons, plated on either Matrigel or POL, was quantified using qPCR. Dissociated cells plated on POL had significantly lower *MAP2* mRNA expression than cells plated on Matrigel (Fig 2.4J).

Comparison of neural progenitor cell (NPC) isolation by multiple methods

There are a number of ways to select desirable day 17 neuroepithelial rosette structures

for further differentiation. We next sought to compare different NPC isolation methods at day 17 of differentiation (Fig 2.5A). First, manual neural rosette selection was compared to enzymatic neural rosette selection. Manual rosette selection involved manually scraping away the large, clear cells (neural crest morphology) that surround neural rosette structures to remove these contaminating cell types. For enzymatic rosette selection, the StemCell Technologies STEMdiff Neural Rosette Selection Reagent was used to selectively detach neural rosettes from the dish (Fig 2.5B). Immunostaining at day 18 (one day after selection) shows that both manual and enzymatic rosette selection enrich for Pax6+ (Fig 2.5C, top row), Nestin+ (Fig 2.5C, top and bottom rows) and Oct4- (Fig 2.5C, middle row) cells, compared to cells that were not subjected to any NPC selection. Manual selection resulted in fewer Oct4+ cells than rosette selection (Fig 2.5C, middle row). Sox2 expression was similar between the three conditions, but there were several Sox2+/Nestin- cells without NPC selection, and a few Sox2+/Nestin- cells after rosette selection (Fig 2.5C, bottom row, asterisks). Immunostaining of differentiated neurons at day 40 (after enzymatic rosette selection) shows that 85% (±5.1 SEM) are MAP2+, similar to the 93% MAP2+ neurons resulting from manual selection.

We hypothesized that employing a cell-sorting technique would help decrease non-neuronal cell contamination in our cultures. To test this, we sorted day 17 cells using magnetic affinity cell sort (MACS) technology with a PSA-NCAM antibody. Manually selected NPCs and PSA-NCAM+ cells were plated on Matrigel in neural differentiation media for 23 days and immunostained for various neuronal markers (Fig 2.5D). Both conditions (manual selection and PSA-NCAM+) expressed neuronal markers TuJ1, MAP2 and Tau. However, sorted cells (Fig 2.5D, right column) had high background levels of non-neuronal cells, indicated by non-neuronal morphology and absence of neuronal markers. Additionally, Tbr1 immunoreactivity was less abundant in MACS preparations compared to manually selected cells (Fig 2.5D, middle row). Quantification following PSA-NCAM sorting from these experiments showed 47% (±2.3 SEM)

Figure 2.5. Comparison of NPC isolation methods. (A) Schematic indicating the time course of differentiation and the techniques used to isolate neural progenitor cells (NPCs). Human iPSCs were differentiated for 17 days. NPCs were isolated by manual scraping of non-NPCs under a microscope (manual selection), using a proprietary neural rosette selection reagent (rosette selection), or by FACS for CD184+/CD44-/CD271-/CD24+ cells (FACS). **(B)** Representative bright field images are shown for selection of rosettes using rosette selection reagent. White arrows indicate rosette structures to be isolated. After use of the reagent, rosettes are isolated. Scale bars=100 μm. **(C)** Immunostaining for various cell fate markers at day 18 after isolation at day 17. Asterisks in the bottom panel show Sox2+Nestin- cells. Scale bars=100 μm. **(D)** Day 17 NPCs were either manually selected or dissociated using accutase and processed for cell sorting. Manually selected or PSANCAM+ cells were plated on Matrigel for 23 days in neural differentiation media and immunostained at day 40 for neuronal markers. Scale bars=100 μm. **(E)** Day 17 cells were dissociated and subjected to FACS. CD184+/CD44-/CD271-/CD24+ cells ("NPCs") and all other cells ("non-NPCs") were plated on Matrigel and maintained in neural progenitor media for 20 days prior to immunostaining. Scale bar = 50 um. **(F,G)** RNA was harvested from cells at day 17 after isolation and used in the NanoString assay. Expression profiles of selected NPC fate markers (**F**) or other cell fate markers (**G**) are shown. Gene expression was normalized to the geometric mean of seven housekeeping genes. Data are represented as mean ± SEM. Data are from 5-6 independent differentiations and 3 lines, n=6-30. Significance is shown compared to "manual selection." Statistics were calculated using two-way ANOVA with Holm-Sidak multiple comparisons correction: *, $p < 0.05$; **, $p < 0.01$; ***, $p < 0.001$.

Figure 2.5 (Continued)

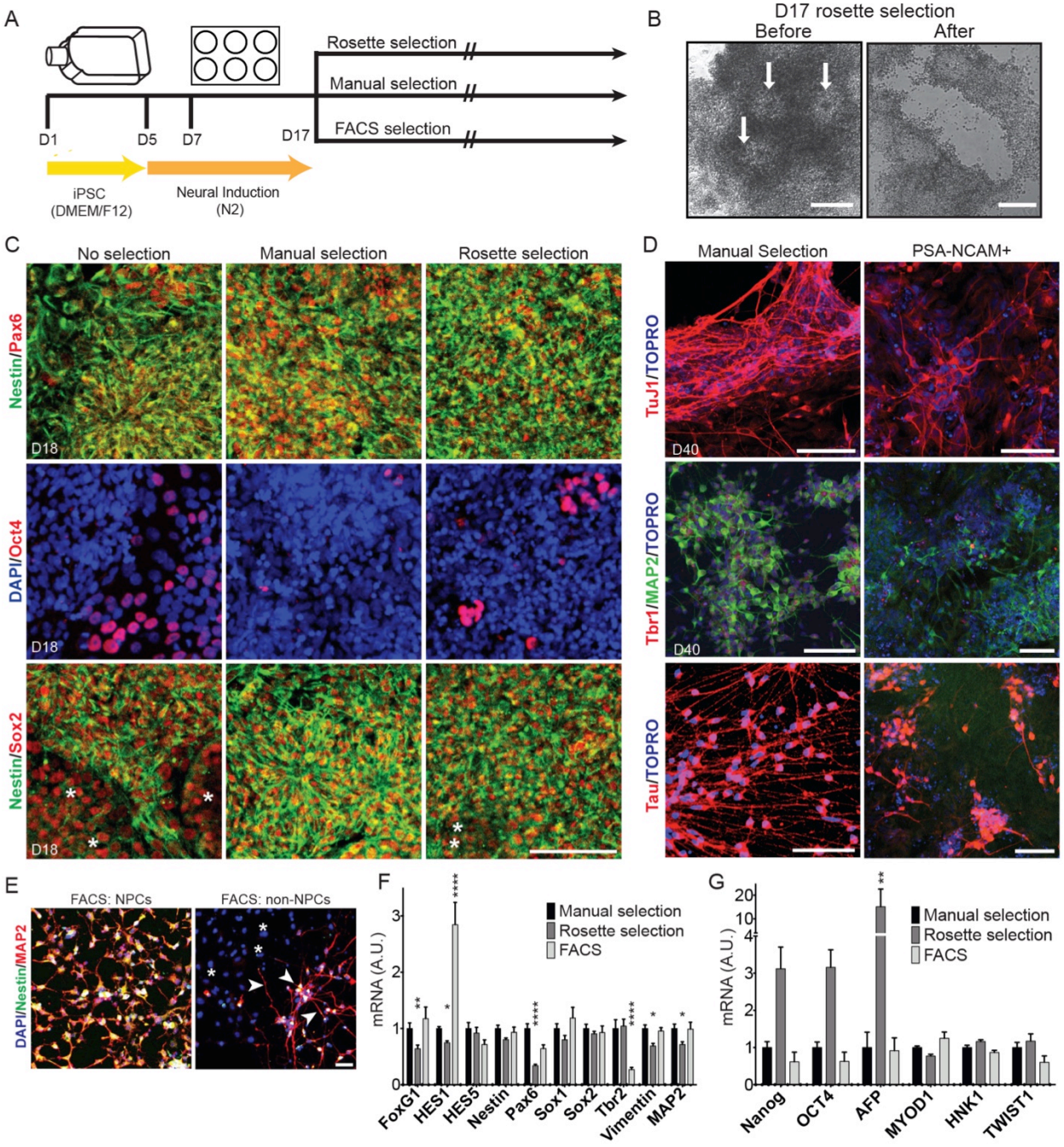

MAP2+ cells.

Because MACS did not improve neuronal purity above other NPC selection strategies, we then tested the ability of FACS to enrich for NPCs by isolating CD184+/CD44-/CD271-/CD24+ cells using the BD Stemflow Human Neural Cell Sorting Kit (based largely on a published study[22]), wherein day 17 cells are dissociated and labeled with these antibodies that mark specific cell populations. CD184+/CD44-/CD271-/CD24+ cells ("NPCs") and flow-through cells ("non-NPCs") were maintained in neural progenitor media for 20 days after sorting, followed by immunostaining for Nestin and MAP2 (Fig 2.5E). This media, consisting of a DMEM/F12 base with B27, FGF2, EGF, and heparin, supports culture of adherent neural progenitor cells[23]. Fig 2.5E shows that FACS reduced the number of Nestin-/MAP2- cells present (asterisks), but was highly stringent and also excluded some cells expressing neuronal markers (arrowheads).

Finally, we compared the gene expression profiles of manual-, rosette-, and FACS-isolated NPCs at day 17 by NanoString (Fig 2.5F,G). Gene expression analyses show that enzymatic rosette selection appeared to be most permissive to other cell types, with decreased expression of NPC markers *FoxG1*, *HES1*, *Pax6*, *Vimentin (VIM)*, and *MAP2* (Fig 2.5F), and higher expression of non-NPC cell fate markers, including the endodermal marker *AFP* (Fig 2.5G). There was also a trend for increased expression of pluripotent cell markers *nanog* and *Oct4* (*POU5F1*), but this did not achieve significance. FACS-isolated NPCs showed similar overall gene expression to manually isolated NPCs with a few differences, including increased *HES1* and decreased *Tbr2* expression (Fig 2.5F). Overall, these three NPC isolation methods each enrich for neural progenitors, with slight differences in NPC purity and identity.

Consequences of Neural Progenitor Expansion on Neuronal Identity

Differentiation protocols are time-consuming and costly; thus, we hoped to establish a protocol in which we could generate neuronal cells from an expandable NPC pool. This would

allow for neuronal differentiation without differentiating cells for 17 days prior to the NPC stage, and for expansion of neural progenitors for increased neuronal yield. Fig 2.6A shows the differentiation schematic that was used to culture NPCs. Differentiation was performed using the embryoid aggregate protocol (Fig 2.1A) until day 17. At day 17, neural rosettes were selected and isolated using the Neural Rosette Selection Reagent from StemCell Technologies. Harvested cells were either maintained in suspension as neural aggregates in N2/B27 neural induction media, plated for expandable monolayer culture in neural progenitor media, or plated on Matrigel in 96-well plates for final differentiation in neural differentiation media. We first compared neurons resulting from aggregates to neurons differentiated from monolayer NPCs. Rosette-selected NPCs were maintained on POL-coated plates in neural progenitor media with EGF, FGF2, and heparin. Cells were plated for final neuronal differentiation from a pool of monolayer-maintained NPCs after the first or second passage (~3-5 days per passage) or directly from day 24 aggregates without passaging. Cells were subsequently maintained in neural differentiation media for 16 days (Fig 2.6A).

Differentiation of monolayer-maintained NPCs from two subsequent passages showed a trend for decreased *MAP2* mRNA expression after the first passage and significantly lower *MAP2* expression after the second passage compared to neurons derived directly from day 24 aggregates (Fig 2.6B). These data indicate decreased potential for neuronal identity with extended monolayer NPC expansion, which could result from expansion of contaminating adherent non-neuronal cells. We also observed a corresponding decrease in MAP2 immunostaining in day 40 neurons derived from NPC monolayer passage 2 compared to neurons derived from day 24 aggregates (Fig 2.6C).

We then examined effects of suspension neural aggregate progenitor expansion on resulting neuronal identity. NPCs were maintained in suspension as neural aggregates for 2 days after selection (day 19) or 18 days after selection (day 35) before plating for final neuronal

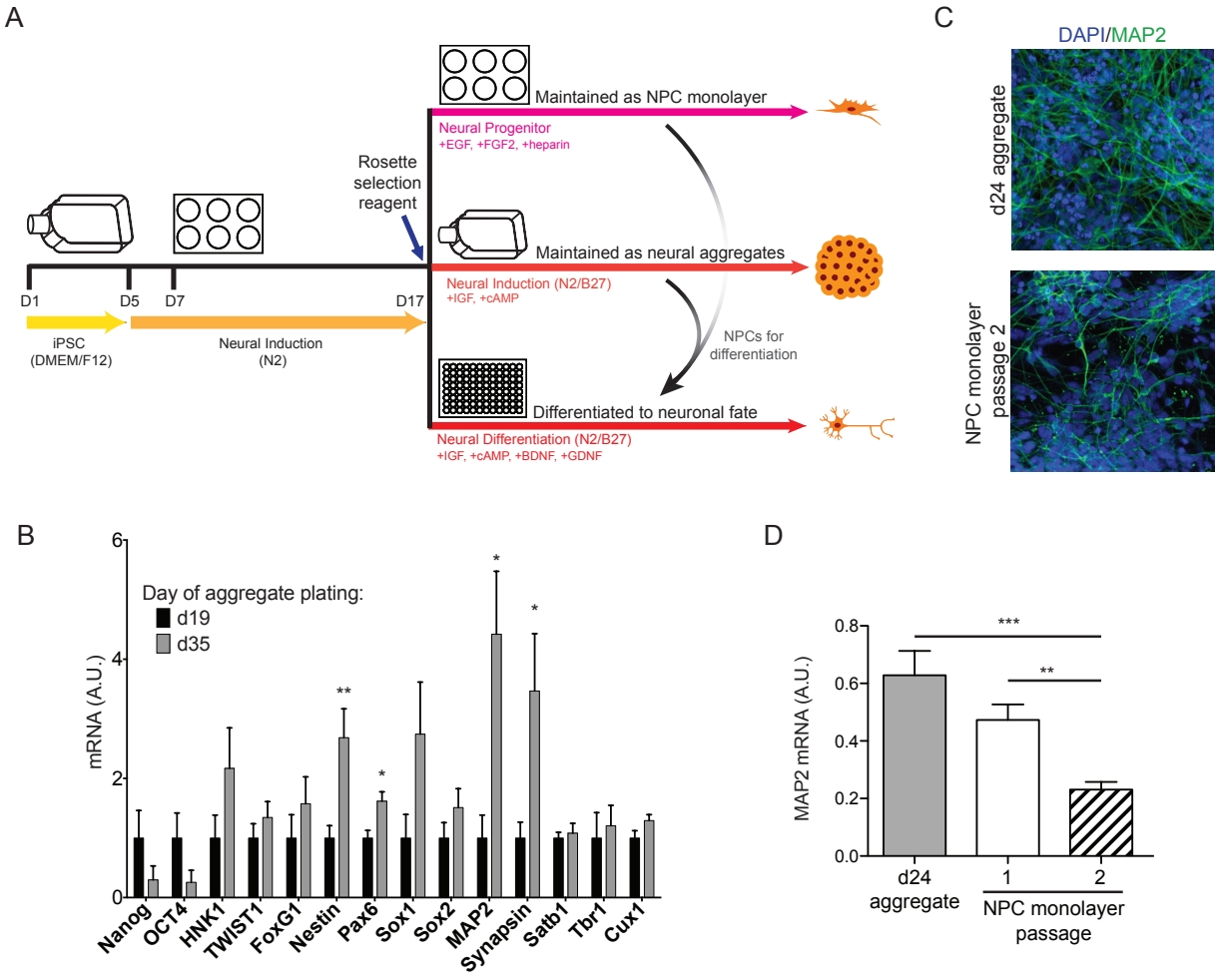

Figure 2.6. Effects of neural progenitor cell maintenance and expansion on differentiation efficiency. (A) Schematic indicating the time course of differentiation and the techniques used to maintain/differentiate neural progenitor cells (NPCs) after NPC isolation with neural rosette selection reagent at day 17. **(B**) qPCR analysis of MAP2 expression after 16 days of differentiation of day 24 aggregates or passage 1 or 2 monolayer NPCs. Data normalized to *GAPDH*. **(C**) Immunostaining of day 40 (D40) neurons, following differentiation from either day 24 aggregates or passage 2 NPCs. Scale bars = 100 μm. Representative images are shown. **(D**) NanoString analysis of cell fate markers of neural aggregates plated at day 19 or 35, after 16 days of plating in neural differentiation media, normalized to the geometric mean of seven housekeeping genes. Data are represented as mean ± SEM, n=6. Significance was determined by student's t-test: *, $p < 0.05$; **, $p < 0.01$; ***, $p<0.001$.

differentiation. These cells were cultured in neural differentiation media for 16 days before analysis of mRNA expression by NanoString (Fig 2.6D). Prolonged neural aggregate culture did not appreciably alter resulting neuronal identity, as demonstrated by comparable expression of cortical markers *Satb1*, *Tbr1*, and *Cux1* (Fig 2.6D). However, the NPC/neural purity of the cultures appeared to be improved with longer neural aggregate culture, shown by higher *nestin (Nes), Pax6, MAP2, and synapsin I (SYN)* expression, as well as a trend for lower *nanog* and *Oct4* (*POU5F1*) expression (Fig 2.6D). Thus, if long-term culture and/or expansion of NPCs is desired, maintenance in aggregates may be superior to maintenance as a monolayer.

The emergence of endogenous astrocytes

Neuronal markers change over the course of differentiation, such that over time there is an upregulation of synaptic markers. We also were interested in whether endogenous astrocytes emerged in our cultures within 100 days of differentiation (Fig 2.7A, green arm). Immunostaining and confocal microscopy of day 42 and day 100 neuronal cultures showed an increase in expression of glial fibrillary acidic protein (GFAP), a marker of astrocytes, at day 100 (Fig 2.7B). Additionally, using the NanoString platform, we evaluated RNA harvested from either day 40 or day 100 neuronal cultures for a subset of neuron and astrocyte markers (Fig 2.7C) and synaptic markers (Fig 2.7D). Day 100 cultures showed a significant increase in expression of the astrocytic markers *GFAP* and *S100B* (Fig 2.7C), as well as in markers of mature neurons, *VLGUT1* (*SLC17A7*), *NMDAR* (*GRIN1*) and *KCC2* (Fig 2.7D). There was no significant difference in *MAP2*, *Tbr1, Tau*, *SYN, PSD95, or VGAT* between day 40 and day 100 cultures.

Neuronal maturation with astrocyte co-culture

Lastly, we aimed to address the possible benefits of astrocyte co-culture on differentiation, i.e. if we could accelerate maturation of neuronal cultures before day 100. Differentiated neurons were cultured alone or co-cultured with mouse astrocytes (Sciencell)

Figure 2.7. Astrocyte co-culture increases neuronal maturation and endogenous astrocytes arise at later time-points in differentiation. (A) Schematic of differentiation up to 100 days. For astrocyte co-culture, astrocytes were added to neuronal cultures at ~day 24 of differentiation. Endogenous astrocytes gradually emerged over the course of 100 days, after day 40. **(B)** Day 42 and day 100 neuronal cultures were immunostained and imaged for GFAP. Scale bars=50 μm. **(C)** After 40-50 (D40) or 100 days (D100), cells were lysed, RNA extracted, and expression of 150 genes analyzed using the NanoString platform. A subset of neuronal markers (**C**) and synaptic markers (**D**) are shown. Data are from at least 6 independent differentiations (3 lines). For day 40-50 n=29-38, for day 100 n=15-19. **(E)** Neuron cultures with or without astrocytes were immunostained and imaged using confocal microscopy at day 40. Insets in right column show VGLUT1 staining along the length of a neuronal process. Representative images are shown. Scale bars=50 μm. **(F)** qPCR was performed using RNA harvested from day 40 cultures. Data normalized to *GAPDH* expression. For neurons alone n=20 for MAP2, TBR1, CUX1, GAD1, n= 37 for SYP, n=38 for VGLUT1; for astrocyte co-culture n=17 for GAD1, n=18 for MAP2, TBR1, CUX1, n=27 for SYP, n=25 for VGLUT1. Data are represented as mean ± SEM. Significance determined by student's t-test: **, $p<0.01$; ***, $p<0.001$; ****, $p<0.0001$.

Figure 2.7 (Continued)

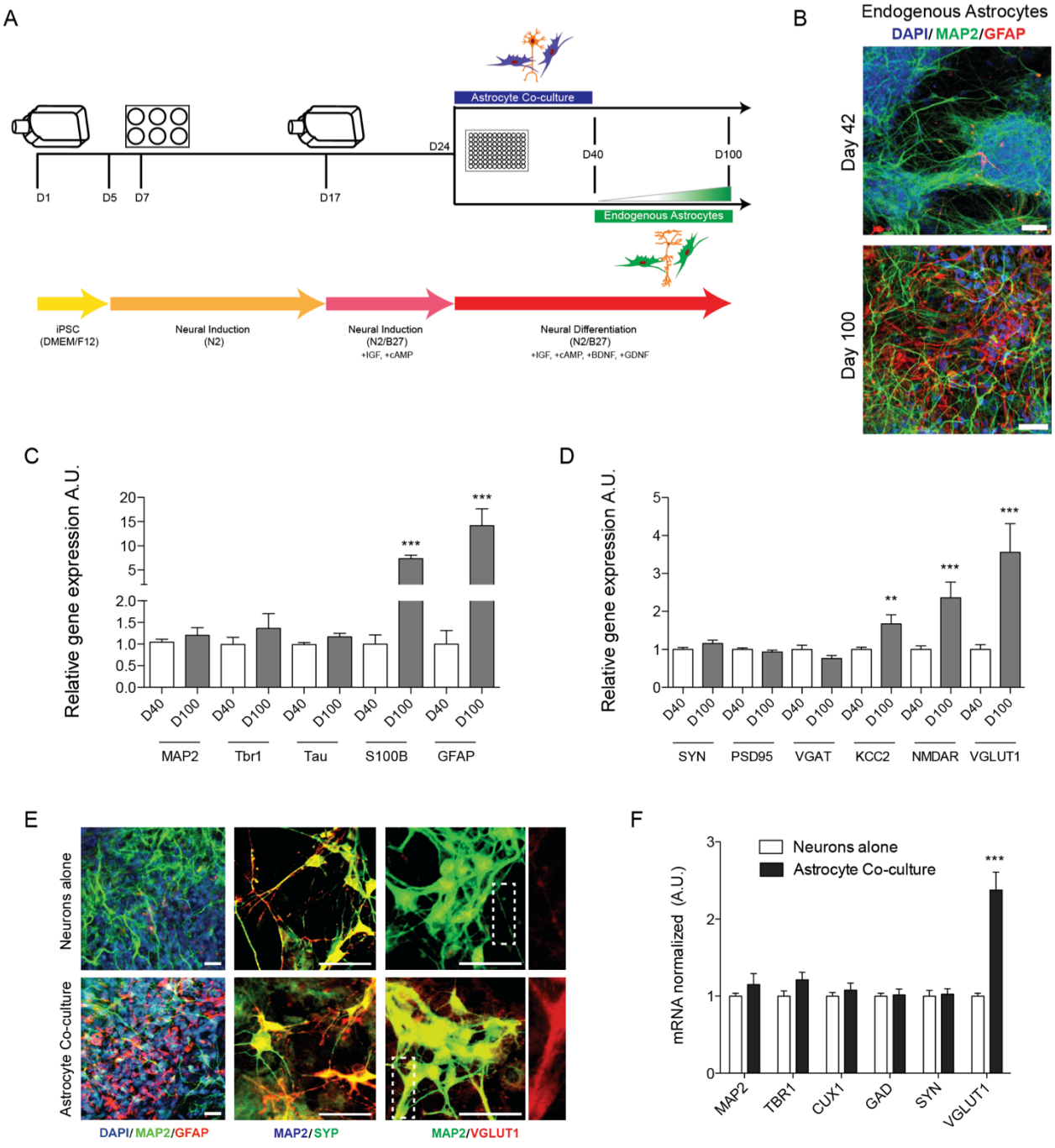

after plating at day 24 (Fig 2.7A, purple arm). Samples were harvested at day 40, before the emergence of endogenous astrocytes. By immunostaining, there were no qualitative differences in MAP2 or SYP expression between culture conditions (Fig 2.7E). However, we were able to visualize protein expression of VGLUT1 at day 40 only when differentiated neurons were co-cultured with exogenous astrocytes (Fig 2.7E, bottom row). qPCR analysis showed no changes in *MAP2*, *Tbr1, CUX1*, *GAD1* or *SYP* expression, but significantly increased *VGLUT1* (*SLC17A7*) expression at day 40 with astrocyte co-culture (Fig 2.7F).

DISCUSSION

With advancements in iPSC neuronal differentiation, it has been possible to examine human neural development and consequences of neurological disease-associated mutations at the cellular level. However, there exist a multitude of techniques to get from point A (iPSCs) to point B (differentiated neurons). Here, we evaluated several methods that are regularly used to generate forebrain cortical neurons, the "default" neuronal fate generated in the absence of exogenously provided patterning factors. We compared the outcomes of these protocols using gene expression, cell morphology, and protein expression by immunostaining (Table 2.1). Notably, these protocols resulted in robust expression of forebrain cortical transcription factors with negligible expression of midbrain and hindbrain transcription factors, as assessed by NanoString counts (Fig 2.8).

The percentage of cells expressing MAP2 was quantified following immunostaining from many of the various differentiation schemes employed here. The manual embryoid aggregate method with manual rosette selection as well as enzymatic rosette selection, generated the highest percentage of MAP2+ cells at day 40 of differentiation (~93% and ~85%, respectively). Other differentiation methods resulted in significantly fewer MAP2+ cells, such as monolayer dual SMAD inhibition differentiation (~45%), AggreWell embryoid aggregate differentiation

Table 2.1: Key comparisons of methods tested

Optimization Parameter	Key Benchmarks	Results	Notes
Differentiation Protocols			
Embryoid Aggregate vs. Monolayer Dual SMAD Inhibition	MAP2 %, qPCR of neuronal markers	Consistent neuronal yield with over 90% MAP2+ neurons using embryoid aggregate protocol. Decreased MAP2 % with dual SMAD inhibition method.	Zeng et al., 2010[19]; Chambers et al., 2009[8]
Aggregate Formation			
Manual vs. AggreWell	MAP2 %, qPCR of neuronal markers, brightfield microscopy	Manual formation more variable in aggregate size than Aggrewell. More consistent aggregate size and decreased MAP2 % using Aggrewell	Zeng et al., 2010[19]; StemCell Technologies
Plating Substrates			
Matrigel vs. POL	MAP2 %, qPCR of neuronal markers, immunostaining of NPC and iPSC markers	Matrigel promotes aggregate adherence better than POL at D7. Matrigel generates higher percentage of cortical neurons than POL at D40.	Matrigel from BD Biosciences. Lot-to-lot variations in protein content may affect outcome.
Progenitor Selection			
Manual/Cell Sort/Rosette Selection	MAP2 %, immunostaining of neuronal markers, Nanostring of NPC and non-neuronal markers	Rosette Selection is rapid and efficient but most permissive to non-neural cells. FACS and manual selection are equally effective for eliminating non-neural cells, but FACS is more time-consuming, has a lower yield, and selects NPCs with slightly different marker expression.	Manual: Zeng et al., 2010[19]; Hu et al. 2010[9]; FACS: BD Biosciences, Yuan et al., 2011[22]; Rosette Selection: StemCell Technologies
Co-culture			
None vs. Astrocytes	qPCR of neuronal markers, Nanostring of neuronal and astrocyte markers, immunostaining of neuronal markers	Astrocyte-free cultures express neuronal markers, but express less VGLUT1 than co-culture with astrocytes or cultures containing endogenous astrocytes	

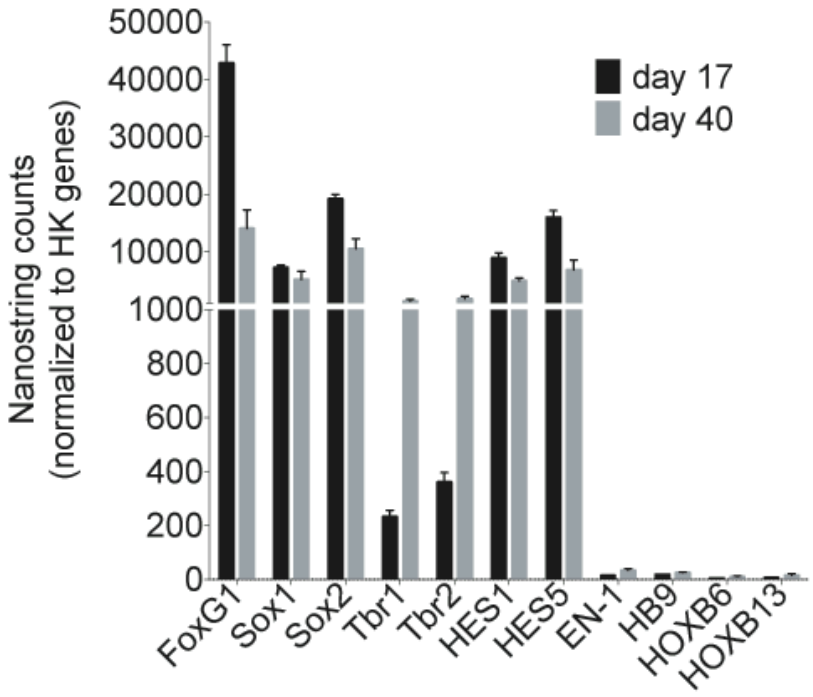

Figure 2.8. Expression of forebrain cortical vs. mid- or hindbrain transcription factors. Day 17 (NPC) or day 40 (neuron) RNA (same samples as used in Figures 2.5 or 2.6D, respectively). Nanostring counts show robust cortical transcription factor expression (FoxG1, Sox1, Sox2, Tbr1, Tbr2, HES1, HES5) and negligible expression of non-cortical transcription factors (EN-1, HB9, HOXB6, HOXB13).

(~46%), and PSA-NCAM sorting (~47%). It has been reported that different iPSC lines can vary in their ability to differentiate into neural cells[9,24-31]. For the embryoid aggregate-based differentiation variations examined herein, we did not observe obvious differences in efficiency of final neuronal differentiation or cell isolation method across cell lines. As this protocol includes steps to minimize or exclude undesirable cell types (e.g. selection of NPCs at day 17 and subsequent NPC culture in suspension), differences in differentiation capacity of different lines are minimized. However, we did note that certain lines differentiated better than others using the dual-SMAD inhibition protocol, with the most promising neuronal differentiations shown here.

At both plating steps of the embryoid aggregate protocol, Matrigel appears to be a superior substrate for promoting cell adherence and acquisition of neuronal identity. Use of Matrigel in the second plating generates >90% MAP2+ cells at day 40 of differentiation, compared to 56% MAP2+ cells using POL for the second plating. Plating cells on Matrigel at the second step leads to higher *MAP2* mRNA expression compared to the POL plating, despite whether the cells are plated as aggregates or dissociated and plated as a monolayer.

Matrigel likely serves as a better substrate due to its complex composition, which includes laminin, collagen IV and entactin, as well as a variety of growth factors that may promote neuronal differentiation. Notably, we have found that the lot-to-lot variability in Matrigel protein concentration is important for its differentiation- and adherence-promoting capability in the second plating step. Matrigel lots with higher initial protein concentrations are often more suitable for neuronal differentiation, even when plated at the same final protein concentration as lower protein concentration lots.

Isolation of NPCs may be done by a variety of methods, four of which we compared here: manual selection, enzymatic rosette selection, PSA-NCAM MACS, and FACS. PSA-NCAM sorting was less effective than manual NPC selection, with decreased neuronal purity in

PSA-NCAM+ sorted populations. Each of the remaining methods serves to enrich for NPCs, with some differences. Rosette selection appears to be more permissive to undesirable cell types, including pluripotent cells and endodermal cells, than manual selection or FACS. However, this method still generates neurons with high purity. The increased *HES1* expression with FACS could reflect increased purity of proliferative, undifferentiated neuroepithelial cells with FACS isolation[32,33]. Decreased *Tbr2* expression with FACS isolation suggests that this method may enrich for earlier neural progenitors at the expense of decreased enrichment for intermediate progenitors[34].

The less selective nature of the neural rosette selection reagent should be balanced with the cost (in both time and money) of each method. The manual selection method can be the most time-consuming and requires an experienced user, but requires no additional reagents and thus has the lowest reagent cost. The rosette selection method is fastest, but requires use of a proprietary reagent and so comes with a moderate cost. Finally, FACS selection is somewhat time-consuming and is the most expensive method. FACS also greatly reduces the total yield of viable cells, as there is significant cell loss due to prolonged dissociation and sorting time. The decision to choose one of these methods should be determined by the experimental setup and subsequent use of the isolated NPCs. If a highly sensitive and/or expensive method will be used on the isolated NPCs and purity is of the utmost importance, FACS isolation may be optimal. For experiments with few cell lines, manual selection is the cheapest and most effective method. If many different hiPSC lines are being differentiated, manual rosette selection would be time-prohibitive and rosette selection may be a better option. For an experiment in which NPCs will be further purified as neural aggregates (where many non-NPC fates will adhere while NPCs float as aggregates), rosette selection should be acceptable.

Culturing cells as NPCs has the advantage of expanding the neural progenitor pool for

subsequent neuronal differentiation without having to repeat days 1-17 of differentiation. This can save time and resources while increasing neuronal yield per differentiation experiment. If expansion of cells at the NPC stage is desired, our data suggest that maintenance as neural aggregates is superior to maintenance in a monolayer. Differentiation of later passage cells from aggregates show increased purity without obvious alterations in neuronal identity (as assayed by our 150-probe NanoString profile), whereas extended culture in monolayer decreased neuronal identity of the resulting cells. This may be related to the suspension nature of aggregate culture, wherein many contaminating cell types (e.g. neural crest cells) will preferentially adhere to the flask, whereas desirable cell types (e.g. NPCs) will be maintained as suspended aggregates. There also is a possibility that the slightly different media formulations of N2/B27 neural induction media versus neural progenitor media may alter cell fate and differentiation capacity (e.g. N2, cAMP, IGF-1 only in the former and FGF2, EGF only in the latter). Of note, neural aggregate size increases as cells proliferate, which eventually limits nutrient access for cells inside the aggregate. To allow cells to continue proliferating while maximizing access of cells to nutrients, neural aggregates can be broken up by gentle trituration[12]. Other groups have reported the establishment of NPC lines from hESCs or hiPSCs, often using more than one purification strategy to generate a highly pure and homogenous NPC population[23,35-41]. These strategies could be considered to generate NPC lines for longer-term use, but it is less sustainable to execute multiple purification techniques for many lines over multiple differentiations.

We also sought to study the emergence of endogenous astrocytes from neuronal cultures and examine the effect of exogenous astrocytes on iPSC-derived neurons. Over differentiation time, remaining neural progenitor cells begin to produce astrocytes, shown by increasing astrocyte marker expression and immunostaining by day 100. This confirms data presented by other groups showing emergence of astrocytes with long-term differentiation of

hiPSC-derived neural progenitors[42-44]. Concurrently, there is an increase in the excitatory neuronal marker *VGLUT1* (*SLC17A7*) (but not *SYN*) expression. Co-culture of human iPSC-derived neurons with mouse astrocytes promoted increased expression of *VGLUT1* (*SLC17A7*) at day 40, without affecting other neuronal subtype and synaptic markers. This suggests that exogenous astrocyte co-culture promotes the maturation of iPS-derived neurons without altering cell fate. These data are consistent with reports of accelerated hESC- and hiPSC-derived neuronal maturity with astrocyte co-culture[45,46]. Addition of exogenous astrocytes has the advantage of accelerating neuronal maturation, which may be desirable depending on the phenotype to be studied.

Achieving a "standard" protocol for neural differentiation across laboratories is unrealistic, due to the wide range of studied phenotypes and continual development of new protocols. Because small variations in methods can have dramatic effects on the resulting cells (and studied cellular properties), it is imperative that groups utilizing iPSC-derived neural cells carefully report how differentiation was performed and thoroughly characterize the resulting cell populations. The data included here provide a framework upon which researchers can base decisions regarding differentiation protocols. We hope this may aid in selection of optimal protocols, promote awareness of the many variables that can affect differentiation, and encourage detailed reporting of differentiation methods in published studies.

EXPERIMENTAL PROCEDURES

iPSC reprogramming and generation

Human iPSCs were obtained from the UCONN Stem Cell Core. Lines YK26, YZ1 and TZ1 were generated by retroviral vectors containing the reprogramming factors OCT4, SOX2, NANOG and LIN28 or c-Myc and KLF4[19]. Additional lines were reprogrammed by retroviral vectors containing the reprogramming factors OCT4, SOX2, c-Myc and KLF4 in conjunction with

the Harvard Stem Cell Institute as previously described[21].

iPSC karyotype analysis and characterization

The NanoString nCounter Human Karyotype Panel CNV CodeSet was used to assay iPSC genomic DNA every ~10 passages in order to ensure a stable chromosome number over time.

iPSC culture

iPSCs were cultured in iPSC media as previously described[21]. FGF2 (Millipore) was added fresh daily at 10 ng/ml. Cells were maintained at 37°C/5% CO_2 and were split as necessary based on colony growth (~6 days). iPSCs were manually groomed by removing any colonies with irregular borders, spontaneous differentiation or transparent centers, prior to splitting. iPSCs were maintained on a mouse embryonic fibroblast (MEF) feeder layer at 1.7-2.0 $x10^5$ cells/well of a 6-well plate (Globalstem).

Embryoid aggregate differentiation protocol

For the induction of forebrain neurons, iPSCs were differentiated using an embryoid body-based protocol[19], further optimized here. Colonies with irregular borders, spontaneous differentiation or transparent centers were removed prior to splitting. iPSC colonies were dissociated from MEFs at day 1 with collagenase (StemCell Technologies) and cultured as aggregates for 4 days in suspension with iPSC media (no FGF2), with media changes every day. At day 5, aggregates were washed 1X with N2 Neural Induction media and then fed with N2 Neural Induction media. On day 7, aggregates were plated on either Matrigel-coated culture dishes (used per the manufacturer's instructions, BD Biosciences) or poly-ornithine (4 µg/cm2) and laminin-coated plates (1 $\mu g/cm^2$), at about 20-30 aggregates/well. Cells were fed every 2 days with N2 Neural Induction media. Over the course of 10 days, primitive neuroepithelial (NE) structures were formed. By day 17 definitive NE structures were present and rosettes selected.

Neural rosette selection

Neural rosettes were selected manually, selected with STEMDiff Neural Rosette Selection reagent (used per the manufacturer's instructions, StemCell Technologies), or purified by MACS/FACS (further information below). For manual selection, cells with non-rosette morphology were scratched off culture plates using either sterile glass pipettes or sterile plastic pipette tips, followed by aspiration of undesirable material. Remaining rosettes were then scraped from the plate for further use. For each selection method, neural progenitor cells (NPCs) were either dissociated and plated for further differentiation or re-cultured in non-adherent culture flasks. Alternatively, NPCs were cultured as an adherent monolayer.

Neural progenitor cell monolayer culture

NPCs were maintained in neural progenitor media (+FGF2, EGF, heparin) and passaged 1:3 every 3-5 days or as necessary when confluent. Cells were split onto poly-ornithine (4μg/cm^2) and laminin (1μg/cm^2) coated plates. Plates were coated overnight in a humidified 37^{o}C incubator.

Neural aggregate culture

After NPC selection, cells were cultured in suspension and fed with N2/B27 neural induction media with cAMP and IGF-1. At day 24 (or as otherwise noted) cells maintained as aggregates were either plated as aggregates (3-5 aggregates/well of 96 well plate) or dissociated to single cells with Accutase (Invitrogen) (40,000-50,000 cells/well of 96 well plate) and plated on Matrigel for final differentiation in Neural Differentiation media with ROCK inhibitor (Stem RD, 10 μM). Cells plated at day 17 were also switched to neural differentiation media at day 24 for the remainder of the experiment. A full media change was performed every 2-3 days.

Astrocyte co-culture

Mouse astrocytes (Sciencell) were plated on top of differentiated human neurons at day

26 in a 1:1 media mix of Neural Differentiation media and Astrocyte media (Sciencell). Approximately 120,000 cells/cm^2 were plated. Prior to plating, mouse astrocytes were maintained per the manufacturer's directions.

Monolayer differentiation protocol

Using an alternate method for the induction of forebrain neurons, iPSCs were differentiated using a monolayer protocol[8,10]. iPSCs were manually groomed by removing any colonies with irregular borders, spontaneous differentiation or transparent centers. To initiate differentiation, cells were dissociated with Accutase (Invitrogen) for 30 minutes at room temperature. The cells were then triturated to form a single cell suspension and subsequently filtered through a 0.45 μm cell strainer to remove any cell clumps. Remaining cells on the plate were rinsed with additional iPSC media. Cells were washed and centrifuged (200g, 5 minutes) 2x and then resuspended in 10 mL iPSC media with ROCK inhibitor (StemRD, 10 μM). The cell suspension was then plated on a pre-coated gelatin 10cm plate, with a density of less than 200,000 cells/cm^2. 10 cm dishes were then incubated at 37°C for 30 minutes to allow MEFS time to adhere to the gelatin, without substantial adherence of iPSCs. After 30 minutes, suspended cells were washed with iPSC media + 10 μM ROCK inhibitor and centrifuged (200g, 5 minutes). Collected cells were resuspended with MEF conditioned media + 10 μM ROCK inhibitor. Cells were re-plated as a monolayer with a concentration of 20,000 cells/cm^2 in MEF conditioned media, supplemented with FGF2 (10 ng/mL). After cells reached 90% confluency, media was changed to 3N neural induction media (defined below) supplemented with Noggin (200ng/mL) and SB431542 (10 μM) [10]. Cells were split at day 11 using dispase and re-plated in neural differentiation media onto 96-well plates coated with Matrigel.

Aggregate formation using AggreWell

Aggregates were formed using either 400 or 800 μm well plates. Plates were used per

the manufacturer's instructions to form aggregates of either 3,000 or 8,000 cells/aggregate. 24 hours after AggreWell plating (day 2), aggregates were resuspended in low-adherence flasks and cultured in the appropriate medias listed above.

Medias

MEF Medium- 435 mL DMEM (Invitrogen), 5 mL 100x Penicillin/Streptomycin (Invitrogen), 5 mL 100x L-glutamine (Invitrogen), 50 mL FBS (Invitrogen)

iPS Medium- 390 mL DMEM/F12, 100 mL KOSR (Invitrogen), 5 mL 100x Penicillin/Streptomycin/Glutamine (Invitrogen), 5 mL 100x MEM-NEAA (Invitrogen), 50 μM b-mercaptoethanol (Invitrogen), with the addition of fresh FGF2 (Millipore, 10 ng/mL) to the medium

N2 Neural Induction Medium- 490 mL DMEM/F12 (Invitrogen), 5 mL N2 supplement (Invitrogen), 5 mL 100x MEM-NEAA (Invitrogen), and Heparin (Sigma-Aldrich, 2 μg/mL).

N2/B27 Neural Induction Medium- 480 mL DMEM/F12, 5 mL N2 supplement (Invitrogen), 10 mL B27 supplement (Invitrogen), 5 mL MEM-NEAA (Gibco) and 2 μg/ml Heparin (Sigma-Aldrich), with the addition of fresh cAMP (1 μM) (Sigma) and IGF1 (PeproTech, 10 ng/mL) to the medium.

Neural Differentiation Medium- 490 mL Neurobasal medium (Invitrogen), 5 mL N2 supplement (Invitrogen), 5 mL 100x MEM-NEAA (Invitrogen), and 10 mL B27 supplement (Invitrogen), with the addition of fresh cAMP (Sigma, 1 μM), BDNF, GDNF, and IGF-1 (all PeproTech, 10 ng/mL) to the medium.

Neural Progenitor Medium: 350 mL DMEM (Invitrogen), 150 mL F12 (Invitrogen), 5 mL 100x sodium pyruvate (Invitrogen, only if not included in DMEM formulation), 5 mL 100x Penicillin/Streptomycin/Glutamine (Invitrogen), 10 mL B27 supplement (Invitrogen) with the addition of fresh EGF (Sigma, 20 ng/mL), FGF2 (Millipore, 20 ng/ml), and heparin (Sigma, 5 μg/ml) to the medium.

MEF Conditioned Medium- 2.8x10^6 mouse embryonic fibroblasts (GlobalStem) were plated on a gelatin-coated dish (1 hour at room temperature) in MEF media. 24 hours later, cells were washed 1X with iPS media and fed with fresh iPS media. Media was incubated for 24 hours and then collected. Additional iPS media was conditioned every 24 hours for up to 2 weeks. All media was pooled and sterile-filtered before use. 10 ng/mL of FGF2 was added fresh before use.

3N Neural Induction Medium- 485 mL DMEM/F12, 5 ml 100x MEM-NEAA (5 μg/mL), 5 mL N2 supplement (Invitrogen), 10 mL B27 supplement (Invitrogen), insulin (Sigma, 5 μg/mL), 50 μM b-mercaptoethanol (5 μg/mL), 5 mL 100x Penicillin/Streptomycin/Glutamine (5 μg/mL).

qPCR

RNA was purified from individual samples and processed through a PureLink RNA Mini Kit (Ambion), followed by reverse transcription using SuperScript II (Invitrogen). qPCR was performed using Fast SYBR Green Master Mix (Applied Biosystems) and run on a ViiA 7 System (Applied Biosystems). Samples were assayed with 3 technical replicates. Data was analyzed using the $\Delta\Delta C_T$ method and expression was normalized to GAPDH expression[47]. Primer efficiency was calculated for each pair of primers and the slope of the dilution line was found to be within the appropriate range. Dissociation curves also showed single peak traces, indicating template-specific products.

Primers

Oct4- Forward: TGGGCTCGAGAAGGATGTG; Reverse: GCATAGTCGCTGCTTGATCG

MAP2- Forward: AACCGAGGAAGCATTGATTG; Reverse: TTCGTTGTGTCGTGTTCTCA

Tbr1- Forward: TCACCGCCTACCAGAACAC; Reverse: GTCCATGTCACAGCCGGT

GAPDH- Forward: GGGAGCCAAAAGGGTCATCA; Reverse: TGGTTCACACCCATGACGAA

CUX1- Forward: GATGCCACCGCAACGGTAT; Reverse: GGACTGCTCACTTTCATCCTG

VGLUT1- Forward: ACTCAGCTCCAGCGTCTCC; Reverse: GAGTTTCGGAAGCTAGCGG

GAD1- Forward: AGGAGAGGCAATCCTCCAAGA; Reverse: ATCCCGGTCGCTGTTTTCAC

SYP- Forward: AGGGAACACATGCAAGGAG; Reverse: CTTAAACACGAACCACAGG

NanoString analysis

We utilized a custom 150 gene probe set designed by NanoString Technologies (nCounter Gene Expression Assay, see Table 2.2) to analyze gene expression for a large number of genes from an individual sample. All assays were performed following NanoString protocols. The initial hybridization reactions were carried out with 100-1000 ng RNA. Post-hybridization samples were processed using the nCounter Prep-station. Following run completion, the cartridge was scanned at max resolution (~1000 images/sample) using the nCounter Digital Analyzer. Data were analyzed using the nSolver Analysis Software and normalized to a set of 7 house-keeping genes (HK) or to the total gene set, as noted. HK genes: *GAPDH, GUSB, HPRT1, LDHA, POLR2A, RPL13a* and *RPL27*.

Antibodies

Immunostaining was performed with the following antibodies: Abcam: [MAP2 (1:5000), Oct4 (1:1000), Tbr1 (1:200), Sox2 (1:1000), SYP (1:250), VGLUT1 (1:500), GFAP (1:1000)]; Millipore, Tbr2 (1:500); Dako, Tau (1:200); Sigma, TuJ1 (1:1000); R+D, Nestin (1:1000); Covance, Pax6 (1:300) and Novus, Sox 1 (1:200). Secondary antibodies were supplied by Jackson ImmunoResearch: anti-chicken Cy2/Cy3/Cy5, anti-rabbit Cy2/Cy3, anti-mouse Cy2/Cy3. Invitrogen, TOPRO3 & DAPI (nuclear markers, 1:1000).

Immunocytochemistry and microscopy

Cultures were fixed with 4% paraformaldehyde, followed by membrane permeabilization and blocking with 0.1% Triton X-100 in donkey serum (Jackson ImmunoResearch). Samples were incubated with primary and secondary antibodies (see Antibodies) overnight and 1 hour,

Table 2.2: Probe sequences for NanoString assay

NanoString genes	Probe Sequence
AFP	GGAGCGGCTGACATTATTATCGGACACTTATGTATCAGACATGAAATGACTCCAG TAAACCCTGGTGTTGGCCAGTGCTGCACTTCTTCATATGCCAACA
Cux1	ACAAACAGCCCTGGAAAAAACTCGAACAGAATTATTTGACCTGAAAACCAAATAC GATGAAGAAACTACTGCAAAGGCCGACGAGATTGAAATGATCATG
EN1	GCAGCATTTTTGAAAAGGGAGAAAGACTCGGACAGGTGCTATCGAAAAATAAGAT CCATTCTCTATTCCCAGTATAAGGGACGAAACTGCGAACTCCTTA
FoxG1	CTGACAAGTCTATCTCTAAGAGCCGCCAGATTTCCATGTGTGCAGTATTATAAGTT ATCATGGAACTATATGGTGGACGCAGACCTTGAGAACAACCTAA
GFAP	AAGCAGATGAAGCCACCCTGGCCCGTCTGGATCTGGAGAGGAAGATTGAGTCGC TGGAGGAGGAGATCCGGTTCTTGAGGAAGATCCACGAGGAGGAGGT
HES1	ATCTGAGCACAGAAAGTCATCAAAGCCTATTATGGAGAAAAGACGAAGAGCAAGA ATAAATGAAAGTCTGAGCCAGCTGAAAACACTGATTTTGGATGCT
HES5	CAGCCTGTAGAGGACTTTCTTCAGGGCCCGTAGCTGCTGGGCGTACCCCTGGCA GGCGGGCTGTGCCGCGGGCACATTTGCCTTTTGTGAAGGCCGAACT
HNK1	GAGGGAGGCCTGAGCACACTGCTTTGGAAATTATTCTAAACACAAAAAAGGGAAA GAAAATGTTATTTCTCCCTAAGTCAGGAGCATGCAGAGCTAGCCC
HB9	CCTGGGCGCTTCCCTTTTAAGCAAGGGCGCCTCACCTGCTCTTCAAGAAACAGC GAGAGGGAGACCCAGGGGGCTGAAACTTGAACTCTGGTTCTTTTAA
HOXB6	CACCCATTCCTTTAAATCCGGAGGGGGAAAAAATCCCAAGGTCTGCAAAGGCGC GGCGCTCGGACTATAAAACACAACAAATCATAAACCCGGCGGAGCA
HOXB13	CCACCAGGGTTCCCAAAGAACCTGGCCCAGTCATAATCATTCATCCTGACAGTGG CAATAATCACGATAACCAGTACTAGCTGCCATGATCGTTAGCCTC
KCC2	ATGAGAGCGACATCTCAGCTTACACCTATGAGAAGACGTTGGTGATGGAGCAGC GTTCCCAGATCCTCAAACAGATGCATTTAACCAAGAATGAGCGGGA
MAP2	TACTCTGTATGCTGGGATTCCGAGGTTCCAACACACTGTTACAAATCTGTGGGGG GTTTCTTTCTTCTGATAATTCTAGAGCCTGTTACCATAGAAAGGC
MYOD1	TGTAATCTATTCCTGTAAATAAGAGTTGCTTTGCCAGAGCAGGAGCCCCTGGGGC TGTATTTATCTCTGAGGCATGGTGTGTGGTGCTACAGGGAATTTG
Nanog	TGCAGGCAACTCACTTTATCCCAATTTCTTGATACTTTTCCTTCTGGAGGTCCTAT TTCTCTAACATCTTCCAGAAAAGTCTTAAAGCTGCCTTAACCTT
Nestin	CAGAGAATCACAAATCACTGAGGTCTTTAGAAGAACAGGACCAAGAGACATTGAG AACTCTTGAAAAAGAGACTCAACAGCGACGGAGGTCTCTAGGGGA
NMDAR	TTCAAGAGAGTGCTGATGTCTTCCAAGTATGCGGATGGGGTGACTGGTCGCGTG GAGTTCAATGAGGATGGGGACCGGAAGTTCGCCAACTACAGCATCA
Oct4	AAGTTCTTCATTCACTAAGGAAGGAATTGGGAACACAAAGGGTGGGGGCAGGGG AGTTTGGGGCAACTGGTTGGAGGGAAGGTGAAGTTCAATGATGCTC
Pax6	GGGAATTAAAGGCCTTCAGTCATTGGCAGCTTAAGCCAAACATTCCCAAATCTAT GAAGCAGGGCCCATTGTTGGTCAGTTGTTATTTGCAATGAAGCAC
PSD95	TGCCCTGAAGAATGCGGGTCAGACGGTCACGATCATCGCTCAGTATAAACCAGA AGAGTACAGCCGATTCGAGGCCAAGATCCACGACCTTCGGGAACAG
S100B	AGAAGGCCATGGTGGCCCTCATCGACGTTTTCCACCAATATTCTGGAAGGGAGG GAGACAAGCACAAGCTGAAGAAATCCGAACTCAAGGAGCTCATCAA
Satb1	TTCCGAAATCTACCAGTGGGTACGCGATGAACTGAAACGAGCAGGAATCTCCCA GGCGGTATTTGCACGTGTGGCTTTTAACAGAACTCAGGGCTTGCTT

Table 2.2 (Continued)

Sox1	AAAGCGTTTTCTTTGCTCGAGGGGACAAAAAAGTCAAAACGAGGCGAGAGGCGA AGCCCACTTTTGTATACCGGCCGGCGCGCTCACTTTCCTCCGCGTT
Sox2	AAAGCGTTTTCTTTGCTCGAGGGGACAAAAAAGTCAAAACGAGGCGAGAGGCGA AGCCCACTTTTGTATACCGGCCGGCGCGCTCACTTTCCTCCGCGTT
Synapsin I	GGATCTACTTCTGTTTTAGAACCTCCACATTCCTGAAGACCTCCGCCCCTGGTTT CCCCAGAGGGCGTTTTCCTTCCTGGAAGTGCCCAAATACCAGGCA
Tau	ATTGGGTCCCTGGACAATATCACCCACGTCCCTGGCGGAGGAAATAAAAAGATTG AAACCCACAAGCTGACCTTCCGCGAGAACGCCAAAGCCAAGACAG
Tbr1	GCCGTCTGCAGCGAATAAGTGCAGGTCTCCGAGCGTGATTTTAACCTTTTTTGCA CAGCAGTCTCTGCAATTAGCTCACCGACCTTCAACTTTGCTGTAA
Tbr2	TCTCTAGATTCCAATGATTCAGGAGTATACACCAGTGCTTGTAAGCGAAGGCGGC TGTCTCCTAGCAACTCCAGTAATGAAAATTCACCCTCCATAAAGT
TWIST1	CAACTCCCAGACACCTCGCGGGCTCTGCAGCACCGGCACCGTTTCCAGGAGGC CTGGCGGGGTGTGCGTCCAGCCGTTGGGCGCTTTCTTTTTGGACCTC
VGAT	CAGGCTGGAACGTGACCAACGCCATCCAGGGCATGTTCGTGCTGGGCCTACCCT ACGCCATCCTGCACGGCGGCTACCTGGGGTTGTTTCTCATCATCTT
VGLUT1	TCGGCTACTCGCACTCCAAGGGCGTGGCCATCTCCTTCCTGGTCCTAGCCGTGG GCTTCAGCGGCTTCGCCATCTCTGGGTTCAACGTGAACCACCTGGA
Vimentin	GAGGAGATGCTTCAGAGAGAGGAAGCCGAAAACACCCTGCAATCTTTCAGACAG GATGTTGACAATGCGTCTCTGGCACGTCTTGACCTTGAACGCAAAG
Housekeeping genes:	
B2M	CGGGCATTCCTGAAGCTGACAGCATTCGGGCCGAGATGTCTCGCTCCGTGGCCT TAGCTGTGCTCGCGCTACTCTCTCTTTCTGGCCTGGAGGCTATCCA
GAPDH	TCCTCCTGTTCGACAGTCAGCCGCATCTTCTTTTGCGTCGCCAGCCGAGCCACAT CGCTCAGACACCATGGGGAAGGTGAAGGTCGGAGTCAACGGATTT
GUSB	CGGTCGTGATGTGGTCTGTGGCCAACGAGCCTGCGTCCCACCTAGAATCTGCTG GCTACTACTTGAAGATGGTGATCGCTCACACCAAATCCTTGGACCC
HPRT1	TGTGATGAAGGAGATGGGAGGCCATCACATTGTAGCCCTCTGTGTGCTCAAGGG GGGCTATAAATTCTTTGCTGACCTGCTGGATTACATCAAAGCACTG
LDHA	AACTTCCTGGCTCCTTCACTGAACATGCCTAGTCCAACATTTTTTCCCAGTGAGTC ACATCCTGGGATCCAGTGTATAAATCCAATATCATGTCTTGTGC
POLR2A	TTCCAAGAAGCCAAAGACTCCTTCGCTTACTGTCTTCCTGTTGGGCCAGTCCGCT CGAGATGCTGAGAGAGCCAAGGATATTCTGTGCCGTCTGGAGCAT
RPL13a	AGTCCAGGTGCCACAGGCAGCCCTGGGACATAGGAAGCTGGGAGCAAGGAAAG GGTCTTAGTCACTGCCTCCCGAAGTTGCTTGAAAGCACTCGGAGAAT
RPL27	GGGCCGGGTGGTTGCTGCCGAAATGGGCAAGTTCATGAAACCTGGGAAGGTGG TGCTTGTCCTGGCTGGACGCTACTCCGGACGCAAAGCTGTCATCGTG

respectively. Imaging was performed using a Zeiss LSM710 confocal microscope and images were acquired using ZEN black software. Software was used to pseudo-color images and add scale bars. Quantified MAP2 immunostaining was performed blind on at least 3 images per condition, with at least 200 cells counted per image, using ImageJ software (NIH).

MACS

Day 17 embryoid aggregate-differentiated cells were utilized for MACS. Cells were dissociated to single cells using Accutase (Invitrogen) + 10 μM ROCK inhibitor (StemRD) for 30-45 minutes. Cell clumps were removed using a 70 μm strainer (Pre-separation filter, Miltenyi). Cells were sorted per the manufacturer's instructions using Anti-PSA-NCAM Microbeads (Miltenyi) and related equipment (MS columns and MACS Separator, Miltenyi).

FACS

Day 17 embryoid aggregate-differentiated cells were utilized for FACS. Cells were dissociated using Accutase (Invitrogen) for 25 minutes and treated per the manufacturer's protocol (Human Neural Cell Sorting Kit, BD Biosciences). The kit was used to isolate CD184+/CD44-/CD271-/CD24+ neural stem cells, which were separated from neural crest and other non-neuronal cells using a BD FACSAria cell sorter. Cells were either harvested after sorting for RNA analysis or plated on Matrigel for immunostaining and confocal microscopy analysis.

Statistics

Data was analyzed using GraphPad PRISM 5/6 software. Values are expressed as means ±S.D. or ±SEM, as indicated by figure legend text. See Table 2.3 for experimental details. Statistical significance was tested by either an unpaired Student's *t*-test (two-tailed), by one-way ANOVA with a Tukey's post-test, or by two-way ANOVA with Holm-Sidak multiple comparisons correction (as indicated by figure legend text). Statistically significant differences were determined by *P* values less than 0.05.

Table 2.3: Number of iPSC lines, differentiations and well numbers contributing to each figure

Figure	Lines used	Independent differentiations	n
Figure 2.1	YZ1, TZ1, YK26, fAD 2a	1D: 6	1D: iPS n=14-15, D17 n=23-25, D40-50 n=19-26
Figure 2.2	YZ1, YK26	*2D: 2	*2D: iPS n=2-3, D1 n=3-4, D7 n=3-4, D11 n=5-6, D40 n=5
Figure 2.3	YZ1, YK26	3B: 4, 3D: 2	3B: manual n=43, AG3000 n=21, AG8000 n=26; 3D: Manual/Aggrewell n=10
Figure 2.4	YZ1, YK26	4H/J: 2	4H: Matrigel and POL n=10; 4J: Matrigel and POL n=22
Figure 2.5	YZ1, YK26	5F,G: manual: 5; rosette: 18; FACS: 6	5F,G: Manual n=15; Rosette n=30; FACS n=6
Figure 2.6	YZ1, YK26, fAD 2a,b	6B/D: 2	6B: n=11-26; 6D: n=6, both time-points
Figure 2.7	YZ1, YK26	7C,D: 6; 7F: 5	7C,D: D40-50 n=29-38, D100 n=15-19; 7F: Neurons alone n=20 for MAP2, TBR1, CUX1, GAD1, n= 37 for SYP, n=38 for VGLUT1; Astrocyte Co-culture n=17 for GAD1, n=18 for MAP2, TBR1, CUX1, n=27 for SYP, n=25 for VGLUT1
* 10/10 differentiations without dissociation failed. 3/5 differentiations with dissociation yielded MAP2+ cells.			

REFERENCES

1. Gaspard, N. *et al.* An intrinsic mechanism of corticogenesis from embryonic stem cells. *Nature* **455,** 351–357 (2008).

2. Zhang, S. C., Wernig, M., Duncan, I. D., Brüstle, O. & Thomson, J. A. In vitro differentiation of transplantable neural precursors from human embryonic stem cells. *Nat Biotechnol* **19,** 1129–1133 (2001).

3. Li, X.-J. & Zhang, S.-C. In vitro differentiation of neural precursors from human embryonic stem cells. *Methods Mol. Biol.* **331,** 169–177 (2006).

4. Pankratz, M. T. *et al.* Directed neural differentiation of human embryonic stem cells via an obligated primitive anterior stage. *Stem Cells* **25,** 1511–1520 (2007).

5. Eiraku, M. *et al.* Self-organized formation of polarized cortical tissues from ESCs and its active manipulation by extrinsic signals. *Cell Stem Cell* **3,** 519–532 (2008).

6. Erceg, S. *et al.* Differentiation of human embryonic stem cells to regional specific neural precursors in chemically defined medium conditions. *PLoS ONE* **3,** e2122 (2008).

7. Elkabetz, Y. *et al.* Human ES cell-derived neural rosettes reveal a functionally distinct early neural stem cell stage. *Genes & Development* **22,** 152–165 (2008).

8. Chambers, S. M. *et al.* Highly efficient neural conversion of human ES and iPS cells by dual inhibition of SMAD signaling. *Nat Biotechnol* **27,** 275–280 (2009).

9. Hu, B.-Y. *et al.* Neural differentiation of human induced pluripotent stem cells follows developmental principles but with variable potency. *Proceedings of the National Academy of Sciences* **107,** 4335–4340 (2010).

10. Shi, Y., Kirwan, P. & Livesey, F. J. Directed differentiation of human pluripotent stem cells to cerebral cortex neurons and neural networks. *Nat Protoc* **7,** 1836–1846 (2012).

11. Srikanth, P. & Young-Pearse, T. L. Stem Cells on the Brain: Modeling Neurodevelopmental and Neurodegenerative Diseases Using Human Induced Pluripotent Stem Cells. *J. Neurogenet.* 1–25 (2014). doi:10.3109/01677063.2014.881358

12. Liu, Y. *et al.* Directed differentiation of forebrain GABA interneurons from human pluripotent stem cells. *Nat Protoc* **8,** 1670–1679 (2013).

13. Takazawa, T. *et al.* Maturation of spinal motor neurons derived from human embryonic stem cells. *PLoS ONE* **7,** e40154 (2012).

14. Hu, B.-Y. & Zhang, S.-C. Differentiation of spinal motor neurons from pluripotent human

stem cells. *Nat Protoc* **4,** 1295–1304 (2009).

15. Cooper, O. *et al.* Differentiation of human ES and Parkinson's disease iPS cells into ventral midbrain dopaminergic neurons requires a high activity form of SHH, FGF8a and specific regionalization by retinoic acid. *Mol Cell Neurosci* **45,** 258–266 (2010).

16. Perrier, A. L. *et al.* Derivation of midbrain dopamine neurons from human embryonic stem cells. *Proc Natl Acad Sci USA* **101,** 12543–12548 (2004).

17. Li, X.-J. *et al.* Specification of motoneurons from human embryonic stem cells. *Nat Biotechnol* **23,** 215–221 (2005).

18. Swistowski, A. *et al.* Efficient generation of functional dopaminergic neurons from human induced pluripotent stem cells under defined conditions. *Stem Cells* **28,** 1893–1904 (2010).

19. Zeng, H. *et al.* Specification of region-specific neurons including forebrain glutamatergic neurons from human induced pluripotent stem cells. *PLoS ONE* **5,** e11853 (2010).

20. Li, X.-J. *et al.* Coordination of sonic hedgehog and Wnt signaling determines ventral and dorsal telencephalic neuron types from human embryonic stem cells. *Development* **136,** 4055–4063 (2009).

21. Muratore, C. R. *et al.* The familial Alzheimer's disease APPV717I mutation alters APP processing and Tau expression in iPSC-derived neurons. *Human Molecular Genetics* **23,** 3523–3536 (2014).

22. Yuan, S. H. *et al.* Cell-surface marker signatures for the isolation of neural stem cells, glia and neurons derived from human pluripotent stem cells. *PLoS ONE* **6,** e17540 (2011).

23. Sheridan, S. D. *et al.* Epigenetic characterization of the FMR1 gene and aberrant neurodevelopment in human induced pluripotent stem cell models of fragile X syndrome. *PLoS ONE* **6,** e26203 (2011).

24. Vitale, A. M. *et al.* Variability in the generation of induced pluripotent stem cells: importance for disease modeling. *Stem Cells Translational Medicine* **1,** 641–650 (2012).

25. Boulting, G. L. *et al.* A functionally characterized test set of human induced pluripotent stem cells. *Nat Biotechnol* **29,** 279–286 (2011).

26. Amenduni, M. *et al.* iPS cells to model CDKL5-related disorders. *Eur J Hum Genet* **19,** 1246–1255 (2011).

27. Bock, C. *et al.* Reference Maps of human ES and iPS cell variation enable high-throughput characterization of pluripotent cell lines. *Cell* **144,** 439–452 (2011).

28. Di Giorgio, F. P., Boulting, G. L., Bobrowicz, S. & Eggan, K. C. Human embryonic stem cell-derived motor neurons are sensitive to the toxic effect of glial cells carrying an ALS-causing mutation. *Cell Stem Cell* **3,** 637–648 (2008).

29. Meyer, J. S. *et al.* Modeling early retinal development with human embryonic and induced pluripotent stem cells. *Proceedings of the National Academy of Sciences* **106,** 16698–16703 (2009).

30. Osafune, K. *et al.* Marked differences in differentiation propensity among human embryonic stem cell lines. *Nat Biotechnol* **26,** 313–315 (2008).

31. Koyanagi-Aoi, M. *et al.* Differentiation-defective phenotypes revealed by large-scale analyses of human pluripotent stem cells. *Proceedings of the National Academy of Sciences* **110,** 20569–20574 (2013).

32. Kageyama, R., Ohtsuka, T. & Kobayashi, T. The Hes gene family: repressors and oscillators that orchestrate embryogenesis. *Development* **134,** 1243–1251 (2007).

33. Ohtsuka, T., Sakamoto, M., Guillemot, F. & Kageyama, R. Roles of the basic helix-loop-helix genes Hes1 and Hes5 in expansion of neural stem cells of the developing brain. *J Biol Chem* **276,** 30467–30474 (2001).

34. Englund, C. *et al.* Pax6, Tbr2, and Tbr1 are expressed sequentially by radial glia, intermediate progenitor cells, and postmitotic neurons in developing neocortex. *Journal of Neuroscience* **25,** 247–251 (2005).

35. Colleoni, S. *et al.* Long-term culture and differentiation of CNS precursors derived from anterior human neural rosettes following exposure to ventralizing factors. *Exp Cell Res* **316,** 1148–1158 (2010).

36. Conti, L. *et al.* Niche-independent symmetrical self-renewal of a mammalian tissue stem cell. *PLoS Biol.* **3,** e283 (2005).

37. Daadi, M. M., Maag, A.-L. & Steinberg, G. K. Adherent self-renewable human embryonic stem cell-derived neural stem cell line: functional engraftment in experimental stroke model. *PLoS ONE* **3,** e1644 (2008).

38. Hong, S., Kang, U. J., Isacson, O. & Kim, K.-S. Neural precursors derived from human embryonic stem cells maintain long-term proliferation without losing the potential to differentiate into all three neural lineages, including dopaminergic neurons. *J Neurochem* **104,** 316–324 (2008).

39. Kim, D.-S. *et al.* Highly pure and expandable PSA-NCAM-positive neural precursors from human ESC and iPSC-derived neural rosettes. *PLoS ONE* **7,** e39715 (2012).

40. Koch, P., Opitz, T., Steinbeck, J. A., Ladewig, J. & Brüstle, O. A rosette-type, self-renewing human ES cell-derived neural stem cell with potential for in vitro instruction and synaptic integration. *Proceedings of the National Academy of Sciences* **106,** 3225–3230 (2009).

41. Shin, S. *et al.* Long-term proliferation of human embryonic stem cell-derived neuroepithelial cells using defined adherent culture conditions. *Stem Cells* **24,** 125–138 (2006).

42. Espuny-Camacho, I. *et al.* Pyramidal neurons derived from human pluripotent stem cells integrate efficiently into mouse brain circuits in vivo. *Neuron* **77,** 440–456 (2013).

43. Shi, Y. *et al.* A human stem cell model of early Alzheimer's disease pathology in Down syndrome. *Science Translational Medicine* **4,** 124ra29 (2012).

44. Shi, Y., Kirwan, P., Smith, J., Robinson, H. P. C. & Livesey, F. J. Human cerebral cortex development from pluripotent stem cells to functional excitatory synapses. *Nat Neurosci* **15,** 477–486 (2012).

45. Johnson, M. A., Weick, J. P., Pearce, R. A. & Zhang, S.-C. Functional neural development from human embryonic stem cells: accelerated synaptic activity via astrocyte coculture. *J Neurosci* **27,** 3069–3077 (2007).

46. Tang, X. *et al.* Astroglial cells regulate the developmental timeline of human neurons differentiated from induced pluripotent stem cells. *Stem Cell Research* **11,** 743–757 (2013).

47. Livak, K. J. & Schmittgen, T. D. Analysis of relative gene expression data using real-time quantitative PCR and the 2(-Delta Delta C(T)) Method. *Methods* **25,** 402–408 (2001).

Chapter III.

Genomic *DISC1*-disruption in hiPSCs alters Wnt signaling and neural cell fate

Priya Srikanth, Karam Han, Dana G. Callahan, Eugenia Makovkina, Christina R. Muratore,

Matthew A. Lalli, Kenneth S. Kosik, Dennis J. Selkoe, Tracy L. Young-Pearse

Experimental contributions to this chapter: P.S. led and was involved in every aspect of the project. D.G.C. assisted with sample preparation, cell culture, and Western blots. K.H. and E.M. assisted with sample preparation and imaging. C.R.M. performed MEA experiments. M.L. and K.K. assisted with RNA-seq analyses.

ABSTRACT

Genetic and clinical association studies have identified disrupted-in-schizophrenia 1 (*DISC1*) as a strong candidate risk gene for major mental illness. *DISC1* is interrupted by a balanced chr(1;11) translocation in a Scottish family, in which the translocation predisposes to the development of psychiatric disorders. We investigate the consequences of *DISC1* interruption in human neural cells using TALENs or CRISPR-Cas9 to target the *DISC1* locus. We show that disease-relevant *DISC1* targeting results in decreased DISC1 protein expression, increased canonical Wnt signaling activity, and a shift in neural cell fate. DISC1-dependent Wnt signaling and cell fate changes can be reversed by antagonizing the Wnt pathway during a critical window in neural progenitor development. These experiments suggest that *DISC1*-disruption increases Wnt signaling, which alters the identity of neural progenitors, thereby modifying Wnt responsiveness and cell fate. These studies shed light on the roles of DISC1 during human brain development, and further our understanding of the pathogenesis of major mental illness.

INTRODUCTION

Schizophrenia is a debilitating psychiatric disorder that affects ~1% of the world's population. Schizophrenia and other major mental illnesses (MMIs) are widely regarded to result from a combination of genetic susceptibility and environmental insults[1-3]. A diagnosis of schizophrenia is marked by clinical and neurobiological heterogeneity, without striking universal pathological hallmarks[4]. However, clinical and genetic studies indicate that schizophrenia and other MMIs are likely diseases of altered circuitry resulting from disruptions in neurodevelopment[5-8]. The precise developmental step(s) and affected cell type(s) that lead to altered circuitry are not known, but are also likely to be heterogeneous. The recent expansion of GWAS studies has identified many interesting but generally weak genetic linkages[9-14]. There are

also rare strong genetic variants that have been associated with mental illness, including various CNVs and a balanced translocation interrupting the gene disrupted in schizophrenia 1 (*DISC1*)[1,15,16]. *DISC1* was initially associated with mental illness upon the discovery that its coding sequence is interrupted by a balanced chr(1;11) translocation in a Scottish family, in which the translocation cosegregates with schizophrenia, bipolar disorder and major depression[17-19]. The diversity of phenotypes in subjects harboring the translocation suggests that a subtle underlying disruption in development may exist, which predisposes subjects to MMI by increasing vulnerability to other environmental and genetic risk factors. While such rare variants are not likely to contribute significantly to the incidence of sporadic disease, they offer valuable opportunities for investigation. Studying biological effects of known rare mutations with high penetrance has the potential to illuminate cellular and molecular processes implicated in disease pathophysiology, as has been demonstrated with familial mutations in neurodegenerative diseases[20].

Though the genetics of major mental illness are incredibly complex, genetic association studies have implicated *DISC1* as a candidate risk gene for schizophrenia, schizoaffective disorder, bipolar disorder, major depression, and autism spectrum disorders (ASD)[21-29]. The involvement of *DISC1* and other susceptibility genes in both adult-onset major mental illnesses and childhood-onset ASD indicate that a disturbance of proper neurodevelopment may contribute to each of these disorders[30-32]. This hypothesis is further strengthened by involvement of mental illness risk-associated proteins in neurodevelopmental processes, such as neural progenitor proliferation, neuronal migration, neurite outgrowth, neuron maturation, and myelination (reviewed here[30,33-35]). DISC1 has been implicated in several neurodevelopmental processes, including proliferation, Wnt signaling, synaptic maturation, neurite outgrowth, and neuronal migration (reviewed here[30]). In addition, many known DISC1 interacting proteins have independently been associated with neuropsychiatric diseases, further implicating this network

of proteins in the pathophysiology of mental illness (reviewed here[30]). In order to understand how DISC1 mutations increase susceptibility to mental illness, intensive study is necessary to elucidate the pathways by which it normally functions in the human brain and how disease-predisposing *DISC1* variants affect neurodevelopment.

The discovery of the Scottish chr(1;11) translocation stimulated several hypotheses regarding the pathological mechanisms of this abnormality. The balanced translocation could lead to a C-terminally-truncated DISC1 protein, a DISC1 fusion protein, or loss of protein production from one allele via nonsense-mediated decay. Several rodent models have been developed to address these possibilities, using mutations in endogenous *DISC1*, overexpression of truncated DISC1, or *DISC1* knockdown. These models have identified interesting effects of *DISC1* perturbation on cell signaling, neuronal migration, morphology, physiology, and in some instances, behavior[36-45]. Without brain tissue from human t(1;11) carriers, it is difficult to know which (if any) of these models mimic the human disease state.

DISC1 has a very complex splicing pattern, with over 50 splice variants identified to date in human brain[46]. Given the complexities of *DISC1* splicing, a detailed study examining the consequences of *DISC1* interruption is best accomplished in human brain cells. The advent of human induced pluripotent stem cells (iPSCs) that can be differentiated to many somatic lineages, including neurons, has allowed a dramatic expansion in the investigation of cellular mechanisms of human disease[47-49]. The ability to recapitulate aspects of corticogenesis by differentiating iPSCs makes these cells a particularly powerful tool for studying disorders of human neurodevelopment, including major mental illnesses[50-54]. While somatic cell-derived iPSCs from multiple subjects can be used to study disease processes, there exist wide variations in genomic content and epigenetic modifications across cell lines that alter gene expression and cellular phenotypes[55]. When using iPSCs to model a subtle disease phenotype *in vitro*, the effects of background genetic variation between control and patient samples can

obscure or falsely identify differences between these groups. In the study of a known disease-predisposing mutation, one way to avoid this problem is to use “isogenic” lines, which differ only at a single locus. Here, we study the consequences of *DISC1* disruption in isogenic stem cell lines generated using transcription activator-like effector nucleases (TALENs) or clustered regularly interspaced short palindromic repeats (CRISPR)-Cas9 to interrupt *DISC1* near the site of the balanced translocation or else in an exon common to all isoforms. In these studies, multiple isogenic clonal lines are compared for each genotype, allowing for careful study of the effects of genomic *DISC1* interruption on gene expression and neuronal development.

Recent models of mental illness using human iPSCs have utilized sporadic disease lines[56-60] as well as rare variants[61,62]. These studies have implicated multiple neurodevelopmental steps that may be disrupted in the pathophysiology of mental illness. Here, we investigate the effects of disease-relevant genomic *DISC1* disruption on DISC1 expression and human cortical neurodevelopment. We explore the functional consequences of genomic *DISC1*-interruption in human iPSC-derived human cortical neural progenitor cells (NPCs) and neurons. We find that disease-relevant *DISC1*-interruption decreases DISC1 expression due to nonsense-mediated decay and increases NPC Wnt signaling, which subtly alters cell fate in NPCs and neurons. This study further clarifies the functions of DISC1 and identifies how these functions are perturbed in a human disease model, providing insights into a form of neurodevelopmental disruption that may contribute to the pathophysiology of mental illness.

RESULTS

Genomic *DISC1* exon 8 interruption results in loss of DISC1 expression due to nonsense-mediated decay

In order to investigate the effects of *DISC1* interruption at the site of the Scottish translocation in human neurons, we introduced *DISC1* frameshift mutations into control iPSCs.

Mutations were introduced either into exon 8 (near the site of the translocation) or exon 2 (intended to disrupt all known coding isoforms) (Fig 3.1). This strategy allowed us to examine in detail the effects of genomic *DISC1* interruption on DISC1 expression and neural progenitor and neuronal phenotypes in the absence of other genetic variation. Using either TALEN or CRISPR-Cas9 technology, we generated isogenic human iPSC lines that are wild-type (wt) or have frameshift mutations in either exon 8 (monoallelic: exon 8 wt/mut or "ex8wm", biallelic: "exon 8 mut/mut" or "ex8mm") or exon 2 (biallelic: exon 2 mut/mut or "ex2mm"). Exon 8 mutations were generated using a TALEN pair (constructed using a hierarchical ligation procedure[63]), while exon 2 mutations were generated by CRISPR-Cas9 targeting. Using these techniques, multiple *DISC1* mutant genotypes were attained at each locus. Exon 8 targeting resulted in 2 distinct heterozygous 1 bp deletions and 1 heterozygous 1 bp insertion, as well as a 1 bp deletion/1 bp insertion compound heterozygous genotype (Fig 3.1C). These indels result in the introduction of a premature termination codon (PTC) within 3 codons (exon 8 ins 1 bp) or 27 codons (exon 8 del 1 bp). Exon 2 targeting resulted in two distinct biallelic mutation genotypes: a 1 bp/2 bp insertion compound heterozygote and a 1 bp insertion homozygote (Fig 3.1D), resulting in a PTC within 12 codons (exon 2 ins 1 bp) or 65 codons (exon 2 ins 2 bp). Targeted cells maintained iPSC colony morphology, expressed iPSC markers Nanog, Oct4, SSEA4, Sox2, and TRA-1-60 (Fig 3.1E; Fig 3.2), and maintained a euploid karyotype (Fig 3.3). No predicted off-target cleavage events were detected using RNA-sequencing data (data not shown, see Experimental Procedures). Multiple iPSC clones of each genotype were used for the studies described herein to minimize the potential effects of clonal variability and off-target cleavage events (Table 3.1).

Genomic *DISC1* interruption has been hypothesized to cause expression of a truncated or mutant DISC1 or to decrease DISC1 expression from the mutated allele[30]. The limited evidence that exists from t(1;11) patients suggests that the translocation lowers DISC1

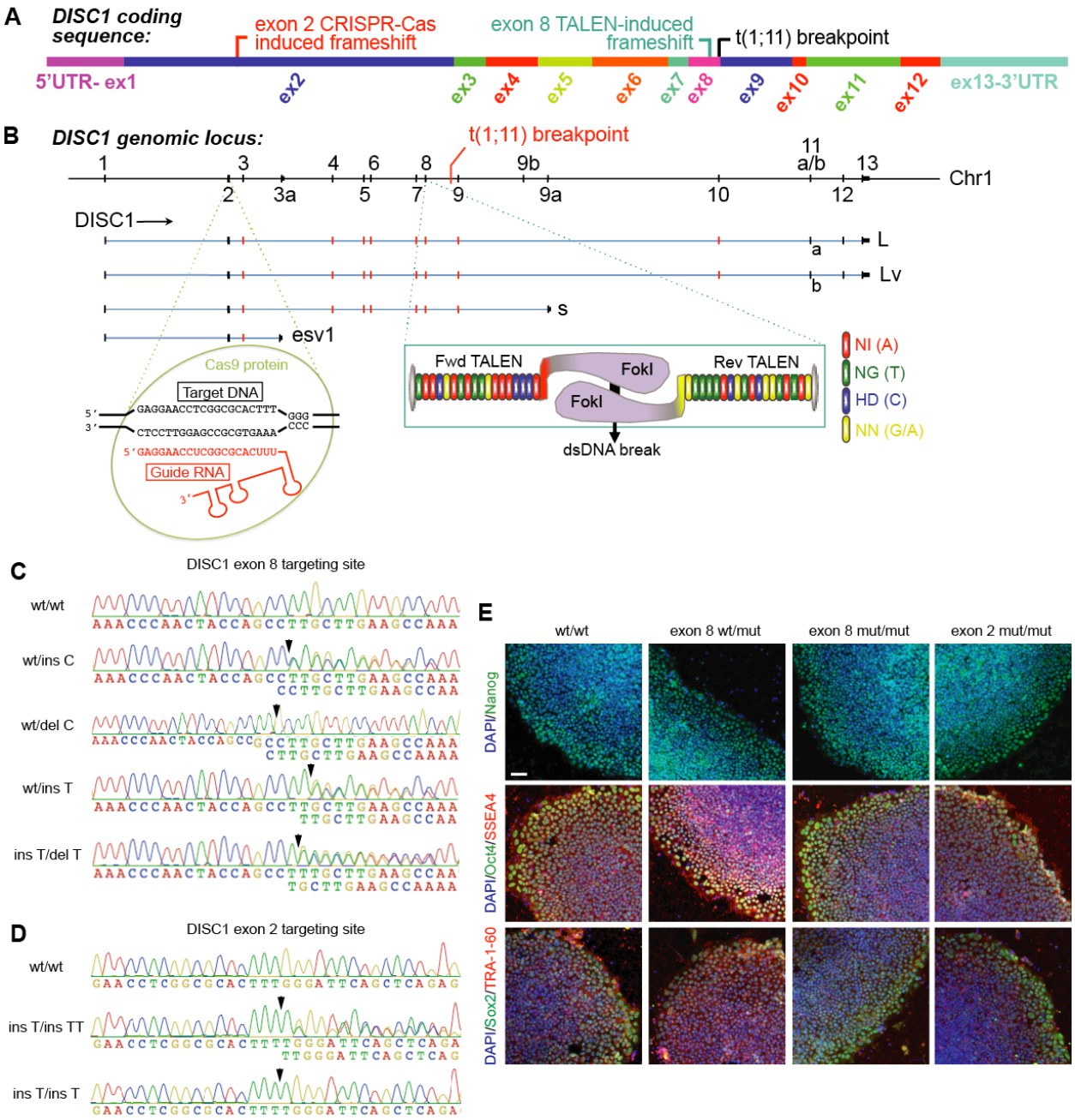

Figure 3.1. **Targeting the human *DISC1* locus**. **(A)** Diagram of the coding sequence of *DISC1*, with the sites of induced frame shifts and the Scottish chr(1;11) translocation indicated. **(B)** Diagram of the *DISC1* genomic locus, with exons shown on the top line and sample transcripts shown below. A selection of alternatively spliced isoforms are shown in red. **(C,D)** Wild-type and mutant sequences around the exon 8 (**C**) or exon 2 (**D**) targeting sites, obtained by Sanger sequencing of targeted iPS colonies. Mutation sites are indicated with black arrowheads. **(E)** Immunostaining for pluripotent cell markers Nanog, Oct4, SSEA4, Sox2, and TRA-1-60 following genome-editing. Scale bar = 50 um.

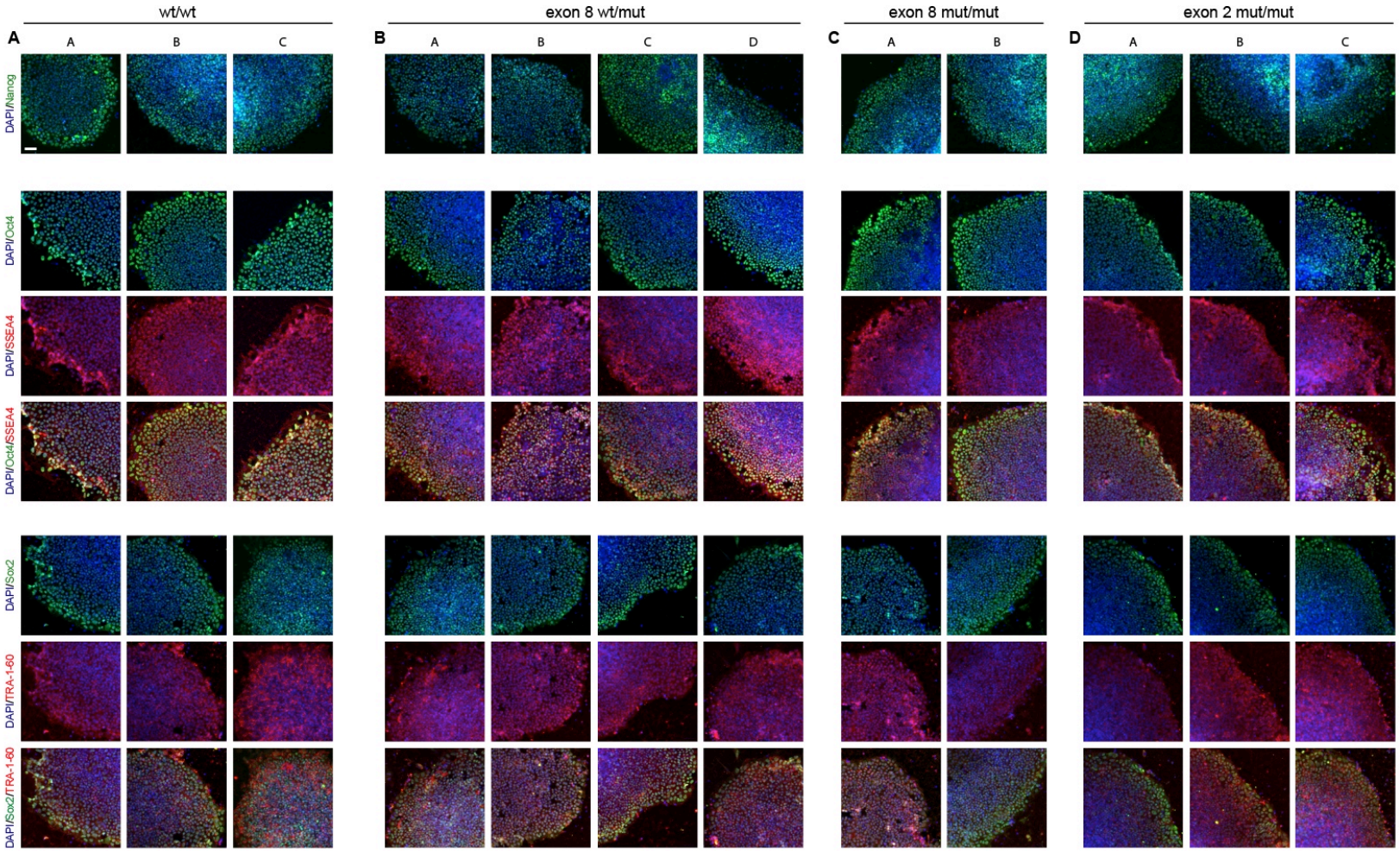

Figure 3.2. **Characterization of iPSC lines**. Example immunostaining of iPSC colonies from wt/wt **(A)**, exon 8 wt/mut **(B)**, exon 8 mut/mut **(C)**, and exon 2 mut/mut (**D)** lines. Markers are labeled at left; cell lines are labeled at top. Scale bar = 50 um.

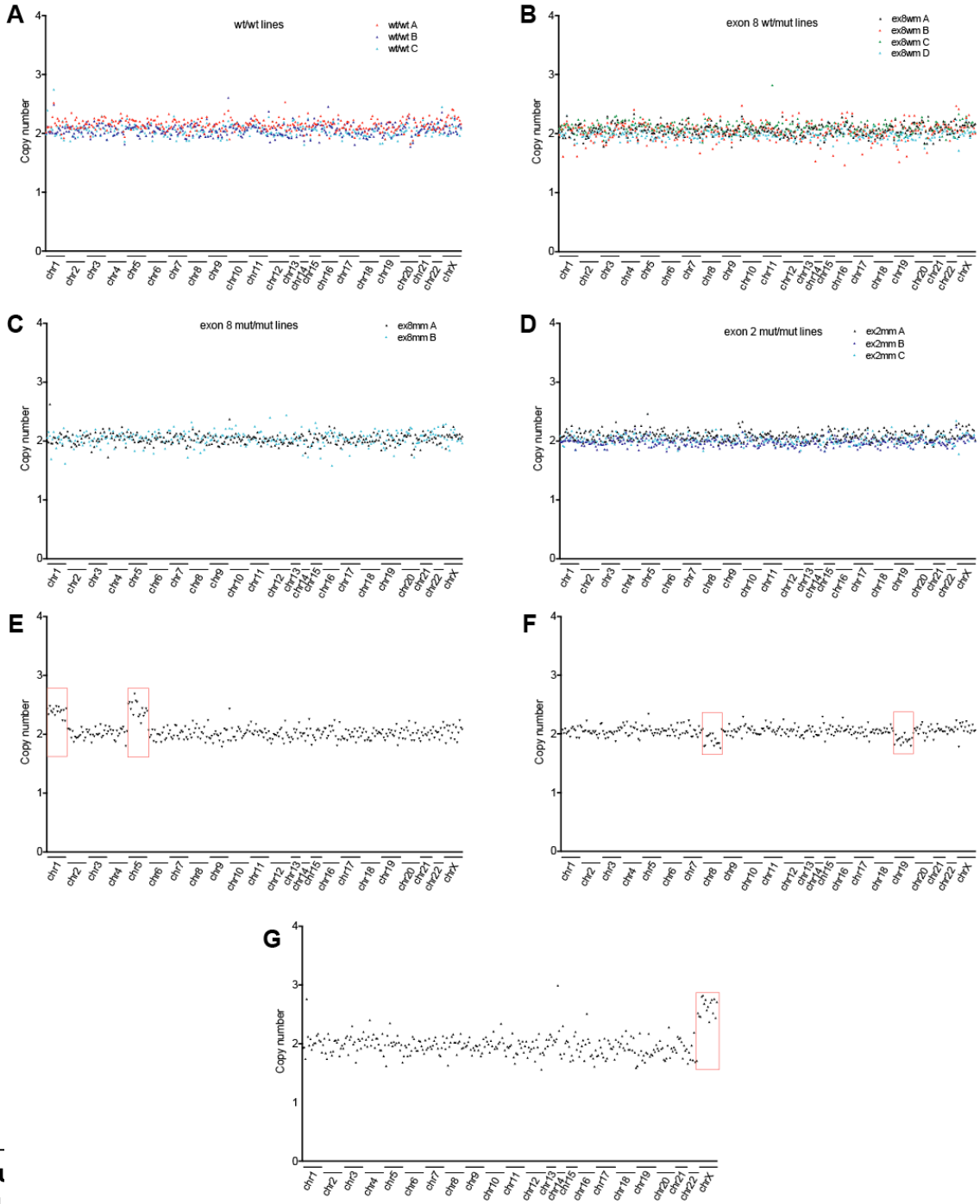

Figu …he
and … analyses are shown for wt/wt lines **(A)**, exon 8 wt/mut lines **(B)**, exon 8 mut/mut lines **(C)**, and exon 2 mut/mut lines **(D)**. Examples of abnormal CNV profiles that resulted in discarding iPSC lines are shown in **(E-G)**, with abnormalities in red boxes. Karyotyping was performed routinely on all lines to examine genomic stability.

Table 3.1. Summary of lines used to generate data. (x) indicates data not shown.

Genotype	Line	DISC1 Mutation	Pluripotency marker expression	CNV karyotyping	DISC1 expression qPCR	DISC1 expression WB	DISC1 RNA CHX	DISC1 protein CHX	Nanostring d17	Nanostring d50	WB d40	Ngn2 iN d28 Nanostring	RNA-seq d17	RNA-seq d50	Luciferase, NPCs, no patterning	Luciferase, iPSCs	Luciferase, NPCs, DMSO/cyc	Nanostring d40, DMSO/cyc	Luciferase, NPCs, DMSO/XAV/CHIR	Nanostring d40, DMSO/XAV/CHIR
wt/wt	A	--	x	x	x	x	x	x	x	x	x	x	x	x	x	x	x	x	x	x
	B		x	x		x		x	x	x	x	x		x	x	x	x	x	x	x
	C		x	x	x	x	x	x	x	x	x			x	x	x	x	x	x	x
	D		(x)	(x)					x				x			x				
	E		(x)	(x)	x		x		x	x					x	x				
	F		(x)	(x)					x	x			x	x	x	x				
exon 8 wt/mut	A	wt/del C	x	x	x	x	x	x	x	x	x	x	x	x	x	x	pooled	pooled	pooled	pooled
	B		x	x	x	x	x		x	x				x	x					
	C		x	x	x	x	x	x												
	D	wt/ins T	x	x	x	x	x	x			x	x			x					
	E	wt/ins C	(x)	(x)					x	x					x	x				
	F		(x)	(x)	x		x		x	x					x	x				
exon 8 mut/mut	A	ins T/ del T	x	x	x	x	x		x	x	x		x	x	x	x	pooled	pooled		
	B		x	x	x	x	x		x	x	x			x	x	x				
	C		(x)	(x)					x						x	x				
	D		(x)	(x)					x	x			x		x	x				
exon 2 mut/mut	A	ins T/ ins T	x	x	x	x	x	x	x	x	x		x	x	x		pooled	pooled		
	B		x	x	x	x	x	x	x	x	x		x		x					
	C		x	x	x	x	x	x	x	x	x		x	x	x					
	D			(x)	x		x		x	x				x	x					
	E	ins T/ ins TT		(x)	x		x		x	x				x	x					
	F			(x)	x	x	x		x	x	x			x	x					
	G			(x)	x	x	x		x	x	x		x		x					
	H			(x)					x	x			x		x					
	I		(x)	(x)	x	x	x				x									

transcript and protein levels in patient-derived cell lines[64]. However, the effects of t(1;11) have not yet been studied in human neurons. Based on the genomic structure surrounding the t(1;11)breakpoints, if splicing occurs between *DISC1* exon 8 and the next available exon on chr11, the resulting transcript would contain a premature stop codon. The introduction of a PTC into a coding RNA often results in nonsense-mediated decay (NMD) if the PTC occurs prior to the last exon-exon junction of the transcript[65]. Thus, we hypothesized that genomic *DISC1* interruption would cause decay of those PTC-containing mRNAs that extended at least one exon past the interruption (i.e. beyond exon 8 for exon 8 targeting; beyond exon 2 for exon 2 targeting). Given the complexity of *DISC1* splicing, we chose to analyze transcription at multiple *DISC1* coding regions to assess levels of distinct groups of isoforms. For example, exons 12 and 13 are only present in the longest *DISC1* transcripts (L and Lv), whereas exon 2 is present in all identified *DISC1* coding transcripts[46]. We therefore predicted that exon 8 targeting would decrease expression of longer splice variants from the mutant allele(s), whereas biallelic exon 2 targeting would ablate DISC1 expression, due to degradation of all coding RNAs.

To examine the effects of genomic *DISC1* interruption on *DISC1* RNA expression, RNA was harvested from NPCs and/or differentiated neurons. Wild-type and *DISC1*-targeted iPSCs were differentiated to neural fates using an embryoid aggregate-based protocol[66], which results in definitive neuroepithelium by day 17 and expression of neuronal makers past day 25. We sought to characterize the expression of multiple isoforms of *DISC1* by examining RNA expression of distinct exons or exon junctions. Initial qPCR analyses of day 40 neuronal samples revealed that the presence of a single exon 8 mutant allele (exon 8 wt/mut) does not significantly decrease total *DISC1* expression (assessed by qPCR of *DISC1* exon 2) but does significantly decrease expression of the longest *DISC1* isoforms (*DISC1* exon 12/13) (Fig 3.4A,B). Biallelic exon 8 interruption (exon 8 mut/mut) significantly decreased total *DISC1* and long *DISC1* transcripts (Fig 3.4A,B). Surprisingly, the biallelic exon 2 mutation did not reduce

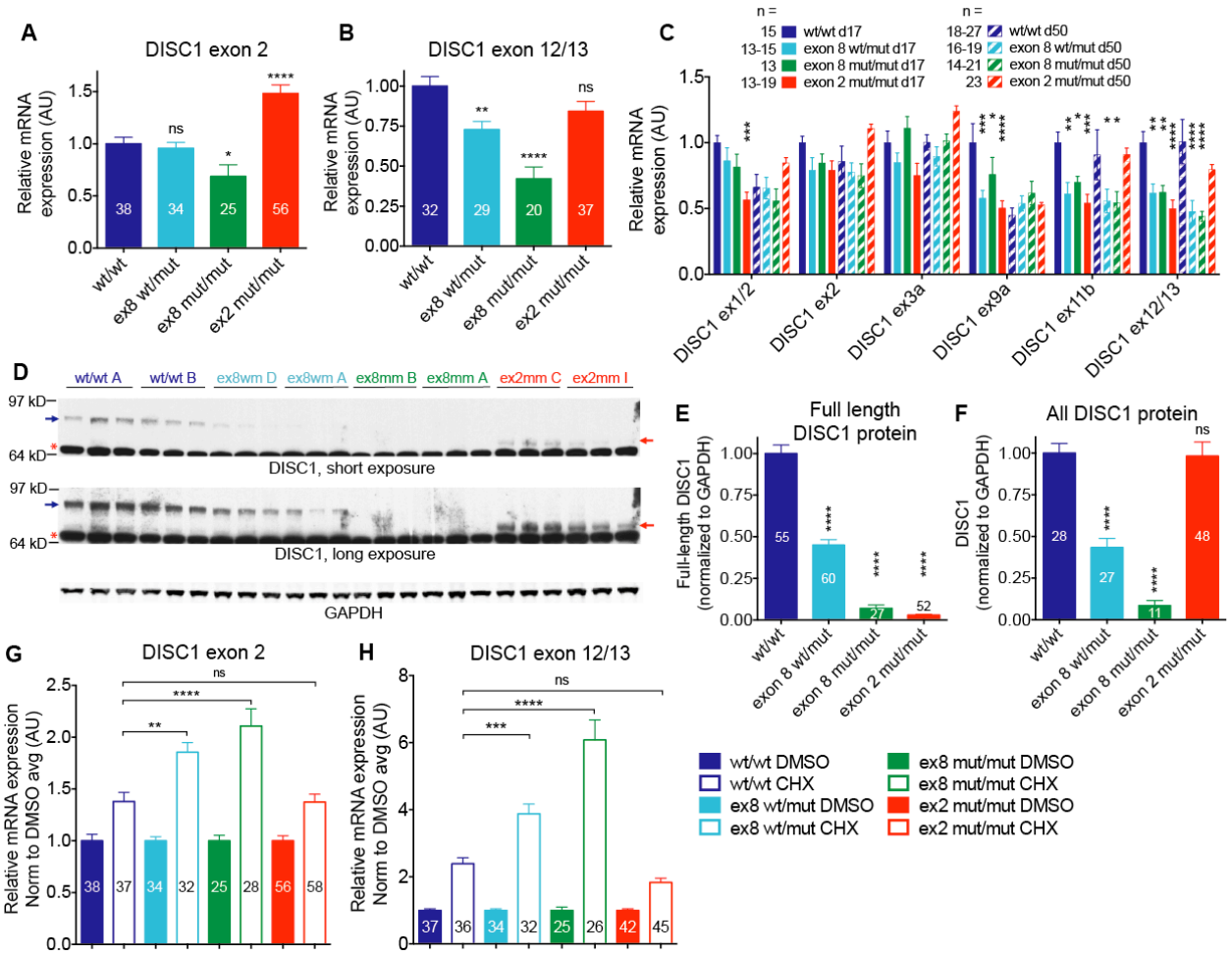

Figure 3.4. *DISC1* exon 8-disruption causes loss of full length *DISC1* expression via NMD. **(A,B)** Wild-type and DISC1-disrupted iPSCs were differentiated to day 40 neural fates and RNA was harvested for qRT-PCR of *DISC1* exon 2 (**A**) or exons 12/13 (**B**). Expression is normalized to *GAPDH* and wt/wt levels. (**C**) iPSCs were differentiated to NPCs (day 17) and neurons (day 50) and RNA was harvested for NanoString. *DISC1* probe expression is normalized to expression of 8 housekeeping genes & average wt/wt d17 levels. Statistics shown versus wt of corresponding differentiation day. (**D**) Representative Western blot of DISC1 in day 40 neuronal lysates. Full length DISC1 is indicated with blue arrows; novel truncated DISC1 is indicated by red arrows. The red asterisks denote a nonspecific band. **(E,F)** Quantification of full-length (**E**) or all (**F**) DISC1 from Western blots of day 40 neuronal lysates, normalized to GAPDH and wt/wt levels. **(G,H)** Day 40 neurons were treated with 100 ug/ml cycloheximide (CHX) or vehicle (DMSO) for 3 hrs, followed by RNA harvest and qRT-PCR for exon 2 (**G**) or the exon 12/13 junction (**H**) of *DISC1*. Expression normalized to *GAPDH* and average DMSO expression within genotype. All data derived from at least 5 independent differentiations. Stats: (C) 2-way ANOVA, (A,B,E-H) 1-way ANOVA. Mean ± SEM shown. ns = not significant, * $p < 0.05$, ** $p < 0.01$, *** $p < 0.001$, **** $p < 0.0001$.

DISC1 expression, but instead modestly increased total *DISC1* (exon 2) RNA levels and did not alter expression of long isoforms (Fig 3.4A). We further investigated levels of various *DISC1* isoforms in NPCs (day 17) and neurons (day 50) using a custom NanoString probeset which included probes targeting multiple *DISC1* exons. The NanoString analyses confirmed the qPCR data, showing isoform-specific effects of genomic *DISC1* disruption, where introduction of a PTC into exon 8 decreased expression of longer (extending beyond exon 8) but not shorter *DISC1* transcripts at day 17 (NPC) and day 50 (neuron) (Fig 3.4C). Unexpectedly, exon 2 targeting appeared to decrease *DISC1* expression at day 17 (Fig 3.4C), but either did not change or increased expression of various *DISC1* isoforms at days 40-50 (Fig 3.4A-C).

To investigate the effects of *DISC1* interruption at the protein level, we performed Western blots of day 40 neuronal lysates and analyzed DISC1 expression using a monoclonal antibody we generated against the C-terminus of DISC1. Single allelic DISC1 exon 8 mutation resulted in a ~55% decrease in full-length DISC1 protein expression, while biallelic exon 8 mutation led to total loss of full length protein, consistent with a loss of expression from longer transcripts (Fig 3.4D-F). Biallelic exon 2 targeting showed a total loss of full length protein, but surprisingly led to the expression of a shorter, novel DISC1 protein product in day 40 neural cells (Fig 3.4D, red arrows). This truncated protein was expressed at levels nearly identical to that of wild-type full-length DISC1 (Fig 3.4F). Although unexpected, the truncated DISC1 protein resulting from exon 2 mutation provided an opportunity to include in our analyses the effects of an independent *DISC1* mutation in a system that was isogenic to our disease-relevant (exon 8-disruption) *DISC1* disruption model. As several prior studies have demonstrated that misexpression of a mutant truncated DISC1 can phenocopy *DISC1* knockdown[30], we used our exon 2- and exon 8-targeted cells to explore whether these observations would hold true in a human neuronal context.

To determine whether the observed changes in DISC1 expression in the exon 2- and

exon 8-targeted cells were due to NMD of RNAs containing a PTC, we treated day 40 neurons with cycloheximide (CHX), which inhibits NMD by interfering with the "pioneer" round of translation required to detect the PTC[67]. Analysis of *DISC1* expression after CHX treatment revealed significantly increased NMD of exon 2- and exon 12/13-containing mRNAs in exon 8- but not exon 2-targeted cells (Fig 3.4G,H). These data suggest that introduction of a PTC into *DISC1* exon 8, but not exon 2, results in NMD of PTC-containing transcripts. This result supports a loss-of-function (LOF) model, whereby genomic *DISC1* interruption at exon 8 causes loss of DISC1 expression from the disrupted allele. In the chr(1;11) balanced translocation, splicing of exon 8 to the next available exon (in chromosome 11) results in a premature termination codon within 2 or 61 codons (depending on usage of 2 different predicted exons), prior to the last exon of the chr11 gene. This fusion transcript should therefore also recruit the NMD pathway, as observed in our model. The common effect of 1 bp insertion or deletion on decreasing *DISC1* expression suggests that the number of codons (3 or 27) preceding the PTC does not alter targeting of the transcript for NMD.

We further explored the effects of *DISC1* genomic disruption on DISC1 protein stability, using cycloheximide (CHX) to prevent translation in day 40 neurons. DISC1 protein was remarkably refractory to turnover under these conditions, showing very little or no degradation over 24 hours (Fig 3.5). These data contrast with a recent report of a 1-4 hr DISC1 half-life in PC12 cells[68]. Efficacy of the CHX treatment was confirmed by detecting APP levels, which showed a half life of ~4 hr for this protein, in agreement with measurements of APP half life in the literature[69-73]. There was no indication from these studies that DISC1 mutation resulted in an unstable DISC1 protein product.

Genomic *DISC1* interruption alters expression of NPC fate markers

To examine the effects of *DISC1* disruption in NPC and neuronal cell populations, we characterized broader gene expression profiles and cell fate in wild-type and *DISC1*-targeted

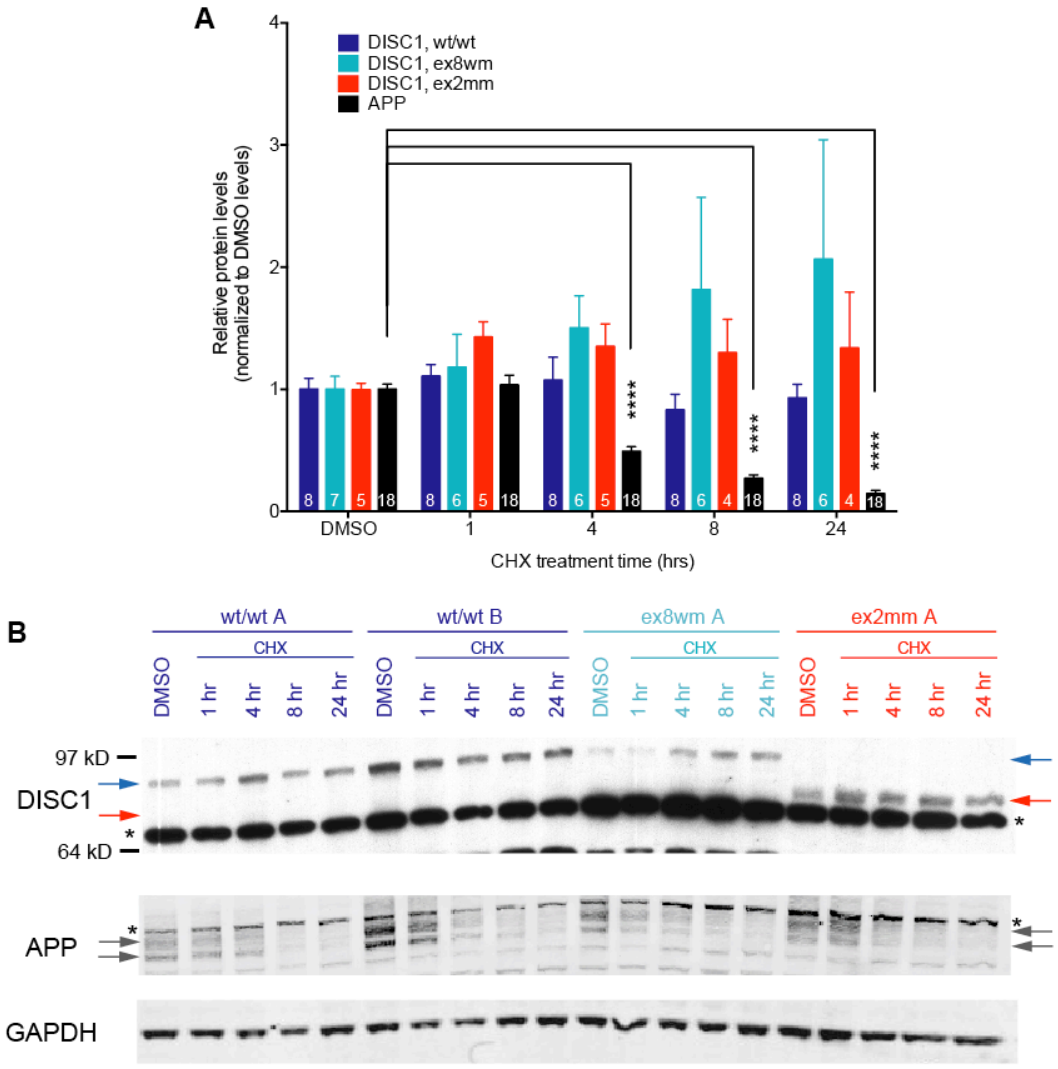

Figure 3.5. ***DISC1* mutations do not destabilize DISC1 protein**. Day 40 neurons were treated with DMSO (vehicle) or 100 ug/ml cycloheximide (CHX) for the indicated time periods. Cells were then lysed and equal protein amounts were used for Western blotting. **(A)** Quantification of protein levels over time with CHX treatment. Mean ± SEM shown. Statistics: two-way ANOVA, **** $p < 0.0001$. Sample number shown in white within bars. **(B)** Representative Western blot showing DISC1, APP, and GAPDH protein levels. Blue arrows indicate full-length DISC1, red arrows indicate exon 2 truncated DISC1, grey arrows indicate APP, asterisks indicate nonspecific bands. Data derived from at least 3 independent differentiations.

cells. Neural differentiation resulted in dorsal forebrain NPC fates across all genotypes (Fig 3.6A, expressing Nestin, Pax6, Brn2, Ngn2, FoxG1, Tbr2). In order to quantitatively measure expression of a broad selection of neural markers, we used a custom NanoString codeset to assay RNA expression in rosette-selected day 17 NPCs. NanoString analyses showed that *DISC1* exon 8 and exon 2 interruption significantly decreased FoxG1 and Tbr2 expression (Fig 3.6B). There also was decreased Sox1 and increased Pax6 expression in exon 2-targeted NPCs, suggesting that exon 2 mutation causes more dramatic cell fate changes than exon 8 interruption (Fig 3.6B,C). *DISC1* interruption did not alter expression of other broad progenitor markers, such as Sox2, HES1, Nestin, or Vimentin (Fig 3.6B,C). The decrease in FoxG1 and Tbr2 RNA in the absence of decreased expression of other cortical progenitor markers argued against a deficit in telencephalic differentiation. Furthermore, immunostaining did not reveal any qualitative changes in the proportion of FoxG1+ cells, suggesting that FoxG1 levels were decreased on an individual cell basis (Fig 3.6A).

DISC1 interruption subtly alters neuronal fate but not neuronal maturity

We further investigated effects of *DISC1* disruption on cell fate in iPSC-derived neurons. Differentiation for 40 days resulted in neurons of mixed layer identity (lower layer: CTIP2, Tbr1; upper layer: Cux1, Brn2, Satb2) that expressed neuronal markers MAP2, Tau, SYP, PSD-95, and VGLUT2 (Fig 3.7A). A population of neural progenitors persisted in these cultures (Nestin, Tbr2; Fig 3.7A). Neurons demonstrated spontaneous action potentials by day 42 when co-cultured with astrocytes (Fig 3.7B, Fig 3.8A). Gene expression was assayed in day 50 neurons by NanoString, revealing a persistent decrease in Tbr2 expression across all genotypes and decreased FoxG1 in exon 8 wt/mut and exon 2 mut/mut neurons (Fig 3.7C). There were no significant expression changes of general neuronal markers (including TUJ1, Tau, PSD-95, Syn I, and SYP; Fig 3.7D). Exon 2 mut/mut neurons expressed lower levels of select mature neuronal genes VGLUT1, GRIN1, and MAP2 (Fig 3.7D). Exon 8 interruption did not significantly

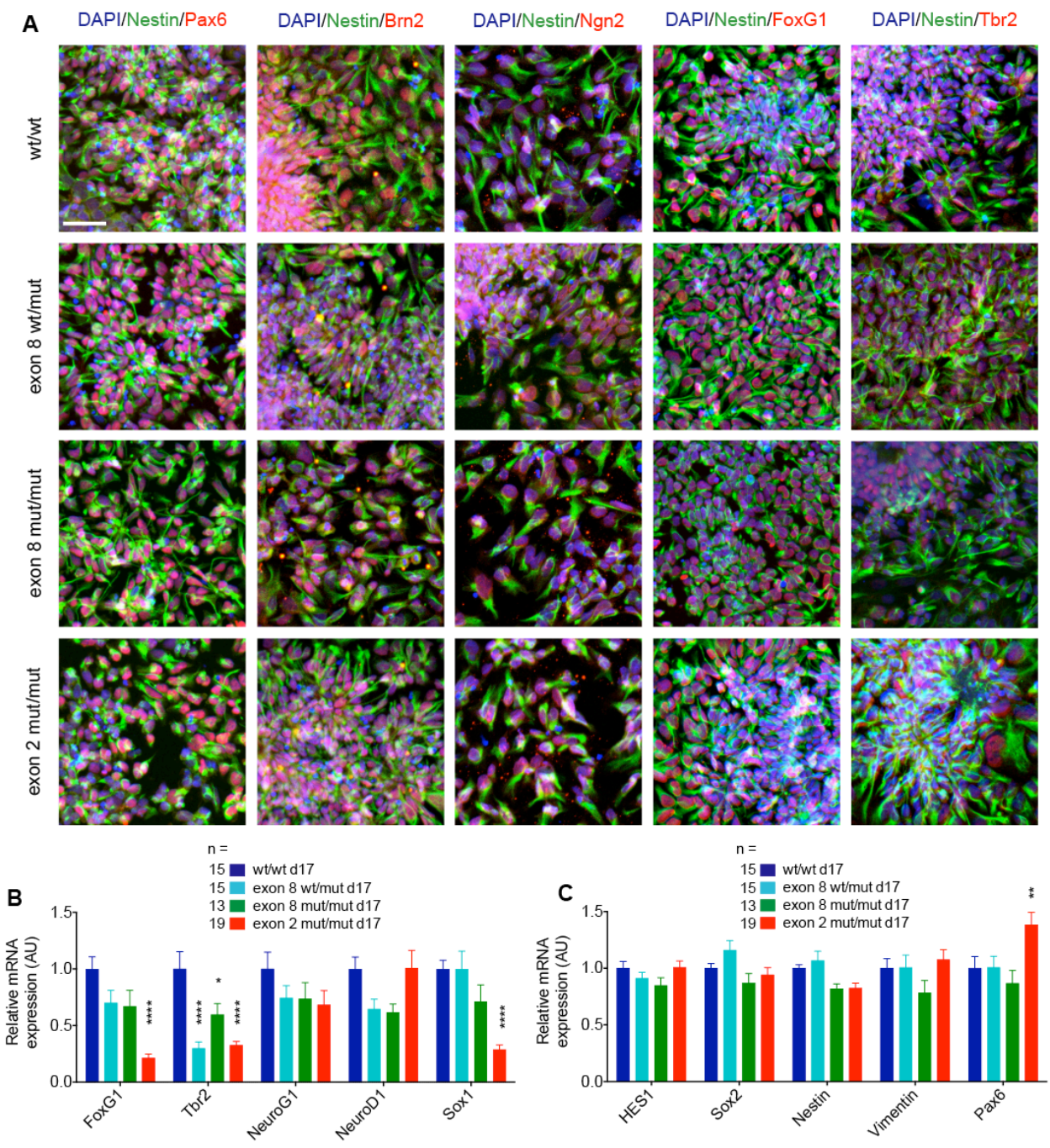

Figure 3.6. ***DISC1*** **disruption causes subtle alterations in NPC fate**. **(A)** iPSCs were differentiated to day 17 NPCs, rosette selected, and immunostained for the NPC markers as shown. Scale bar = 50 um. **(B,C)** iPSCs were differentiated to day 17 NPCs, rosette selected, and RNA was harvested for NanoString. Gene expression is normalized to expression of 8 housekeeping genes and wt/wt levels. Data derived from at least 8 independent differentiations. Statistics: 2-way ANOVA. Mean ± SEM shown. * $p < 0.05$, ** $p < 0.01$, **** $p < 0.0001$.

Figure 3.7. ***DISC1*** **disruption does not alter neuronal differentiation capacity or maturity but causes subtle alterations in cell fate. (A)** iPSCs were differentiated to day 40 neurons and immunostained for the markers labeled. Scale bar = 50 um top 8 rows, 25 um bottom 3 rows. **(B)** Day 24 cells were dissociated and plated with human astrocytes on microelectrode arrays. Day 42 single unit waveforms are shown. **(C-E)** iPSCs were differentiated to day 50 neurons and RNA was harvested for NanoString. Gene expression is normalized to expression of 8 housekeeping genes and wt/wt levels. **(F,G)** Quantification of SYP (**F**) and SYN I (**G**) protein expression in day 40 neuronal lysates, normalized to Tau. **(H)** Representative Western blot of neuronal markers SYN I, SYP, MAP2, Tau, and loading control GAPDH in day 40 neuronal lysates. Same membrane as shown in Fig 3.4D. Data derived from at least 8 independent differentiations. Statistics: (C-E) 2-way ANOVA, (F,G) 1-way ANOVA. Mean ± SEM shown. ns = not significant, * $p < 0.05$, ** $p < 0.01$, *** $p < 0.001$, **** $p < 0.0001$.

Figure 3.7 (Continued)

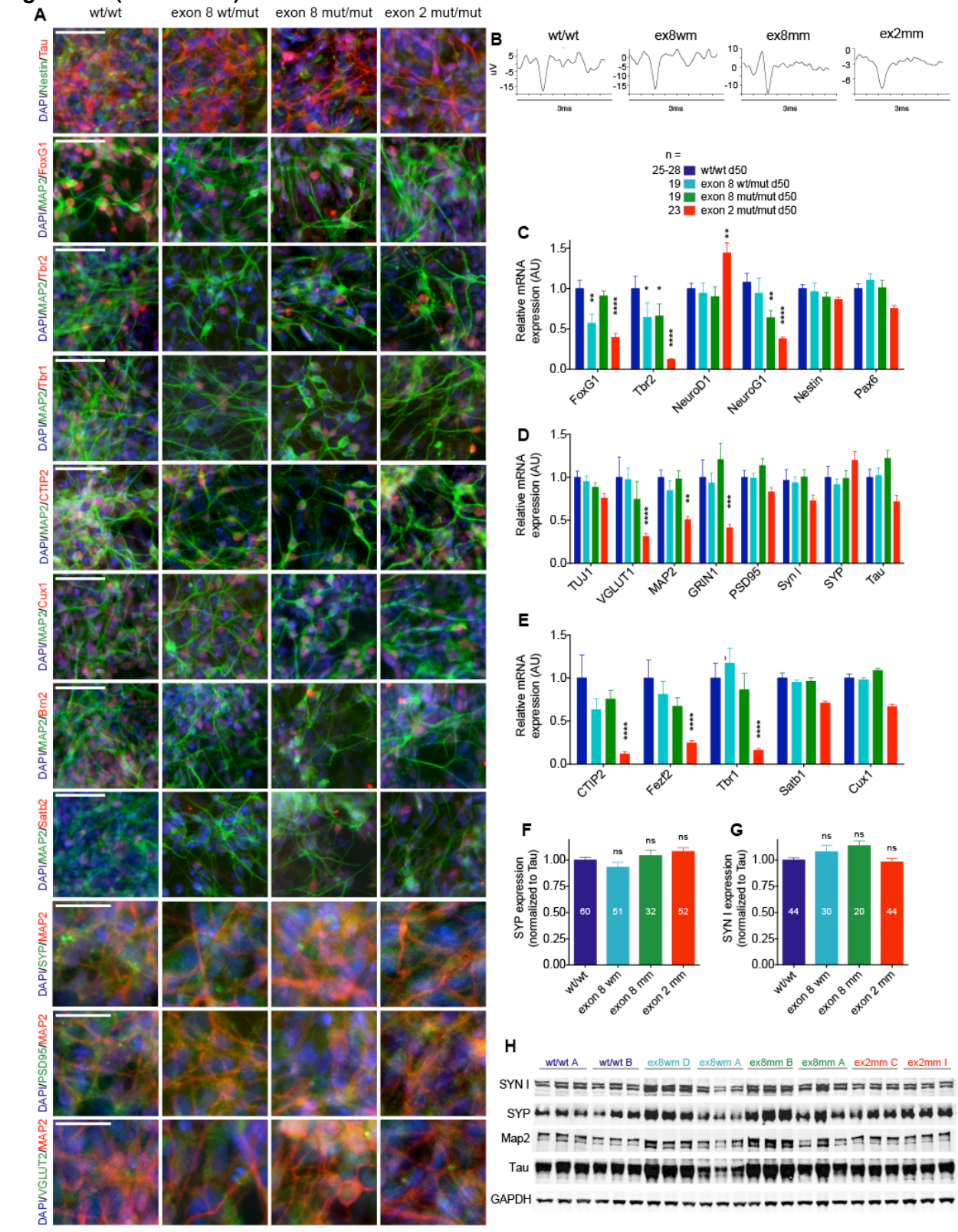

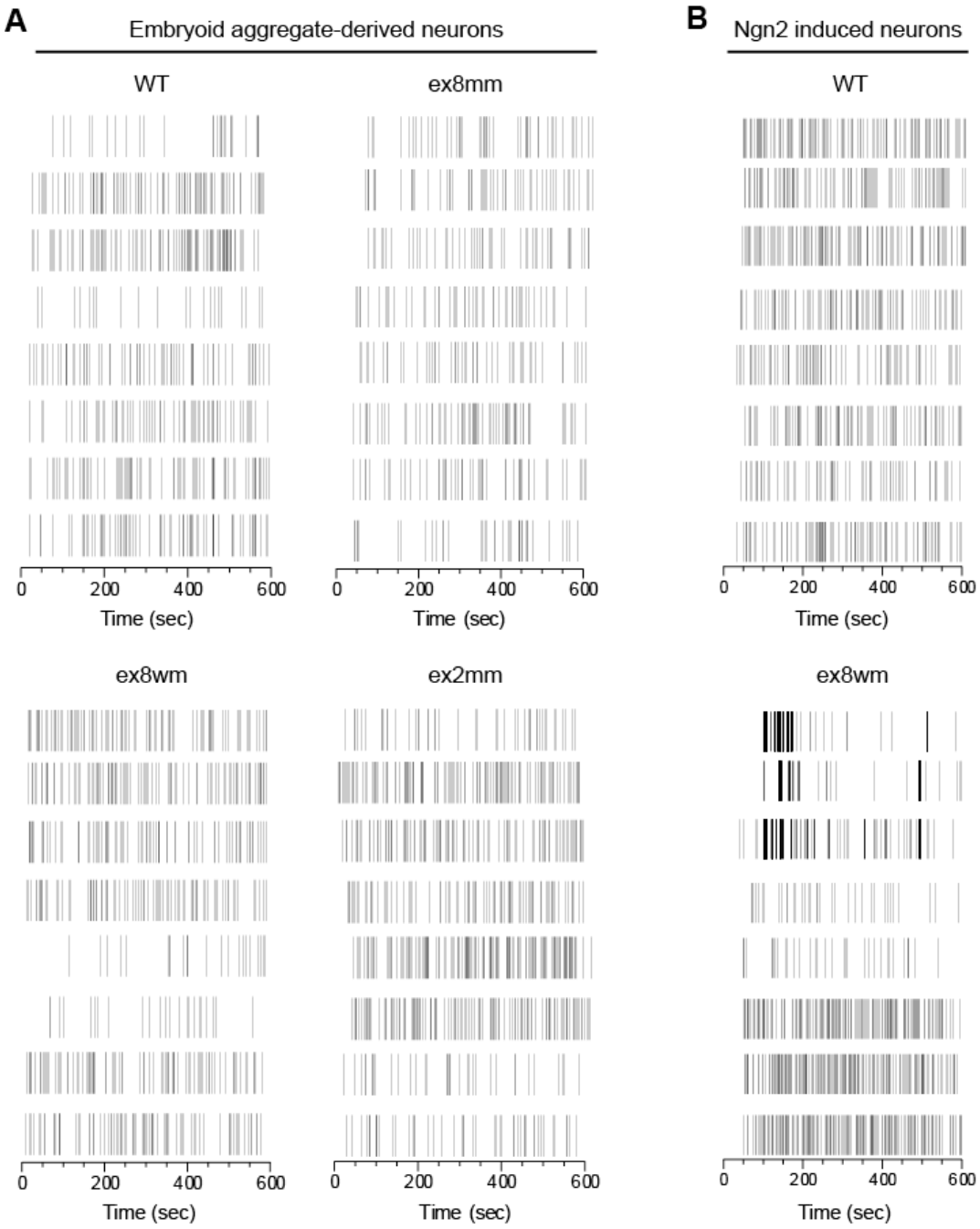

Figure 3.8. Microelectrode array (MEA) recordings show spontaneous activity from embryoid aggregate and Ngn2-transduced iPSC-derived neurons. Example raster plots from embryoid aggregate day 47 neurons (**A**) and Ngn2-transduced day 29 induced neurons (**B**). Each row represents one electrode; 8 representative electrodes were selected from 1 recording of each of the genotypes as shown.

alter neuronal layer marker expression, while exon 2 interruption significantly decreased lower layer neuron markers CTIP2, FezF2, and Tbr1, with a trend for decreased upper layer markers Satb1 and Cux1 (Fig 3.7E). These gene expression changes support the day 17 NPC data, where exon 8 interruption subtly shifts cell fate without impairing neuronal differentiation, and exon 2 interruption causes a broader dysregulation of neurogenesis. We further investigated neuronal maturity by assessing expression of presynaptic proteins. Western blot analyses revealed no significant alterations in SYP or Syn I expression with *DISC1* disruption (Fig 3.7F-H), in contrast to a different clinical *DISC1* mutation (exon 12 Δ4bp[74]), which was found to result in a dramatic increase in both[62].

The effects of *DISC1* disruption on neuronal cell fate confounded further analyses of neuronal phenotypes, as differences in cell fate can affect many neuronal properties. In addition, while the embryoid aggregate-based protocol employed here is a valuable tool for studying neurodevelopment, iPSC differentiation results in a heterogeneous pool of neurons that follows a human developmental timeline[54]. These factors can complicate analyses requiring a homogenous cell population or mature neurons, which may not develop in these cultures for months. In order to study gene expression in a more homogenous and mature neuronal population, we utilized a single-step induction protocol, wherein Neurogenin2 (Ngn2) viral transduction directly converts iPSCs to layer 2/3 excitatory neurons[75]. For these analyses, we narrowed our focus to our disease model, *DISC1* exon 8 wt/mut lines, in parallel with wild-type lines. Immunostaining confirmed that this protocol induces rapid neuronal fate conversion and results in neurons expressing Tau, MAP2, PSD-95, and SYP (Fig 3.9A). These neurons expressed upper-layer markers Brn2, Cux1, Cux2, and Satb2, and excitatory neuron markers VGLUT1 and VGLUT2 (Fig 3.9A). Ngn2 induced neurons (iNs) demonstrated spontaneous action potentials when co-cultured with astrocytes (Fig 3.8B, 3.9B). In order to first compare the population of neurons generated by Ngn2 expression to our standard embryoid aggregate-

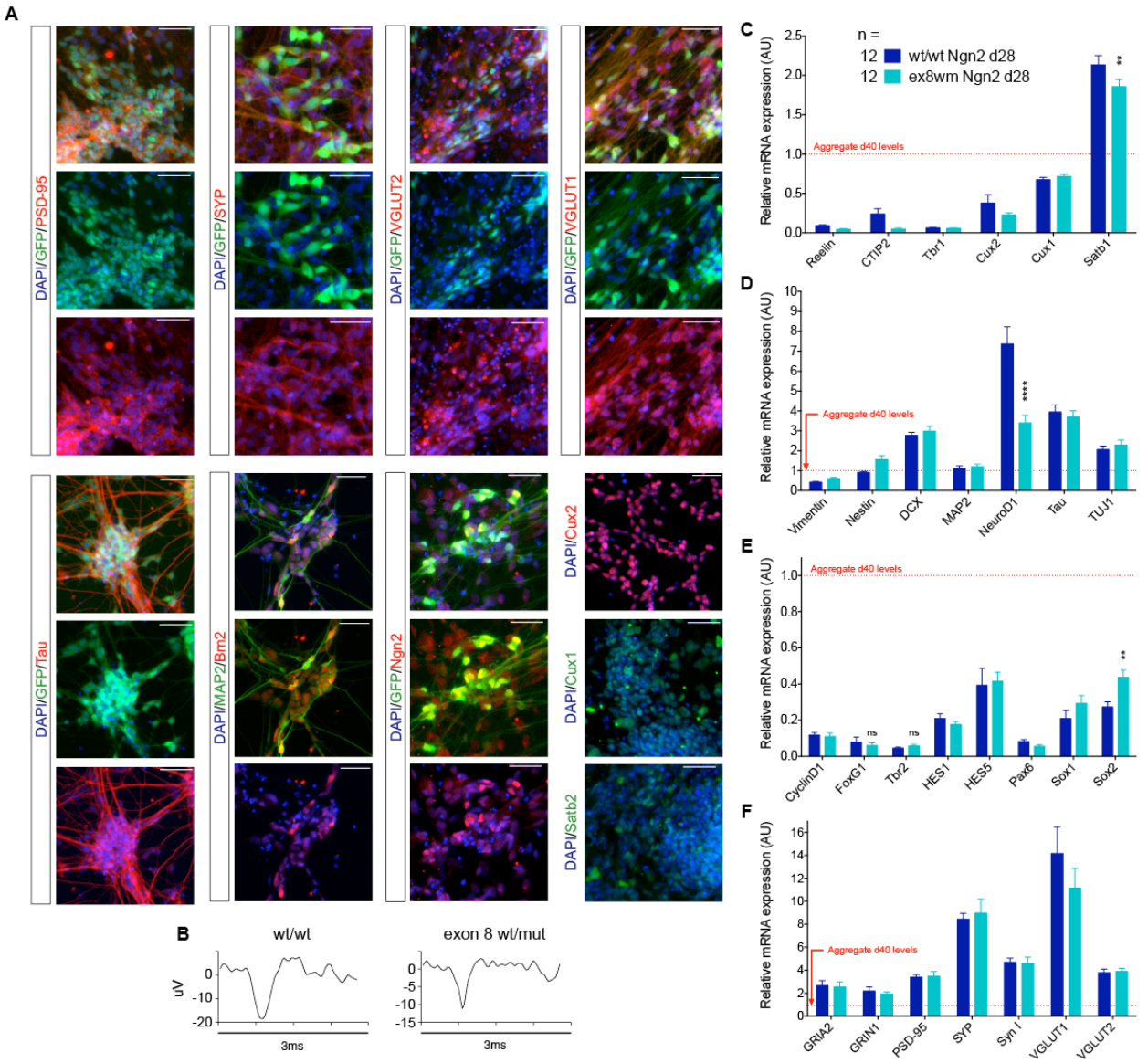

Figure 3.9. **Induced neuron differentiation modifies the neurodevelopmental effects of *DISC1* disruption. (A)** iPSCs were transduced with Neurogenin 2 and differentiated for 28 days to yield a homogenous and mature population of excitatory layer II-III neurons. Day 28 neurons were immunostained for the markers labeled. Scale bar = 50 um. **(B)** Day 4 cells were dissociated and plated with human astrocytes on microelectrode arrays. Day 24 single unit waveforms are shown. **(C-F)** Ngn2-transduced iPSCs were differentiated to day 28 neurons and RNA was harvested for NanoString. Gene expression is normalized to all genes and day 40 embryoid aggregate-derived neurons (average of 19 samples, shown by red dotted line). Data derived from 6 independent differentiations. Statistics: (C-F) 2-way ANOVA. Mean ± SEM shown. ns = not significant, ** $p < 0.01$, **** $p < 0.0001$.

based protocol, we compared gene expression of day 40 aggregate-derived neural cells to day 28 Ngn2-transduced cells. NanoString showed downregulation of layer I marker Reelin and lower layer markers Tbr1 and CTIP2 and upregulation of upper layer marker Satb1 in Ngn2-transduced neurons relative to aggregate-derived neurons (Fig 3.9C). Decreased Cux1/2 expression in the iNs may reflect the decrease in the progenitor population, as these markers can be expressed in upper-layer precursor cells as well as upper-layer neurons[76]. Expression of some general neuronal markers was increased with Ngn2 transduction, including DCX, NeuroD1, Tau, and TUJ1 (Fig 3.9D). Confirming the increased maturity of the induced neuron cultures, neural progenitor marker levels were decreased (FoxG1, HES1, Pax6, Sox1; Fig 3.9E), and mature neuronal markers were increased (PSD-95, SYP, Syn I, VGLUT1/2; Fig 3.9F) compared to embryoid aggregate neurons.

Comparison of wild-type and ex8wm induced neuron cultures revealed comparable expression of many neuronal markers in these cultures. However, decreased expression of Satb1 and NeuroD1, with increased expression of Sox2 may reflect decreased neuronal maturity in exon 8 wt/mut neurons (Fig 3.9C-E)[77,78]. The decreased levels of neural progenitors and low FoxG1 expression obscure the decrease in FoxG1 and Tbr2 expression observed with embryoid aggregate differentiation (Fig 3.9 E), making these induced neurons a less attractive model in which to study the neurodevelopmental consequences of *DISC1* interruption.

RNA-sequencing shows a dorsal fate shift in *DISC1*-interrupted NPCs and neurons

In order to get a genome-wide view of gene expression changes, we performed RNA-sequencing (RNA-seq) on day 17 NPC samples and day 50 neuronal samples of wild-type and *DISC1*-disrupted cells. These data show that exon 8 interruption did not substantially alter global gene expression, whereas exon 2 interruption had a greater effect in disrupting gene

expression, including genes crucial for neurogenesis (Fig 3.10 and by DEseq, data not shown). Examination of cell fate markers largely confirmed and extended the NanoString findings, suggesting a subtle shift in cell fate with *DISC1* interruption (Fig 3.10). RNA-seq confirmed the decrease in FoxG1 expression in NPCs (Fig 3.10D). To investigate for potential dorsal-ventral fate shifts, we evaluated expression of a subset of dorsal and ventral markers. Among telencephalic progenitor markers, a selection of dorsal markers were increased (Pax3, Pax7, Msx2, NeuroG2, Dbx2, Wnt8B) and ventral markers were decreased (ASCL1, DLX1/2, Gsx2) by *DISC1* interruption (Fig 3.10A,B). Notably, Pax3, Pax7, NeuroG2, Msx2, Dbx2, Wnt8B, ASCL1, DLX1/2, GSX2, FoxG1, and Tbr2 (EOMES) are identified in select DEseq comparisons, especially at day 17 (data not shown). While this RNA-seq analysis is limited by low sample numbers, it supports a subtle dorsal shift in cell fate with *DISC1* interruption. Beyond these cell fate changes, a number of other genes were identified by DEseq analysis that are outside the scope of the current study, including differential expression of several protocadherin genes across all genotypes. This gene family has several roles in neural development and neuronal function, and provides interesting candidates for future studies.

The observed changes in gene expression suggested that disease-relevant *DISC1* exon 8 interruption did not drastically alter neuronal differentiation capacity or neuronal maturation but did cause subtle but significant changes in cell fate, including decreased FoxG1 and Tbr2 expression. FoxG1 is a marker of telencephalic progenitors[79-82], while Tbr2 is expressed in intermediate progenitor (IP) cells of the cortex[83-85]. While FoxG1 is expressed broadly in the progenitor cells of the developing neocortex, it is particularly critical for differentiation of ventral forebrain neurons[82,86,87] and is expressed in a high-ventral to low-dorsal gradient in the developing forebrain[88]. We hypothesized that *DISC1*-disruption might subtly alter neural cell fate via an established patterning pathway. The Wnt proteins are a major family of patterning molecules that regulate the dorsal-ventral axis in neurodevelopment[89]. During

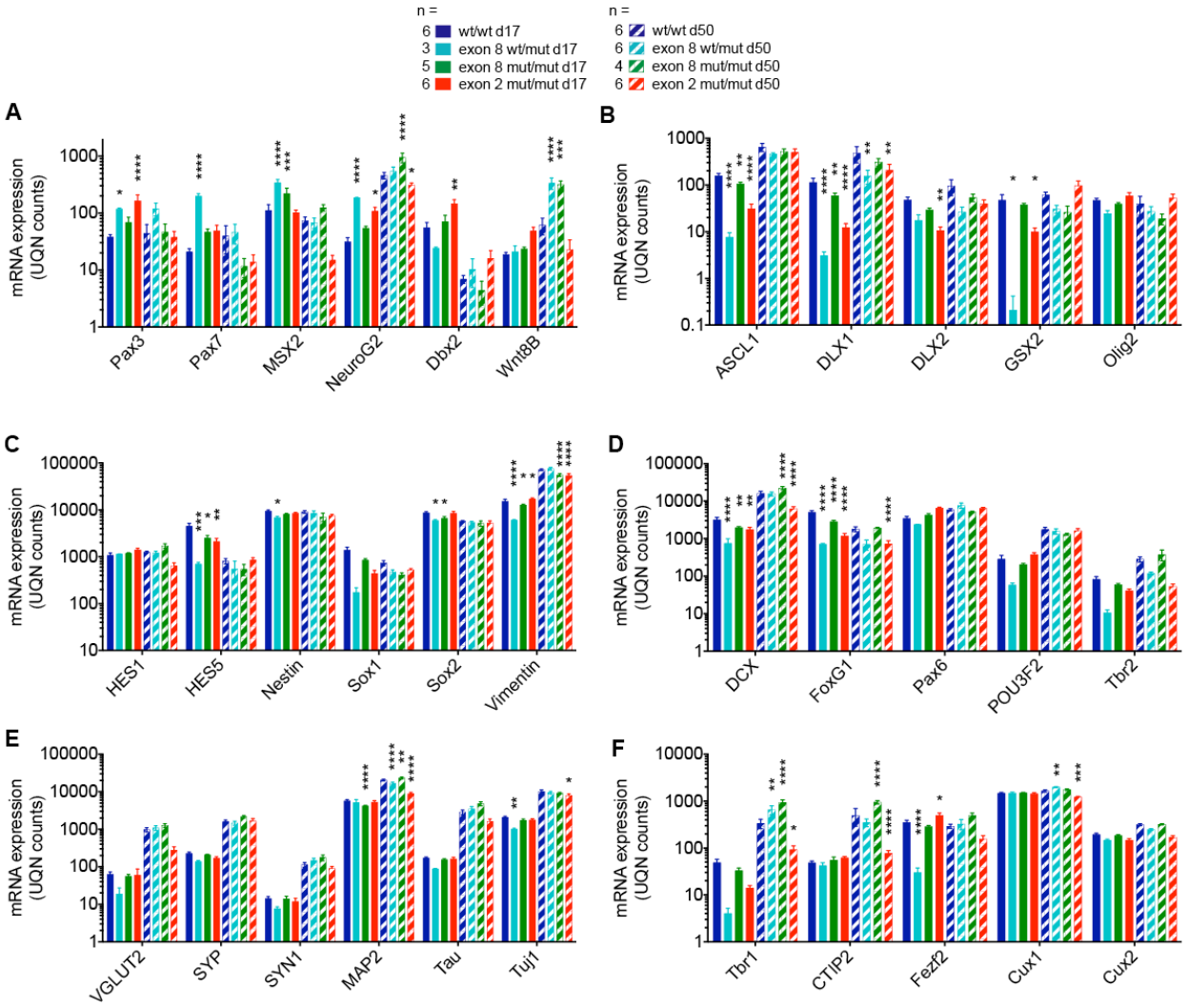

Figure 3.10. **RNA-seq of *DISC1*-targeted NPCs and neurons.** iPSCs were differentiated to NPCs (day 17) and neurons (day 50) and RNA was harvested for RNAseq. Counts were upper-quartile normalized. **(A)** Dorsal telencephalic markers, **(B)** ventral telencephalic markers, **(C,D)** NPC markers, **(E,F)** neuronal markers. Statistics shown versus wt of corresponding differentiation day. Data derived from 2-6 independent differentiations. Statistics: 2-way ANOVA. Mean ± SEM shown. * $p < 0.05$, ** $p < 0.01$, *** $p < 0.001$, **** $p < 0.0001$.

forebrain development, Wnts are present in a dorsal to ventral gradient and act on neural progenitors to create a dorsal neuronal population. In contrast, Shh is present in a ventral to dorsal gradient and ventralizes neural progenitors in the developing cortex[90-92]. Artificially elevating Wnt signaling in the developing cortex has been shown to decrease FoxG1 expression and cause a dorsal shift in neural identity[89]. Wnts have also been shown to trigger IP differentiation and premature neuronal differentiation, thus reducing the abundance of Tbr2-positive cells in the cortex[93,94]. As DISC1 has been shown to participate in the Wnt signaling pathway, we next sought to investigate the Wnt signaling properties of *DISC1*-targeted neural progenitors.

DISC1-disrupted NPCs display elevated baseline Wnt signaling activity, independent of dorsal identity

DISC1 has been identified as both a positive and negative regulator of Wnt signaling[40,95-97]. Accordingly, we investigated Wnt signaling in NPCs derived from our isogenic wild-type and *DISC1*-disrupted iPSCs. We evaluated Wnt signaling by introducing a TCF/LEF-responsive luciferase into cells by Amaxa nucleofection, followed by incubation with control (L) or Wnt3a (W) conditioned media (CM) for 24 hrs. Cells were then lysed and used for luciferase assays. Analysis of luciferase activity showed that *DISC1*-disrupted NPCs display decreased Wnt responsiveness, with a decreased fold change in luciferase activity with Wnt3a application relative to control (Fig 3.11C). However, this decreased Wnt response is driven by increased baseline Wnt signaling in DISC1-disrupted cells (wt vs. DISC1 mutant L CM luciferase activity, Fig 3.11B). Interestingly, this phenotype is not present in iPSCs (Fig 3.12), highlighting the cell-fate specificity of this DISC1-mediated alteration in Wnt signaling. These results suggest that *DISC1* disruption decreases the Wnt response in NPCs by increasing basal Wnt signaling.

The cell fate changes and increased baseline Wnt signaling observed in *DISC1*-

Figure 3.11. *DISC1* interruption increases basal Wnt signaling and decreases Wnt responsiveness in NPCs, independent of dorsal identity. **(A)** Schematic of experimental design. iPSC-derived day 24 NPCs were nucleofected with plasmids encoding the Super8XTOPFlash luciferase reporter and beta-galactosidase (b-gal) as a marker of transfection efficiency. After 18 hr, media were changed to control (L) or Wnt3a (W) conditioned media (CM) for 24 hr, followed by cell lysis. Cell lysate luciferase activity (luc) was normalized to beta-galactosidase activity (b-gal) and wt/wt L levels **(B)**, L levels within genotype **(C)**, wt/wt DMSO L levels **(D)**, or L levels within condition **(E)**. **(B,C)** DISC1-disruption causes increased baseline Wnt signaling (**B**), which drives decreased Wnt response (**C**). **(D,E)** Wild-type and DISC1-disrupted cells treated with vehicle (DMSO) or cyclopamine (cyclop) to dorsalize NPCs for days 5-17 do not show changes in baseline Wnt signaling (**D**) or Wnt response (**E**). Statistics in (D) versus wt DMSO L; statistics in (E) versus wt DMSO W. Sample numbers shown in bars. (F) RNA was harvested from day 40 neurons and used for Nanostring. Gene expression was normalized to all genes. Statistics shown versus wt DMSO. Mean ± SEM shown. Data derived from at least 3 independent differentiations. Stats: (B-E) 1 way ANOVA, (F) 2 way ANOVA. * $p < 0.05$, ** $p < 0.01$, *** $p < 0.001$, **** $p < 0.0001$.

Figure 3.11 (Continued)

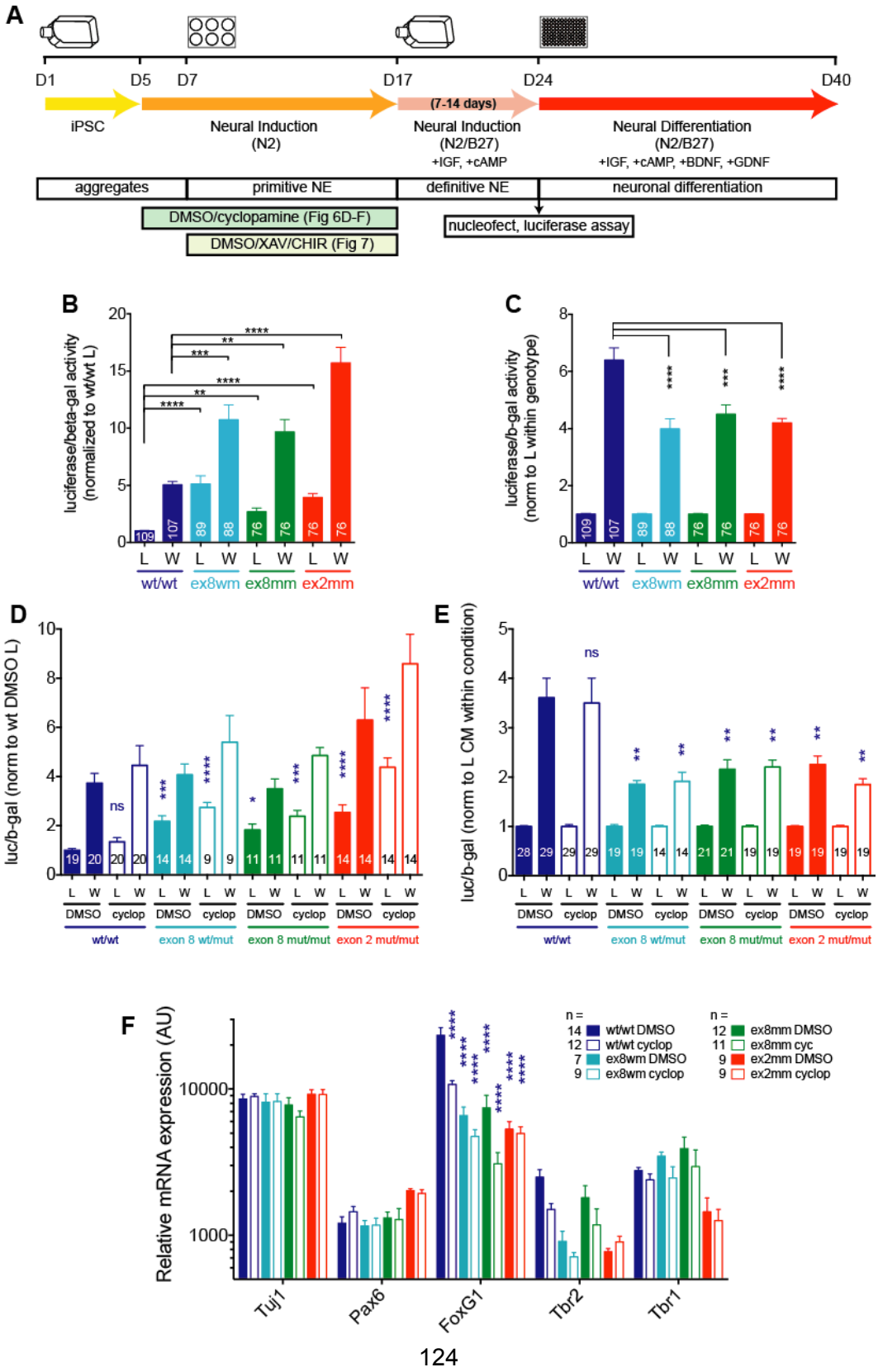

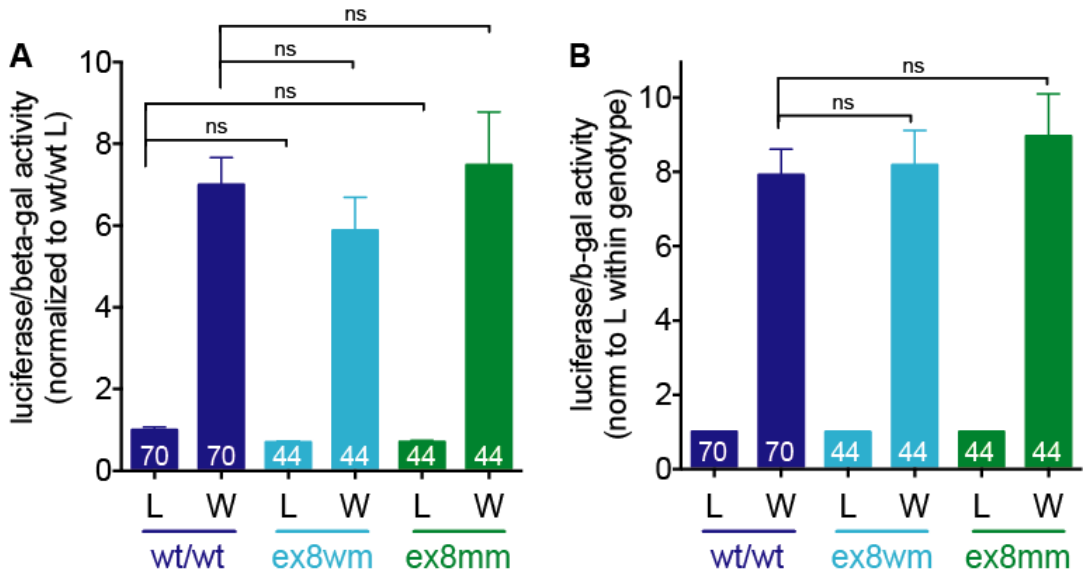

Figure 3.12. ***DISC1* disruption does not alter Wnt signaling in iPSCs.** iPSCs were nucleofected with plasmids encoding the Super8XTOPFlash luciferase reporter (luc) and beta-galactosidase (b-gal) as a marker of transfection efficiency. After 18 hr, media were changed to control (L) or Wnt3a- (W) conditioned media for 24 hr followed by cell lysis. **(A)** Cell lysate luciferase activity was normalized to beta-galactosidase activity. **(B)** Wnt3a-stimulated luc/b-gal was normalized to the average L CM level within each genotype. Mean ± SEM shown. Data derived from at least 10 independent sets of samples. Stats: 1 way ANOVA. ns = not significant.

disrupted cells could be related or independent phenotypes. Altered cell fate could result in changes in observed Wnt signaling by changing the pool of cells being assayed. Conversely, increased baseline Wnt signaling could alter cell fate. A third possibility is that these phenotypes are interrelated, where altered Wnt signaling and cell fate each feed into one another. If dorsal NPC fates have different intrinsic Wnt signaling properties than more ventral NPCs, changes in Wnt signaling may be observed in dorsal-shifted NPCs.

To assess whether the observed alteration in Wnt signaling could be induced in wild-type cells by forcing a dorsal fate, we pushed NPCs to more dorsal fates by antagonizing Shh signaling with cyclopamine during days 5-17 of differentiation[60,62,98]. NPCs were then rosette selected and cultured as neural aggregates without cyclopamine for ~13 days prior to Wnt signaling assays (schematic in Fig 3.11A). Cyclopamine treatment did not alter baseline levels of Wnt signaling or Wnt responsiveness in wild-type or *DISC1*-disrupted lines (Fig 3.11D,E). Dissociated NPCs were also plated and differentiated as neurons for 16 days, followed by RNA harvest. NanoString showed that a window of prior cyclopamine exposure did not alter expression of many cell fate markers, supporting previous studies demonstrating the “default” dorsal fate of NPCs differentiated from human pluripotent cells[91,99,100]. Cyclopamine treatment did decrease FoxG1 expression in wild-type cells (Fig 3.11F), suggesting that decreased FoxG1 expression in *DISC1*-disrupted cells can be mimicked in wild-type cells using cyclopamine to dorsalize NPCs. However, the increased baseline Wnt signaling and decreased Wnt-responsiveness of *DISC1*-disrupted NPCs is not induced in wild-type cells with cyclopamine treatment. Thus, the altered Wnt signaling seen in *DISC1*-disrupted cells does not appear to result from altered dorsal identity of these NPCs.

Wnt signaling and gene expression changes in *DISC1*-disrupted cells can be rescued with Wnt antagonism in a critical window of neurodevelopment

The elevation in baseline Wnt signaling in *DISC1*-disrupted NPCs suggested a mechanism by which *DISC1* interruption may alter cell fate. As Wnts act to dorsally pattern NPCs during neural development, increased baseline Wnt signaling with *DISC1* disruption may cause NPCs to attain a slightly more dorsal fate than wild-type cells. In order to test this hypothesis, we treated wild-type and *DISC1* exon 8 wt/mut NPCs with either a Wnt agonist (CHIR99021) or antagonist (XAV939) during days 7-17 of differentiation. Immunostaining of NPCs showed dramatic cell fate changes with CHIR99021 treatment, including decreased FoxG1 and Tbr2 expression, and increased MAP2 expression (Fig 3.13A). Neural rosettes were then cultured in suspension as neural aggregates in the absence of these small molecules prior to assaying Wnt signaling. Previous treatment with Wnt antagonist XAV939 decreased baseline Wnt signaling and increased Wnt responsiveness in *DISC1* exon 8 wt/mut NPCs (Fig 3.13B,C). The altered Wnt response of *DISC1*-targeted NPCs can thus be rescued by prior Wnt antagonism during a 10-day window early in neural development. In contrast, Wnt agonism caused wild-type cells to mimic the decreased Wnt responsiveness of *DISC1*-targeted cells (Fig 3.13C). CHIR99021 treatment also caused a dramatic decrease in Wnt baseline signaling, likely due to the observed decrease in NPCs and increase in neuronal cell fates at early progenitor time points (Fig 3.13 A,B).

In parallel with Wnt signaling assays, NPCs were plated and differentiated as neurons for 16 days prior to RNA harvest and cell fate analyses. Antagonizing NPC Wnt signaling with XAV939 rescued decreased FoxG1, Brn2, and Tbr2 expression in exon 8 wt/mut neurons (Fig 3.13D,E). Stimulating Wnt signaling with CHIR99021 pushed NPCs to spontaneously differentiate, decreasing expression of progenitor markers and cortical layer markers (Fig 3.13 D,E).

CHIR99021 treatment resulted in decreased expression of ventral marker GSX2 and increased expression of caudal genes HOXA1/2 and HOXB4, consistent with the effects of Wnt

Figure 3.13. Wnt antagonism rescues altered Wnt signaling and cell fate in *DISC1*-disrupted cells. iPSCs were differentiated to NPCs and treated with vehicle (DMSO), Wnt antagonist XAV939 (XAV), or Wnt agonist CHIR99021 (CHIR) during days 7-17. After rosette selection, small molecules were withdrawn. **(A)** Examples of immunostained NPCs are shown. Scale bar = 50 um. **(B,C)** Prior exposure to Wnt antagonist XAV939 decreases baseline Wnt signaling and increases Wnt responsiveness in NPCs, whereas Wnt agonist CHIR99021 decreases Wnt responsiveness. iPSC-derived NPCs were nucleofected with plasmids encoding the Super8XTOPFlash luciferase reporter and beta-galactosidase as a marker of transfection efficiency. After 18 hr, media were changed to control (L) or Wnt3a- (W) conditioned media (CM) for 24 hr followed by cell lysis. Cell lysate luciferase activity (luc) was normalized to beta-galactosidase activity (b-gal) and wt/wt DMSO L levels (**B**) or L levels within treatment condition (**C**). Sample numbers shown in bars. **(D-F)** RNA was harvested from day 40 neurons and used for Nanostring. (**D,E**) Progenitor and neuronal, dorsal, ventral, caudal markers. (**F**) Wnt pathway genes. Gene expression is normalized to all genes. Significance asterisks in dark blue are versus wt/wt DMSO; asterisks in light blue are versus ex8wm DMSO. All luciferase assay and Nanostring samples are independent of samples used in Fig 6. Mean ± SEM shown. Data derived from at 3 independent differentiations. Stats: (B,C) 1 way ANOVA, (D-F) 2 way ANOVA. * $p < 0.05$, ** $p < 0.01$, *** $p < 0.001$, **** $p < 0.0001$.

Figure 3.13 (Continued)

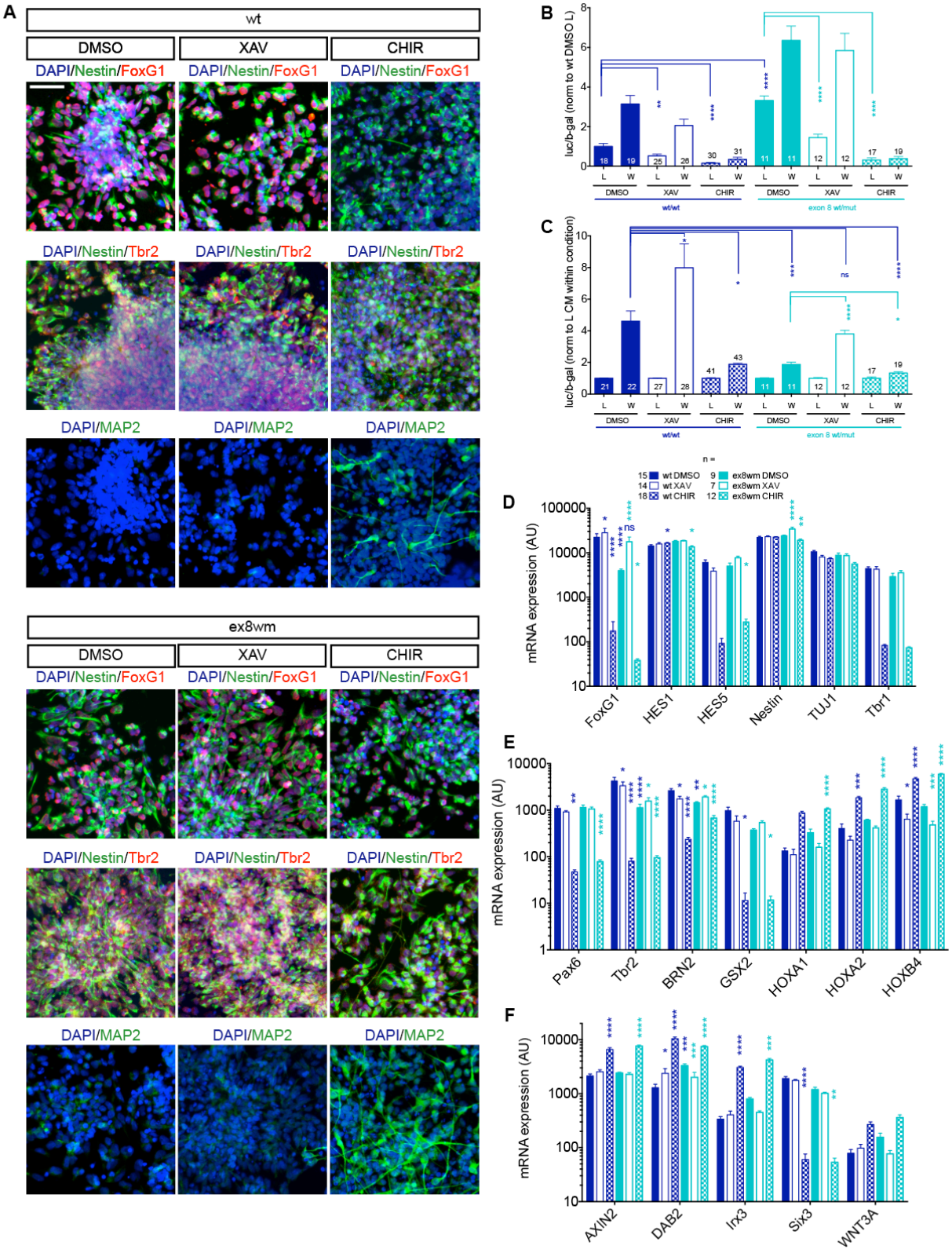

in dorsal and posterior patterning (Fig 3.13E). XAV939 opposed many of these effects in wild-type and exon 8 wt/mut cells. XAV939 also rescued increased DAB2 expression in exon 8 wt/mut cells, whereas CHIR99021 increased DAB2 levels in wt and ex8wm neurons. Furthermore, prior treatment of NPCs with CHIR99021 altered neuronal expression of Wnt pathway genes AXIN2, Irx3 and Six3 (Fig 3.13F). The reversal of gene expression changes in exon 8-targeted neurons with Wnt antagonism during NPC development suggests that altered cell fate in *DISC1*-disrupted cells is downstream of increased Wnt signaling. Rescue of cell fate changes by Wnt antagonism in *DISC1* exon 8 wt/mut cells also rescues increased baseline Wnt signaling and decreased Wnt responsiveness in *DISC1*-targeted NPCs. These studies support a model in which altered Wnt signaling and cell fate are interdependent phenotypes in *DISC1*-disrupted NPCs and neurons (Fig 3.14).

DISCUSSION

The study of genetic predispositions to mental illness, even if found only in a subset of patients, will improve our understanding of the pathophysiology of these debilitating disorders. Both rare, highly-penetrant and common, weaker *DISC1* variants have been associated with multiple MMIs (reviewed here[30]). The Scottish chr(1;11) translocation provides a unique opportunity to investigate the pathophysiology of a rare genetic alteration that has been rigorously linked to MMI[101]. Without brain tissue from patients, it has been difficult to identify the pathological mechanisms of the Scottish translocation. Even with the study of t(1;11) patient-derived cells, it would be impossible to attribute findings specifically to *DISC1* disruption due to the presence of background genetic variability between control and t(1;11) lines and the disruption of other genes by the translocation (e.g. the long non-coding RNA (lncRNA) *DISC2*). DISC1 fragment overexpression in mice yields schizophrenia-associated phenotypes[36,37,41,44], while *DISC1* knockdown in embryonic rodent brain impairs neural progenitor cell (NPC)

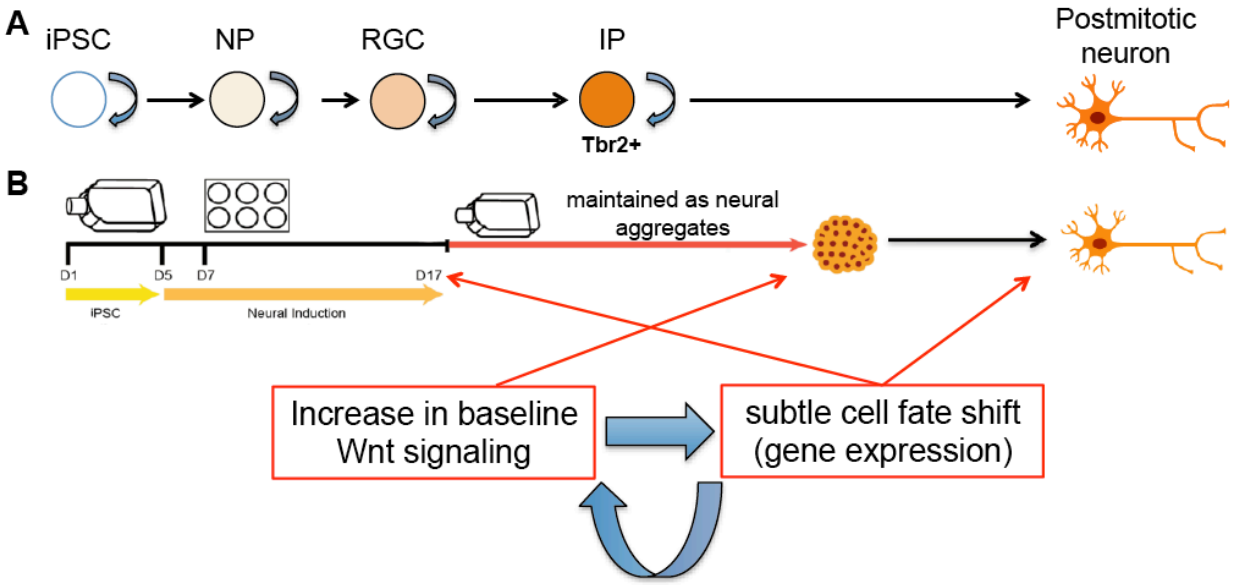

C

	wild-type	wild-type + XAV	wild-type + CHIR	DISC1 ex8 wm	DISC1 ex8 wm + XAV	DISC1 ex8 wm + CHIR
Changes in gene expression (Tbr2, FoxG1)	=	↑	↓↓↓↓	↓↓↓	=/↓	↓↓↓↓
Baseline Wnt signaling (luciferase)	=	↓	↓↓↓	↑↑↑	=/↑	↓↓↓
Wnt responsiveness (luciferase)	=	↑↑	↓↓	↓↓	=	↓↓↓

Figure 3.14. Summary of Wnt modulation findings with wild-type and *DISC1* ex8wm cells. (A) Schematic of neural progenitor populations. **(B)** Schematic of differentiation. The increase in baseline Wnt signaling observed in dissociated neural aggregates appears to be interdependent on a subtle fate shift of NPCs and neurons, observed at days 17 and days 40-50, respectively. **(C)** The Wnt signaling and gene expression changes observed with *DISC1* disruption can be rescued with Wnt antagonism and induced with Wnt agonism. iPSC: induced pluripotent stem cell, NP: neural precursor, RGC: Radial glial cell, IP: intermediate progenitor, XAV: Wnt antagonist XAV939, CHIR: Wnt agonist CHIR99021.

proliferation and alters neuronal migration[39,43,44]. Animal models have thus identified critical neurodevelopmental roles for DISC1 that could be perturbed by either loss-of-function (LOF) or gain-of-function (GOF) mechanisms. Due to differences in *DISC1* splicing between human and rodent samples[46,102], there is a need to complement animal models with studies of human neurons and glia.

Human induced pluripotent stem cells (iPSCs) provide a tremendous advantage when studying otherwise inaccessible human cells and tissues. To investigate the consequences of *DISC1* interruption in human neurons with a controlled genetic background, we TALEN- and CRISPR-Cas9-targeted iPSCs to create isogenic lines, which differ only at a single locus. We did not find evidence for off-target mutations with CRISPR-Cas9 or TALEN targeting, in agreement with recent reports of the high specificity of genome editing in human iPSCs[103-106].

The model described herein allows investigation of the effects of *DISC1* interruption on DISC1 expression and neurodevelopment. As the clinical presentation of subjects with t(1;11) is relatively modest, in that patients can develop normally for decades before diagnosis of any neuropsychiatric disorder, we predicted that phenotypic alterations resulting from *DISC1* interruption in neurons would also be mild. We found that genomic *DISC1* interruption near the site of the Scottish chr(1;11) translocation causes loss of expression of longer *DISC1* transcripts from the mutated allele by NMD, which increases baseline Wnt signaling and alters the transcriptional profile of NPCs and neurons. These data support a loss-of-function model, wherein *DISC1* interruption causes decreased full-length DISC1 expression (confirmed by Western blotting) and has downstream consequences on DISC1-dependent Wnt signaling, which results in a subtle NPC and neuronal fate shift. The exon 2 biallelic mutant lines demonstrate that an independent *DISC1* mutation can dysregulate many of the same processes as our disease-relevant exon 8 disruption, and has even stronger effects on neuronal cell fate. These data support studies in the field showing that *DISC1* knockdown and overexpression of

many different DISC1 mutants share several phenotypic consequences (reviewed here[30]). As exon 2 mutation does not dramatically alter *DISC1* transcript structure by RNA-seq (Appendix 1), we hypothesize that the truncated DISC1 protein may result from forced usage of an alternate start codon downstream of the introduced frameshift mutation, resulting in an N-terminally truncated protein.

The similarity in effects of heterozygous and biallelic *DISC1* exon 8 interruption suggest that *DISC1* is subject to haploinsufficiency, where loss of long isoform expression from one allele is sufficient to alter neurodevelopment. Unexpectedly, biallelic exon 8 mutation did not exacerbate the changes in gene expression or Wnt signaling observed in exon 8 wt/mut lines. This phenomenon has been demonstrated for other genes important for neural patterning, including presenilin 2 (PS2), where loss of a single copy of *PS2* on a *PS1* null background phenocopies the developmental defects of the *PS2/PS1* double knockout[107]. It is also possible that our phenotypic assays may not have the resolution to detect subtle differences between *DISC1*-mutant genotypes. Furthermore, other phenotypes related to *DISC1*-disruption, not assayed here, may be stronger in exon 8 biallelic mutant cell lines than in exon 8 wt/mut cells.

It should be noted that because we have not generated the chr(1;11) translocation, we cannot assess for presence of a fusion transcript or evaluate the effects of disruption of the antisense lncRNA *DISC2*. In patients carrying t(1;11), there has been no evidence of expression of a truncated DISC1 or a DISC1 fusion protein with the nearest downstream chromosome 11 gene (*DISC1FP1* or *Boymaw*). Patient lymphoblastoid cell lines showed a decrease in detectable DISC1 protein and mRNA without the appearance of any truncated or novel protein species[64], supporting a loss of DISC1 expression from the mutated allele. PCR from patient cell lines has revealed expression of a transcript from the der 1 chromosome, fusing *DISC1* exons 1-8 to *DISC1FP1*/*Boymaw* exons 1-4, but there is no evidence that this transcript results in a translated protein product[108]. Indeed, the presence of a PTC in the fusion transcript prior to the

last exon of the chr11 gene suggests that this protein would be targeted for NMD. Thus, there is little evidence to suggest that a fusion protein plays a large role in the pathophysiology of the disease process. However, the role of *DISC2*, which is also interrupted by t(1;11), cannot be addressed here and remains unknown. Disruption of *DISC2* in the human chr(1;11) translocation could exacerbate or modify our observed phenotypes with *DISC1* interruption.

The ability to identify defects in neurodevelopment with human iPSCs depends on recapitulating human corticogenesis in a dish. The advent of newer "induced neuron" differentiation methods, which accelerate differentiation by overexpressing master regulators of cell fate, may obscure developmental effects of disease mutations. Here we found that Ngn2-induced neurons were unable to reproduce the developmental phenotype observed in embryoid aggregate-derived neurons, but did display distinct gene expression changes suggestive of altered development. Therefore, the choice of differentiation protocol can greatly impact the ability to detect consequences of disease mutations. Traditional differentiation methods follow a developmental timeline of cell fate generation, but result in heterogeneous and immature cultures. Induced neuron differentiation results in more homogenous and mature neurons, but bypasses critical regulatory processes of neurodevelopment.

The results described herein reveal a role of *DISC1* disruption in disordered neurodevelopment. Previous analyses of psychiatric disease with human iPSCs have also reported changes in neural development. Studies with sporadic schizophrenic patient-derived (SCZ) lines identified decreased neuronal connectivity and synaptic density, normal electrophysiological activity, and altered expression of glutamate receptors and Wnt signaling pathway genes in schizophrenic patient-derived cortical neurons[56]. SCZ cortical NPCs and immature neurons displayed decreased migration and increased oxidative stress[59]. Modeling hippocampal neurogenesis also revealed a deficit in neurogenesis and reduced neuronal activity in these lines[60]. A model of 15q11.2 deletion, which predisposes to schizophrenia,

showed disordered adherens junctions and apical polarity in del15q11.2 cortical NPCs[61]. Another study used iPSCs with a distinct *DISC1* mutation found in an American family, in which a 4 bp deletion in exon 12 co-segregates with schizophrenia[62,74]. This mutation resulted in dysregulation of presynaptic biology, with decreased synaptic density and synaptic transmission and increased presynaptic protein expression in cortical neurons[62].

Our findings differ from the study of the *DISC1* Δ4 bp mutation, as we do not observe an upregulation of presynaptic proteins[62]. Because there were insufficient family members in the American pedigree to conclusively associate the C-terminal 4 bp deletion with schizophrenia, the clinical causality of this mutation in human patients remains unclear[74]. There exist numerous possibilities to explain the distinct phenotypes resulting from different *DISC1* mutations. It is possible that different genetic backgrounds alter the phenotype of *DISC1* disruption, or that the mutations used in the present study act through a distinct pathological mechanism from the 4 bp deletion. Furthermore, the differentiation methods used in that study were slightly different than those utilized here, including the use of dual SMAD inhibition (antagonizing BMP signaling) and cyclopamine (antagonizing Shh signaling), which likely results in a different population of neural progenitors and neurons, as BMPs and Shh are critical regulators of dorsal-ventral patterning of the telencephalon[109]. Future studies should address whether differentiating these lines in parallel illuminates common pathological mechanisms of these distinct disease-associated *DISC1* mutations.

Here, we found that disease-relevant *DISC1* disruption alters Wnt signaling in human NPCs. DISC1 is thought to play a role in the Wnt signaling pathway by binding to and inhibiting the action of GSK3β, thus allowing accumulation of beta-catenin and promoting Wnt signaling in the cell[40,95,110]. An alternative role for DISC1 in Wnt signaling has been proposed in rat striatum, where a DISC1-D2R complex is important for facilitating GSK3β activity and thus negatively regulates Wnt signaling[97]. Based on these two models, disruption of DISC1 expression might

lead to either decreased or increased Wnt signaling in the cell. We observed that decreased expression of DISC1 or misexpression of truncated DISC1 increases baseline Wnt signaling and decreases Wnt responsiveness in NPCs. Our results are consistent with the decreased Wnt response upon *DISC1* knockdown in murine NPCs, but do not support a model in which DISC1 increases Wnt signaling[40,96]. It is also unlikely that the DISC1-D2R complex plays a significant role in cortical NPCs, which differ greatly from striatal neurons. The data described herein do support a role of DISC1 in negatively regulating Wnt signaling, such that altered DISC1 expression increases baseline NPC Wnt signaling.

The Wnt signaling pathway has been implicated in the pathophysiology of neuropsychiatric disorders, making the role of DISC1 in this pathway of particular interest[111-113]. However, we are not aware of any previous studies investigating Wnt signaling in a human neuronal model of mental illness. Perturbation of Wnt signaling in animal models supports a role of Wnt signaling in positional patterning (on the dorsal-ventral and anterior-posterior axes) as well as in regulating the balance of progenitor proliferation vs. differentiation. Artificial dysregulation of this system can result in disordered corticogenesis and defects in neural progenitor behavior[114].

We found that *DISC1* disruption causes altered NPC and neuronal cell fate via increased baseline Wnt signaling. The Wnt signaling and gene expression data are consistent with animal models in which increased Wnt signaling in the developing brain causes dorsal NPC fate shift, decreases FoxG1 expression, and decreases Tbr2 expression by promoting IP differentiation [89,94,115]. Wnt inhibition with XAV939 for a 10 day window in *DISC1*-targeted NPCs rescued neuronal cell fate changes, suggesting that increased Wnt signaling with *DISC1*-disruption is upstream of cell fate alterations. The increase in Tbr2 expression with XAV939 treatment upholds previous reports that Wnt antagonism causes expansion of Tbr2+ IPs [94,116,117]. The ability of prior Wnt antagonism to restore Wnt responsiveness in *DISC1*-targeted NPCs

suggests that the altered *DISC1*-disrupted neural progenitor population also has different intrinsic Wnt signaling properties. Although we found evidence that *DISC1*-disrupted cells displayed a dorsal fate shift, forcing a dorsal fate in wild-type NPCs did not induce the Wnt phenotype seen with *DISC1* disruption. These studies suggest a model in which *DISC1* interruption increases Wnt signaling, which alters the pool of NPCs, resulting in decreased Wnt responsiveness. The inability of cyclopamine to induce altered Wnt signaling in wild-type NPCs suggests that the relevant cell fate change in *DISC1*-disrupted NPCs is a Wnt-stimulated dysregulation of progenitor proliferation vs. differentiation, rather than purely a dorsal fate shift.

The involvement of long *DISC1* isoforms in neuronal migration (identified in rodent knockdown studies) could also reflect a role of DISC1 in proper acquisition of neuronal cell fate. Studies of genetic disorders of neuronal development and migration have found that defects in cell fate transitions underlie the migration deficit[118,119]. Furthermore, expression of FoxG1 has been shown to be required for the exit of migrating neurons out of the multipolar phase and for entry into the cortical plate[120]. The observed alterations in cell fate may thus cause defects in migration and cortical plate entry with *DISC1* disruption, in agreement with *in vivo DISC1* knockdown studies.

Further work will be required to elucidate the exact mechanism by which *DISC1*-disruption alters Wnt signaling in human NPCs. We have also identified other candidate gene expression changes that result from *DISC1* interruption by RNA-sequencing, which provide interesting candidates for future study. This work shows the utility of human iPSCs in modeling mental illness-associated defects in human neurodevelopment. Taken together, this study strengthens the association between Wnt signaling, neurodevelopment, and major mental illness.

EXPERIMENTAL PROCEDURES

Genome editing

Healthy control human iPSC line YZ1 was obtained from the UCONN Stem Cell Core (generated by retroviral vectors containing reprogramming factors OCT4, SOX2, c-Myc, and KLF4)[121]. TALENs were designed and constructed using a hierarchical ligation procedure[63]. TALE monomer plasmids and TALEN backbone plasmids were a generous gift from Feng Zhang. Exon 8 TALENs were designed targeting unique genomic sequences in DISC1 exon 8 (5'-TTAACGATATTGAAACCCAA-CTACCAGCCTTGCTTGAAG-CCAAAATGCATGCCATATCA-3') (TALEN sites underlined). For CRISPR-Cas9 targeting, a unique genomic site in DISC1 exon 2 (GAGGAACCTCGGCGCACTTTGGG) was cloned into a gRNA cloning vector using Gibson assembly. The pCAG-Cas9-T2A-GFP plasmid was a gift from Kiran Musunuru (Addgene plasmid #44719); the gRNA cloning vector was a gift from George Church (Addgene plasmid #41824)[122]. Targeting plasmids (exon 8: TALENs (3 ug each) and pCAG-GFP (1 ug) or exon 2: pCAG-Cas9-T2A-GFP (2.5 ug) and gRNA (2.5 ug)) were electroporated into dissociated YZ1 iPSCs (~5E6 cells, dissociated in Accutase (Life Technologies) supplemented with 10 uM ROCK inhibitor, Y-27632 (Stem RD)) using the Amaxa 4D-Nucleofector X Unit (Lonza, program DN-100). Transfected cells were plated onto Matrigel- (BD Biosciences) coated plates in mTeSR1 media (Stemcell Technologies) + 10 uM ROCK inhibitor. 48 hours after transfection, iPSCs were dissociated and GFP+ cells were collected by FACS. GFP+ cells were plated at low density onto irradiated MEFs (GFP+ cells: ~3000 cells/cm^2, MEFs: ~17500 cells/cm^2, GlobalStem). Cells were cultured in standard iPS cell medium until small, isolated colonies appeared (~7-10 days). Clones were transferred to individual wells of a matrigel-coated 96 well plate and expanded in mTeSR1 media. Genomic DNA was harvested using QuickExtract DNA Extraction solution (Epicentre). Clones were screened for genomic mutation by PCR amplification around the target site, followed by Sanger sequencing.

Karyotype analysis

The NanoString nCounter human karyotype panel (NanoString Technologies) was used per manufacturer's instructions to evaluate cell lines for large-scale CNVs. Briefly, 200-600 ng genomic DNA (gDNA), extracted using PureLink Genomic DNA Mini Kit (Life Technologies), was AluI-digested for 2 hrs at 37°C, denatured for 5 min at 95°C, and cooled on ice for 2 min to prevent renaturation. Denatured gDNA was combined with capture and reporter probesets and hybridized at 65°C for 16-30 hrs. Hybridized samples were processed using the nCounter Prep Station and imaged using the nCounter Digital Analyzer (NanoString Technologies). Sample counts were normalized to a reference sample with a normal karyotype.

iPSC culture

Human iPSCs were cultured as previously described[66]. Briefly, cells were cultured on an irradiated MEF feeder layer (GlobalStem, ~17500 cells/cm^2) in 10 ng/ml FGF2 (PeproTech), added fresh daily. Cells were maintained at 37°C/5% CO_2 and split every ~6 days. Differentiated cells were manually removed prior to splitting.

Embryoid aggregate neuronal differentiation

Neuronal differentiation was performed using an embryoid aggregate-based protocol, as previously described[66]. Briefly, iPSC colonies were removed from MEFs and cultured as embryoid aggregates in suspension for 4 days in iPSC media (without FGF2), followed by 2 days in N2 neural induction media. Day 7 aggregates were plated onto Matrigel-coated 6 well plates and maintained in N2 neural induction media, forming neuroepithelial structures. For dorsal-ventral patterning, cells were treated with 1/1000 DMSO (Sigma) or 2 uM cyclopamine (Santa Cruz) as indicated during days 5-17 of differentiation. For Wnt manipulation, cells were treated with 1/5000 DMSO (Sigma), 2 uM XAV939 (Stemgent), or 3 uM CHIR99021 (Tocris) as indicated during days 7-17 of differentiation. At day 17, neural rosettes were enzymatically

isolated using STEMDiff Neural Rosette Selection Reagent (Stemcell Technologies) and cultured in suspension for 7-14 days in N2/B27 neural induction media containing cAMP (1 uM, Sigma) and IGF-1 (10 ng/ml, Peprotech). Neural aggregates were dissociated using Accutase in the presence of 10 uM ROCK inhibitor and plated for final differentiation at ~85000 cells/cm^2 in neural differentiation media containing cAMP (10 uM, Sigma), IGF-1, BDNF, and GDNF (10 ng/ml, Peprotech). The day of neural aggregate dissociation was considered "day 24". Cells were cultured for another 16 days to day 40 or 26 days to day 50.

Induced neuron differentiation

Induced neurons were generated as described[75], with some modifications. iPSCs were cultured on Matrigel-coated plates in mTeSR1 media, infected with lentivirus encoding Ub-rtTA, TetO-Ngn2-T2A-puro, and TetO-GFP, and expanded. Viruses were a generous gift from Kevin Eggan. Transduced cells were dissociated with Accutase and plated onto Matrigel-coated plates at 50000 cells/cm^2 in mTeSR1 (day 0). On day 1, media was changed to KSR media with SB413542 (10 uM, Tocris), LDN-193189 (100 nM, Stemgent), XAV939 (2 uM, Stemgent), and doxycycline (2 ug/ml, Sigma). Doxycycline was maintained in the media for the remainder of the differentiation. On day 2, media was changed to 1:1 (KSR + SB413542/LDN-193189/XAV939):N2B media with puromycin (5 ug/ml, Gibco). Media was changed to N2B media + 1:100 B27 supplement (Life Technologies) on day 3. From day 4 on, cells were cultured in NBM media + 1:50 B27 + BDNF, GDNF (10 ng/ml, Peprotech), CNTF (10 ng/ml, R&D systems). Puromycin was maintained in the media until day 4-6.

Medias

MEF media: DMEM, 10% FBS, 100 U/ml Penicillin-Streptomycin, 2 mM L-glutamine (Life Technologies).

iPSC media: DMEM/F12, 20% KOSR, 1x MEM-NEAA, 1x Penicillin-Streptomycin-Glutamine, 55

uM beta-mercaptoethanol (Life Technologies).

N2 neural induction media: DMEM/F12, 1x N2 supplement, 1x MEM-NEAA (Life Technologies), 2 ug/ml heparin (Sigma).

N2/B27 neural induction media: DMEM/F12, 1x N2 supplement, 1x B27 supplement, 1x MEM-NEAA (Life Technologies), 2 ug/ml heparin (Sigma).

Neural differentiation media: Neurobasal medium, 1x N2 supplement, 1x B27 supplement, 1x MEM-NEAA (Life Technologies), 2 ug/ml heparin (Sigma).

KSR media: Knockout DMEM, 15% KOSR, 1x MEM-NEAA, 55 uM beta-mercaptoethanol, 1x GlutaMAX (Life Technologies).

N2B media: DMEM/F12, 1x GlutaMAX (Life Technologies), 1x N2 supplement B (Stemcell Technologies), 0.3% dextrose (D-(+)-glucose, Sigma).

NBM media: Neurobasal medium, 0.5x MEM-NEAA, 1x GlutaMAX (Life Technologies), 0.3% dextrose (D-(+)-glucose, Sigma).

Cycloheximide treatment

Day 40 embryoid aggregate differentiated neurons were treated with neural differentiation media + 1/500 DMSO (vehicle) or 100 ug/ml cycloheximide (Sigma) for the times indicated. Cells were then harvested for RNA and subsequent qRT-PCR analysis or lysed for Western blots.

Microelectrode array recordings

MEA recordings were performed as previously described[66]. Sterile single-well MEA culture dishes were coated with poly-D-lysine (Sigma) for 1 hr at room temperature, washed 3 times with sterile water, and dried overnight. The electrode area of each well was coated with Matrigel for 1 hr at 37°C. For embryoid aggregate-derived neurons, neural aggregates (day 24) were dissociated with Accutase + 10 uM ROCK Inhibitor. For induced neurons, cells were

dissociated on day 4 of differentiation with Accutase + 10 uM ROCK Inhibitor + DNase I (5U/ml, NEB). Human astrocytes (ScienCell), maintained in Astrocyte Medium (ScienCell), were dissociated with 0.25% Trypsin-EDTA (Life Technologies). Approximately 75000 neurons and 75000 astrocytes were resuspended in a 3:2 mixture of neural media:astrocyte media in a 50 ul volume and plated directly onto the electrode surface. Cells were incubated at 37°C for 30 min to allow cells to adhere before adding 500 ul 3:2 neural:astrocyte media to the well. Cells were fed with either neural differentiation media (embryoid aggregate neurons) or NBM media (induced neurons) for the remainder of the protocol.

MEA recordings were performed using the Muse system (Axion Biosystems). Each well contains 64 nano-porous platinum electrodes arranged in an 8x8 grid. Data were acquired using AxIS software (Axion Biosystems) at a sampling rate of 12.5 kHz, filtered using a 200-2500 Hz Butterworth band-pass filter. The detection threshold was set to ±5.5x SD baseline electrode noise. Raster plots were analyzed using NeuroExplorer (NEX Technologies). Waveform data were filtered and plotted using custom MATLAB scripts (The Mathworks).

qPCR

RNA was extracted using the Pure Link RNA Mini Kit (Life Technologies) and reverse transcribed using SuperScript II (Life Technologies). cDNA was used for qPCR with Fast SYBR Green Master Mix (Life Technologies) on a ViiA 7 System (Life Technologies). Samples were run using 3 technical replicates (n in figures represent biological replicates only). Data were normalized to GAPDH expression using the $\Delta\Delta C_T$ method as previously described[123]. Primer efficiency was calculated for each primer pair and the slope of a template dilution curve was found to be within an appropriate range. Melting curves after amplification showed single peaks at the appropriate temperature for each amplicon, indicating specificity of amplification. Primers are listed below.

Primers

Gene	Application	Primer	Sequence
DISC1	Exon 2 Sanger genotyping	Forward	CTACATGAGAAGCTCGACAGGGCCTGGGAT
		Reverse	CAAGAGACTGAAGGGCCGAGAGAGACATC
DISC1	Exon 8 Sanger genotyping	Forward	AAACCCAGAAATCTCTGACCTGGCTGTTCC
		Reverse	CCCAAATACGGTACTCACTTAAACACCTTGTGC
GAPDH	qPCR	Forward	GGGAGCCAAAAGGGTCATCA
		Reverse	TGGTTCACACCCATGACGAA
DISC1	qPCR, exon 2	Forward	CCCCTACTGTGACCTCTGTGA
		Reverse	AATCTGGTGCCACCTCTGA
DISC1	qPCR, exon 12/13	Forward	AAAGTGTGAAGACATAGGCAAGAA
		Reverse	CCCTCCTGAGAGAATGAATGAG

NanoString gene expression analysis

Two 150-gene nCounter Custom CodeSets were designed by NanoString Technologies to facilitate analysis of 150 genes from a single sample. One codeset was used to generate initial embryoid aggregate expression data (Appendix 2). Data were analyzed by subtracting counts from a blank control and normalizing to 8 housekeeping genes (B2M, GAPDH, GUSB, HPRT1, LDHA, POLR2A, RPL13a and RPL27). After this codeset was depleted, another codeset was made, which greatly overlapped with the initial codeset (but with some substitutions) – this codeset was used to generate induced neuron and patterning embryoid aggregate data (Appendix 2). Data were analyzed with nSolver Analysis Software (NanoString Technologies) and normalized to the total gene set.

Assays were performed according to the manufacturer's instructions. Briefly, 200-1000 ng RNA was hybridized with capture and reporter probesets at 65°C for 12-30 hours. Hybridized samples were processed using an nCounter Prep Station and imaged using an nCounter Digital Analyzer (NanoString Technologies).

Immunocytochemistry and microscopy

Cells were fixed with 4% paraformaldehyde (Sigma), followed by membrane

permeabilization and blocking with 0.2% Triton X-100 (Sigma) and 2% donkey serum (Jackson Immunoresearch) in PBS for 1 hour at room temperature. Cells were then incubated with primary antibodies overnight at 4°C, secondary antibodies for 1 hr at room temperature, and 1:1000 DAPI (Life Technologies) for 10 minutes, with multiple washes between each step. Samples were imaged using a Zeiss LSM710 confocal microscope and Zen black software. Zen black and FIJI were used to pseudo-color images and add scale bars. Antibodies are listed below.

Western blots

Lysates were prepared in a buffer containing 1% NP40, 10 mM EDTA, 150 mM NaCl, 50 mM Tris, cOmplete Protease Inhibitors and phosSTOP (Roche). BCA protein assays were performed on all samples to normalize for protein content (Pierce). Equal protein amounts were loaded onto 4-12% Bis-Tris NuPAGE gels (Life Technologies) and transferred to nitrocellulose membranes. Blots were either incubated with HRP-conjugated secondary antibodies and developed using ECL substrate (for DISC1 only, Pierce) or incubated with fluorophore-conjugated secondary antibodies and imaged on the Odyssey system (all other antigens, LI-COR).

Antibodies

Antigen	Host	Application	Dilution	Vendor	Catalog #
MAP2	Chicken	ICC, WB	1/2500, 1/5000	Abcam	ab5392
Brn2	Rabbit	ICC	1/300	Abcam	ab137469
Satb2	Mouse	ICC	1/100	Abcam	ab51502
Nestin	Mouse	ICC	1/1000	R&D	MAB1259
PSD-95	Mouse	ICC	1/400	Abcam	ab2723
Cux2	Rabbit	ICC		Abcam	ab130395
Cux1	Mouse	ICC	1/300	Abcam	ab54583
Ngn2	Rabbit	ICC	1/200	Abcam	ab109236
VGLUT1	Rabbit	ICC	1/300	Synaptic systems	135303
VGLUT2	Mouse	ICC	1/1000	Abcam	ab79157
CTIP2	Rat	ICC	1/300	Abcam	ab18465
Tbr2	Rabbit	ICC		(gift from Hevner lab)	

Tbr2	Rabbit	ICC	1/250	Abcam	ab23345
FoxG1	Rabbit	ICC	1/300	Abcam	ab18259
Pax6	Rabbit	ICC	1/300	Covance	PRB-278P
Tau	Rabbit	ICC, WB	1/200	Dako	A0024
Tbr1	Rabbit	ICC	1/250	Abcam	ab32454
SYP	Rabbit	ICC, WB	1/200, 1/1000	Abcam	ab14692
DISC1 (3G10)	Mouse	WB	1/1000	(from TYP/DJS labs)	
GAPDH	Mouse	WB	1/2000	Millipore	MAB374
SYN I	Rabbit	WB	1/200	Millipore	574777
APP (C9)	Rabbit	WB	1/1000	(from DJS lab)	

RNA-sequencing

RNA was extracted from embryoid aggregate differentiated day 17 (NPC) or day 50 (neuron) samples using the Pure Link RNA Mini Kit (Life Technologies). Total RNA samples were converted into cDNA libraries using the TruSeq Stranded Total RNA-RiboZero Gold Sample Prep Kit (Illumina). Starting with 100 ng of total RNA, ribosomal RNA was removed by hybridization to a biotinylated probe selective for ribosomal RNA species, followed by streptavidin bead binding and sample purification. The resulting rRNA-depleted sample was chemically fragmented and converted into single-stranded cDNA using reverse transcriptase and random hexamer primers, with the addition of Actinomycin D to suppress DNA-dependent synthesis of the second strand. Double-stranded cDNA was created by removing the RNA template and synthesizing the second strand in the presence of dUTP in place of dTTP. A single A base was added to the 3' end to facilitate ligation of sequencing adapters, which contain a single T base overhang. Adapter-ligated cDNA was amplified by polymerase chain reaction to increase the amount of sequence-ready library. During this amplification the polymerase stalls when it encounters a U base, rendering the second strand a poor template. Accordingly, amplified material used the first strand as a template, thereby preserving the strand information. Final cDNA libraries were analyzed for size distribution and using an Agilent Bioanalyzer (DNA 1000 kit, Agilent), quantitated by qPCR (KAPA Library Quant Kit, KAPA Biosystems), then

normalized to 2 nM in preparation for sequencing. RNA was sequenced using stranded paired-end reads, with ~50 millions reads per sample.

Differential gene expression analysis

Reads were mapped to the UCSC Human Reference Genome (hg19) using TopHat v2.0.10[124]. Reads mapping to genes were counted using htseq (v0.6.1)[125]. Counts were upper quartile normalized using SVS (Golden Helix) for limited gene comparisons. Alternatively, differential gene expression analysis between lines was performed using the edgeR package in R[126]. To evaluate for differential exon usage across the lines, the DEXSeq package was used[127].

Off-target mutagenesis analysis

Off-target cleavage sites were predicted for the exon2 CRISPR/Cas9 construct using CCTop (http://crispr.cos.uni-heidelberg.de/) and <crispr.mit.edu>[128]. For the exon 8 TALEN constructs, potential off target cleavage sites were predicted using PROGNOS[129] and TALENoffer[130]. Variants in the RNA-seq datasets were called using the GATK Best Practices for Variant Discovery[131]. No indels or SNPs were observed at any of the top 10 overall or top 10 coding predicted CRISPR/Cas9 or TALEN cleavage sites from each of these prediction tools.

Luciferase assays

Control (“L”) and Wnt3a conditioned media (CM) was produced using Wnt3a-expressing and control (“L”) cells (ATCC). Conditioned medias were generated according to the ATCC protocol. Neural aggregates (~day 27-31) were dissociated using Accutase + 10 uM ROCK Inhibitor. Cells were resuspended in in P3 solution (Lonza) and DNA was added (3 ug Super8XTOPFlash, 1.5 ug pMIR-REPORT-beta-galactosidase, 1-5E6 cells). Super8XTOPFlash was a gift from Randall Moon[132]; pMIR-REPORT-b-gal was purchased from Life Technologies. Cells were electroporated by the Amaxa 4D-Nucleofector X Unit (Lonza, program CU-133). Electroporated cells were recovered in RPMI (Life Technologies) + 10% B27 supplement + 20

uM ROCK Inhibitor for 15 minutes and subsequently plated onto poly-ornithine/laminin coated 96 well plates (4 ug/cm^2 poly-ornithine, 1 ug/cm^2 laminin, coated overnight at 37°C) containing N2/B27 neural induction media + 10 uM ROCK-Inhibitor. 16 hours later, media was changed to L or Wnt3a CM for 24 hours. Cells were then lysed in luciferase assay lysis buffer (Biotium) and used for a firefly luciferase assay (Biotium) and beta-galactosidase assay (Promega). Luciferase and beta-galactosidase activities were assayed using a Synergy H1 reader (BioTek). Luciferase activity was normalized to beta-galactosidase activity for each sample.

Data collection and statistics

All data represent at least three independent experiments, utilizing the iPSC lines as shown in Table 3.1. Data were analyzed using GraphPad PRISM 6 software. Values are expressed as means ±SEM. Statistical significance was tested by either one-way or two-way ANOVA with Holm-Sidak's multiple comparisons post-test, as indicated in figure legends. Statistical significance was determined by *P*-values of < 0.05.

ACKNOWLEDGEMENTS

We thank N. Sanjana and F. Zhang for help designing TALENs and providing TALE monomer and TALEN backbone plasmids; R. Nehme and K. Eggan for valuable guidance in performing induced neuron differentiations and generously providing the Ngn2 induced neuron protocol viruses; R. Hevner for sharing Tbr2 antibody; and C. Zhou, F. Abawi, and P. Mouradian for technical assistance.

REFERENCES

1. Williams, H. J., Owen, M. J. & O'Donovan, M. C. Schizophrenia genetics: new insights from new approaches. *Br. Med. Bull.* **91,** 61–74 (2009).

2. Tsuang, M. Schizophrenia: genes and environment. *Biol Psychiatry* **47,** 210–220 (2000).

3. van Os, J., Kenis, G. & Rutten, B. P. F. The environment and schizophrenia. *Nature* **468,** 203–212 (2010).

4. Tamminga, C. A. & Holcomb, H. H. Phenotype of schizophrenia: a review and formulation. *Mol Psychiatry* **10,** 27–39 (2005).

5. Harrison, P. J. The neuropathology of schizophrenia. A critical review of the data and their interpretation. *Brain* **122 (Pt 4),** 593–624 (1999).

6. Harrison, P. J. & Weinberger, D. R. Schizophrenia genes, gene expression, and neuropathology: on the matter of their convergence. *Mol Psychiatry* **10,** 40–68; image 5 (2005).

7. Weinberger, D. R. From neuropathology to neurodevelopment. *Lancet* **346,** 552–557 (1995).

8. Weinberger, D. R. Implications of normal brain development for the pathogenesis of schizophrenia. *Archives of General Psychiatry* **44,** 660–669 (1987).

9. Ripke, S. *et al.* Genome-wide association analysis identifies 13 new risk loci for schizophrenia. *Nat Biotechnol* **45,** 1150–1159 (2013).

10. Cross-Disorder Group of the Psychiatric Genomics Consortium. Identification of risk loci with shared effects on five major psychiatric disorders: a genome-wide analysis. *Lancet* **381,** 1371–1379 (2013).

11. Lee, S. H. *et al.* Estimating the proportion of variation in susceptibility to schizophrenia captured by common SNPs. *Nat Biotechnol* **44,** 247–250 (2012).

12. International Schizophrenia Consortium *et al.* Common polygenic variation contributes to risk of schizophrenia and bipolar disorder. *Nature* **460,** 748–752 (2009).

13. Reinhardt, P. *et al.* Genetic correction of a LRRK2 mutation in human iPSCs links parkinsonian neurodegeneration to ERK-dependent changes in gene expression. *Cell Stem Cell* **12,** 354–367 (2013).

14. Schizophrenia Working Group of the Psychiatric Genomics Consortium. Biological

insights from 108 schizophrenia-associated genetic loci. *Nature* **511,** 421–427 (2014).

15. Sullivan, P. F., Daly, M. J. & O'Donovan, M. Genetic architectures of psychiatric disorders: the emerging picture and its implications. *Nat Rev Genet* **13,** 537–551 (2012).

16. Mitchell, K. J. The genetics of neurodevelopmental disease. *Curr Opin Neurobiol* **21,** 197–203 (2011).

17. St Clair, D. *et al.* Association within a family of a balanced autosomal translocation with major mental illness. *Lancet* **336,** 13–16 (1990).

18. Millar, J. K. *et al.* Disruption of two novel genes by a translocation co-segregating with schizophrenia. *Human Molecular Genetics* **9,** 1415–1423 (2000).

19. Blackwood, D. H. *et al.* Schizophrenia and affective disorders--cosegregation with a translocation at chromosome 1q42 that directly disrupts brain-expressed genes: clinical and P300 findings in a family. *Am J Hum Genet* **69,** 428–433 (2001).

20. Selkoe, D. J. Alzheimer's disease. *Cold Spring Harb Perspect Biol* **3,** (2011).

21. Hodgkinson, C. A. *et al.* Disrupted in schizophrenia 1 (DISC1): association with schizophrenia, schizoaffective disorder, and bipolar disorder. *Am J Hum Genet* **75,** 862–872 (2004).

22. Cannon, T. D. *et al.* Association of DISC1/TRAX haplotypes with schizophrenia, reduced prefrontal gray matter, and impaired short- and long-term memory. *Archives of General Psychiatry* **62,** 1205–1213 (2005).

23. Thomson, P. A. *et al.* Association between the TRAX/DISC locus and both bipolar disorder and schizophrenia in the Scottish population. *Mol Psychiatry* **10,** 657–68– 616 (2005).

24. Hashimoto, R. *et al.* Impact of the DISC1 Ser704Cys polymorphism on risk for major depression, brain morphology and ERK signaling. *Human Molecular Genetics* **15,** 3024–3033 (2006).

25. Kilpinen, H. *et al.* Association of DISC1 with autism and Asperger syndrome. *Mol Psychiatry* **13,** 187–196 (2008).

26. Saetre, P. *et al.* Association between a disrupted-in-schizophrenia 1 (DISC1) single nucleotide polymorphism and schizophrenia in a combined Scandinavian case-control sample. *Schizophrenia Research* **106,** 237–241 (2008).

27. Hennah, W. *et al.* Haplotype transmission analysis provides evidence of association for

DISC1 to schizophrenia and suggests sex-dependent effects. *Human Molecular Genetics* **12,** 3151–3159 (2003).

28. Callicott, J. H. *et al.* Variation in DISC1 affects hippocampal structure and function and increases risk for schizophrenia. *Proc Natl Acad Sci USA* **102,** 8627–8632 (2005).

29. Hamshere, M. L. *et al.* Genomewide linkage scan in schizoaffective disorder: significant evidence for linkage at 1q42 close to DISC1, and suggestive evidence at 22q11 and 19p13. *Archives of General Psychiatry* **62,** 1081–1088 (2005).

30. Brandon, N. J. & Sawa, A. Linking neurodevelopmental and synaptic theories of mental illness through DISC1. *Nat Rev Neurosci* **12,** 707–722 (2011).

31. Insel, T. R. Rethinking schizophrenia. *Nature* **468,** 187–193 (2010).

32. Lewis, D. A. & Levitt, P. Schizophrenia as a disorder of neurodevelopment. *Annu Rev Neurosci* **25,** 409–432 (2002).

33. Corfas, G., Roy, K. & Buxbaum, J. D. Neuregulin 1-erbB signaling and the molecular/cellular basis of schizophrenia. *Nat Neurosci* **7,** 575–580 (2004).

34. Jaaro-Peled, H. *et al.* Neurodevelopmental mechanisms of schizophrenia: understanding disturbed postnatal brain maturation through neuregulin-1-ErbB4 and DISC1. *Trends Neurosci* **32,** 485–495 (2009).

35. Arnold, S. E., Talbot, K. & Hahn, C.-G. Neurodevelopment, neuroplasticity, and new genes for schizophrenia. *Prog Brain Res* **147,** 319–345 (2005).

36. Hikida, T. *et al.* Dominant-negative DISC1 transgenic mice display schizophrenia-associated phenotypes detected by measures translatable to humans. *Proc Natl Acad Sci USA* **104,** 14501–14506 (2007).

37. Pletnikov, M. V. *et al.* Inducible expression of mutant human DISC1 in mice is associated with brain and behavioral abnormalities reminiscent of schizophrenia. *Mol Psychiatry* **13,** 173–86, 115 (2008).

38. Clapcote, S. J. *et al.* Behavioral phenotypes of Disc1 missense mutations in mice. *Neuron* **54,** 387–402 (2007).

39. Kamiya, A. *et al.* A schizophrenia-associated mutation of DISC1 perturbs cerebral cortex development. *Nat Cell Biol* **7,** 1167–1178 (2005).

40. Mao, Y. *et al.* Disrupted in schizophrenia 1 regulates neuronal progenitor proliferation via modulation of GSK3beta/beta-catenin signaling. *Cell* **136,** 1017–1031 (2009).

41. Li, W. *et al.* Specific developmental disruption of disrupted-in-schizophrenia-1 function results in schizophrenia-related phenotypes in mice. *Proc Natl Acad Sci USA* **104,** 18280–18285 (2007).

42. Kvajo, M. *et al.* A mutation in mouse Disc1 that models a schizophrenia risk allele leads to specific alterations in neuronal architecture and cognition. *Proc Natl Acad Sci USA* **105,** 7076–7081 (2008).

43. Duan, X. *et al.* Disrupted-In-Schizophrenia 1 regulates integration of newly generated neurons in the adult brain. *Cell* **130,** 1146–1158 (2007).

44. Young-Pearse, T. L., Suth, S., Luth, E. S., Sawa, A. & Selkoe, D. J. Biochemical and functional interaction of disrupted-in-schizophrenia 1 and amyloid precursor protein regulates neuronal migration during mammalian cortical development. *J Neurosci* **30,** 10431–10440 (2010).

45. Niwa, M. *et al.* Knockdown of DISC1 by in utero gene transfer disturbs postnatal dopaminergic maturation in the frontal cortex and leads to adult behavioral deficits. *Neuron* **65,** 480–489 (2010).

46. Nakata, K. *et al.* DISC1 splice variants are upregulated in schizophrenia and associated with risk polymorphisms. *Proceedings of the National Academy of Sciences* **106,** 15873–15878 (2009).

47. Takahashi, K. *et al.* Induction of pluripotent stem cells from adult human fibroblasts by defined factors. *Cell* **131,** 861–872 (2007).

48. Yu, J. *et al.* Induced pluripotent stem cell lines derived from human somatic cells. *Science* **318,** 1917–1920 (2007).

49. Park, I.-H. *et al.* Reprogramming of human somatic cells to pluripotency with defined factors. *Nature* **451,** 141–146 (2008).

50. Lancaster, M. A. *et al.* Cerebral organoids model human brain development and microcephaly. *Nature* **501,** 373–379 (2013).

51. Eiraku, M. *et al.* Self-organized formation of polarized cortical tissues from ESCs and its active manipulation by extrinsic signals. *Cell Stem Cell* **3,** 519–532 (2008).

52. Mariani, J. *et al.* Modeling human cortical development in vitro using induced pluripotent stem cells. *Proceedings of the National Academy of Sciences* **109,** 12770–12775 (2012).

53. Gaspard, N. *et al.* An intrinsic mechanism of corticogenesis from embryonic stem cells. *Nature* **455,** 351–357 (2008).

54. Shi, Y., Kirwan, P., Smith, J., Robinson, H. P. C. & Livesey, F. J. Human cerebral cortex development from pluripotent stem cells to functional excitatory synapses. *Nat Neurosci* **15,** 477–486 (2012).

55. Bock, C. *et al.* Reference Maps of human ES and iPS cell variation enable high-throughput characterization of pluripotent cell lines. *Cell* **144,** 439–452 (2011).

56. Brennand, K. J. *et al.* Modelling schizophrenia using human induced pluripotent stem cells. *Nature* **473,** 221–225 (2011).

57. Paulsen, B. D. S. *et al.* Altered oxygen metabolism associated to neurogenesis of induced pluripotent stem cells derived from a schizophrenic patient. *ct* **21,** 1547–1559 (2012).

58. Robicsek, O. *et al.* Abnormal neuronal differentiation and mitochondrial dysfunction in hair follicle-derived induced pluripotent stem cells of schizophrenia patients. *Mol Psychiatry* **18,** 1067–1076 (2013).

59. Brennand, K. *et al.* Phenotypic differences in hiPSC NPCs derived from patients with schizophrenia. *Mol Psychiatry* **20,** 361–368 (2015).

60. Yu, D. X. *et al.* Modeling hippocampal neurogenesis using human pluripotent stem cells. *Stem Cell Reports* **2,** 295–310 (2014).

61. Yoon, K.-J. *et al.* Modeling a Genetic Risk for Schizophreniain iPSCs and Mice Reveals Neural Stem Cell Deficits Associated with Adherens Junctions and Polarity. *Stem Cell* **15,** 79–91 (2014).

62. Wen, Z. *et al.* Synaptic dysregulation in a human iPS cell model of mental disorders. *Nature* 1–15 (2014). doi:10.1038/nature13716

63. Sanjana, N. E. *et al.* A transcription activator-like effector toolbox for genome engineering. *Nat Protoc* **7,** 171–192 (2012).

64. Millar, J. K. *et al.* DISC1 and PDE4B are interacting genetic factors in schizophrenia that regulate cAMP signaling. *Science* **310,** 1187–1191 (2005).

65. Silva, A. L. & Romão, L. The mammalian nonsense-mediated mRNA decay pathway: to decay or not to decay! Which players make the decision? *FEBS Lett* **583,** 499–505 (2009).

66. Muratore, C. R. *et al.* The familial Alzheimer's disease APPV717I mutation alters APP processing and Tau expression in iPSC-derived neurons. *Human Molecular Genetics* **23,** 3523–3536 (2014).

67. Ishigaki, Y., Li, X., Serin, G. & Maquat, L. E. Evidence for a pioneer round of mRNA translation: mRNAs subject to nonsense-mediated decay in mammalian cells are bound by CBP80 and CBP20. *Cell* **106,** 607–617 (2001).

68. Barodia, S. K., Park, S. K., Ishizuka, K., Sawa, A. & Kamiya, A. Half-life of DISC1 protein and its pathological significance under hypoxia stress. *Neuroscience Research* (2015). doi:10.1016/j.neures.2015.02.008

69. Savage, M. J. *et al.* Turnover of amyloid beta-protein in mouse brain and acute reduction of its level by phorbol ester. *J Neurosci* **18,** 1743–1752 (1998).

70. Lyckman, A. W., Confaloni, A. M., Thinakaran, G., Sisodia, S. S. & Moya, K. L. Post-translational processing and turnover kinetics of presynaptically targeted amyloid precursor superfamily proteins in the central nervous system. *J Biol Chem* **273,** 11100–11106 (1998).

71. Morales-Corraliza, J. *et al.* In vivo turnover of tau and APP metabolites in the brains of wild-type and Tg2576 mice: greater stability of sAPP in the beta-amyloid depositing mice. *PLoS ONE* **4,** e7134 (2009).

72. Vieira, S. I. *et al.* Retrieval of the Alzheimer's amyloid precursor protein from the endosome to the TGN is S655 phosphorylation state-dependent and retromer-mediated. *Mol Neurodegener* **5,** 40 (2010).

73. Lefort, R., Pozueta, J. & Shelanski, M. Cross-linking of cell surface amyloid precursor protein leads to increased β-amyloid peptide production in hippocampal neurons: implications for Alzheimer's disease. *Journal of Neuroscience* **32,** 10674–10685 (2012).

74. Sachs, N. A. *et al.* A frameshift mutation in Disrupted in Schizophrenia 1 in an American family with schizophrenia and schizoaffective disorder. *Mol Psychiatry* **10,** 758–764 (2005).

75. Zhang, Y. *et al.* Rapid single-step induction of functional neurons from human pluripotent stem cells. *Neuron* **78,** 785–798 (2013).

76. Nieto, M. *et al.* Expression of Cux-1 and Cux-2 in the subventricular zone and upper layers II-IV of the cerebral cortex. *J Comp Neurol* **479,** 168–180 (2004).

77. Balamotis, M. A. *et al.* Satb1 ablation alters temporal expression of immediate early genes and reduces dendritic spine density during postnatal brain development. *Mol Cell Biol* **32,** 333–347 (2012).

78. Gao, Z. *et al.* Neurod1 is essential for the survival and maturation of adult-born neurons. *Nat Biotechnol* **12,** 1090–1092 (2009).

79. Tao, W. & Lai, E. Telencephalon-restricted expression of BF-1, a new member of the HNF-3/fork head gene family, in the developing rat brain. *Neuron* **8,** 957–966 (1992).

80. Molyneaux, B. J., Arlotta, P., Menezes, J. R. L. & Macklis, J. D. Neuronal subtype specification in the cerebral cortex. *Nat Rev Neurosci* **8,** 427–437 (2007).

81. Shimamura, K., Hartigan, D. J., Martinez, S., Puelles, L. & Rubenstein, J. L. Longitudinal organization of the anterior neural plate and neural tube. *Development* **121,** 3923–3933 (1995).

82. Xuan, S. *et al.* Winged helix transcription factor BF-1 is essential for the development of the cerebral hemispheres. *Neuron* **14,** 1141–1152 (1995).

83. Englund, C. *et al.* Pax6, Tbr2, and Tbr1 are expressed sequentially by radial glia, intermediate progenitor cells, and postmitotic neurons in developing neocortex. *Journal of Neuroscience* **25,** 247–251 (2005).

84. Hevner, R. F., Hodge, R. D., Daza, R. A. M. & Englund, C. Transcription factors in glutamatergic neurogenesis: conserved programs in neocortex, cerebellum, and adult hippocampus. *Neuroscience Research* **55,** 223–233 (2006).

85. Sessa, A., Mao, C.-A., Hadjantonakis, A.-K., Klein, W. H. & Broccoli, V. Tbr2 directs conversion of radial glia into basal precursors and guides neuronal amplification by indirect neurogenesis in the developing neocortex. *Neuron* **60,** 56–69 (2008).

86. Manuel, M. *et al.* The transcription factor Foxg1 regulates the competence of telencephalic cells to adopt subpallial fates in mice. *Development* **137,** 487–497 (2010).

87. Martynoga, B., Morrison, H., Price, D. J. & Mason, J. O. Foxg1 is required for specification of ventral telencephalon and region-specific regulation of dorsal telencephalic precursor proliferation and apoptosis. *Developmental Biology* **283,** 113–127 (2005).

88. Danesin, C. *et al.* Integration of telencephalic Wnt and hedgehog signaling center activities by Foxg1. *Dev. Cell* **16,** 576–587 (2009).

89. Backman, M. *et al.* Effects of canonical Wnt signaling on dorso-ventral specification of the mouse telencephalon. *Developmental Biology* **279,** 155–168 (2005).

90. Ulloa, F. & Martí, E. Wnt won the war: antagonistic role of Wnt over Shh controls dorso-ventral patterning of the vertebrate neural tube. *Dev Dyn* **239,** 69–76 (2010).

91. Li, X.-J. *et al.* Coordination of sonic hedgehog and Wnt signaling determines ventral and dorsal telencephalic neuron types from human embryonic stem cells. *Development* **136,** 4055–4063 (2009).

92. Wilson, S. W. & Rubenstein, J. L. Induction and dorsoventral patterning of the telencephalon. *Neuron* **28,** 641–651 (2000).

93. Hirabayashi, Y. *et al.* The Wnt/beta-catenin pathway directs neuronal differentiation of cortical neural precursor cells. *Development* **131,** 2791–2801 (2004).

94. Munji, R. N., Choe, Y., Li, G., Siegenthaler, J. A. & Pleasure, S. J. Wnt signaling regulates neuronal differentiation of cortical intermediate progenitors. *Journal of Neuroscience* **31,** 1676–1687 (2011).

95. Singh, K. K. *et al.* Common DISC1 Polymorphisms Disrupt Wnt/GSK3β Signaling and Brain Development. *Neuron* **72,** 545–558 (2011).

96. Singh, K. K. *et al.* Dixdc1 is a critical regulator of DISC1 and embryonic cortical development. *Neuron* **67,** 33–48 (2010).

97. Su, P. *et al.* A Dopamine D2 Receptor-DISC1 Protein Complex may Contribute to Antipsychotic-Like Effects. *Neuron* **84,** 1302–1316 (2014).

98. Chen, J. K., Taipale, J., Cooper, M. K. & Beachy, P. A. Inhibition of Hedgehog signaling by direct binding of cyclopamine to Smoothened. *Genes & Development* **16,** 2743–2748 (2002).

99. Espuny-Camacho, I. *et al.* Pyramidal neurons derived from human pluripotent stem cells integrate efficiently into mouse brain circuits in vivo. *Neuron* **77,** 440–456 (2013).

100. Kim, J.-E. *et al.* Investigating synapse formation and function using human pluripotent stem cell-derived neurons. *Proc Natl Acad Sci USA* **108,** 3005–3010 (2011).

101. Porteous, D. J. *et al.* DISC1 as a genetic risk factor for schizophrenia and related major mental illness: response to Sullivan. *Mol Psychiatry* **19,** 141–143 (2014).

102. Ma, L. *et al.* Cloning and characterization of Disc1, the mouse ortholog of DISC1 (Disrupted-in-Schizophrenia 1). *Genomics* **80,** 662–672 (2002).

103. Veres, A. *et al.* Low incidence of off-target mutations in individual CRISPR-Cas9 and TALEN targeted human stem cell clones detected by whole-genome sequencing. *Cell Stem Cell* **15,** 27–30 (2014).

104. Smith, C. *et al.* Whole-genome sequencing analysis reveals high specificity of CRISPR/Cas9 and TALEN-based genome editing in human iPSCs. *Cell Stem Cell* **15,** 12–13 (2014).

105. Suzuki, K. *et al.* Targeted gene correction minimally impacts whole-genome mutational load in human-disease-specific induced pluripotent stem cell clones. *Cell Stem Cell* **15,** 31–36 (2014).

106. Yang, L. *et al.* Targeted and genome-wide sequencing reveal single nucleotide variations impacting specificity of Cas9 in human stem cells. *Nature Communications* **5,**

5507 (2014).

107. Donoviel, D. B. *et al.* Mice lacking both presenilin genes exhibit early embryonic patterning defects. *Genes & Development* **13,** 2801–2810 (1999).

108. Eykelenboom, J. E. *et al.* A t(1;11) translocation linked to schizophrenia and affective disorders gives rise to aberrant chimeric DISC1 transcripts that encode structurally altered, deleterious mitochondrial proteins. *Human Molecular Genetics* **21,** 3374–3386 (2012).

109. Hebert, J. M. & Fishell, G. The genetics of early telencephalon patterning: some assembly required. *Nat Rev Neurosci* **9,** 678–685 (2008).

110. Ishizuka, K. *et al.* DISC1-dependent switch from progenitor proliferation to migration in the developing cortex. *Nature* **473,** 92–96 (2011).

111. Freyberg, Z., Ferrando, S. J. & Javitch, J. A. Roles of the Akt/GSK-3 and Wnt signaling pathways in schizophrenia and antipsychotic drug action. *Am J Psychiatry* **167,** 388–396 (2010).

112. Inestrosa, N. C., Montecinos-Oliva, C. & Fuenzalida, M. Wnt signaling: role in Alzheimer disease and schizophrenia. *J Neuroimmune Pharmacol* **7,** 788–807 (2012).

113. Toro, C. T. & Deakin, J. F. W. Adult neurogenesis and schizophrenia: a window on abnormal early brain development? *Schizophrenia Research* **90,** 1–14 (2007).

114. Guillemot, F. Cell fate specification in the mammalian telencephalon. *Prog. Neurobiol.* **83,** 37–52 (2007).

115. Esfandiari, F. *et al.* Glycogen synthase kinase-3 inhibition promotes proliferation and neuronal differentiation of human-induced pluripotent stem cell-derived neural progenitors. *Stem Cells and Development* **21,** 3233–3243 (2012).

116. Fang, W.-Q., Chen, W.-W., Fu, A. K. Y. & Ip, N. Y. Axin directs the amplification and differentiation of intermediate progenitors in the developing cerebral cortex. *Neuron* **79,** 665–679 (2013).

117. Fang, W.-Q. *et al.* Overproduction of upper-layer neurons in the neocortex leads to autism-like features in mice. *CellReports* **9,** 1635–1643 (2014).

118. LoTurco, J. J. & Bai, J. The multipolar stage and disruptions in neuronal migration. *Trends Neurosci* **29,** 407–413 (2006).

119. La Fata, G. *et al.* FMRP regulates multipolar to bipolar transition affecting neuronal migration and cortical circuitry. *Nat Neurosci* **17,** 1693–1700 (2014).

120. Miyoshi, G. & Fishell, G. Dynamic FoxG1 expression coordinates the integration of

multipolar pyramidal neuron precursors into the cortical plate. *Neuron* **74,** 1045–1058 (2012).

121. Zeng, H. *et al.* Specification of region-specific neurons including forebrain glutamatergic neurons from human induced pluripotent stem cells. *PLoS ONE* **5,** e11853 (2010).

122. Mali, P. *et al.* RNA-guided human genome engineering via Cas9. *Science* **339,** 823–826 (2013).

123. Livak, K. J. & Schmittgen, T. D. Analysis of relative gene expression data using real-time quantitative PCR and the 2(-Delta Delta C(T)) Method. *Methods* **25,** 402–408 (2001).

124. Kim, D. *et al.* TopHat2: accurate alignment of transcriptomes in the presence of insertions, deletions and gene fusions. *Genome Biol* **14,** R36 (2013).

125. Anders, S., Pyl, P. T. & Huber, W. HTSeq--a Python framework to work with high-throughput sequencing data. *Bioinformatics* **31,** 166–169 (2015).

126. Robinson, M. D., McCarthy, D. J. & Smyth, G. K. edgeR: a Bioconductor package for differential expression analysis of digital gene expression data. *Bioinformatics* **26,** 139–140 (2010).

127. Anders, S., Reyes, A. & Huber, W. Detecting differential usage of exons from RNA-seq data. *Genome Research* **22,** 2008–2017 (2012).

128. Hsu, P. D. *et al.* DNA targeting specificity of RNA-guided Cas9 nucleases. *Nat Biotechnol* **31,** 827–832 (2013).

129. Fine, E. J., Cradick, T. J., Zhao, C. L., Lin, Y. & Bao, G. An online bioinformatics tool predicts zinc finger and TALE nuclease off-target cleavage. *Nucleic Acids Res* **42,** e42 (2014).

130. Grau, J., Boch, J. & Posch, S. TALENoffer: genome-wide TALEN off-target prediction. *Bioinformatics* **29,** 2931–2932 (2013).

131. Van der Auwera, G. A. *et al.* From FastQ data to high confidence variant calls: the Genome Analysis Toolkit best practices pipeline. *Curr Protoc Bioinformatics* **11,** 11.10.1–11.10.33 (2013).

132. Veeman, M. T., Slusarski, D. C., Kaykas, A., Louie, S. H. & Moon, R. T. Zebrafish prickle, a modulator of noncanonical Wnt/Fz signaling, regulates gastrulation movements. *Curr. Biol.* **13,** 680–685 (2003).

Chapter IV.

Discussion

The study of human neuropsychiatric diseases is a complex task, due in part to our relatively incomplete knowledge of the underlying genetic alterations and molecular pathways implicated in these disorders. Only recently have tools been developed and genetic studies performed that facilitate investigation of the cellular and molecular pathophysiology of neuropsychiatric diseases. It will continue to be essential to combine work in heterologous cell lines, animal models, and human iPSCs to carefully model the molecular, cellular, and circuit defects that accompany mental illness-associated genetic mutations. When using iPSC-derived neurons, rare variants of strong effect will be important for identifying crucial pathways that can be dysregulated to contribute to disease. Given the variability inherent to iPSC differentiation protocols, stronger variants are more likely to yield reproducible, statistically significant phenotypes. The use of isogenic cell lines will be essential to control for effects of genetic background, which can greatly impact neuronal differentiation and neuronal phenotypes[1,2]. While off-target effects of genome editing remain a legitimate concern, several studies have found that use of genetic engineering technologies in human iPSCs is specific, with very few off-target mutations identified[3-6].

The studies cited above have nevertheless identified substantial clonal genomic variation among “isogenic” lines, which is attributed to somatic mutations that accumulate in individual clonal lines during passaging[3,6]. This somatic variation should be considered a source of potential phenotypic variability among lines with “identical” genotypes. Variation can be minimized by limiting cell passage number and regularly assaying for large-scale genomic variation (e.g. large CNVs). However, some accrual of genetic variation is likely unavoidable with extended cell culture. As a result, even with “isogenic” lines, ideally multiple lines of each genotype should be used to demonstrate disease phenotypes. Showing that a phenotype is reproducible when multiple wild-type and disease lines are used diminishes the chance of false phenotype discovery due to clonal variation.

Pioneering studies of neuropsychiatric disease in human neurons have identified developmental processes altered in different disease contexts, including neural progenitor organization, oxidative stress, hippocampal neurogenesis, neuronal migration, neuronal connectivity, and neuronal activity. These studies do not overlap much in their study of mutations and phenotypes, but differing results do exist between studies and mutations. For example, a study of sporadic SCZ lines identified decreased postsynaptic protein expression and synaptic density but normal spontaneous electrophysiological activity in neurons, whereas *DISC1* exon 12 Δ4bp lines showed decreased synaptic density, increased presynaptic protein expression, and decreased neuronal activity[7,8]. The current study does not evaluate synaptic density or activity in-depth, but shows unchanged expression of presynaptic proteins in neurons with frameshift mutations in exon 2 or exon 8 of *DISC1*. A recent report identified disorganization of NPC polarity with del15q11.2, but not with *DISC1* exon 12 Δ4bp[9]. Differences in phenotypes across disease models could result from distinct differentiation protocols, variability in the neuronal populations studied, and *bona fide* differences in the consequences of different disease-predisposing mutations. As increasing numbers of iPSC lines become available from different patients and with different mutations, future studies can assess phenotypes of interest across many disease-associated cell lines. Such studies will be able to identify those phenotypes that are unique to specific mutations and which, if any, are common across multiple mutations.

Genetic studies of major mental illnesses have revealed linkage of disease to many neurodevelopmental and synaptic genes[10-12]. It is very unlikely that most or all of these mutations, even if they are genuinely linked to development of mental illness, will impact the same cellular or developmental pathways. Rather, different mutations will likely impact distinct steps in development, and may exhibit phenotypes in distinct neuronal (or non-neuronal) subtypes. Different disease-predisposing mutations are likely to converge downstream onto

alterations in circuitry. Changes in neural circuitry in the adolescent brain may result from alterations in one or more upstream steps in development, including neural progenitor proliferation and patterning, neuronal migration and differentiation, and neurotransmission (Fig 4.1). Refining our knowledge of human neural development and identifying those processes that are altered with rare, but strongly penetrant, genetic variants linked to major mental illness will expedite the study of common, weaker variants. As technologies expand the possibilities for large-scale, high-throughput cell culture and phenotypic assays, mutations may eventually be studied in a combinatorial fashion. Introducing combinations of multiple mutations could evaluate additive effects on disease-relevant phenotypes, which may be easier to detect than the consequences of single, weak variants.

The ability to directly convert stem cells and somatic cells to specific neuronal populations of interest will increase our power to detect phenotypic alterations, but reduce the possibility of discovering alterations in unexpected cell types and processes. One example is demonstrated here, where *DISC1* interruption resulted in a consistent reduction of progenitor markers FoxG1 and Tbr2 in cortical NPCs derived from an embryoid aggregate differentiation protocol. However, iPSCs that were directly converted to a mature, homogenous population of upper layer neurons using Ngn2 transduction did not display these gene expression changes. As we show that *DISC1*-disruption alters Wnt signaling and NPC patterning during a window of neural progenitor development, this phenotype cannot be studied with a protocol, like Ngn2 induction, that largely bypasses this developmental time point. Expression of FoxG1 and Tbr2 is dramatically decreased in Ngn2-transduced “induced neurons” (iNs), and the effect of *DISC1* mutation on neurodevelopment is masked. However, iNs would be a more appropriate cell population to use to study synaptic biology, as this protocol greatly reduces heterogeneity (decreasing experimental noise) and increases maturity (making synaptic studies more

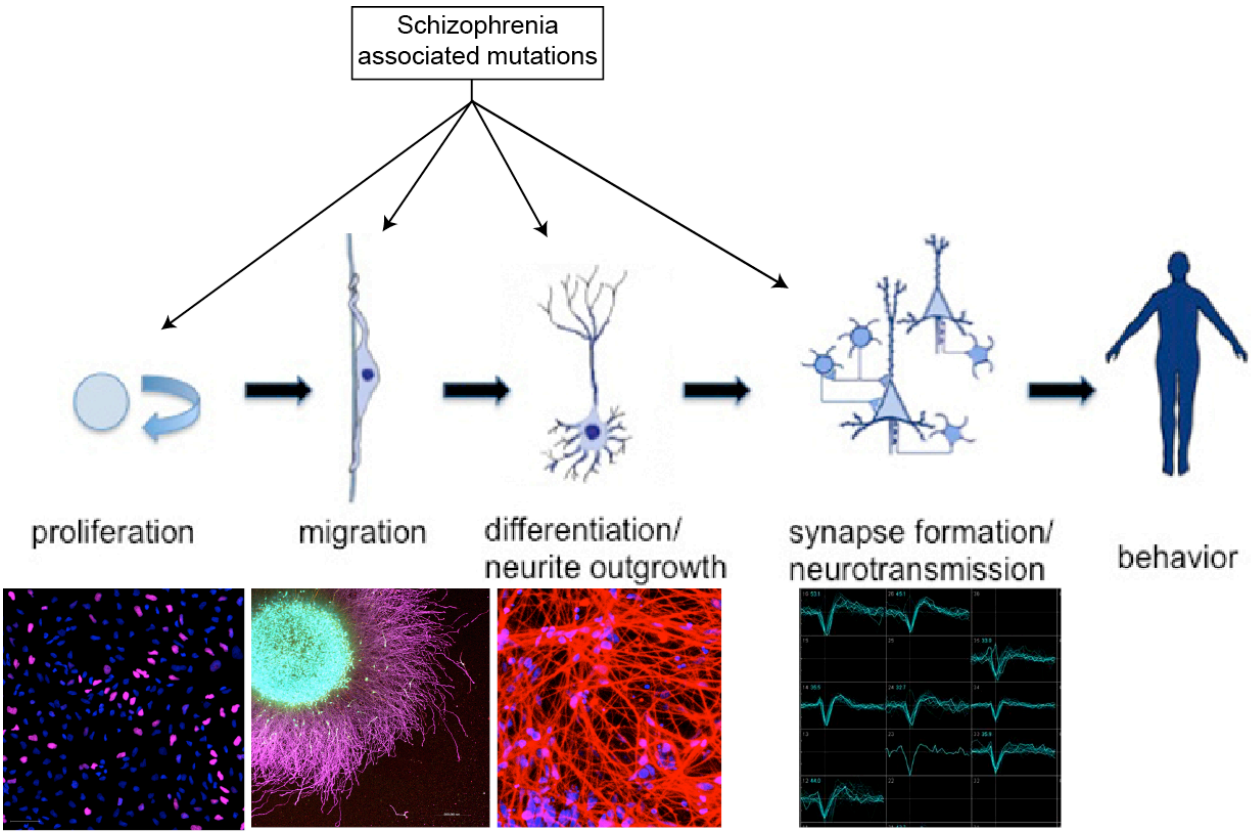

Figure 4.1. Schematic of developmental steps that may be affected by schizophrenia-associated mutations.

relevant). Our work demonstrates how selection of a differentiation protocol inherently biases a study to the discovery of different phenotypic alterations.

Combinations of multiple differentiation strategies will be crucial in narrowing the processes and cell types affected in major mental illnesses. As induced and directed differentiation protocols are refined and become more efficient, reproducible, and homogenous, the arsenal of potential iPSC-derived neuronal and glial subtypes will continually expand. While a variety of cell types have been implicated in major mental illness, one cell type of great interest in schizophrenia are cortical interneurons[13]. As protocols now exist to generate cortical interneurons from human iPSCs[14,15], these are a particularly appealing target for further study. Investigations of the inhibitory-excitatory balance using mixed cultures of excitatory and inhibitory neurons will also facilitate the recognition of circuit dysfunction.

While most studies of psychiatric disease thus far have focused on neurons, iPSCs also can be used to investigate the role of disease-associated mutations in glial biology and neuron-glia interactions. Although investigation into glial dysfunction is less prevalent, there is evidence supporting glial abnormalities in schizophrenia[16]. This may be of interest in the case of DISC1 mutations, as DISC1 is expressed in microglia, astrocytes, and oligodendrocytes, in addition to neurons[17]. Furthermore, the association of many immunity-related genes in recent schizophrenia GWAS makes astrocytes and microglia attractive cell types in which to study mutations and variants in these genes[12].

Three-dimensional models of human neurodevelopment will be crucial in expanding current findings by examining human neuronal development in a setting closer to the *in vivo* context. While these “cerebral organoid” protocols currently generate heterogeneous cultures, with high inter-organoid variability, they still offer valuable information on cortical development[18]. Future protocols will likely address this variability, making these models more attractive for disease modeling. This method would be particularly interesting for further study of the

developmental dysregulation that accompanies DISC1 mutation. In three-dimensional organoids, one could investigate cell fate and cell position in the “cortex”, refining the phenotype observed here (i.e. are cell fate changes accompanied by disruption of proper cell migration or positioning?). Organoids also can be used for “in-organoid” electroporation studies, to assay the effects of local manipulation of gene expression on human neurons in a developing cortical structure.

The current work opens many doors for future studies of the functions of DISC1 in human neurons. DISC1 has been implicated in several distinct neuronal processes, and the potential phenotypes available for investigation are abundant[19]. Given the synaptic deficits identified in some other models of mental illness (discussed above), further investigation into synaptic biology using *DISC1*-disrupted neurons is warranted. The involvement of DISC1 in Wnt signaling points to neural progenitor cell proliferation as an interesting target for further analysis. NPC subtype-specific proliferation and cell cycle analyses would be particularly interesting, in light of the data presented here showing alterations in NPC fate with *DISC1* disruption. DISC1 has been linked to neuronal migration by multiple *in vivo* knockdown studies in rodent cortex, as well as through the identification of centrosomal binding partners[20-22]. Investigation of neuronal migration in culture is limited, as the process of neuronal migration in the developing brain is a highly regulated and context-dependent process[23]. Xenografting studies would allow for observation of human iPSC-derived neuronal migration in a developing rodent cortex. This method is technically challenging but offers an exciting opportunity for studying how *DISC1* disruption affects cell fate and migration in human neurons in an *in vivo* environment.

A further advantage of using human iPSCs to model neurological diseases is that these cells have the potential to recapitulate species-specific steps of neurodevelopment. Dramatic changes in neocortical structure and development have occurred over evolution, with the human brain characterized by an expansion of progenitor layer numbers and size and consequent

enlargement of the neocortex[24,25]. The increase in brain size over evolutionary time has been attributed in part to an expansion of intermediate progenitors and the presence of non-apical radial glial cells in the outer subventricular zone (oSVZ) of the developing primate cortex[26,27]. A recent study profiling human neural progenitors, purified from human fetal brains, identified unique transcriptional signatures of apical vs. non-apical radial glia. Using single-cell analyses, these cell types were further subdivided based on gene expression. When compared to purified mouse neural progenitors, this study found that human NPCs displayed a greater number of distinct transcriptional states, often defined by expression of genes that were not present in mouse progenitors[28].

The pronounced diversity of neural progenitors in human cortex, defined by unique transcriptional signatures, highlights both a challenge and advantage of modeling neurological disease using human cells. The vast majority of our knowledge regarding markers of different neural progenitor and neuronal states is derived from rodent studies, which harbor a distinct developmental program. This can make interpreting data derived from human neuronal differentiations challenging, as the relevance of these genes in human neurodevelopment is less well-studied. An expansion of studies of human neural development, from primary human tissues as well as from human stem cells, will help to address these challenges in the future. Furthermore, disease modeling using human cells allows for the discovery of alterations in cell types that are not present in rodent cortex, and therefore have not been previously studied. The present study identifies alterations in a human neural progenitor population with *DISC1* mutation, including decreased expression of the intermediate progenitor marker Tbr2. Future single-cell transcriptional studies of wild-type versus *DISC1*-disrupted progenitors may identify alterations in the balance of primate-specific NPC fates, which could not be identified using rodent models.

Modeling neuropsychiatric disease with human iPSCs has several caveats. Culture and

differentiation of neurons *in vitro* is distinct from *in vivo* neurodevelopment in many ways, making the study of neurodevelopment with iPSCs challenging. However, these cells provide novel opportunities for investigating disease processes in otherwise inaccessible human cells. When iPSC studies are combined with existing *in vivo* models of brain development and neurological diseases, the potential for investigation and discovery in this field is extraordinary.

REFERENCES

1. Bock, C. *et al.* Reference Maps of human ES and iPS cell variation enable high-throughput characterization of pluripotent cell lines. *Cell* **144,** 439–452 (2011).

2. Boulting, G. L. *et al.* A functionally characterized test set of human induced pluripotent stem cells. *Nat Biotechnol* **29,** 279–286 (2011).

3. Veres, A. *et al.* Low incidence of off-target mutations in individual CRISPR-Cas9 and TALEN targeted human stem cell clones detected by whole-genome sequencing. *Cell Stem Cell* **15,** 27–30 (2014).

4. Smith, C. *et al.* Whole-genome sequencing analysis reveals high specificity of CRISPR/Cas9 and TALEN-based genome editing in human iPSCs. *Cell Stem Cell* **15,** 12–13 (2014).

5. Suzuki, K. *et al.* Targeted gene correction minimally impacts whole-genome mutational load in human-disease-specific induced pluripotent stem cell clones. *Cell Stem Cell* **15,** 31–36 (2014).

6. Ding, Q. *et al.* A TALEN genome-editing system for generating human stem cell-based disease models. *Cell Stem Cell* **12,** 238–251 (2013).

7. Brennand, K. J. *et al.* Modelling schizophrenia using human induced pluripotent stem cells. *Nature* **473,** 221–225 (2011).

8. Wen, Z. *et al.* Synaptic dysregulation in a human iPS cell model of mental disorders. *Nature* 1–15 (2014). doi:10.1038/nature13716

9. Yoon, K.-J. *et al.* Modeling a Genetic Risk for Schizophreniain iPSCs and Mice Reveals Neural Stem Cell Deficits Associated with Adherens Junctions and Polarity. *Stem Cell* **15,** 79–91 (2014).

10. Sullivan, P. F., Daly, M. J. & O'Donovan, M. Genetic architectures of psychiatric disorders: the emerging picture and its implications. *Nat Rev Genet* **13,** 537–551 (2012).

11. Bergen, S. E. & Petryshen, T. L. Genome-wide association studies of schizophrenia: does bigger lead to better results? *Curr Opin Psychiatry* **25,** 76–82 (2012).

12. Schizophrenia Working Group of the Psychiatric Genomics Consortium. Biological insights from 108 schizophrenia-associated genetic loci. *Nature* **511,** 421–427 (2014).

13. Marín, O. Interneuron dysfunction in psychiatric disorders. *Nat Rev Neurosci* **13,** 107–120 (2012).

14. Maroof, A. M. *et al.* Directed differentiation and functional maturation of cortical interneurons from human embryonic stem cells. *Cell Stem Cell* **12,** 559–572 (2013).

15. Liu, Y. *et al.* Directed differentiation of forebrain GABA interneurons from human pluripotent stem cells. *Nat Protoc* **8,** 1670–1679 (2013).

16. Takahashi, N. & Sakurai, T. Roles of glial cells in schizophrenia: possible targets for therapeutic approaches. *Neurobiology of Disease* **53,** 49–60 (2013).

17. Seshadri, S. *et al.* Disrupted-in-Schizophrenia-1 expression is regulated by beta-site amyloid precursor protein cleaving enzyme-1-neuregulin cascade. *Proc Natl Acad Sci USA* **107,** 5622–5627 (2010).

18. Lancaster, M. A. *et al.* Cerebral organoids model human brain development and microcephaly. *Nature* **501,** 373–379 (2013).

19. Brandon, N. J. & Sawa, A. Linking neurodevelopmental and synaptic theories of mental illness through DISC1. *Nat Rev Neurosci* **12,** 707–722 (2011).

20. Young-Pearse, T. L., Suth, S., Luth, E. S., Sawa, A. & Selkoe, D. J. Biochemical and functional interaction of disrupted-in-schizophrenia 1 and amyloid precursor protein regulates neuronal migration during mammalian cortical development. *J Neurosci* **30,** 10431–10440 (2010).

21. Kamiya, A. *et al.* A schizophrenia-associated mutation of DISC1 perturbs cerebral cortex development. *Nat Cell Biol* **7,** 1167–1178 (2005).

22. Duan, X. *et al.* Disrupted-In-Schizophrenia 1 regulates integration of newly generated neurons in the adult brain. *Cell* **130,** 1146–1158 (2007).

23. Nadarajah, B. & Parnavelas, J. G. Modes of neuronal migration in the developing cerebral cortex. *Nat Rev Neurosci* **3,** 423–432 (2002).

24. Abdel-Mannan, O., Cheung, A. F. P. & Molnár, Z. Evolution of cortical neurogenesis. *Brain Res. Bull.* **75,** 398–404 (2008).

25. Molnár, Z. Evolution of cerebral cortical development. *Brain Behav. Evol.* **78,** 94–107 (2011).

26. Martínez-Cerdeño, V., Noctor, S. C. & Kriegstein, A. R. The role of intermediate progenitor cells in the evolutionary expansion of the cerebral cortex. *Cereb. Cortex* **16 Suppl 1,** i152–61 (2006).

27. Reillo, I., de Juan Romero, C., García-Cabezas, M. Á. & Borrell, V. A role for intermediate radial glia in the tangential expansion of the mammalian cerebral cortex. *Cerebral Cortex* **21,** 1674–1694 (2011).

28. Johnson, M. B. *et al.* Single-cell analysis reveals transcriptional heterogeneity of neural progenitors in human cortex. *Nat Neurosci* (2015). doi:10.1038/nn.3980

Appendix 1

Exon usage at the *DISC1* locus by RNA-sequencing

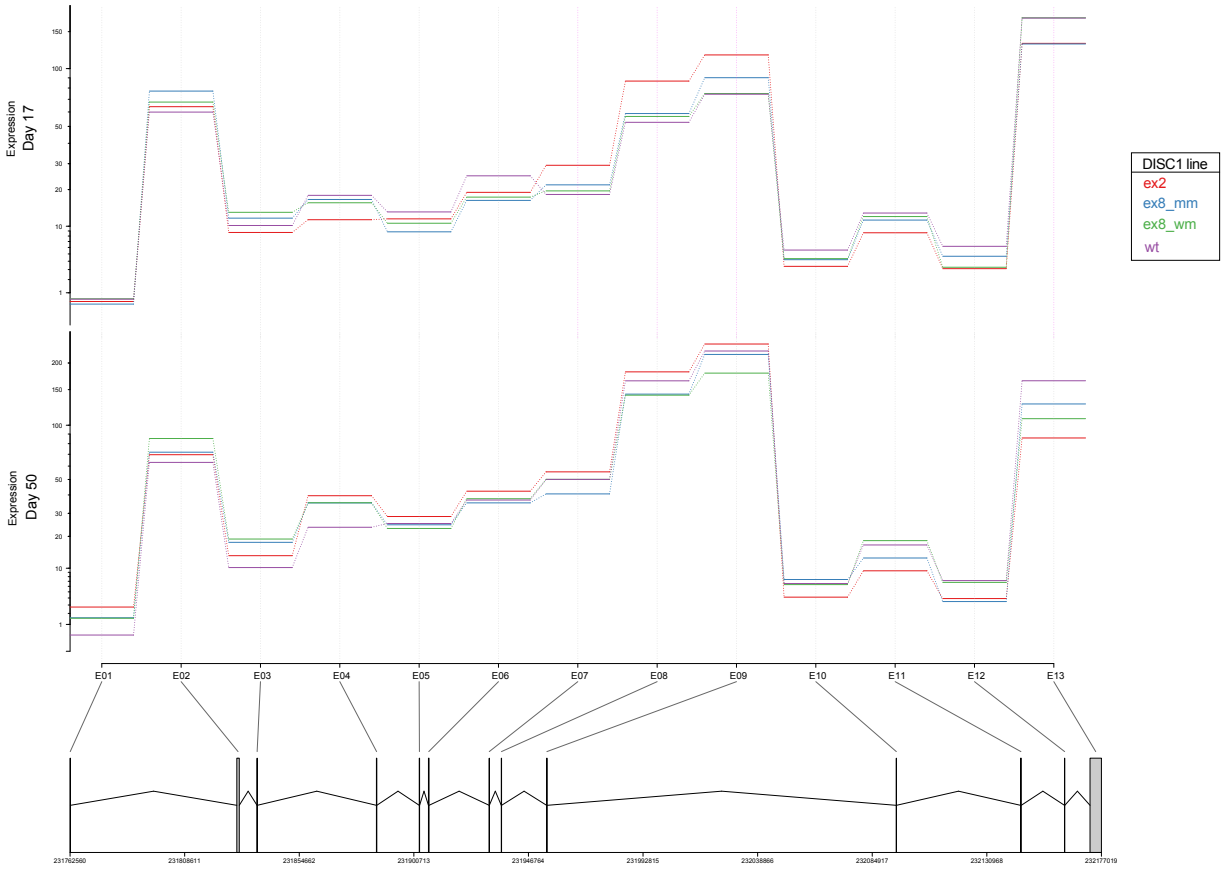

Figure A1. Exon usage at the *DISC1* locus by RNA-sequencing. DEXSeq was used to evaluate for differential exon usage in wild-type (wt) and *DISC1*-disrupted cells at day 17 (top) and day 50 (bottom). DISC1 exon structure is shown at bottom. There is no evidence for alteration of transcript structure with exon 8 or exon 2 mutations.

Appendix 2

Nanostring codeset tables

Table A2.1. Nanostring probe sequence for codeset 1.

CTIP2	GTGAAAAGTAAGGAAATCAGCCTTTCATCCCGGTCCTAAGTAACCGTCAGCCGA AGGTCTCGTGGAACACAGGCAAACCCGTGATTTTGGTGCTCCTTGT
Cux1	ACAAACAGCCCTGGAAAAAACTCGAACAGAATTATTTGACCTGAAAACCAAATAC GATGAAGAAACTACTGCAAAGGCCGACGAGATTGAAATGATCATG
DISC1 ex1/2	CCGGCGGCGGCGGCGTGAGCCACCGCGCAGGCAGCCGGGATTGCTTACCACC TGCAGCGTGCTTTCGGAGGCGGCGGCTGGCACGGAGGCCGGGCTACAT
DISC1 ex11b	CCCCAGGCTCCACTCCGAGGATAAAAGGAAGACCCCTTTGAAGGAATCTTACAT CCTTTCTGCAGAACTTGGAGAAAAGTGTGAAGACATAGGCAAGAAG
DISC1 ex12/13	CTTGGAAGATCAACTTCACACAGCAATCCACAGTCATGATGAAGATCTCATTCAG TCTCTCAGGAGGGAGCTCCAGATGGTGAAGGAAACTCTGCAGGCC
DISC1 ex2	CCCCAACCCCTCCTGGCTCTCACAGTGCCTTTACCTCAAGCTTTAGCTTTATTCG GCTCTCGCTTGGCTCTGCCGGGGAACGTGGAGAAGCAGAAGGCTG
DISC1 ex3a	GCGTAGATCATGACTTCTTTAGACATCATGAAAAGAAAAAGAGGACCCACGTGGA AGAATACGCTCATTTATGATCAGGGTAGCATCATATTCCTCTCCC
DISC1 ex9a	TATAAGTACTGTGATGCAGAGTCCTGGACACAGAGAAGTCAGCAACTTGCCTGA GGACAGCCTGCAGGACACAGCACTGTGATTTGAACCCAGAGAGTCT
Fezf2	GGGGCAGCCAGTTTTAACCCCAGCCTGTCACCGTGAGCGCCCCAGAAGAGCGC GGCGCCCCTAGCCATCTTTATACAGCCATGTAAATCCTCCTGTACAA
FoxG1	CTGACAAGTCTATCTCTAAGAGCCGCCAGATTTCCATGTGTGCAGTATTATAAGT TATCATGGAACTATATGGTGGACGCAGACCTTGAGAACAACCTAA
MAP2	TACTCTGTATGCTGGGATTCCGAGGTTCCAACACACTGTTACAAATCTGTGGGGG GTTTCTTTCTTCTGATAATTCTAGAGCCTGTTACCATAGAAAGGC
Nestin	CAGAGAATCACAAATCACTGAGGTCTTTAGAAGAACAGGACCAAGAGACATTGA GAACTCTTGAAAAAGAGACTCAACAGCGACGGAGGTCTCTAGGGGA
NeuroD1	GTGCCCAGCTCAATGCCATATTTCATGATTAGAGGCACGCCAGTTTCACCATTTC CGGGAAACGAACCCACTGTGCTTACAGTGACTGTCGTGTTTACAA
NeuroG1	GCCCCTAGACGGCCTTTCCTTTTGCACTTTCTGAACTCCACAAAACCTCCTTTGT GACTGGCTCAGAACTGACCCCAGCCACCACTTCAGTGTGATTTAG
Pax6	GGGAATTAAAGGCCTTCAGTCATTGGCAGCTTAAGCCAAACATTCCCAAATCTAT GAAGCAGGGCCCATTGTTGGTCAGTTGTTATTTGCAATGAAGCAC
PSD-95	TGCCCTGAAGAATGCGGGTCAGACGGTCACGATCATCGCTCAGTATAAACCAGA AGAGTACAGCCGATTCGAGGCCAAGATCCACGACCTTCGGGAACAG
Satb1	TTCCGAAATCTACCAGTGGGTACGCGATGAACTGAAACGAGCAGGAATCTCCCA GGCGGTATTTGCACGTGTGGCTTTTAACAGAACTCAGGGCTTGCTT
Sox1	AAAGCGTTTTCTTTGCTCGAGGGGACAAAAAAGTCAAAACGAGGCGAGAGGCGA AGCCCACTTTTGTATACCGGCCGGCGCGCTCACTTTCCTCCGCGTT
Sox2	AGCGCCCTGCAGTACAACTCCATGACCAGCTCGCAGACCTACATGAACGGCTCG CCCACCTACAGCATGTCCTACTCGCAGCAGGGCACCCCTGGCATGG
Syn I	GGATCTACTTCTGTTTTAGAACCTCCACATTCCTGAAGACCTCCGCCCCTGGTTT CCCCAGAGGGCGTTTTCCTTCCTGGAAGTGCCCAAATACCAGGCA
SYP	TAGTGCCTGTGATCGTGTGTTGCCATTTTGTCTGGCTGTGGCCCCTCCTTCTCCC CTCCAGACCCCTACCCTTTCCCAAACCCTTCGGTATTGTTCAAAG
Tau	ATTGGGTCCCTGGACAATATCACCCACGTCCCTGGCGGAGGAAATAAAAAGATT GAAACCCACAAGCTGACCTTCCGCGAGAACGCCAAAGCCAAGACAG
Tbr1	GCCGTCTGCAGCGAATAAGTGCAGGTCTCCGAGCGTGATTTTAACCTTTTTTGCA CAGCAGTCTCTGCAATTAGCTCACCGACCTTCAACTTTGCTGTAA
Tbr2	TCTCTAGATTCCAATGATTCAGGAGTATACACCAGTGCTTGTAAGCGAAGGCGGC TGTCTCCTAGCAACTCCAGTAATGAAAATTCACCCTCCATAAAGT

(Table A2.1, continued)

TUJ1	GCCGCCCTCCTGCAGTATTTATGGCCTCGTCCTCCCCACCTAGGCCACGTGTGA GCTGCTCCTGTCTCTGTCTTATTGCAGCTCCAGGCCTGACGTTTTA
VGLUT1	TCGGCTACTCGCACTCCAAGGGCGTGGCCATCTCCTTCCTGGTCCTAGCCGTGG GCTTCAGCGGCTTCGCCATCTCTGGGTTCAACGTGAACCACCTGGA
Vimentin	GAGGAGATGCTTCAGAGAGAGGAAGCCGAAAACACCCTGCAATCTTTCAGACAG GATGTTGACAATGCGTCTCTGGCACGTCTTGACCTTGAACGCAAAG

Table A2.2. Nanostring probe sequences for codeset 2.	
AXIN2	CTTGTCCAGCAAAACTCTGAGGGCCACGGCGAGTGTGAGGTCCACGGAAACTGTT GACAGTGGATACAGGTCCTTCAAGAGGAGCGATCCTGTTAATCCT
BRN2	GGGCACGGAGCTGCTTCGGGTGCATCACGCTGCTCGTTCCTGAGGTATGGGAACT GGCCTTTAGTGAAGCTATCCAGAGCAGGGCAAATAGCCACTGGTA
CCND2	TAGATTGCAAAGCAATGAACTCAAGAAGGAATTGAAATAAGGAGGGACATGATGGG GAAGGAGTACAAAACAATCTCTCAACATGATTGAACCATTTGGG
CTIP2	GTGAAAAGTAAGGAAATCAGCCTTTCATCCCGGTCCTAAGTAACCGTCAGCCGAAG GTCTCGTGGAACACAGGCAAACCCGTGATTTTGGTGCTCCTTGT
Cux1	ACAAACAGCCCTGGAAAAAACTCGAACAGAATTATTTGACCTGAAAACCAAATACGA TGAAGAAACTACTGCAAAGGCCGACGAGATTGAAATGATCATG
Cux2	GATAACAGAATGTCCGTGCCATTGTAAATGTTGTAGAGATGTGGGCCGTGGCCCAA CCGTCCTATATGAGATGTAGCATGGTACAGAACAAACTGCTTAC
CyclinD1	TTGAACACTTCCTCTCCAAAATGCCAGAGGCGGAGGAGAACAAACAGATCATCCGC AAACACGCGCAGACCTTCGTTGCCCTCTGTGCCACAGATGTGAA
DAB2	TTATTTGAGACTTCTCCATCGGGATCGCCTGGTGTCACCAAGTGTCCACTGGTACTG AGGTTTGCTGCCTGCCTTCTTGCCATGTCTAACGAAGTAGAAA
DCX	AAAGCTATGTCTGTTCCTCAGACAACTTCTTTAAAAAGGTGGAGTACACCAAGAATG TCAATCCCAACTGGTCTGTCAACGTAAAAACATCTGCCAATAT
FoxG1	CTGACAAGTCTATCTCTAAGAGCCGCCAGATTTCCATGTGTGCAGTATTATAAGTTA TCATGGAACTATATGGTGGACGCAGACCTTGAGAACAACCTAA
GRIA2	TGACCTATGATGCCGTTCAAGTGATGACTGAAGCCTTCCGCAACCTAAGGAAGCAA AGAATTGAAATCTCCCGAAGGGGGAATGCAGGAGACTGTCTGGC
GRIN1	TTCAAGAGAGTGCTGATGTCTTCCAAGTATGCGGATGGGGTGACTGGTCGCGTGGA GTTCAATGAGGATGGGGACCGGAAGTTCGCCAACTACAGCATCA
GSX2	TCTATGTCGACTCGCTCATCATCAAGGACACCTCACGGCCTGCGCCCTCGCTGCCT GAACCGCACCCCGGGCCGGATTTCTTCATCCCGCTTGGCATGCC
HES1	ATCTGAGCACAGAAAGTCATCAAAGCCTATTATGGAGAAAAGACGAAGAGCAAGAA TAAATGAAAGTCTGAGCCAGCTGAAAACACTGATTTTGGATGCT
HES5	CAGCCTGTAGAGGACTTTCTTCAGGGCCCGTAGCTGCTGGGCGTACCCCTGGCAG GCGGGCTGTGCCGCGGGCACATTTGCCTTTTGTGAAGGCCGAACT
HOXA1	CAGATAATTCTGGACCAGAGACTTGGTGCGGGGTTAACACCTTCATCCAGATTGGG TGCCAGCATACATTTTCTGGTGGGCCTTAACATCCCTCCTGCTT
HOXA2	CCCAAAGTTTCCCAGTCTCGCCTTTAACCAGCAATGAGAAAAATCTGAAACATTTTC AGCACCAGTCACCCACTGTTCCCAACTGCTTGTCAACAATGGG
HOXB4	CCTTTTCTCTTTCTGACATTCCAAAACCAGGCCCCTTCCTACCTCTGGGGCTGCTTG AGTCTAGAACCCTTCGTATGTGTGAATATCTGTGTGCTGTACA
Irx3	AGTCGCTTCTGTGGCACCCCGCATTCGCTGTGAGGTTTGTTTGTCCGGTTGATTTTG GGGGGTGGAGTTTCAGTGAGAATAAACGTGTCTGCCTTTGTGT
MAP2	TACTCTGTATGCTGGGATTCCGAGGTTCCAACACACTGTTACAAATCTGTGGGGGG TTTCTTTCTTCTGATAATTCTAGAGCCTGTTACCATAGAAAGGC

(Table A2.2, continued)

Nestin	CAGAGAATCACAAATCACTGAGGTCTTTAGAAGAACAGGACCAAGAGACATTGAGA ACTCTTGAAAAAGAGACTCAACAGCGACGGAGGTCTCTAGGGGA
NeuroD1	GTGCCCAGCTCAATGCCATATTTCATGATTAGAGGCACGCCAGTTTCACCATTTCCG GGAAACGAACCCACTGTGCTTACAGTGACTGTCGTGTTTACAA
Pax6	GGGAATTAAAGGCCTTCAGTCATTGGCAGCTTAAGCCAAACATTCCCAAATCTATGA AGCAGGGCCCATTGTTGGTCAGTTGTTATTTGCAATGAAGCAC
PSD-95	TGCCCTGAAGAATGCGGGTCAGACGGTCACGATCATCGCTCAGTATAAACCAGAAG AGTACAGCCGATTCGAGGCCAAGATCCACGACCTTCGGGAACAG
Reelin	TATTCAGACCCCAGCATCATCGTGTTATATGCCAAGAATAACTCTGCGGACTGGATT CAGCTAGAGAAAATTAGAGCCCCTTCCAATGTCAGCACAATCA
Satb1	TTCCGAAATCTACCAGTGGGTACGCGATGAACTGAAACGAGCAGGAATCTCCCAGG CGGTATTTGCACGTGTGGCTTTTAACAGAACTCAGGGCTTGCTT
Six3	CAGCCTGACGGAGCGCGCGGACACCGGCACCTCCATCCTCTCGGTAACCTCCAGC GACTCGGAATGTGATGTATGATAGCCAAGGCCGCCCTCCTCCCTC
Sox1	AAAGCGTTTTCTTTGCTCGAGGGGACAAAAAAGTCAAAACGAGGCGAGAGGCGAAG CCCACTTTTGTATACCGGCCGGCGCGCTCACTTTCCTCCGCGTT
Sox2	AGCGCCCTGCAGTACAACTCCATGACCAGCTCGCAGACCTACATGAACGGCTCGC CCACCTACAGCATGTCCTACTCGCAGCAGGGCACCCCTGGCATGG
Syn I	GGATCTACTTCTGTTTTAGAACCTCCACATTCCTGAAGACCTCCGCCCCTGGTTTCC CCAGAGGGCGTTTTCCTTCCTGGAAGTGCCCAAATACCAGGCA
SYP	TAGTGCCTGTGATCGTGTGTTGCCATTTTGTCTGGCTGTGGCCCCTCCTTCTCCCCT CCAGACCCCTACCCTTTCCCAAACCCTTCGGTATTGTTCAAAG
Tau	ATTGGGTCCCTGGACAATATCACCCACGTCCCTGGCGGAGGAAATAAAAAGATTGA AACCCACAAGCTGACCTTCCGCGAGAACGCCAAAGCCAAGACAG
Tbr1	GCCGTCTGCAGCGAATAAGTGCAGGTCTCCGAGCGTGATTTTAACCTTTTTTGCACA GCAGTCTCTGCAATTAGCTCACCGACCTTCAACTTTGCTGTAA
Tbr2	TCTCTAGATTCCAATGATTCAGGAGTATACACCAGTGCTTGTAAGCGAAGGCGGCT GTCTCCTAGCAACTCCAGTAATGAAAATTCACCCTCCATAAAGT
TUJ1	GCCGCCCTCCTGCAGTATTTATGGCCTCGTCCTCCCCACCTAGGCCACGTGTGAGC TGCTCCTGTCTCTGTCTTATTGCAGCTCCAGGCCTGACGTTTTA
TWIST1	CAACTCCCAGACACCTCGCGGGCTCTGCAGCACCGGCACCGTTTCCAGGAGGCCT GGCGGGGTGTGCGTCCAGCCGTTGGGCGCTTTCTTTTTGGACCTC
VGLUT1	TCGGCTACTCGCACTCCAAGGGCGTGGCCATCTCCTTCCTGGTCCTAGCCGTGGG CTTCAGCGGCTTCGCCATCTCTGGGTTCAACGTGAACCACCTGGA
VGLUT2	TACGACAGTGAGAAAGATCATGAATTGTGGTGGTTTTGGCATGGAAGCCACACTGC TCCTGGTCGTTGGCTATTCTCATACTAGAGGGGTAGCAATCTCA
Vimentin	GAGGAGATGCTTCAGAGAGAGGAAGCCGAAAACACCCTGCAATCTTTCAGACAGGA TGTTGACAATGCGTCTCTGGCACGTCTTGACCTTGAACGCAAAG
WNT3A	TCTCTCCGCGGGTGGGACTCTTCCCTGGGAACCGCCCTCCTGATTAAGGCGTGGC TTCTGCAGGAATCCCGGCTCCAGAGCAGGAAATTCAGCCCACCAG

Appendix 3

Neuronal migration and neurite outgrowth of *DISC1*-targeted cells

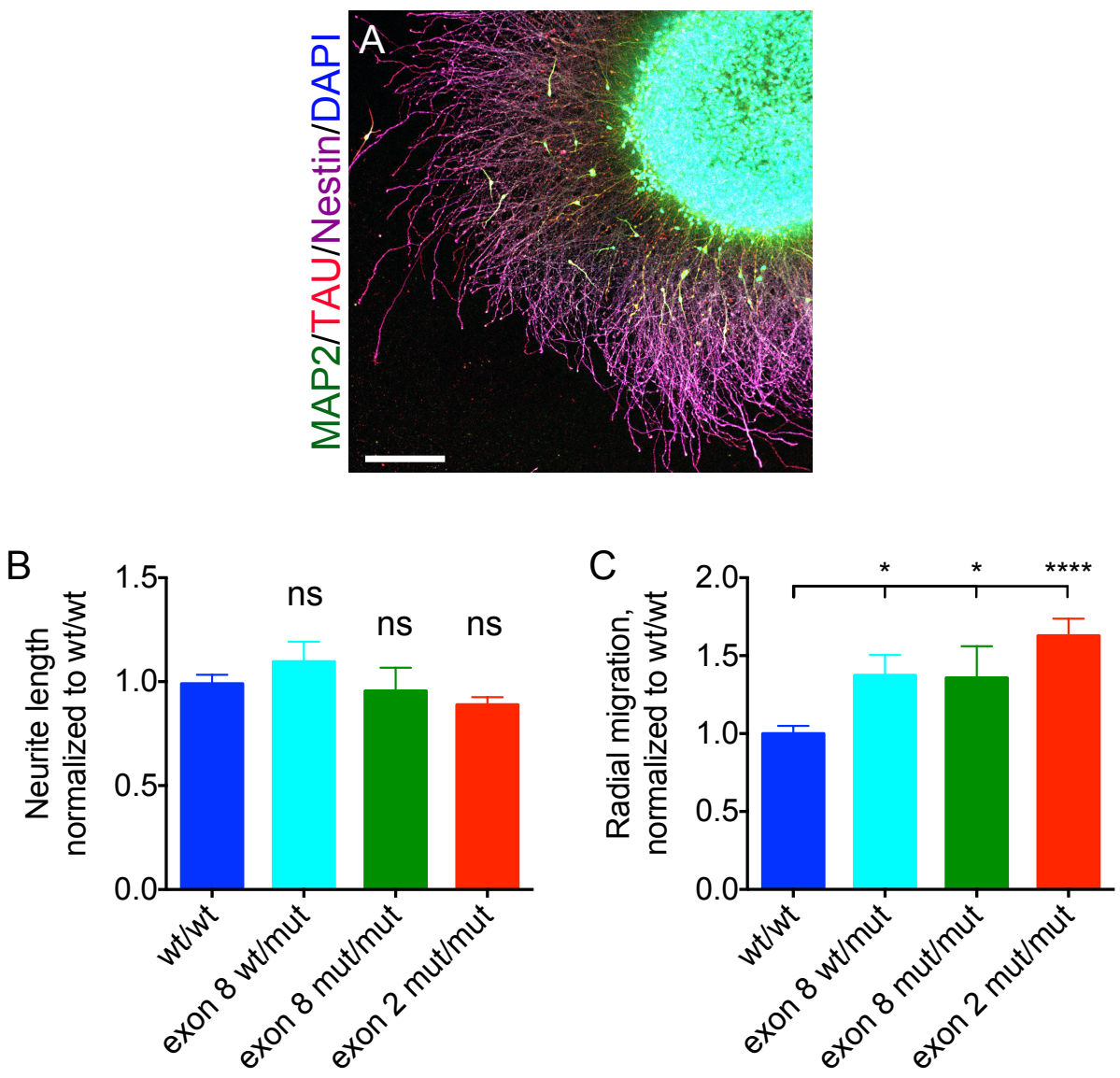

Figure A3. *DISC1* disruption does not affect neurite outgrowth but increases neuronal migration *in vitro*. *In vitro* assay: day 24 neural aggregates were plated onto poly-ornithine/laminin-coated plates and cultured for 72 hr in neural differentiation media. **(A)** Representative image of a neural aggregate, immunostained as shown. Scale bar = 200 μm. **(B)** Quantification of neurite outgrowth (each dot represents avg of 10 longest neurites from 1 aggregate, n = 21-69), using Simple Neurite Tracer in FIJI. **(C)** Migration was measured by subtracting average aggregate radius from average radius of migrated cells in FIJI. n = 42-86 Data represent at least 3 independent differentiations. Mean ± SEM shown, statistics: one way ANOVA. ns = not significant, * $p < 0.05$, **** $p < 0.0001$.

Appendix 4

Proliferation of *DISC1* targeted NPCs

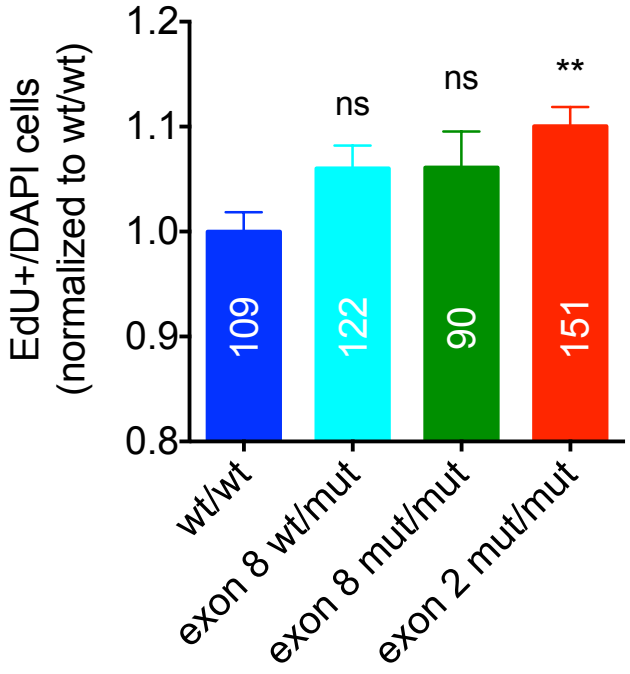

Figure A4. *DISC1* exon 2 disruption increases EdU incorporation in NPCs. NPCs from dissociated day 24 neural aggregates were plated and cultured in L (control) conditioned media for 24 hours, in the presence of 10 uM EdU for hours 16-20. The proportion of EdU+/DAPI+ cells was quantified using CellProfiler. Data represent at least 5 independent differentiations. Number of images counted shown in bars. Mean ± SEM shown, statistics: one way ANOVA. ns = not significant, * $p < 0.05$, **** $p < 0.0001$.